2 mip

FINAL REPORT

(1R

[redacted]

RESEARCH STUDY ON STABILIZATION AND CONTROL

MODERN SAMPLED-DATA CONTROL THEORY

SYSTEMS RESEARCH LABORATORY

P.O. BOX 2277, STATION A
3206 VALLEY BROOK DRIVE
CHAMPAIGN, ILLINOIS 61820

PREPARED FOR GEORGE C. MARSHALL SPACE FLIGHT CENTER

HUNTSVILLE, ALABAMA

FINAL REPORT

RESEARCH STUDY ON STABILIZATION AND CONTROL – MODERN SAMPLED-DATA CONTROL THEORY

SUBTITLE: CONTINUOUS AND DISCRETE DESCRIBING FUNCTION ANALYSIS OF THE LST SYSTEM

January 1, 1974 NAS8-29853

BY **B.C. KUO**
G. SINGH

PREPARED FOR GEORGE C. MARSHALL SPACE FLIGHT CENTER
HUNTSVILLE, ALABAMA

CONTRACT NAS8-29853 DCN 1-2-40-23018

SYSTEMS RESEARCH LABORATORY
P.O. BOX 2277, STATION A
CHAMPAIGN, ILLINOIS 61820

TABLE OF CONTENTS

		Page
1.	Modeling of the LST System with the CMG Control Loop	1
2.	Modeling of the CMG Frictional Nonlinearity	20
3.	A Continuous Describing Function for the Gimbal Friction Nonlinearity	35
4.	Computer Simulation of the Simplified LST System	41
5.	A Describing Function of the CMG Nonlinearity Using The Analytical Torque Equation	49
6.	Computer Simulation of the Simplified LST System with the Analytical Torque Expressions	60
7.	Transfer Functions of the Sampled-Data LST System	78
8.	The Discrete Describing Function of the CMG Frictional Nonlinearity	90
9.	Discrete Describing Function Plots of the CMG Frictional Nonlinearity	112
10.	Computer Simulation of the Simplified Sampled-Data LST System with the Analytical CMG Frictional Torque Expressions	122

1. Modeling of the LST System with the CMG Control Loop

The purpose of this section is to study the dynamics of the LST control system, and to arrive at a simplified model for computer simulation without loss of accuracy. A dynamic model for the LST control system with the complete CMG control loop is shown in Figure 1-1. Other than the CMG nonlinearity model, this system is essentially the same as that in reference [1]. It should be noted that the limits on the current command, the gimbal rate command, and the torque amplifier voltage, have been neglected. The model also assumes a second-order pure inertial vehicle dynamics. The cogging torque, ripple torque, and the tachometer ripple of the CMG are also neglected.

Since the LST control system has a sample-and-hold in the forward path, discrete-data system theory should be used when studying the system's behavior. However, because of the complexity of the CMG nonlinearity, an analytical study of the entire system is quite complex. The present task calls for two approaches to the analytical study of the stability of the system. The first analysis involves the assumption that the sampling rate of the system is high, so that the system may be approximated by a continuous-data system. This is accomplished simply by shorting out the sample-and-hold in Figure 1-1. The second approach involves the insertion of a fictitious sample-and-hold at the input of the nonlinearity. This way, the system has two synchronized samplers, and discrete-data techniques such as the discrete-describing function method may be used.

Characteristic Equation and Eigenvalues of the Continuous-Data LST

In this section the LST system modeled in Figure 1-1 is considered to be of continuous-data, that is, without the sample-and-hold. If we represent the input-output relation of the CMG nonlinearity between θ_G and

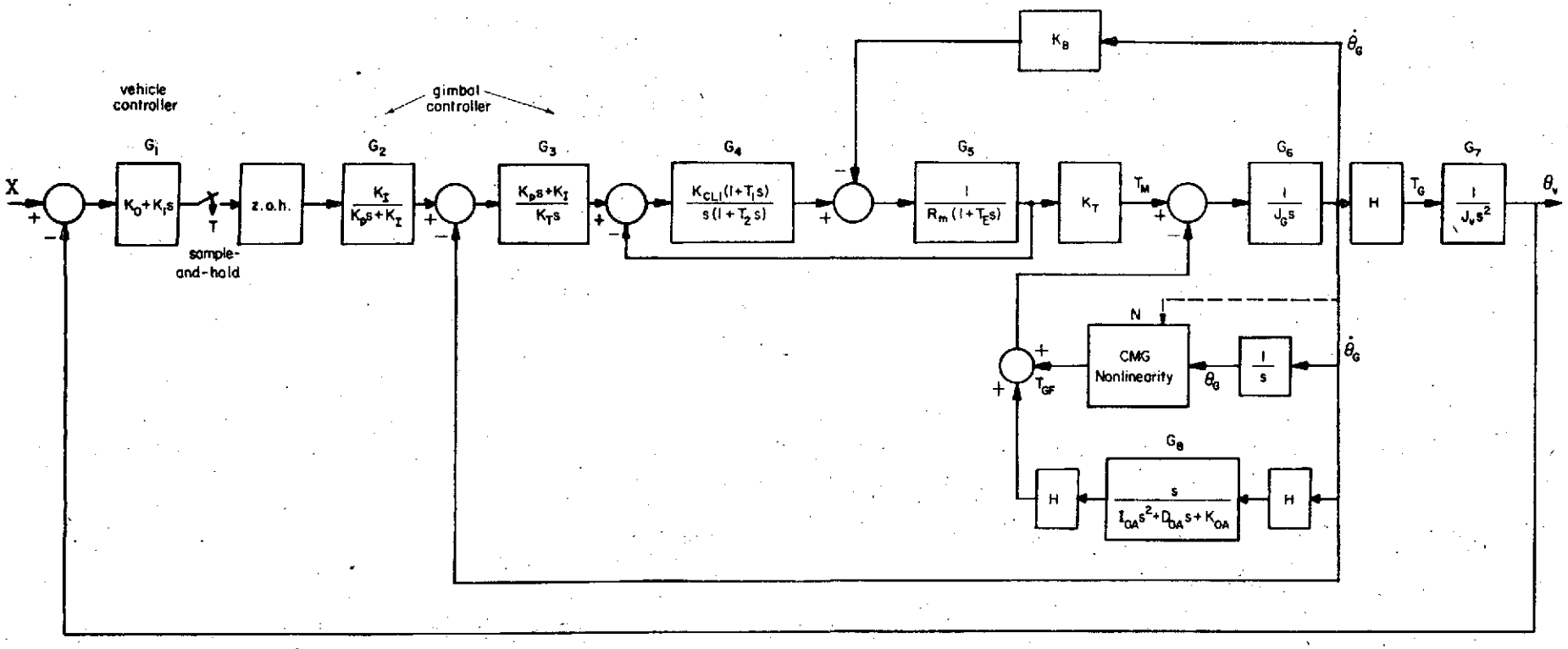

Figure 1-1. A dynamic model for the LST control system with the complete CMG control loop.

T_{GF} by an equivalent gain N, we can derive the characteristic equation and determine the eigenvalues of the linear portion of the system. The characteristic equation and the eigenvalue studies of the system allow us to gain understanding of the dynamic behavior of the system, and eventually lead to the simplification of the system model.

With reference to Figure 1-1, the characteristic equation of the continuous model of the system for stability analysis may be obtained from the following equation:

$$1 + \Sigma \text{ Loop gains} = 0 \tag{1-1}$$

Or,

$$1 + N(1 + G_4G_5)\frac{G_6}{s} + H^2G_6G_8 + G_5G_6K_BK_T + G_4G_5 + G_3G_4G_5G_6 + G_1G_2G_3G_4G_5G_6G_7K_T + G_6G_8H^2G_4G_5 = 0 \tag{1-2}$$

Dividing both sides of the last equation by the terms which do not contain N, we arrive at the equation which is of the form,

$$1 + NG(s) = 0 \tag{1-3}$$

where

$$G(s) = \frac{G_6(1+G_4G_5)}{s\Delta_0} \tag{1-4}$$

and

$$\Delta_0 = 1 + H^2G_6G_8 + G_5G_6G_8K_BK_T + G_4G_5 + G_3G_4G_5G_6 + G_1G_2G_3G_4G_5G_6G_7K_T + G_6G_8G_4G_5H^2 \tag{1-5}$$

$$G_1 = K_0 + K_1s$$

$$G_2 = \frac{K_I}{K_ps+K_I}$$

$$G_3 = \frac{K_p s + K_I}{K_T s}$$

$$G_4 = \frac{K_{CLI}(1+T_1 s)}{s(1+T_2 s)} \qquad (1\text{-}6)$$

$$G_5 = \frac{1}{R_m(1+T_E s)}$$

$$G_6 = \frac{1}{J_G s}$$

$$G_7 = \frac{H}{J_V s^2}$$

$$G_8 = \frac{s}{I_{OA}s^2 + D_{OA}s + K_{OA}}$$

The following system parameters are given:

$H = 600$	ft-lb-sec	CMG Angular Momentum
$J_G = 2.1$	ft-lb-sec^2	Gimbal inertia
$I_{OA} = 2.1$	ft-lb-sec^2	CMG output axis inertia
$D_{OA} = 20$	ft-lb-sec	CMG output axis damping
$K_{OA} = 10^6$	ft-lb	CMG output axis spring constant
$K_0 = 5.75835 \times 10^3$		vehicle controller coefficient
$K_1 = 1.37102 \times 10^3$		vehicle controller coefficient
$K_T = 2.5$	ft-lb/amp	Torque motor sensitivity
$K_B = 3.4$	volts/rad/sec	Torque motor back emf constant
$R_m = 4.4$	ohms	Torque motor armature resistance
$T_E = 6.4$	milliseconds	Torque motor armature time constant
$K_p = 216$	ft-lb/rad/sec	Gimbal rate loop proportional gain

K_I = 9700 ft-lb/rad Gimbal rate loop integral gain

K_{CLI} = $1.6X10^4$ volts/sec/amp Current loop integral gain

T_1 = 6.4 milliseconds Current loop lead time constant

T_2 = 0.16 milliseconds Current loop lag time constant

J_v = 10^5 ft-lb-sec^2 Vehicle inertia

The numerator of Eq. (1-2) may be regarded as the characteristic equation of the overall system. Let us consider that the CMG is without the nonlinear friction chearcteristics. The overall LST system is linear, and the characteristic equation is given by

$$\Delta_0 = 0 \tag{1-7}$$

Substituting Eq. (1-6) into Eq. (1-5), and simplifying, the numerator polynomial of Δ_0 when equated to zero gives the characteristic equation. Thus we have

$$\Delta = b_0 s^9 + b_1 s^8 + b_2 s^7 + b_3 s^6 + b_4 s^5 + b_5 s^4 + b_6 s^3 + b_7 s^2 + b_8 s + b_9 = 0 \tag{1-8}$$

where

$$b_0 = R_m J_G J_V T_E T_2 I_{OA}$$

$$b_1 = R_m J_G J_V [D_{OA} T_E T_2 + I_{OA}(T_E + T_2)]$$

$$b_2 = R_m J_G J_V [I_{OA} + D_{OA}(T_E + T_2) + K_{OA} T_E T_2] + K_{CLI} J_V J_G T_1 I_{OA} + K_B K_T J_V T_2 I_{OA} + H^2 J_V R_m T_2 T_E$$

$$b_3 = R_m J_G J_V [D_{OA} + (T_2 + T_E) K_{OA}] + K_{CLI} J_V J_G (T_1 D_{OA} + I_{OA}) + K_B K_T J_V (T_2 D_{OA} + I_{OA}) + H^2 J_V R_m (T_2 + T_E) + J_V K_{CLI} T_1 I_{OA} K_P$$

$$b_4 = R_m J_G J_V K_{OA} + K_{CLI} J_V J_G (D_{OA} + K_{OA} T_1) + K_B K_T J_V (D_{OA} + K_{OA} T_2) + H^2 J_V R_m + J_V K_{CLI} [(T_1 D_{OA} + I_{OA}) K_P + K_I T_1 I_{OA}] + K_{CLI} J_V H^2 T_1$$

$$b_5 = K_{CLI}J_VJ_GK_{OA} + K_BK_TJ_VK_{OA} + J_VK_{CLI}[K_P(D_{OA} + K_{OA}T_1) + K_I(T_1D_{OA} + I_{OA})] + K_IK_{CLI}HT_1I_{OA}K_1 + K_{CLI}J_VH^2$$

$$b_6 = J_VK_{CLI}[K_{OA}K_P + K_I(D_{OA} + K_{OA}T_1)] + K_IK_{CLI}H[(T_1D_{OA} + I_{OA})K_1 + K_0T_1I_{OA}]$$

$$b_7 = J_VK_{CLI}K_IK_{OA} + [K_0(T_1D_{OA} + I_{OA}) + K_1(D_{OA} + K_{OA}T_1)]$$

$$b_8 = K_IK_{CLI}H[K_{OA}K_1 + K_0(D_{OA} + K_{OA}T_1)]$$

$$b_9 = K_IK_{CLI}HK_0K_{OA} \qquad (1\text{-}9)$$

Substituting the values of the system parameters into these coefficients, we have,

$$b_0 = 1.98697$$

$$b_1 = 12747.9$$

$$b_2 = 0.483289X10^{8}$$

$$b_3 = 0.192517X10^{11}$$

$$b_4 = 0.273187X10^{14}$$

$$b_5 = 0.619189X10^{16}$$

$$b_6 = 0.44553X10^{18}$$

$$b_7 = 0.163408X10^{20}$$

$$b_8 = 0.131112X10^{21}$$

$$b_9 = 0.536217X10^{21}$$

The eigenvalues of the system, or the roots of Eq. (1-8) are found and are tabulated below:

-4.56811 + j4.68534 -4.56811 - j4.68534	vehicle dynamics
-1563.11	CMG torque motor Armature time constant
-39.8505 + j40.9207 -39.8505 - j40.9207	CMG dynamics
-12.4647 + j748.038 -12.4647 - j748.038	CMG output axis torsion dynamics
-3072.85 + j3554.86 -3072.85 - j3554.86	CMG current loop controller

The contribution of the sectors of the LST and the CMG dynamics to these eigenvalues are indicated.

It is essential to investigate the importance and weight of each of these eigenvalues upon the dynamics of the entire system. Since some of these modes have very short time constants and high-frequency oscillations, it is expected that a digital computer simulation of the entire exact model will be time consuming and costly.

We shall show that for computer simulation and analytical purposes some of these fast and oscillatory modes of the system may be neglected.

Figure 1-2 illustrates the root locus diagram of Eq. (1-8) when K_0 and K_1 are varied proportionally from their nominal values which are listed earlier. In Figure 1-2 the variable parameter is indicated as K which is the multiplier of the nominal K_0 and K_1. Table 1-1 gives the location of the roots as a function of K.

It is interesting to note from the root locus diagram that for the nominal K_0 and K_1 both the LST vehicle dynamics and the CMG dynamics have a relative damping ratio of approximately 0.707. Furthermore, the

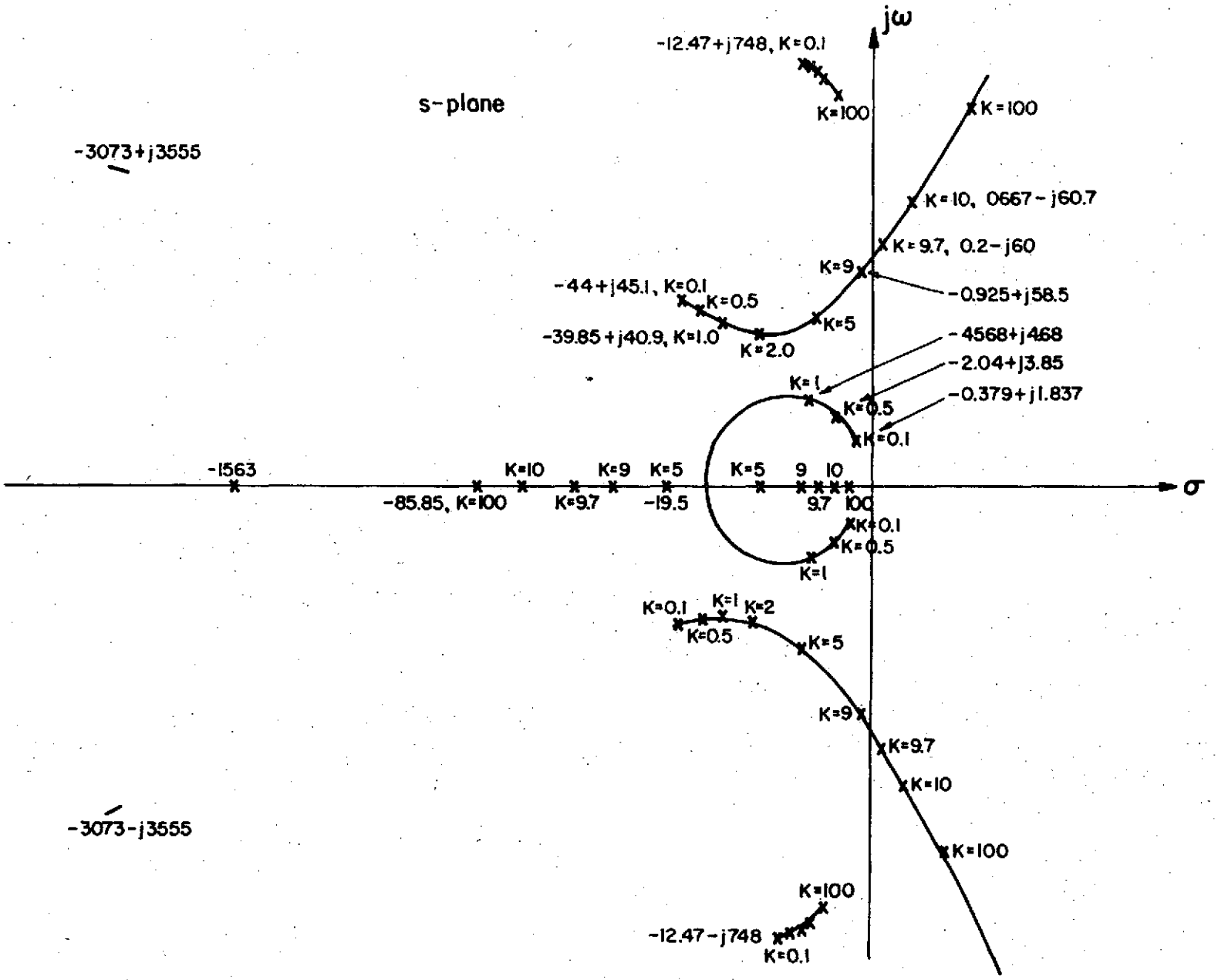

Figure 1-2. A root locus diagram of Eq. (1-8) when K_0 and K_1 are varied proportionally.

Table 1-1. Eigenvalues of the complete LST as

$K_0 = KK_0$ (nominal) and $K_1 = KK_1$ (nominal) vary.

K_0 (nominal) = 5.75835×10^3

K_1 (nominal) = 1.37102×10^3

K	Roots				
0.1	-0.379 ± j1.837	-1563.1	-44.034 ± j45.091	-12.470 ± j748.04	-3072.8 ± j3554.8
0.5	-2.041 ± j3.853	-1563.1	-42.374 ± j43.335	-12.467 ± j748.04	-3072.8 ± j3554.8
1.0	-4.568 ± j4.685	-1563.1	-39.850 ± j40.921	-12.465 ± j748.04	-3072.8 ± j3554.8
2.0	-6.295 -19.522	-1563.1	-31.515 ± j35.779	-12.459 ± j748.04	-3072.8 ± j3554.8
5.0	-4.680 -64.314	-1563.1	-9.943 ± j47.136	-12.443 ± j648.04	-3072.8 ± j3554.8
9.0	-4.441 -82.631	-1563.1	-0.925 ± j58.522	-12.422 ± j748.04	-3072.8 ± j3554.8
9.7	-4.422 -84.921	-1563.1	0.206 ± j60.068	-12.418 ± j748.04	-3072.8 ± j3554.8
10	-4.415 -86.866	-1563.1	0.667 ± j66.774	-12.417 ± j748.04	-3072.8 ± j3554.8
100	-4.220 -156.13	-1563.1	45.437 ± j129.14	-11.94 ± j748.03	-3072.8 ± j3554.8

eigenvalues at -1563.1, -3072.8 ± j3554.8, and -12.465 ± j748.04 are not sensitive to the change of the loop gain at all.

Another way of investigating the significance of each of the eigenvalues toward the dynamics of the entire system is to evaluate the residue of the closed-loop transfer function that corresponds to each of the eigenvalues.

From Figure 1-1 the closed-loop transfer function of the LST system without the CMG nonlinearity is written

$$\frac{\theta_V}{\chi} = \frac{G_1G_2G_3G_4G_5G_6G_7K_T}{\Delta_0} \tag{1-10}$$

After simplification, Eq. (1-10) becomes

$$\frac{\theta_V}{\chi} = \frac{K_TK_{CLI}K_IH(a_0s^4+a_1s^3+a_2s^2+a_3s+a_4)}{\Delta} \tag{1-11}$$

where Δ is given by Eq. (1-8), and

$$a_0 = I_{0A}K_1T_1$$

$$a_1 = D_{0A}K_1T_1 + I_{0A}(K_1 + K_0T_1)$$

$$a_2 = K_{0A}T_1K_1 + D_{0A}(K_1 + K_0T_1) + I_{0A}K_0$$

$$a_3 = K_0D_{0A} + K_{0A}(K_1 + K_0T_1)$$

$$a_4 = K_0K_{0A}$$

Substitution of the system parameters into Eq. (1-11), and performing partial faction expansion, the residues of Eq. (1-11) at its poles are tabulated in Table 1-2. It is interesting to note that only the residues which correspond to the CMG and the vehicle dynamics are of significance. The contributions from the eigenvalues at -1563.1, -3072.8 ± j3554.8, and -12.465 ± j748.04 are very insignificant.

Table 1-2. Residues of Eq. (1-11) at its poles

	Roots	Residues
Vehicle dynamics	-4.56811 ± j4.68534	14.3102 ∓ j0.5256
CMG torque motor armature time constant	-1563.11	0.002778
CMG dynamics	-39.8505 ± j40.9207	-14.2967 ± j12.7188
CMG output axis torsion dynamics	-12.4647 ± j748.038	-0.013248 ± j0.0001275
CMG current loop controller	-3072.85 ± j3554.86	-0.001565 ∓ j0.002523

Still another method of investigating the effects of each of the system components on the system dynamics is to make the frequency-domain plots for G(s) of Eq. (1-4). These plots are also useful for the continuous-data describing function study of the system. In Figure 1-3, curve 1 gives the G(s) plot in decibels versus phase for the 9th-order LST system. In the same figure, curve 2 gives the G(s) plot when the output axis torsional dynamics of the CMG are neglected; that is, $I_{OA} = 0$, $D_{OA} \neq 0$, $K_{OA} = 0$.

In this case, G(s) is simplified to

$$G(s) = \frac{R_m s(1+T_2 s)(1+T_E s)+K_{CLI}(1+T_1 s)}{\Delta} \tag{1-12}$$

where

$$\Delta = R_m J_G T_2 T_E s^5 + R_m J_G (T_2 + T_E) s^4 + (R_m J_G + K_{CLI} J_G T_1 + K_B K_T T_2) s^3 + (K_{CLI} J_G + K_B K_T + K_{CLI} K_p T_1) s^2 + K_{CLI}(K_p + K_I T_1) s + K_{CLI} K_I \tag{1-13}$$

In addition to neglecting the CMG torsional dynamics a further simplification of the LST system can be conducted by neglecting the time constants T_1, T_2, and T_E, as these are small when compared with the time constants of the vehicle and the CMG. Figure 1-4 gives the block diagram of the Gimbal rate control loop and the CMG with these simplifications. Using the block diagram reduction technique, the system in Figure 1-4 is reduced to the block diagram of Figure 1-5. Since K_{CLI}/R_m is very large, the transfer function of the inner loop involving K_{CLI} and R_m is approximately unity. Furthermore, since K_B/K_{CLI} is very small, the back emf loop of Figure 1-5 may also be neglected. The final simplified gimbal rate control loop and CMG dynamics are represented by the block diagram of Figure 1-6. The transfer function of the simplified CMG control loop is

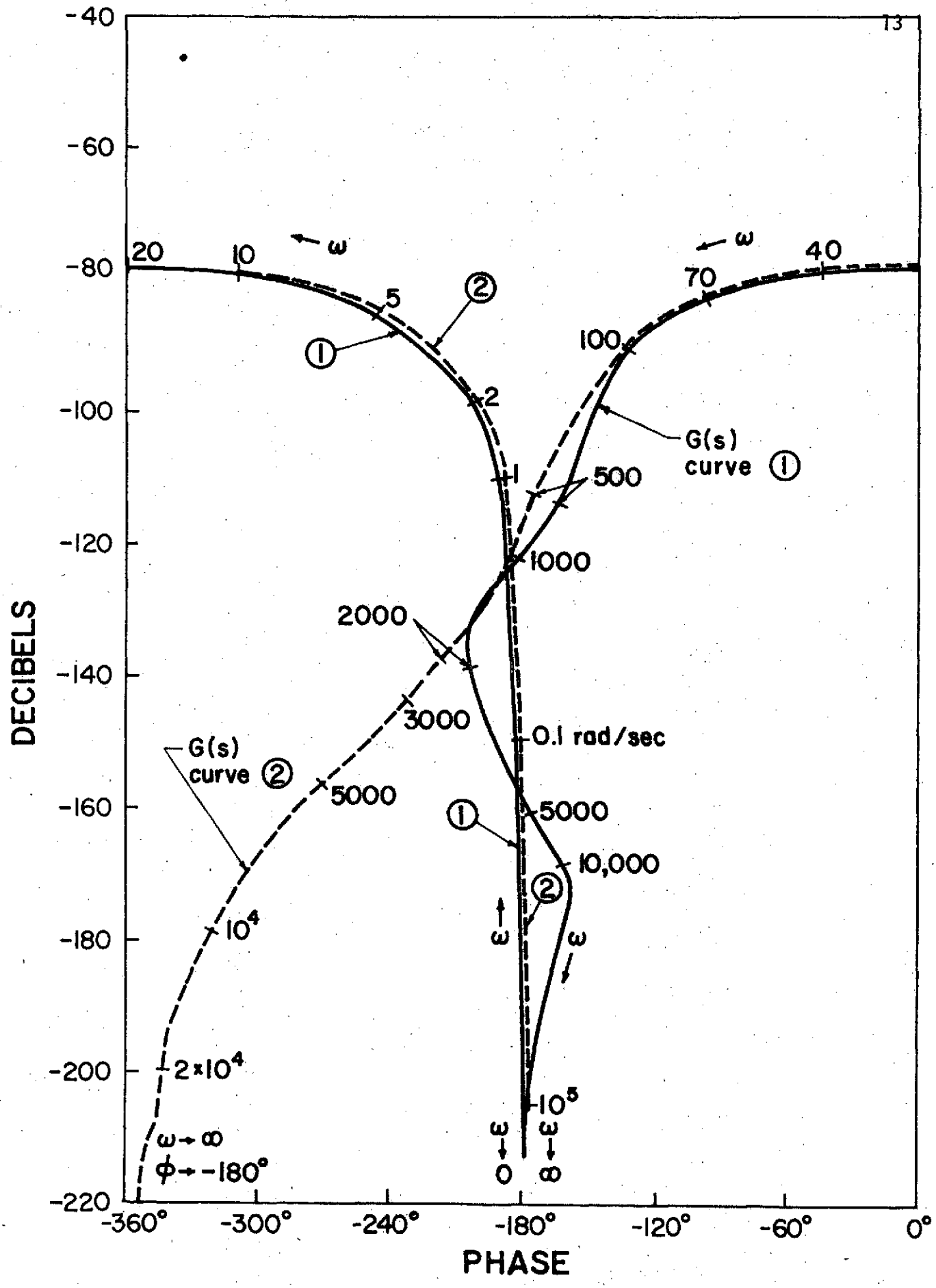

Figure 1-3. Frequency-domain plots of the LST system.

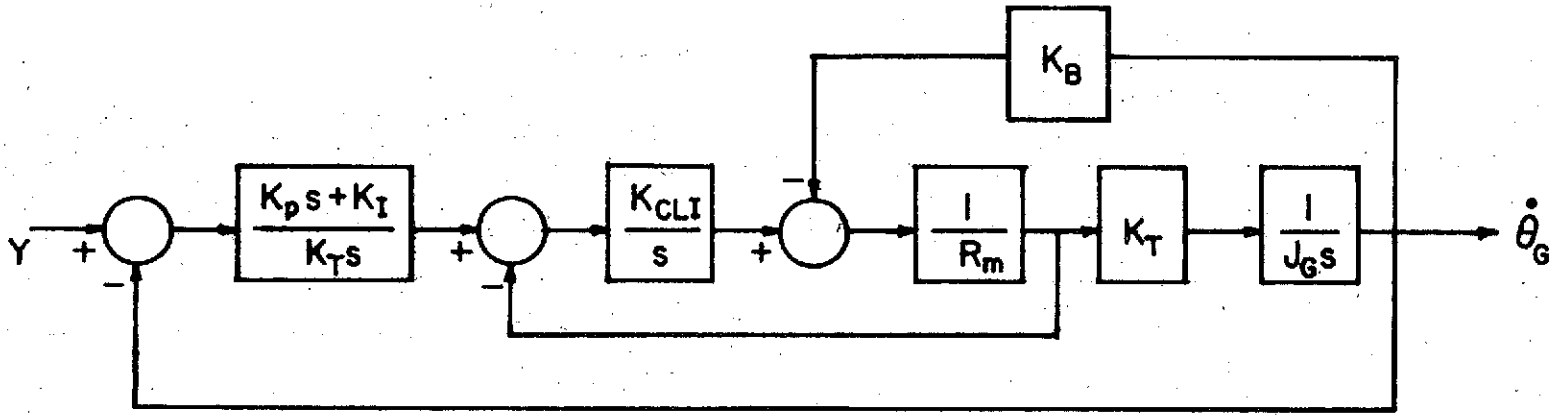

Figure 1-4. Simplified gimbal rate control loop and CMG.

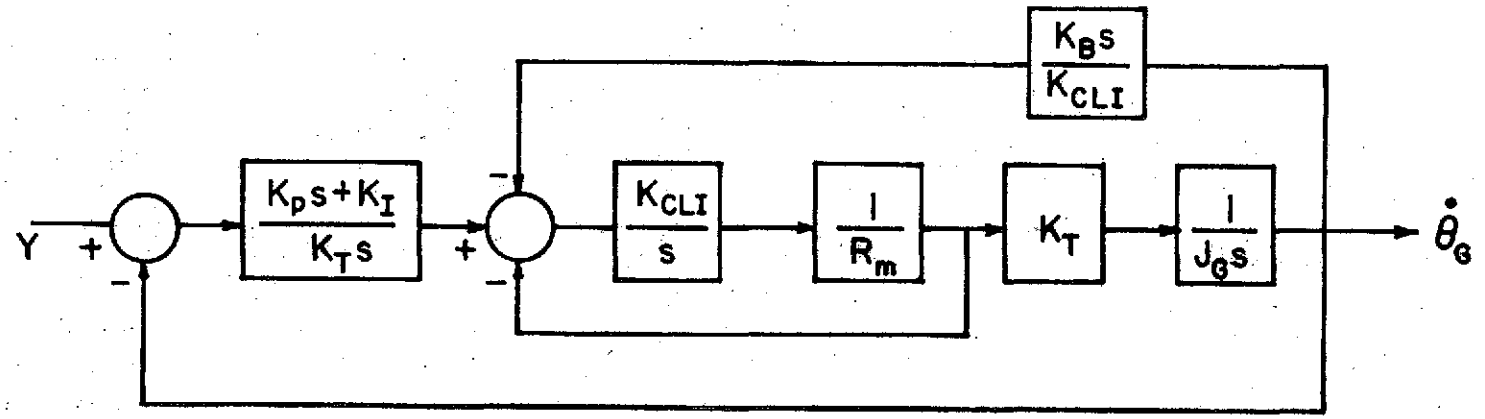

Figure 1-5. An equivalent block diagram of the system in Figure 1-4.

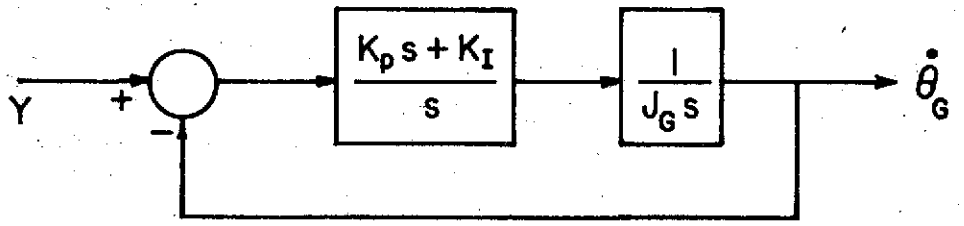

Figure 1-6. Final simplified gimbal rate control loop and the CMG.

$$\frac{\dot{\theta}_G}{Y} = \frac{K_p s + K_I}{J_G s^2 + K_p s + K_I} \tag{1-14}$$

Substituting the system parameters into the last equation, we have

$$\frac{\dot{\theta}_G}{Y} = \frac{102.857(s+44.9074)}{(s+51.428+j44.43)(s+51.428-j44.43)} \tag{1-15}$$

Now replacing the CMG control loop in Figure 1-1 by the simplified diagram of Figure 1-6, we have the block diagram of Figure 1-7 for the simplified LST system without sampling.

The transfer function for G(s) in Eq. (1-4) is simplified to

$$G(s) = \frac{J_V s^2}{J_G J_V s^4 + J_V K_p s^3 + J_V K_I s^2 + K_I H K_1 s + K_I K_0 H} \tag{1-16}$$

Figure 1-8 shows the plot for the G(s) in Eq. (1-16). It is interesting to note that the three G(s) plots in Figures 1-3 and 1-8 are very similar for frequencies below 1000 rad/sec. This proves that the LST system may justifiably approximated by the simplified system of Figure 1-7.

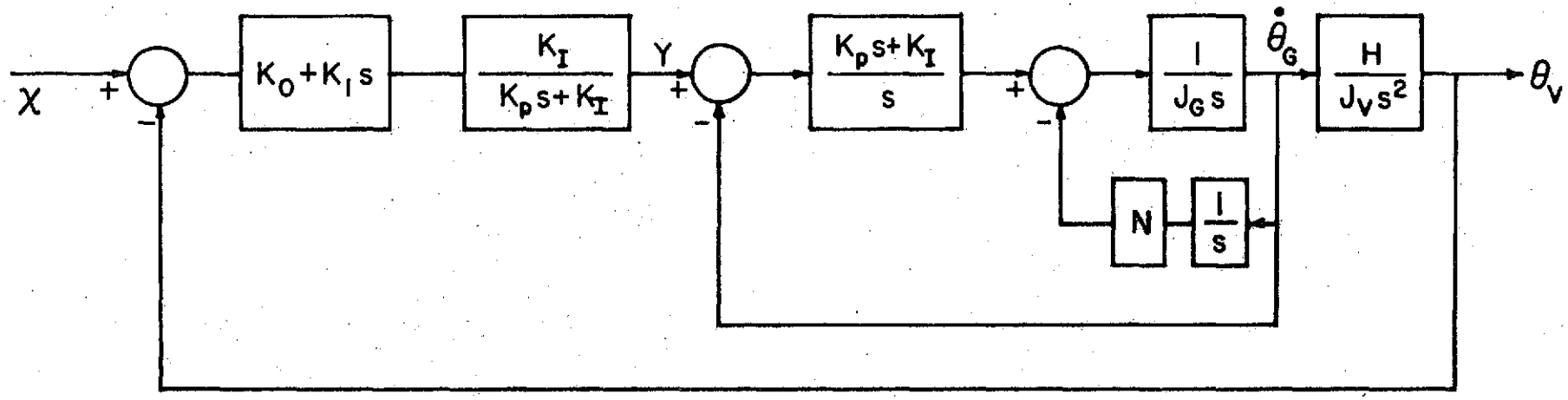

Figure 1-7. A Simplified LST system diagram.

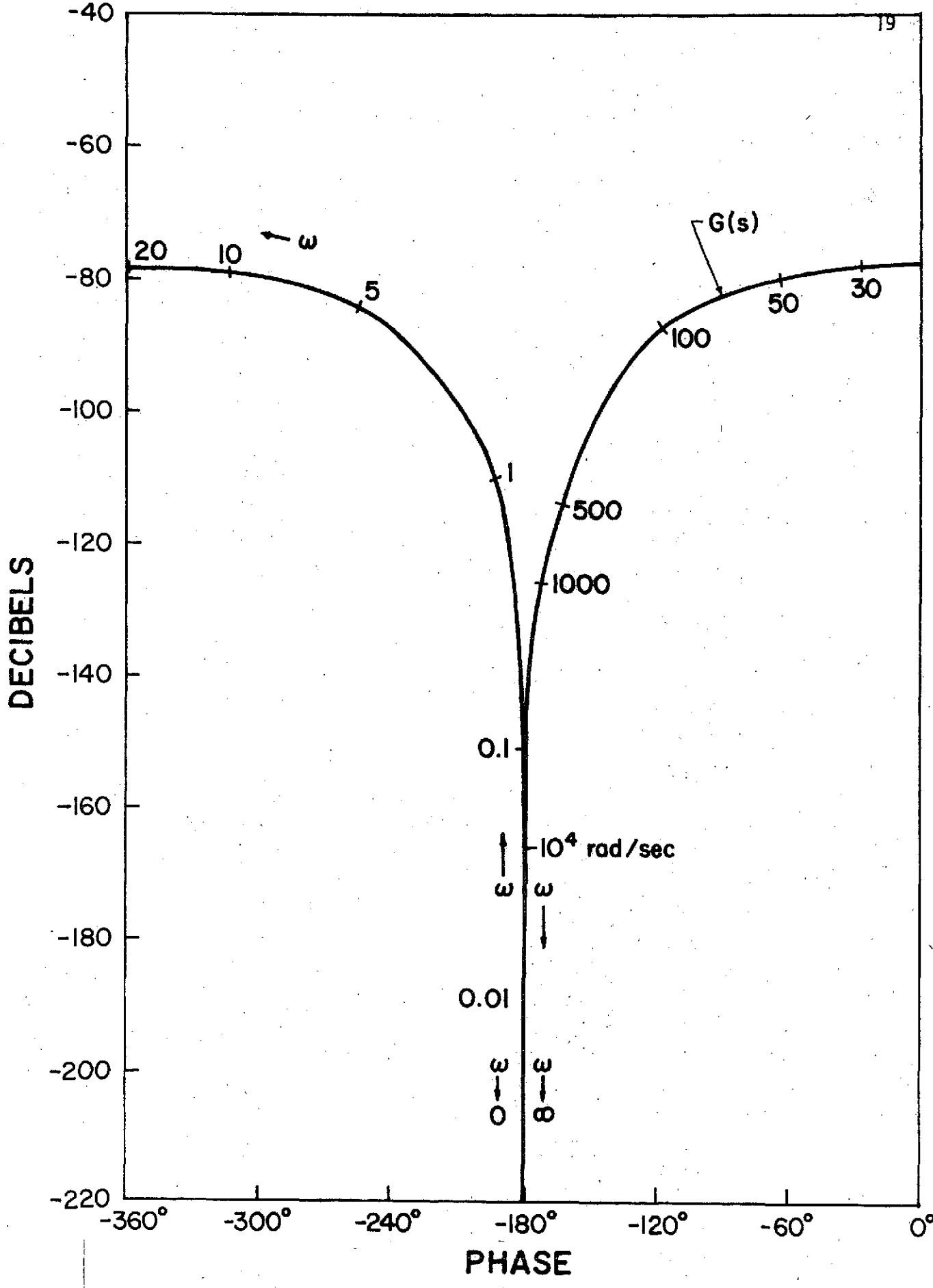

Figure 1-8. Frequency-domain plot of the simplified LST system.

Then T_f can be generated by intebrating both sides of Eq. (2-1) with respect to t. It is observed that T'_{GF} is easily found as a function of χ. However, the simulation model actually has T'_{GF} generated by a function generator with T_{GF} as the input. The simulation block diagram for the CMG friction nonlinearity is shown in Figure 2-1. Notice that this model has $\dot{\theta}_G$ as input and T_{GF} as the output.

Referring to Figure 1-1, the block diagram of Figure 2-1 may replace the blocks for the simplified nonlinearity between $\dot{\theta}_G$ and T_{GF}.

It has been demonstrated experimentally [3] that for the solid rolling friction the relation between T'_{GF} and T_{GF} may be approximated by a square-law expression,

$$T'_{GF} = \frac{dT_{GF}}{d\theta_G} = \gamma(T_{GF} - T_{GFO})^2 \qquad T_{GF} \leq T_{GFO} \tag{2-2}$$

where γ is a positive constant.

$$T'_{GF} = 0 \qquad T_{GF} > T_{GFO} \tag{2-3}$$

However, for the CMG friction, the frictional torque is also velocity dependent, as shown in Figure 2-1. Therefore, Eq. (2-2) should be written

$$T'_{GF} = \gamma(T_{GFI} - T_{GFO})^2 \tag{2-4}$$

$$T_{GFI} = T_{GF}\mathrm{SGN}(\dot{\theta}_G) \tag{2-5}$$

For simulation purpose, the block diagram of Figure 2-1 can be easily programmed on the digital computer, and the program can be used for any input.

Our objective is to investigate the behavior of the nonlinearity under a sinusoidal excitation, so that the describing function can be derived. In the present situation, however,

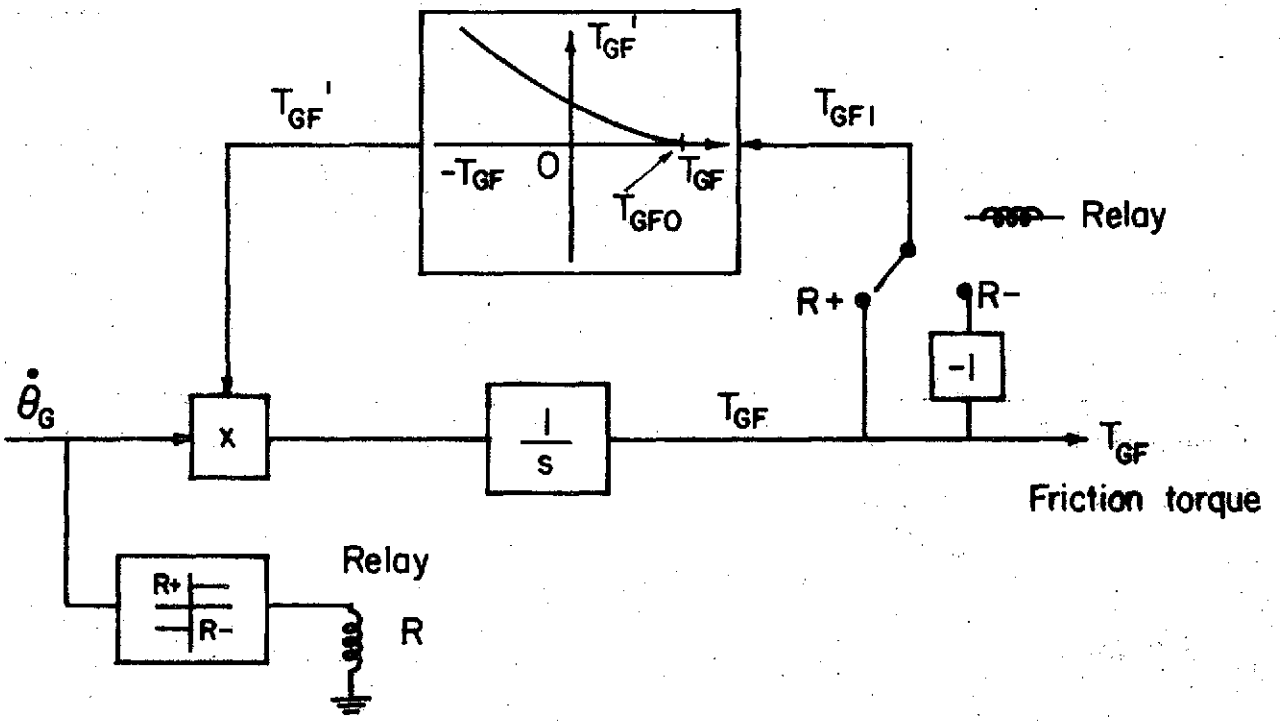

Figure 2-1. A simulation block diagram of the CMG friction nonlinearity.

we shall show that the input-output relation of the CMG nonlinearity is different for sine and cosine inputs. It should be noted that the describing function is a pseudo-sinusoidal steady-state analysis so that either sinusoidal or cosinusoidal inputs may be assumed. These are shown by the following derivations.

(1) Let $\dot{\theta}_G = A \sin\omega t$ (2-6)

then $\theta_G = -\frac{A}{\omega}\cos\omega t$ (2-7)

For $\dot{\theta}_G \geq 0$, Eqs. (2-1),(2-4) and (2-5) lead to

$$\frac{dT_{GF}}{dt} = \gamma A \sin\omega t \, (T_{GF} - T_{GFO})^2 \tag{2-8}$$

$2k\pi \leq \omega t \leq (2k + 1)\pi$, $k = 0, 1, 2, \ldots$.

Solution of the nonlinear differential equation of Eq. (2-8) yields

$$-\frac{1}{T_{GF}-T_{GFO}} = -\frac{\gamma A}{\omega}\cos\omega t + C \tag{2-9}$$

The constant C is found by specifying the initial value of T_{GF} at $t = 0$:

$$t = 0 \qquad T_{GF} = -T_{GFi} \qquad T_{GFi} > 0 \tag{2-10}$$

Thus,

$$C = \frac{\gamma A}{\omega} + \frac{1}{T_{GFi}+T_{GFO}} \tag{2-11}$$

Substitution of the last equation into Eq. (2-9) and simplifying, we have the solution

$$\frac{T_{GF}}{T_{GFO}} = \frac{\frac{b}{2}(1-\cos\omega t) - \frac{R}{R+1}}{\frac{1}{R+1} + \frac{b}{2}(1-\cos\omega t)} \tag{2-12}$$

which is valid for $\dot{\theta}_G \geq 0$, or $2k\pi \leq \omega t \leq (2k + 1)\pi$, $k = 0, 1, 2, \ldots$

where

$$b = \frac{2T_{GFO}\gamma A}{\omega} \tag{2-13}$$

and

$$R = \frac{T_{GFi}}{T_{GFO}} \tag{2-14}$$

For $\dot{\theta}_G \leq 0$, Eqs. (2-1), (2-4), and (2-5) lead to

$$\frac{dT_{GF}}{dt} = \gamma A \sin\omega t(-T_{GF} - T_{GFO})^2 \tag{2-15}$$

$$(2k+1)\pi \leq \omega t \leq (2k+2)\pi, \quad k = 0, 1, 2, \ldots.$$

The solution of Eq. (2-15) is

$$\frac{1}{-T_{GF}-T_{GFO}} = -\frac{\gamma A}{\omega}\cos\omega t + C \tag{2-16}$$

The boundary condition is $T_{GF} = -T_{GFi}$ at $\omega t = 2\pi$ and its integral multiples. Thus,

$$C = \frac{\gamma A}{\omega} + \frac{1}{T_{GFi}-T_{GFO}} \tag{2-17}$$

Substitution of C into Eq. (2-16) and simplifying, the final solution is

$$\frac{T_{GF}}{T_{GFO}} = \frac{-\frac{R}{R-1} - \frac{b}{2}(1-\cos\omega t)}{\frac{b}{2}(1-\cos\omega t)+\frac{1}{R-1}} \tag{2-18}$$

which is valid for $\dot{\theta}_G \leq 0$, or $(2k+1)\pi \leq \omega t \leq (2k+2)\pi$, $k = 0, 1, 2, \ldots$, and $\dot{\theta}_G$ is given by Eq. (2-6).

$-T_{GFi}$, which represents the value of T_{GF} at $\omega t = 2k\pi$, $k = 0, 1, 2, \ldots$, can be determined by matching the values of T_{GF}/T_{GFO} at $\omega t = (2k+1)\pi$, $k = 0, 1, 2, \ldots$, for the two ranges of $\dot{\theta}_G$. Setting $\omega t = \pi$ and equating Eq. (2-12) to Eq. (2-18), we have

$$\frac{b - \frac{R}{R+1}}{\frac{1}{R+1} + b} = \frac{-\frac{R}{R-1} - b}{b + \frac{1}{R-1}} \tag{2-19}$$

which is simplified to

$$R^2 + \frac{2}{b}R - 1 = 0 \tag{2-20}$$

Solving for R gives

$$R = -\frac{1}{b} \pm \sqrt{\frac{b^2+1}{b^2}} \tag{2-21}$$

Since $T_{GFi} \leq T_{GFO}$ and $T_{GFi} > 0$, $R \leq 1$; the plus sign must be chosen in Eq. (2-21).

$$R = -\frac{1}{b} + \sqrt{\frac{b^2+1}{b^2}} = \frac{T_{GFi}}{T_{GFO}} \tag{2-22}$$

The same result for R can be obtained by use of the boundary condition at $\omega t = \pi$ which is $T_{GF} = T_{GFi}$.

The consequence of defining $\dot{\theta}_G$ as a sine function, Eq. (2-6), is that T_{GFi} is dependent on ω, since b depends on ω. Figure 2-2 gives the T_{GF}/T_{GFO} versus $\dot{\theta}_G/A$ relations for various values of A/ω. Notice that the maximum value of T_{GF}/T_{GFO} is different for different ratios of A/ω. Figure 2-3 illustrates the relations between T_{GF}/T_{GFO} and $\theta_G\omega/A$ with θ_G given by Eq. (2-7). Note that the θ_G axis is normalized by ω/A, so that as ω varies not only the bounds of T_{GF}/T_{GFO} will vary but also the bounds of θ_G. These curves are also plotted for various values of A/ω indicated. It would seem that by defining $\dot{\theta}_G$ as a sine function as in Eq. (2-6), there is an advantage of using the nonlinear characteristics of Fig. 2-2 for analytical purposes. In principle, either θ_G or $\dot{\theta}_G$, but not both, may be used as the input to the nonlinearity, provided that the corresponding nonlinear characteristic is used.

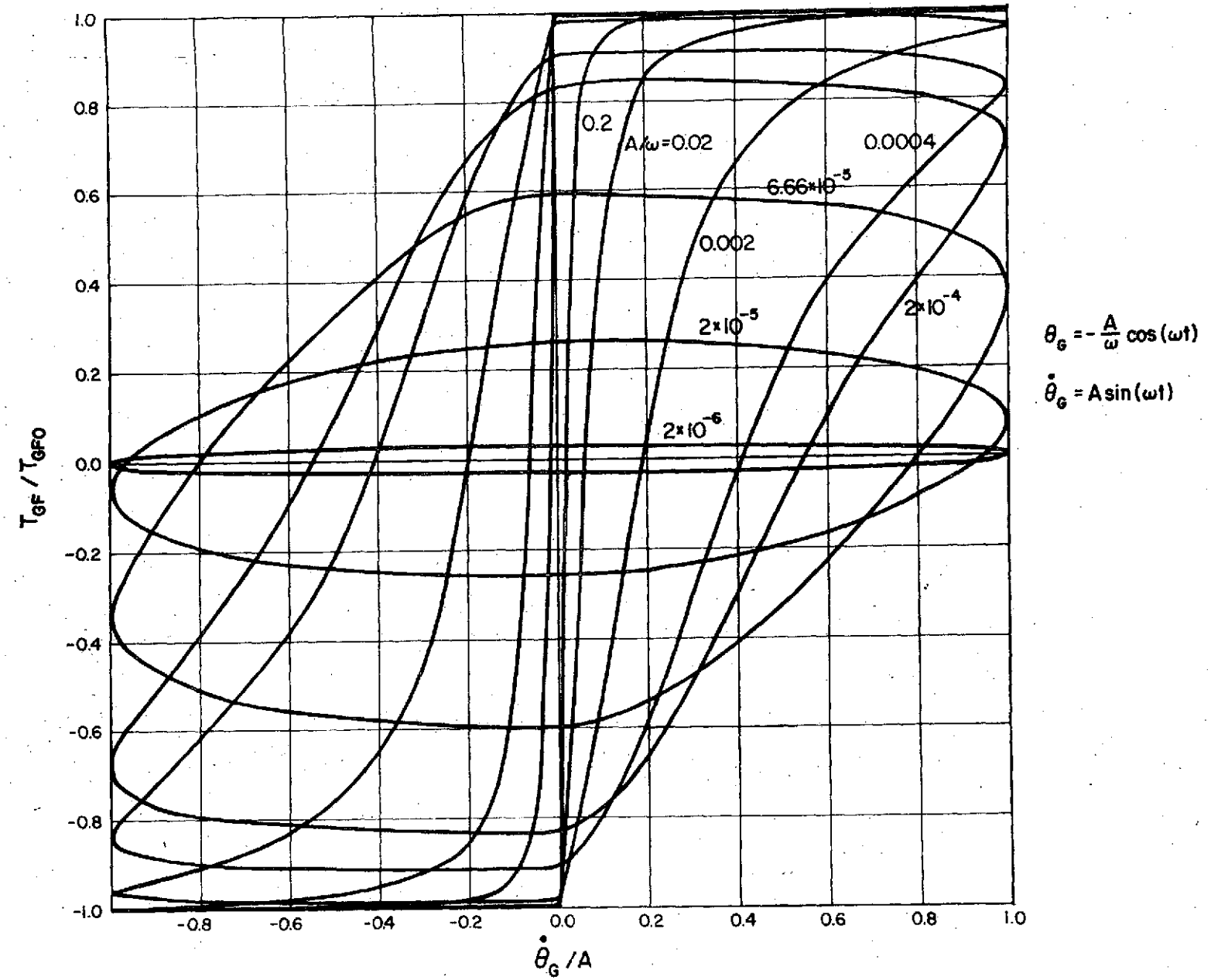

Figure 2-2. Normalized frictional torque versus $\dot{\theta}_G/A$ for CMG nonlinearity, with sine function input.

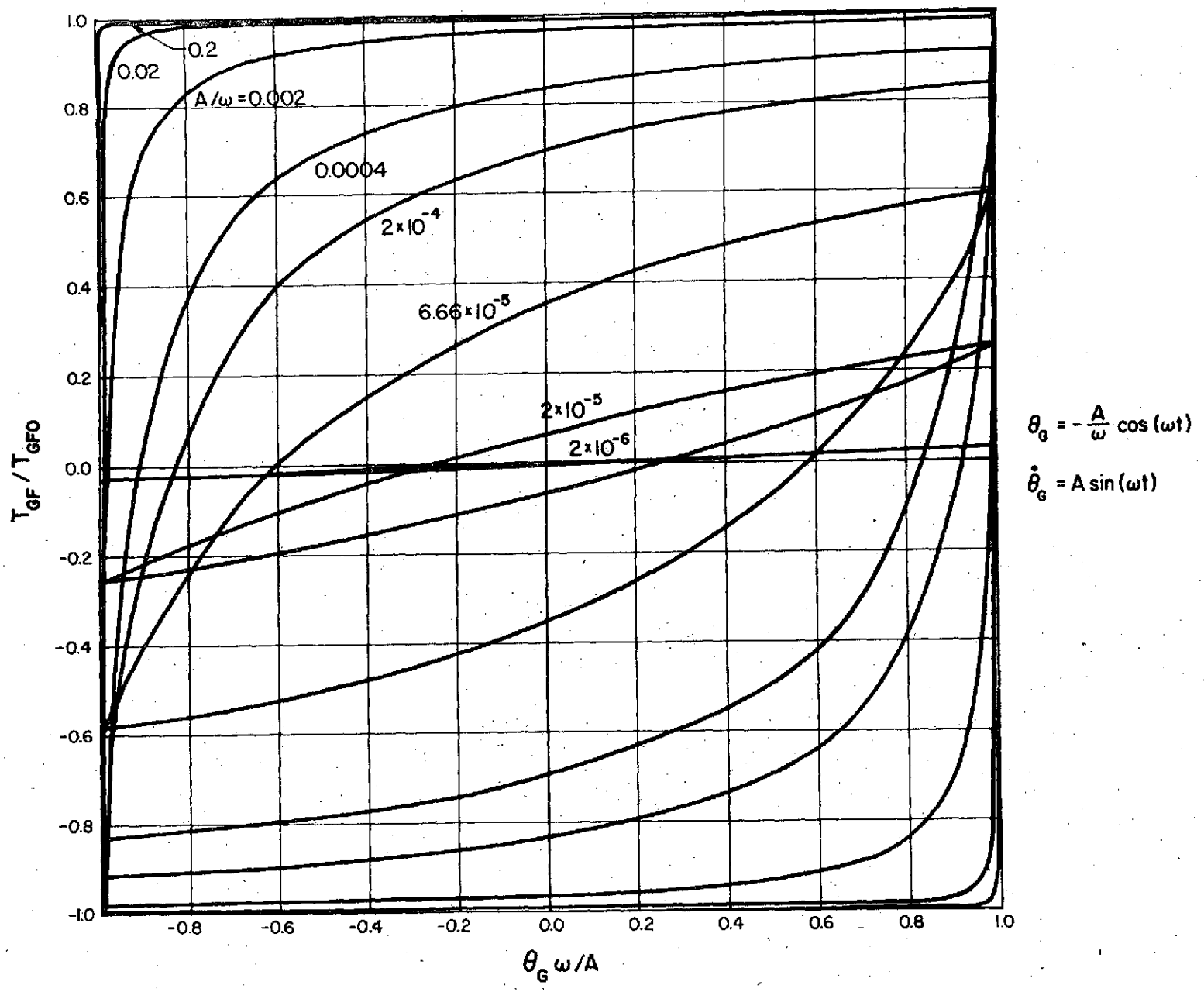

Figure 2-3. Normalized frictional torque versus $\theta_G\omega/A$ for CMG nonlinearity with sine function input.

This is because θ_G and $\dot{\theta}_G$ are directly related. In other words, the T_{GF}/T_{GFO} versus θ_G characteristics contain the same information as those of T_{GF}/T_{GFO} versus $\dot{\theta}_G$.

(2) Let $\theta_G = A \cos \omega t$ (2-23)

Then $\dot{\theta}_G = -A\omega \sin \omega t$ (2-24)

For $\dot{\theta}_G \leq 0$, Eqs. (2-1), (2-4) and (2-5) lead to

$$\frac{dT_{GF}}{dt} = -\gamma A\omega \sin\omega t \, (-T_{GF} - T_{GFO})^2 \tag{2-25}$$

$2k\pi \leq \omega t \leq (2k+1)\pi, \quad k = 0, 1, 2, \ldots$

The solution of Eq. (2-25) is

$$\frac{-1}{T_{GF}+T_{GFO}} = \gamma A \cos \omega t + C \tag{2-26}$$

At $t = 0$, the boundary condition on T_{GF} is $T_{GF} = T_{GFi}$, where $T_{GFi} > 0$. Equation (2-26) gives

$$C = -\gamma A - \frac{1}{T_{GF} + T_{GFO}} \tag{2-27}$$

Substituting Eq. (2-27) into Eq. (2-26) and simplifying, the complete solution is

$$\frac{T_{GF}}{T_{GFO}} = \frac{\frac{R}{R+1} - \frac{a}{2}(1-\cos\omega t)}{\frac{a}{2}(1-\cos\omega t)+\frac{1}{R+1}} \tag{2-28}$$

which is valid for $2k\pi \leq \omega t \leq (2k+1)\pi$, $k = 0, 1, 2, \ldots$, or $\dot{\theta}_G \leq 0$, and

$$a = 2\gamma A T_{GFO} \tag{2-29}$$

For $\dot{\theta}_G \geq 0$,

$$\frac{dT_{GF}}{dt} = -\gamma A\omega \sin\omega t (T_{GF} - T_{GFO})^2 \tag{2-30}$$

$(2k+1)\pi \leq \omega t \leq (2k+2)\pi, \quad k = 0, 1, 2, \ldots$

The solution of Eq. (2-30) is

$$\frac{-1}{T_{GF} - T_{GFO}} = \gamma A\cos\omega t + C \tag{2-31}$$

The boundary condition is $T_{GF} = T_{GFi}$ at $\omega t = 2\pi$. Thus, Eq. (2-31) gives

$$C = -\gamma A - \frac{1}{T_{GFi} - T_{GFO}} \tag{2-32}$$

and the complete solution is

$$\frac{T_{GF}}{T_{GFO}} = \frac{\frac{R}{R-1} + \frac{a}{2}(1-\cos\omega t)}{\frac{a}{2}(1-\cos\omega t) + \frac{1}{R-1}} \tag{2-33}$$

which is valid for $\dot{\theta}_G \geq 0$, or $(2k+1)\pi \leq \omega t \leq (2k+2)\pi$, $k = 0, 1, 2, \ldots$.

Matching Eqs. (2-28) with Eq. (2-33) at $\omega t = \pi$, we have

$$R^2 + \frac{2}{a} R - 1 = 0 \tag{2-34}$$

whose solution of R is

$$R = -\frac{1}{a} + \sqrt{\frac{a^2+1}{a^2}} = \frac{T_{GFi}}{T_{GFO}} \tag{2-35}$$

The significance of this result is that T_{GFi}/T_{GFO} is <u>not</u> a function of ω, since a depends only on γ, A, and T_{GFO}. It is interesting to note that Eq. (2-22) and Eq. (2-35) have the same form, except that in the former equation b is a function of ω, whereas in the latter equation a is not.

Figure 2-4 shows the T_{GF}/T_{GFO} versus θ_G/A characteristics for several values of A. The maximum value that T_{GF} reaches for all values of ω is the same. Figure 2-5 gives the T_{GF}/T_{GFO} versus $\dot{\theta}_G/A$ characteristics with the $\dot{\theta}_G$ axis normalized by $A\omega$. From these curves, it would seem that there is a clear cut advantage in using the T_{GF}/T_{GFO} versus θ_G/A characteristics with $\theta_G = A\cos\omega t$ as the input. Referring to Figure 1-1, for describing function analysis, one difference between

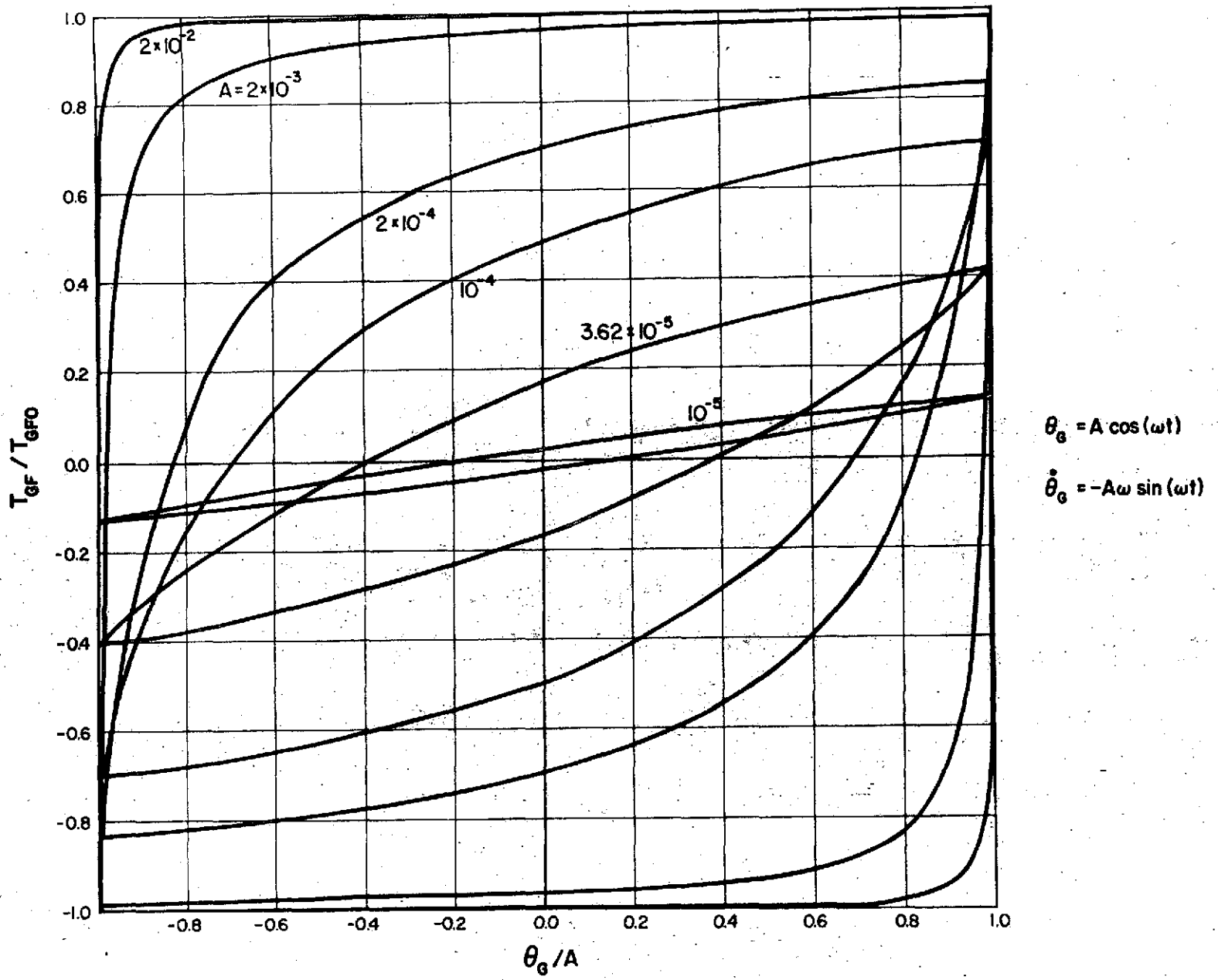

Figure 2-4. Normalized frictional torque versus $\theta_G\omega/A$ for CMG nonlinearity with cosine function input.

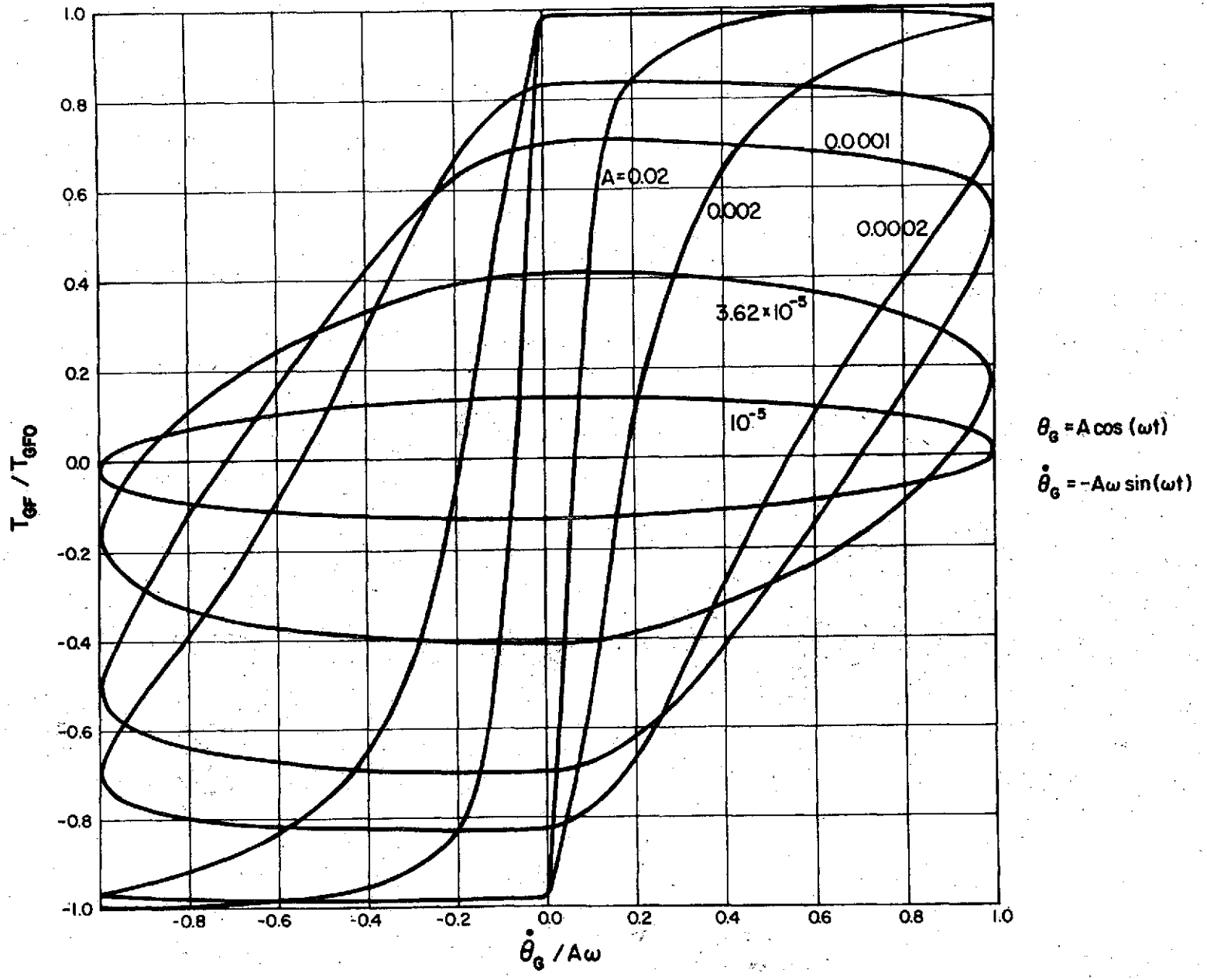

Figure 2-5. Normalized frictional torque versus $\dot{\theta}_G/A$ for CMG nonlinearity with cosine function input.

the use of θ_G and $\dot{\theta}_G$ as the input to the nonlinearity is the linear transfer function G(s) which the nonlinear element sees.

Table 2-1 gives a comparison of the expressions of T_{GF}/T_{GFO} for the two types of inputs. It is interesting to note that if A/ω in b is replaced by A, the expressions for T_{GF}/T_{GFO} differ only by a sign for the two inputs. A similar effect is achieved by replacing $-A/\omega$ by A in Eq. (2-7) for θ_G, and A by $-A\omega$ in Eq. (2-6) for $\dot{\theta}_G$. With the above changes, the torque expressions for the two types of inputs become identical. This means that the curves in Figs. 2-2 and 2-5 and those of Figs. 2-3 and 2-4 are identical for the corresponding values of A/ω and A, respectively.

Table 2-1

$\dot{\theta}_G = A \sin\omega t$ $\qquad$ $\theta_G = A \cos\omega t$

$\theta_G = -\frac{A}{\omega}\cos\omega t$ $\qquad$ $\dot{\theta}_G = -A \sin\omega t$

	$\frac{T_{GF}}{T_{GFO}}$	
$2k\pi \leq \omega t \leq (2k+1)\pi$	$\frac{\frac{b}{2}(1-\cos\omega t) - \frac{R}{R+1}}{\frac{1}{R+1} + \frac{b}{2}(1-\cos\omega t)}$	$\frac{-\frac{a}{2}(1-\cos\omega t) + \frac{R}{R+1}}{\frac{1}{R+1} + \frac{a}{2}(1-\cos\omega t)}$
$(2k+1)\pi \leq \omega t \leq (2k+2)\pi$	$\frac{-\frac{R}{R-1} - \frac{b}{2}(1-\cos\omega t)}{\frac{b}{2}(1-\cos\omega t) + \frac{1}{R-1}}$	$\frac{\frac{R}{R-1} + \frac{a}{2}(1-\cos\omega t)}{\frac{a}{2}(1-\cos\omega t) + \frac{1}{R-1}}$
	$b = \frac{2\gamma A T_{GFO}}{\omega}$	$a = 2\gamma A T_{GFO}$
	$R = -\frac{1}{b} + \sqrt{\frac{b^2+1}{b^2}}$	$R = -\frac{1}{a} + \sqrt{\frac{a^2+1}{a^2}}$

A More General CMG Frictional Nonlinearity Model

A more general expression which is valid for any input can be derived for the CMG frictional torque characteristic. We start with the square-law expression in Eq. (2-4),

$$T'_{GF} = \frac{dT_{GF}}{d\theta_G} = \gamma(T_{GF1}-T_{GFO})^2 \qquad T_{GF} \leq T_{GFO} \tag{2-36}$$

where

$$T_{GF1} = T_{GF}SGN(\dot{\theta}_G) \tag{2-37}$$

Equation (2-36) can be integrated with respect to θ_G directly. The results are:

$$T_{GF} = \frac{(\theta_G-\theta_{Gi})\gamma(T_{GFi}-T_{GFO})T_{GFO}-T_{GFi}}{(\theta_G-\theta_{Gi})\gamma(T_{GFi}-T_{GFO}) - 1} \qquad \dot{\theta}_G \geq 0 \tag{2-38}$$

$$T_{GF} = \frac{-(\theta_G-\theta_{Gi})\gamma(T_{GFi}+T_{GFO})T_{GFO}-T_{GFi}}{(\theta_G-\theta_{Gi})\gamma(T_{GFi}+T_{GFO}) - 1} \qquad \dot{\theta}_G \leq 0 \tag{2-39}$$

where

θ_{Gi} = initial value of θ_G

T_{GFi} = initial value of T_{GF}

These expressions for the frictional torque are valid for any arbitrary input θ_G and initial conditions at the beginning of the process. When $\dot{\theta}_G$ changes sign during the process, the proper expression should be used, and the initial conditions should be appropriately matched at the switching point. It is simple to show that when $\theta_G = -\frac{A}{\omega}\cos\omega t$, $\theta_{Gi} = -\frac{A}{\omega}$, Eqs. (2-38) and (2-39) revert to Eqs. (2-12) and (2-18), respectively. Similarly, if $\theta_G = A\cos\omega t$ and $\theta_{Gi} = A$, Eqs. (2-38) and (2-39) become identical to Eqs. (2-28) and (2-33), respectively.

3. A Continuous Describing Function for the Gimbal Friction Nonlinearity

In chapter 2 the nonlinear characteristic of the gimbal friction is analyzed with sinusoidal inputs. It seems that there is an advantage of using a cosine wave as the input, since, then, the frictional torque saturation level is not a function of frequency. For analytical purposes, the T_{GF}/T_{GFO} versus θ_G/A curves of Figure 2-4 seem to be the most convenient to use.

In the last bimonthly report, No. I-73, the gimbal frictional nonlinearity is approximated by a four-sided polygon. In this section a better approximation is made by the six-sided polygon shown in Figures 3-1 and 3-2. It is apparent from Figure 2-4 that when the input amplitude changes the slope k of the nonlinearity also changes. The continuous-data describing function for the nonlinearity in Figure 3-1 and 3-2 is now derived.

The input to the nonlinearity is a cosine waveform shown in Figure 3-1 and given as

$$\theta_G = E\cos\omega t \tag{3-1}$$

The output waveform of the nonlinearity as a function of ωt is shown in Figure 3-1. The four parts of this waveform are described by the following set of equations.

$$\begin{aligned} f(\theta_G) &= kE\cos\phi - kE && 0 \le \phi \le \alpha_1 \\ &= -M && \alpha_1 \le \phi \le \pi \\ &= kE\cos\phi + kE && \pi \le \phi \le \alpha_2 \\ &= M && \alpha_2 \le \phi \le 2\pi \end{aligned} \tag{3-2}$$

where

$$\phi = \omega t \tag{3-3}$$

$$\alpha_1 = \cos^{-1}(1-M/kE) \tag{3-4}$$

$$\alpha_2 = \alpha_1 + \pi \tag{3-5}$$

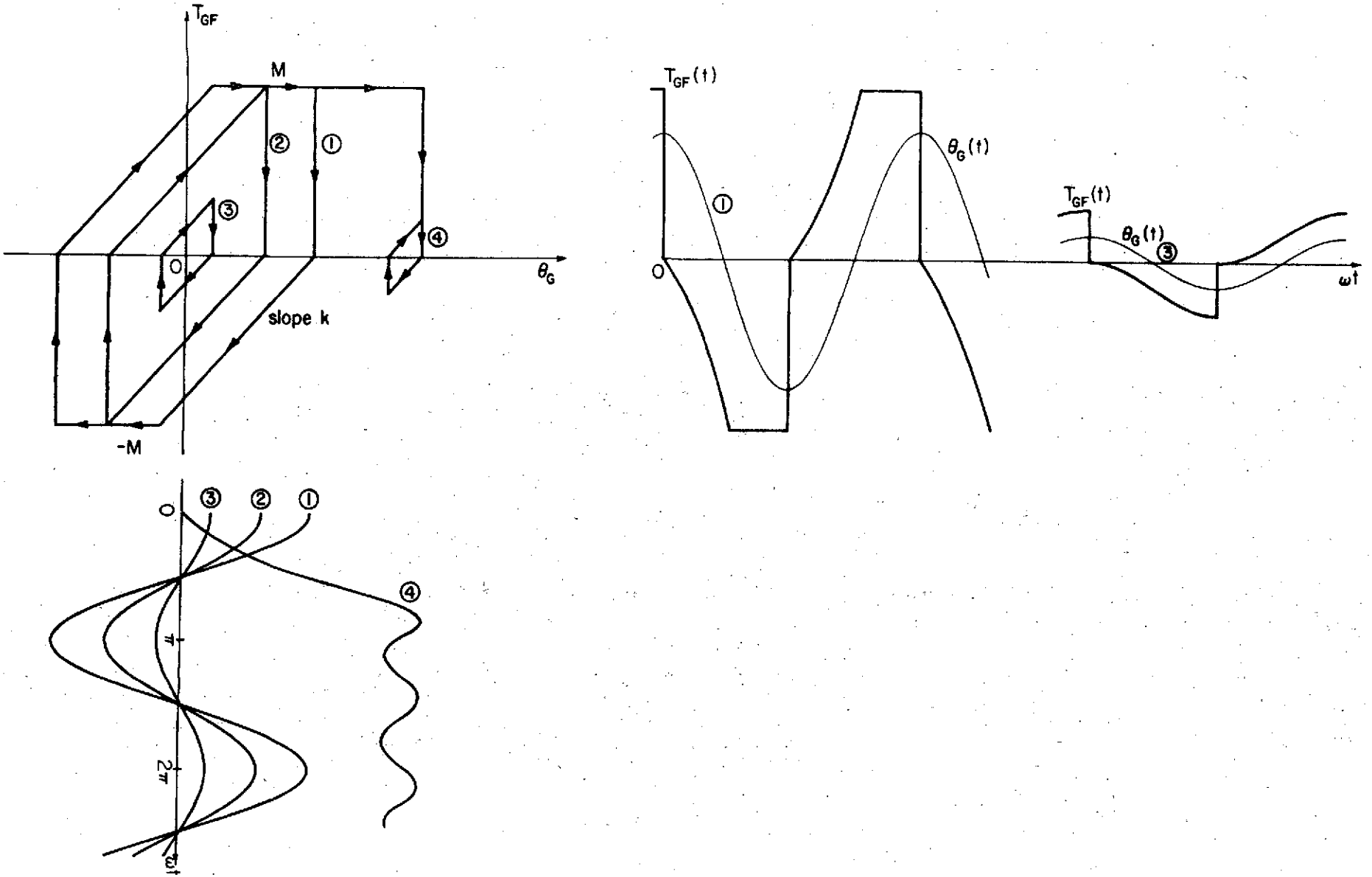

Figure 3-1. Linearized input-output relation of CMG nonlinearity.

The Fourier series for the waveform of the output of the nonlinearity is given by

$$f(t) = A_0/2 + A_1\cos\omega t + B_1\sin\omega t + A_2\cos 2\omega t + B_2\sin 2\omega t + \ldots. \quad (3\text{-}6)$$

where the coefficients are given by

$$A_N = 1/\pi \int_0^{2\pi} f(t)\cos(N\omega t)\,d\omega t \quad (3\text{-}7)$$

$$B_N = 1/\pi \int_0^{2\pi} f(t)\sin(N\omega t)\,d\omega t \quad (3\text{-}8)$$

$$N = 0, 1, 2, \ldots$$

Since there is no bias on the output signal from the nonlinearity, $A_0 = 0$. If the higher frequency harmonics, $N = 2, 3, \ldots$, are neglected, the output waveform is given by

$$f(t) = \sqrt{A_1^2 + B_1^2}\ \cos(\phi - \tan^{-1}B_1/A_1) \quad (3\text{-}9)$$

The phasor notation of $f(t)$ is

$$F(j\omega) = \sqrt{A_1^2 + B_1^2}\ \exp[-j\tan^{-1}B_1/A_1] \quad (3\text{-}10)$$

The describing function of the nonlinearity is defined as

$$N(E) = F(j\omega)/E(j\omega) = \sqrt{A_1^2 + B_1^2}\ /E\cdot\exp[-j\tan^{-1}B_1/A_1] \quad (3\text{-}11)$$
$$= A_1/E - jB_1/E$$

By using Eqs. (3-2) through (3-5) the coefficients in Eqs. (3-7) and (3-8) are solved for $N = 1$ to yield

$$A_1 = kE\cos^{-1}(1 - M/kE)/\pi + \sqrt{2MkE - M^2}\ (M - kE)/\pi kE \quad (3\text{-}12)$$

$$B_1 = -4M/\pi + M^2/\pi kE \quad (3\text{-}13)$$

Describing Function Plots

When evaluating the describing function it is convenient to define a normalized input amplitude H as

$$H = 2kE/M \tag{3-14}$$

Using equation (3-14) in Eqs. (3-12) and (3-13) and dividing both sides of these equations by E gives

$$A_1/E = k\cos^{-1}(1 - 2/H)/\pi + 4k(1 - H/2)\sqrt{H-1}/H^2\pi \tag{3-15}$$

$$B_1/E = -8k/H\pi + 4k/H^2\pi \tag{3-16}$$

The above equations show that the describing function will depend only on H and k.

Figure 3-3 shows the magnitude versus phase curves for -1./N(E) for different values of the slope of the nonlinearity, k. In these curves the magnitude of the normalized input signal to the nonlinearity, H, is varied from 1.0 to 100. When the magnitude of H becomes less than 1, the gimbal torque characteristics decrease as shown in Figure 3-2. For these amplitudes of H, M is set to M = 2kE and the magnitude and phase of 1./N(E) remains constant as H is varied. This can be seen by substituting M = 2kE into equations (3-12) and (3-13).

$$A_1/E = k \tag{3-17}$$

$$B_1/E = -4k/\pi \tag{3-18}$$

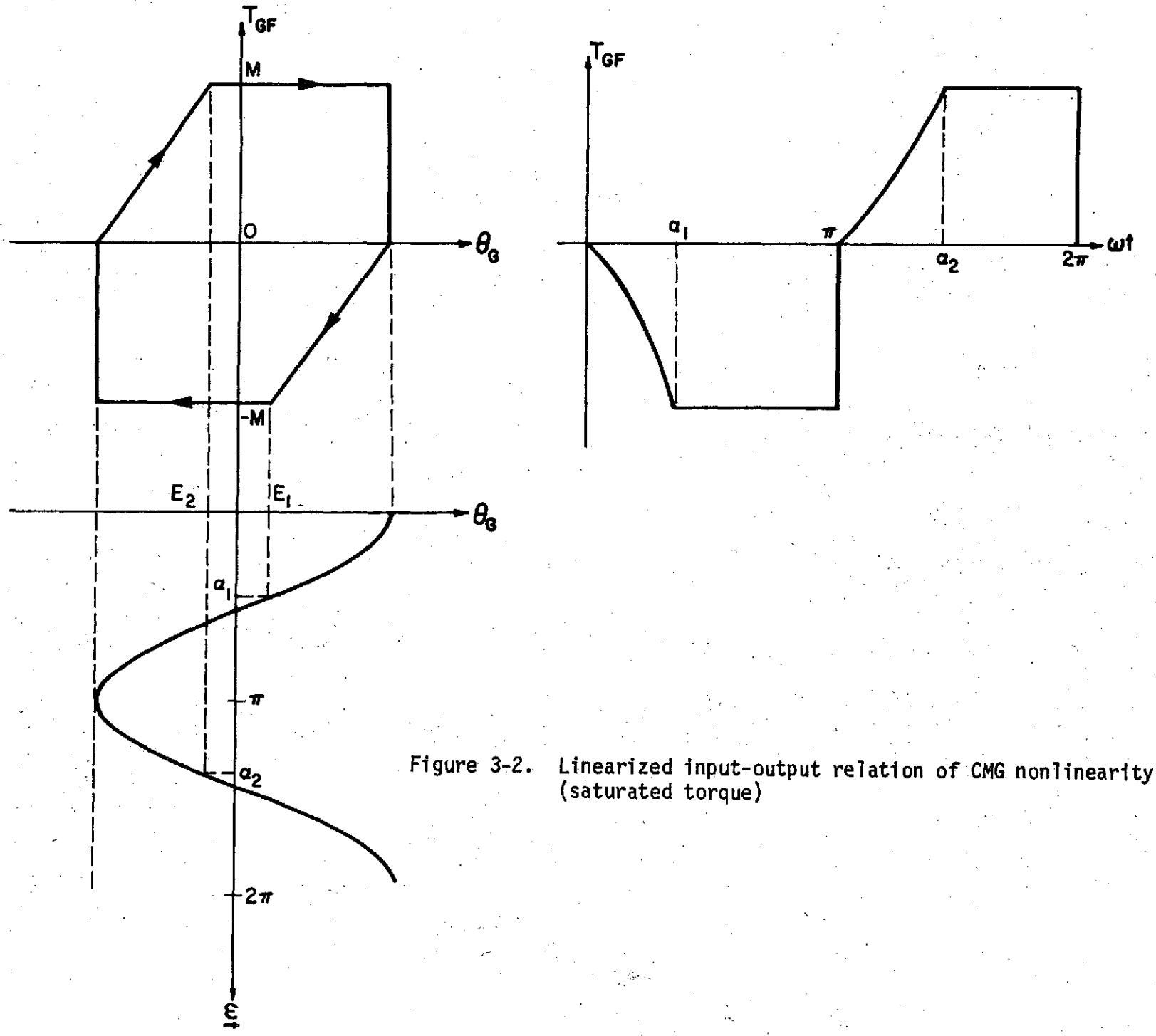

Figure 3-2. Linearized input-output relation of CMG nonlinearity. (saturated torque)

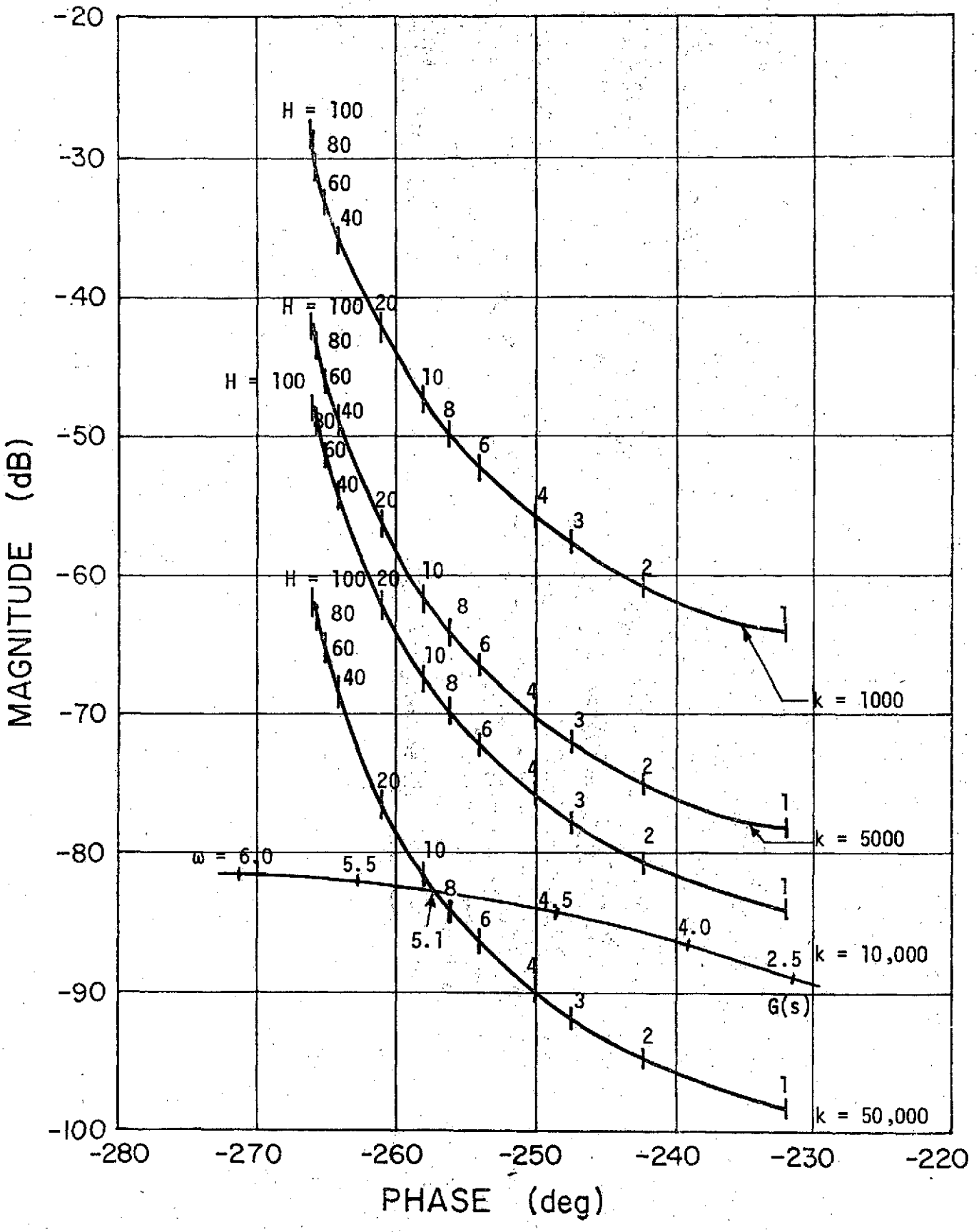

Figure 3-3. Describing function plots of CMG frictional nonlinearity.

4. Computer Simulation of the Simplified LST System

Since the describing function analysis of the CMG nonlinearity has been given in the last chapter, a computer simulation of the LST system is necessary to corroborate the analytical results. It should be noted that the describing function analysis is carried out only for the straight-line approximation of the nonlinearity as illustrated in Figure 3-1. The simulation model of the nonlinearity also has the same characteristics. Future work will include the derivation of the describing function of the exact nonlinearity as modelled in Figure 2-1, as well as a computer simulation with the exact model.

The simplified LST system is represented by the block diagram of Figure 1-7. The linear transfer function which the nonlinear element N sees is given by Eq. (1-16). The frequency-domain plot of G(s) is plotted in Figure 1-8 in db versus phase coordinates. The portion of G(s) for ω = 2.5 to 6 is given in Figure 3-3. For k = 50,000 ft-lb/rad, the G(s) curve intersects the -1/N(E) curve at a frequency of 5.1 rad/sec and H = 9. The saturation level of the gimbal frictional torque is set at M = 0.078 ft-lb. Therefore, the corresponding amplitude of oscillation of the gimbal position, E, is

$$E = MH/2k = 7.2 \times 10^{-6} \text{ rad.}$$

For the computer simulation, the input to the LST system, χ, is set to zero, along with all the initial states, except for the vehicle position θ_V. The initial value of θ_V is set at 5×10^{-5} rad, which is chosen so that the input signal to the nonlinearity, θ_G, would be large enough to cause the torque to saturate, while at the same time the limiting value of the input signal given in [1] is not exceeded.

To fully understand the results of the computer simulation of the LST system it is useful to represent the computer modeling of the nonlinearity by the flow diagram of Figure 4-1. Due to the inherent memory of the nonlinearity it is necessary to initially define the position of the last switching point and the last value of the velocity before entering the flow diagram.

The following quantities are plotted from the simulation runs:

θ_V = vehicle position (rad)

ω_V = vehicle velocity (rad/sec)

θ_G = Gimbal position (rad)

ω_G = Gimbal velocity (rad/sec)

T_{GF} = Torque output of the nonlinearity (ft-lb)

Error = Error input command (rad/sec) to the CMG

$= \chi - K_0\theta_V - K_1\omega_V$

Figures 4-2 through 4-7 show the plots of the above listed quantities. It may be noted from the plot of T_{GF} in Figure 4-6 that the system has a sustained oscillation. This oscillation is not seen on the other plots because of the large initial transients. Figures 4-8 through 4-13 show the continuation of Figures 4-2 through 4-7 with proper scales. These figures show that the amplitude and frequency of the sustained oscillation are quite close to the values predicted in Figure 3-3.

The simulation results show that the LST system is stable for smaller values of k, such as k = 10,000.

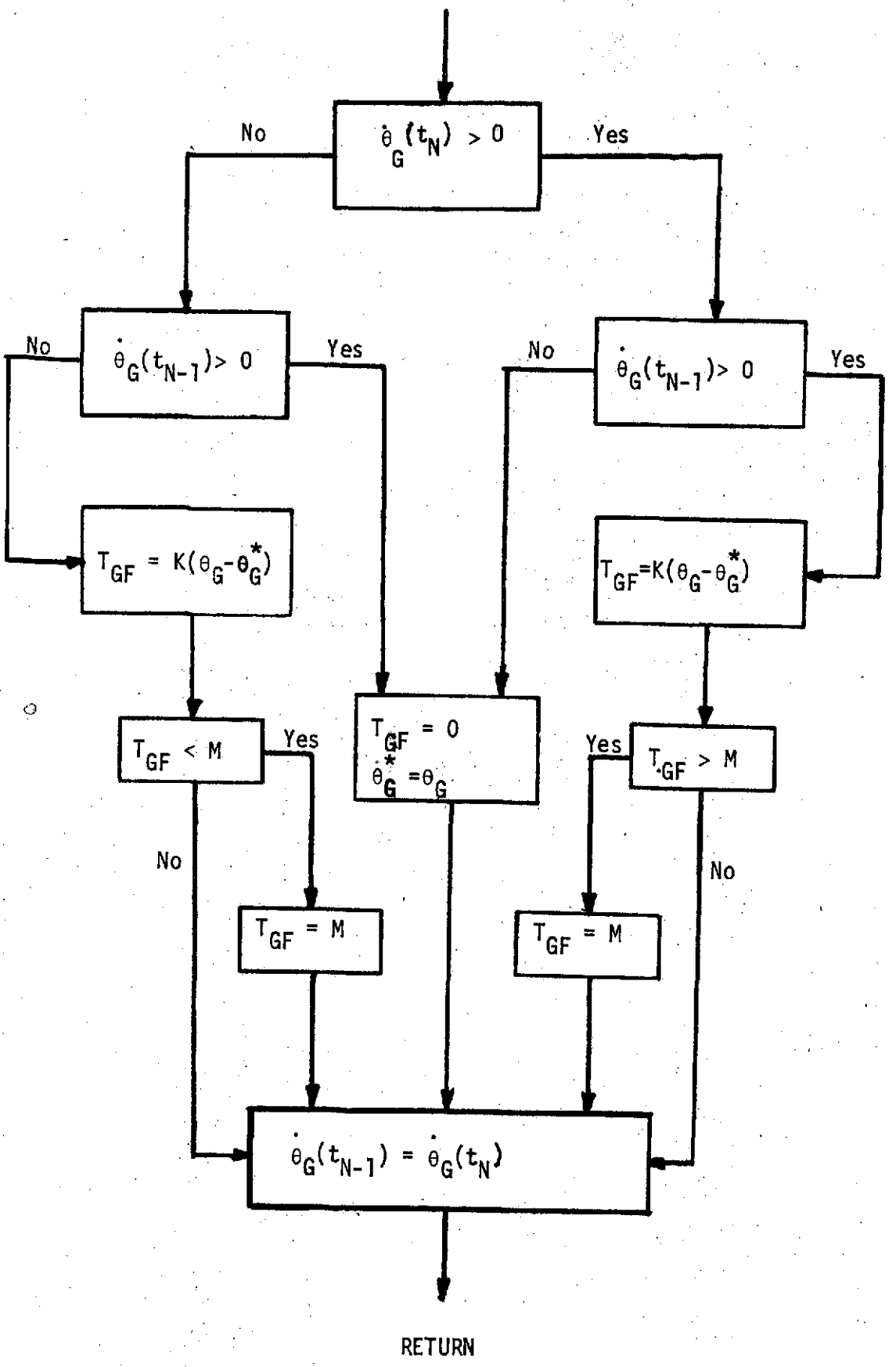

Figure 4.1. Computer flow diagram of CMG nonlinearity.

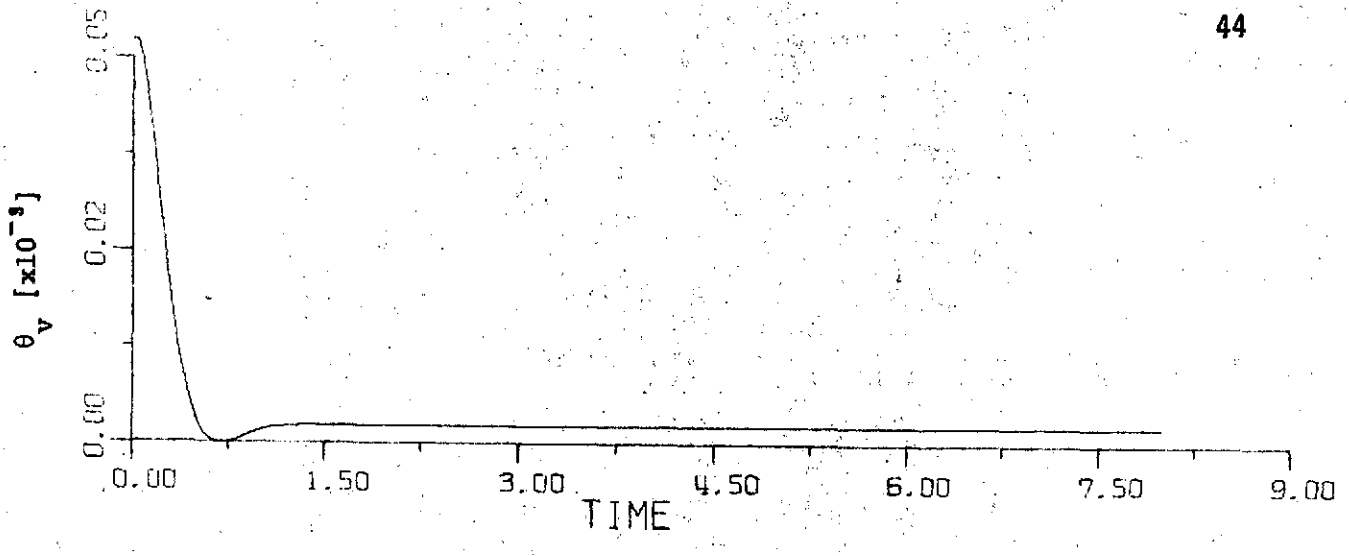

Figure 4-2.

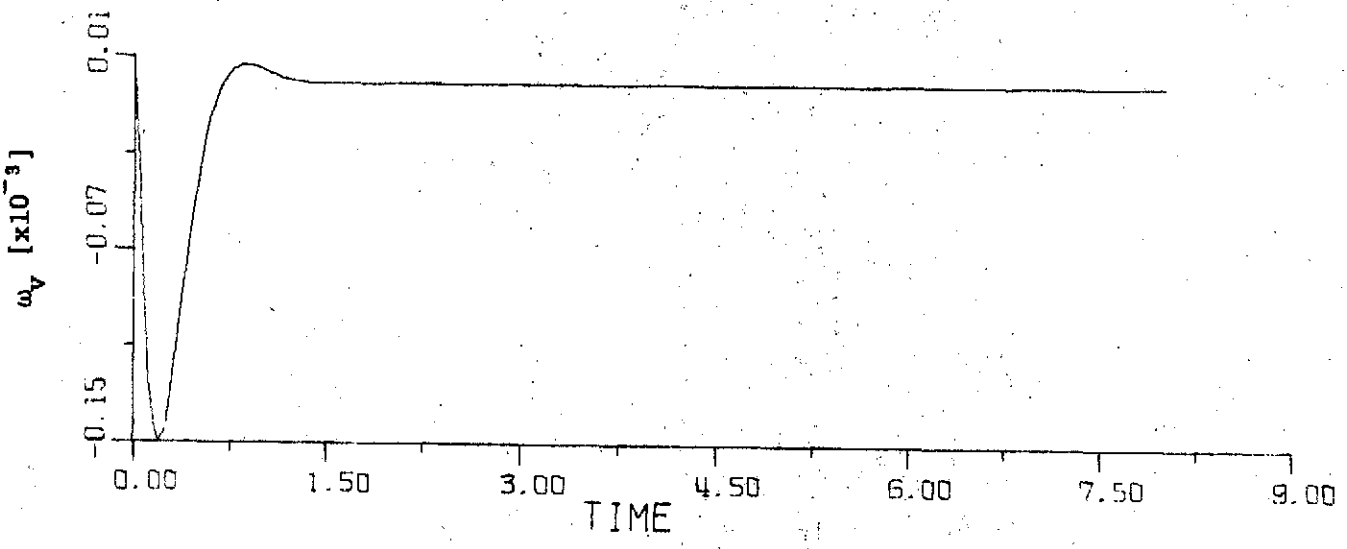

Figure 4-3.

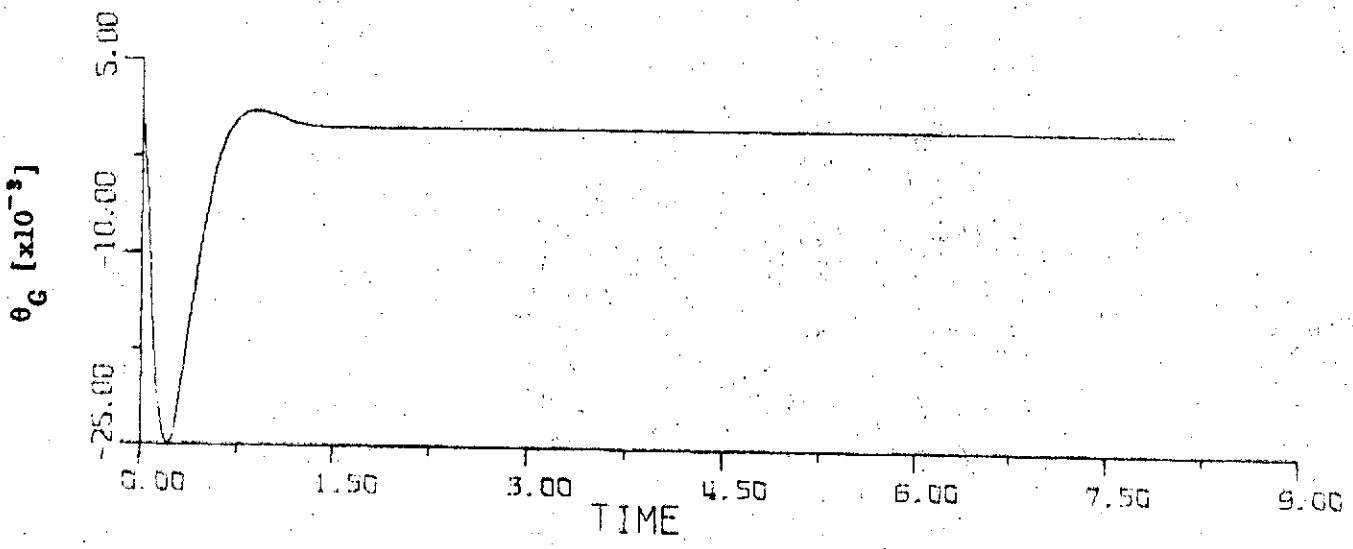

Figure 4-4.

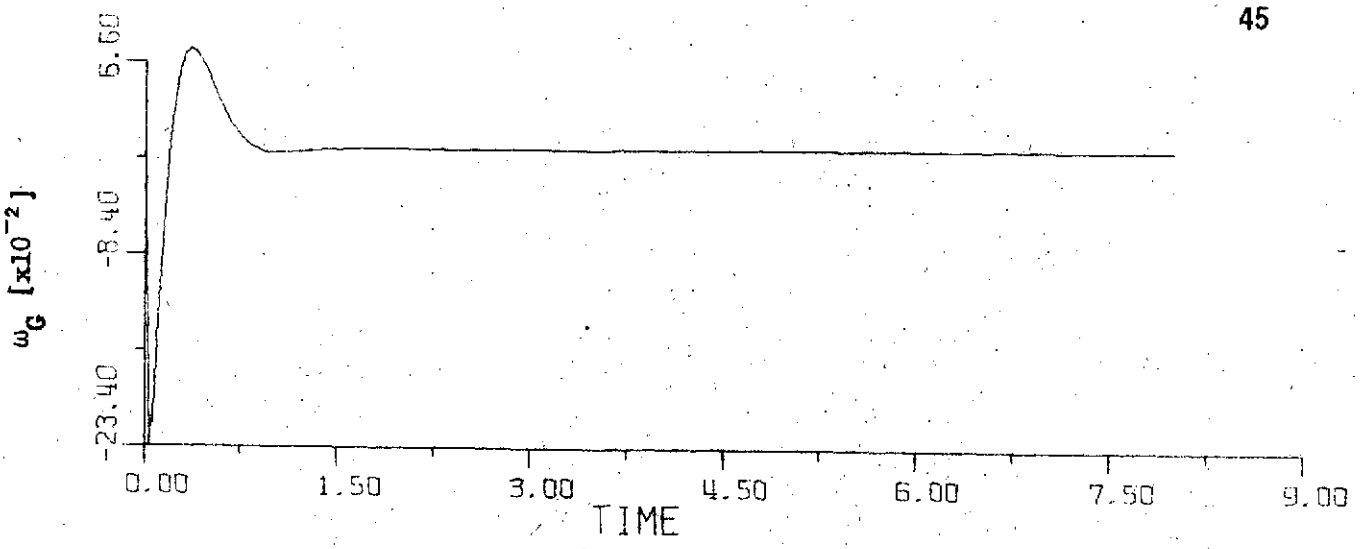

Figure 4-5.

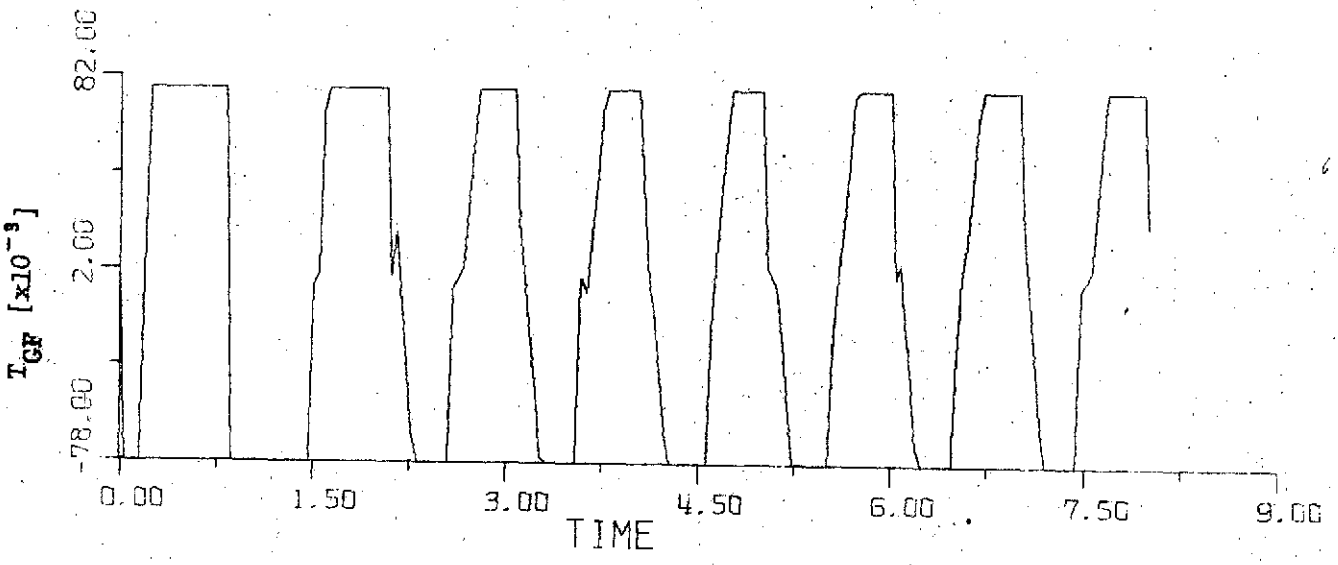

Figure 4-6.

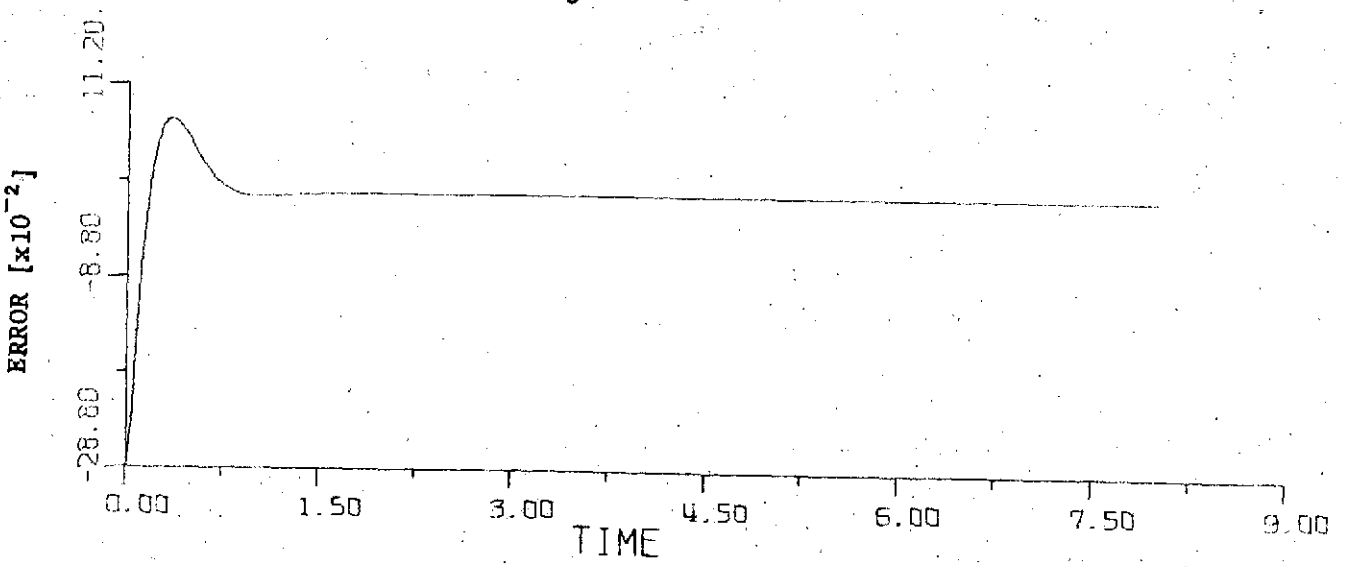

Figure 4-7.

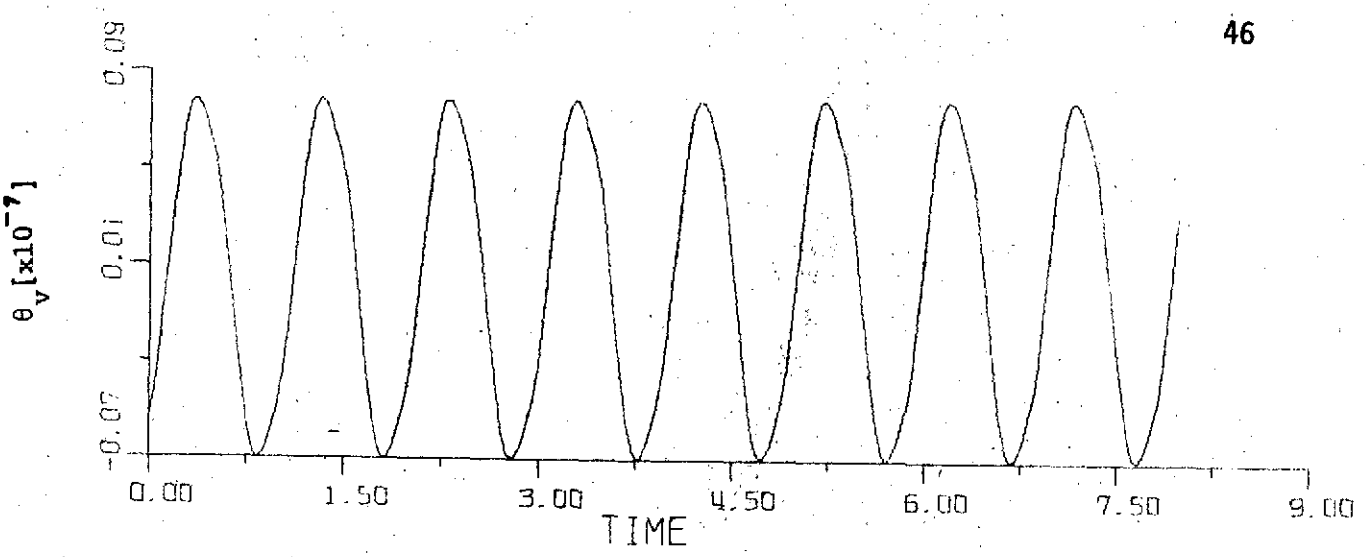

Figure 4-8.

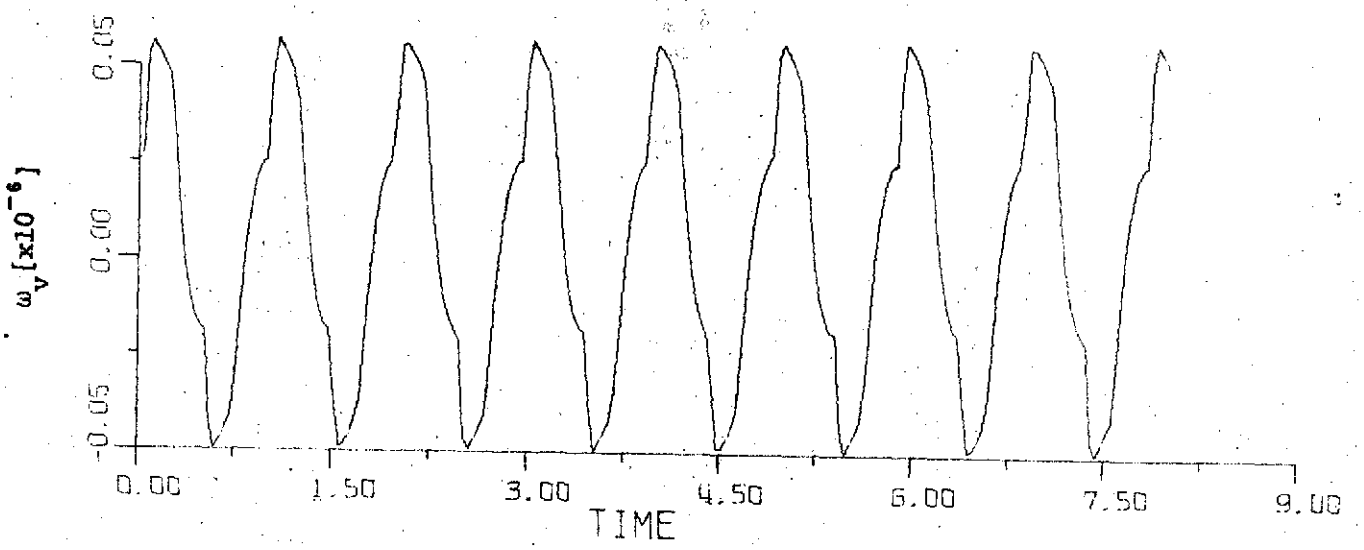

Figure 4-9.

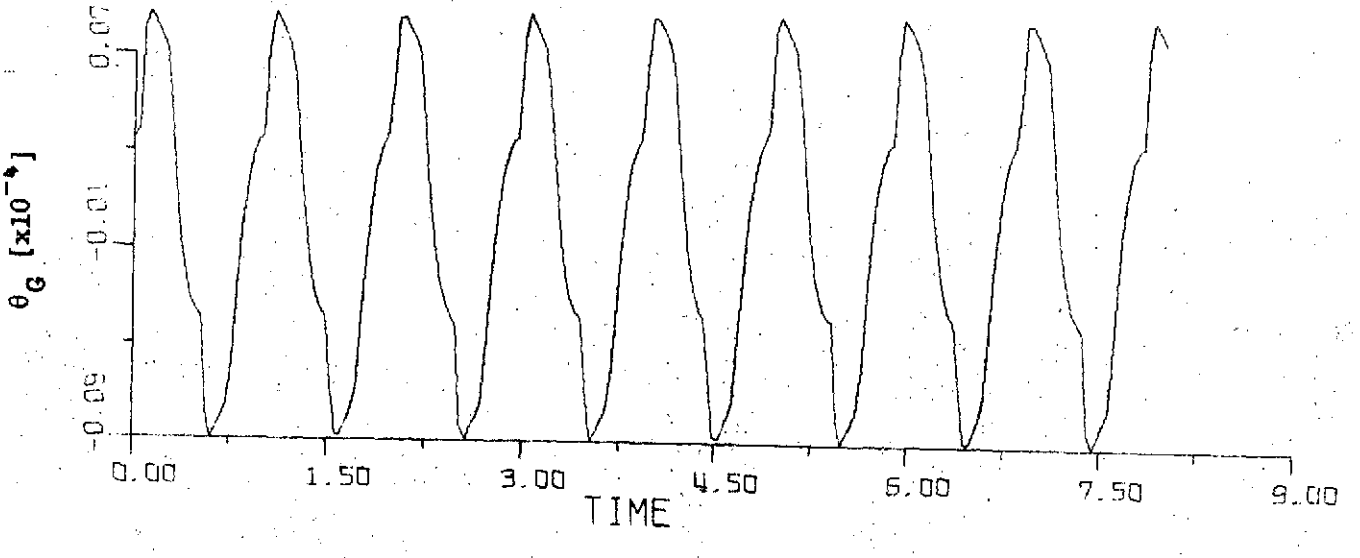

Figure 4-10.

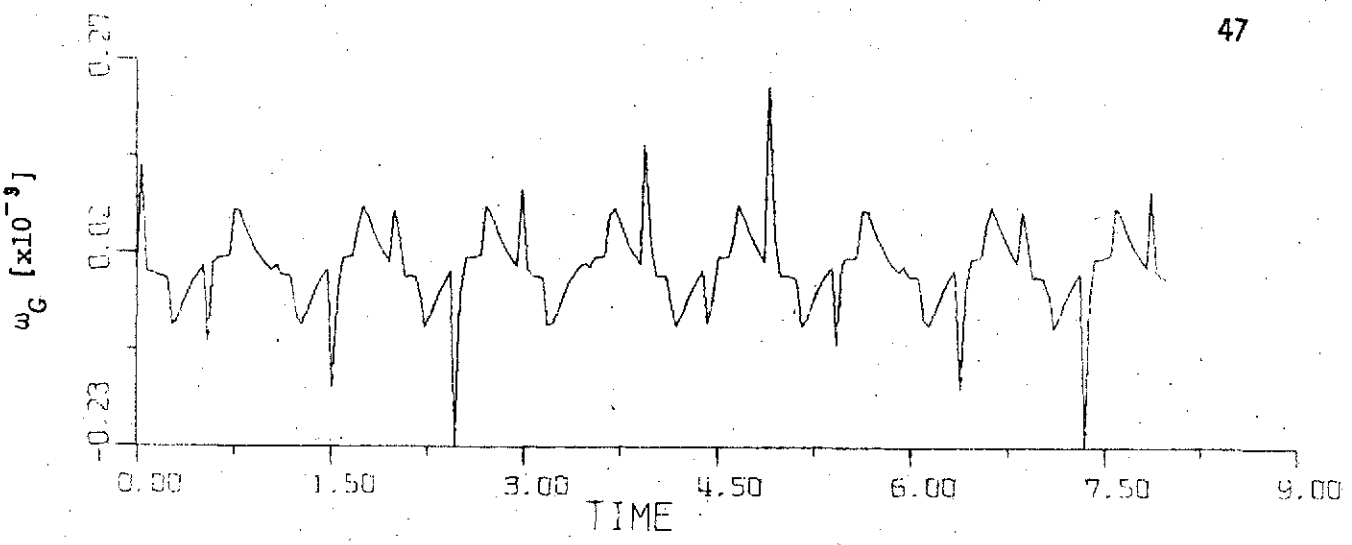

Figure 4-11.

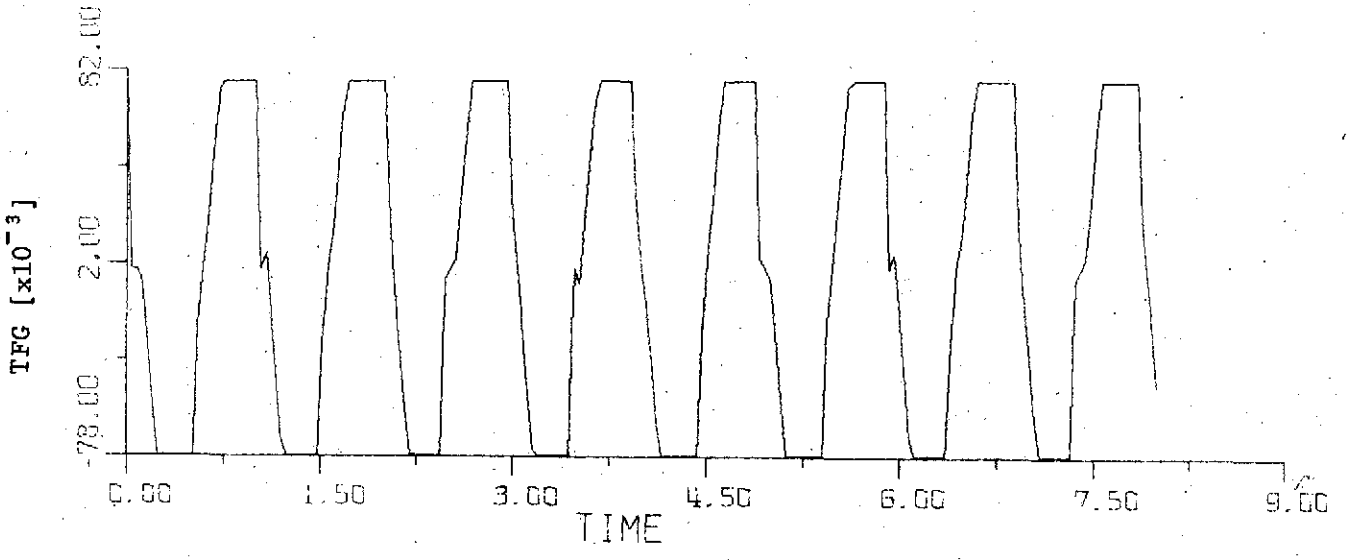

Figure 4-12.

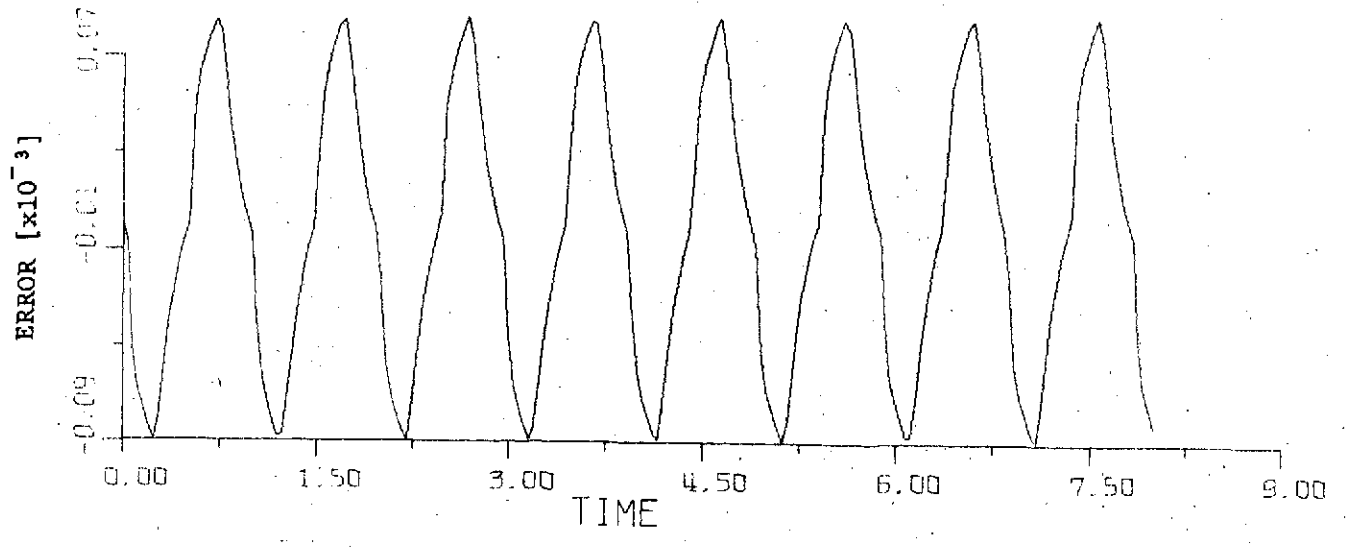

Figure 4-13.

References

1. HEAD Supplemental Information: Gimbal Control System Analysis, Sperry Flight Systems Division, Phoenix, Arizona, May, 1972.

2. Research and Applications Module (RAM) Phase B study, Free Flyer GNeC Trade Study Report, RAM-B-GNC-407, The Bendix Corporation, Navigation and Control Division, Denver Facility, Denver, Colorado.

3. P. R. Dahl, "A Solid Friction Model," Report No. TOR-0158 (3107-18)-1, Aerospace Corporation, El Segundo, California, May, 1968.

5. A Describing Function of the CMG Nonlinearity Using the Analytical Torque Equation

A describing function of the CMG frictional nonlinearity was derived earlier using the straight-line approximated input-output relation between the frictional torque T_{GF} and the CMG angular displacement θ_G.

However, it is possible to derive a describing function for the CMG frictional torque using the analytical relation between T_{GF} and θ_G.

It has been established that the frictional nonlinearity of the CMG can be described by the square-law relation.

$$\frac{dT_{GF}}{d\theta_G} = \gamma(T_{GFI} - T_{GFO})^2 \tag{5-1}$$

where

$$T_{GFI} = T_{GF}\ SGN(\dot{\theta}_G) \tag{5-2}$$

T_{GFO} = saturation level of T_{GF}

γ = positive constant

Carrying out the integration on both sides of Eq. (5-1) yields

$$\theta_G + C_1 = \frac{-1}{\gamma(T_{GF}^{+} - T_{GFO})} \qquad \dot{\theta}_G \geq 0 \tag{5-3}$$

$$\theta_G + C_2 = \frac{-1}{\gamma(T_{GF}^{-} + T_{GFO})} \qquad \dot{\theta}_G \leq 0 \tag{5-4}$$

where C_1 and C_2 are constants of integration, and

$$T_{GF}^{+} = T_{GF} \qquad \dot{\theta}_G \geq 0 \tag{5-5}$$

$$T_{GF}^{-} = T_{GF} \qquad \dot{\theta}_G \leq 0 \tag{5-6}$$

Then, C_1 and C_2 are given by

$$C_1 = -\theta_{Gi} - \frac{1}{\gamma(T_{GFi}^{+} - T_{GFO})} \qquad \dot{\theta}_G \geq 0 \tag{5-7}$$

$$C_2 = -\theta_{Gi} - \frac{1}{\gamma(T_{GFi}^{-} + T_{GFO})} \qquad \dot{\theta}_G \leq 0 \tag{5-8}$$

where θ_{Gi} and T_{GFi} denote the initial values of θ_G and T_{GF}, respectively.

For a sinusoidal input, θ_G is represented by

$$\theta_G = A \cos \omega t \tag{5-9}$$

It is important to note that for the input of Eq. (5-9) $\theta_{Gi} = -A$ when $\dot{\theta}_G \geq 0$, and $\theta_{Gi} = A$ when $\dot{\theta}_G \leq 0$.

Solving for T_{GF}^{+} and T_{GF}^{-} from Eqs. (5-3) and (5-4), respectively, we have

$$T_{GF}^{+} = \frac{-1}{\gamma(A \cos \omega t + C_1)} + T_{GFO} \qquad \dot{\theta}_G \geq 0 \tag{5-10}$$

$$T_{GF}^{-} = \frac{-1}{\gamma(A\cos \omega t + C_2)} - T_{GFO} \qquad \dot{\theta}_G \leq 0 \tag{5-11}$$

with

$$C_1 = A - \frac{1}{\gamma(T_{GFi}^{+} - T_{GFO})} \tag{5-12}$$

$$C_2 = -A - \frac{1}{\gamma(T_{GFi}^{-} + T_{GFO})} \tag{5-13}$$

where

$$T_{GFi}^{+} = - T_{GFO}\left(-\frac{1}{a} + \sqrt{\frac{a^2+1}{a^2}}\right) \tag{5-14}$$

$$T_{GFi}^{-} = T_{GFO}\left(- \frac{1}{a} + \sqrt{\frac{a^2+1}{a^2}}\right) \tag{5-15}$$

$$a = 2\gamma A T_{GFO} \quad . \tag{5-16}$$

With the describing function method, the frictional torque T_{GF} may be approximated by the fundamental component of the Fourier series. The dc component is zero, since the input-output relation is symmetrical about the zero-torque axis.

Thus,

$$T_{GF} = A_1 \sin \omega t + B_1 \cos \omega t$$

$$= \sqrt{A_1^2 + B_1^2} \cos (\omega t - \phi) \tag{5-17}$$

$$\phi = \tan^{-1} \frac{A_1}{B_1} \tag{5-18}$$

$$A_1 = \frac{1}{\pi} \int_0^{2\pi} T_{GF} \sin \omega t \, d\omega t = \frac{1}{\pi} \int_0^{\pi} T_{GF}^{-} \sin\omega t \, d\omega t$$

$$+ \frac{1}{\pi} \int_{\pi}^{2\pi} T_{GF}^{+} \sin\omega t \, d\omega t \tag{5-19}$$

$$B_1 = \frac{1}{\pi} \int_0^{2\pi} T_{GF} \cos\omega t \, d\omega t = \frac{1}{\pi} \int_0^{\pi} T_{GF}^{-} \cos\omega t \, d\omega t$$

$$+ \frac{1}{\pi} \int_{\pi}^{2\pi} T_{GF}^{+} \cos\omega t \, d\omega t \tag{5-20}$$

Substitution of Eqs. (5-10) and (5-11) into Eq. (5-19) gives

$$A_1 = \frac{1}{\pi}\int_0^{\pi} \frac{-1}{\gamma(A\cos\omega t + C_2)}\sin\omega t\, d\omega t - \frac{1}{\pi}\int_0^{\pi} T_{GFO}\sin\omega t\, d\omega t$$

$$+ \frac{1}{\pi}\int_{\pi}^{2\pi} \frac{-1}{\gamma(A\cos\omega t + C_1)}\sin\omega t\, d\omega t + \frac{1}{\pi}\int_{\pi}^{2\pi} T_{GFO}\sin\omega t\, d\omega t \quad (5\text{-}21)$$

$$A_1 = \frac{1}{\pi A\gamma}\ell n\,(A\cos\omega t + C_2)\Big|_0^{\pi} - \frac{2T_{GFO}}{\pi}$$

$$+ \frac{1}{\pi A\gamma}\ell n\,(A\cos\omega t + C_1)\Big|_{\pi}^{2\pi} - \frac{2T_{GFO}}{\pi} \quad (5\text{-}22)$$

Thus

$$A_1 = \frac{1}{\pi A\gamma}\left[\ell n\left(\frac{C_2 - A}{C_2 + A}\right) + \ell n\left(\frac{C_1 + A}{C_1 - A}\right)\right] - \frac{4T_{GFO}}{\pi} \quad (5\text{-}23)$$

In arriving at the last expression it is noted that

$$C_2 < -A$$

$$C_1 > A$$

and $C_1 = -C_2$ over their respective ranges of $\dot{\theta}_G$. Equation (5-23) is simplified further to

$$A_1 = -\frac{4T_{GFO}}{\pi} + \frac{1}{\pi A\gamma}\ell n\left[\frac{(C_2 - A)(C_1 + A)}{(C_2 + A)(C_1 - A)}\right]$$

$$= -\frac{4}{\pi}T_{GFO} + \frac{2}{\pi A\gamma}\ell n\left[\frac{C_1 + A}{C_1 - A}\right] \quad (5\text{-}24)$$

Now substitution of Eqs. (5-10) and (5-11) into Eq. (5-20) yields

$$B_1 = \frac{1}{\pi}\int_0^{\pi} \frac{-1}{\gamma[A\cos\omega t + C_2]}\cos\omega t\, d\omega t - \frac{1}{\pi}\int_0^{\pi} T_{GFO}\cos\omega t\, d\omega t$$

$$+ \frac{1}{\pi}\int_{\pi}^{2\pi} \frac{-1}{\gamma[A\cos\omega t + C_1]}\cos\omega t\, d\omega t + \frac{1}{\pi}\int_{\pi}^{2\pi} T_{GFO}\cos\omega t\, d\omega t \quad (5\text{-}25)$$

Evaluating each of the integrals in the last equation, we have

$$\int_0^{\pi} T_{GFO} \cos\omega t \, d\omega t = \int_{\pi}^{2\pi} T_{GFO} \cos\omega t \, d\omega t = 0 \qquad (5\text{-}26)$$

Since $C_2 < -A$, C_2 is always negative, and $C_2^2 > A^2$, the first integral of B_1 becomes

$$I_1 = \frac{1}{\pi} \int_0^{\pi} \frac{-1}{\gamma(A\cos\omega t + C_2)} \cos\omega t \, d\omega t = \frac{1}{\pi\gamma} \left(\frac{-\omega t}{A}\right)_0^{\pi} + \frac{C_2}{\pi\gamma A} \int_0^{\pi} \frac{d\omega t}{A\cos\omega t + C_2} \qquad (5\text{-}27)$$

or

$$I_1 = -\frac{1}{\gamma A} + \frac{C_2}{\pi\gamma A} \left[\frac{2}{\sqrt{C_2^2 - A^2}} \tan^{-1} \frac{(C_2 - A)\tan(\omega t/2)}{\sqrt{C_2^2 - A^2}} \right]_0^{\pi}$$

$$= -\frac{1}{\gamma A} - \frac{C_2}{\gamma A \sqrt{C_2^2 - A^2}} \qquad (5\text{-}28)$$

where the fact that C_2 is negative has been used. Also, $\tan \pi/2$ is taken to be $+\infty$ since $\omega t/2$ expands from 0 to $\pi/2$.

Similarly, the third integral of B_1 in Eq. (5-25) is written

$$I_2 = \frac{1}{\pi} \int_{\pi}^{2\pi} \frac{-1}{\gamma(A\cos\omega t + C_1)} \cos\omega t \, d\omega t$$

$$= \frac{-1}{\gamma A} + \frac{C_1}{\pi\gamma A} \left[\frac{2}{\sqrt{C_1^2 - A^2}} \tan^{-1} \frac{(C_1 - A)\tan(\omega t/2)}{\sqrt{C_1^2 - A^2}} \right]_{\pi}^{2\pi}$$

$$= \frac{-1}{\gamma A} + \frac{C_1}{\gamma A \sqrt{C_1^2 - A^2}} \qquad (5\text{-}29)$$

In arriving at the last equation, we have recognized that $C_1 > A$ and have used that $\tan \pi/2 = -\infty$, since in this case $\omega t/2$ expands from $\pi/2$ to π. Thus,

$$B_1 = I_1 + I_2 = -\frac{2}{\gamma A} - \frac{C_2}{\gamma A\sqrt{C_2^2-A^2}} + \frac{C_1}{\gamma A\sqrt{C_1^2-A^2}}$$

$$= \frac{2}{\gamma A}\left(\frac{C_1}{\sqrt{C_1^2-A^2}} - 1\right) \qquad (5\text{-}30)$$

The describing function in complex form is written as

$$N(A) = \frac{B_1 - jA_1}{A} \qquad (5\text{-}31)$$

where A_1 and B_1 are given by Eqs. (5-24) and (5-30), respectively. A digital computer program for the computation of N(A) and -1/N(A) is listed in Table 5-1. The constant A is represented by E in this program. The parameters of the nonlinearity are:

$$T_{GFO} = 0.1 \text{ ft-lb}$$

$$\gamma = 1.38 \times 10^5$$

Figure 5-1 shows the magnitude (db) versus phase (degrees) plots of $-1/N(A)$ for $\gamma = 1.38 \times 10^4$, 0.69×10^5, 1.38×10^5, 0.69×10^6, and 1.38×10^6, as the magnitude of A varies. Note that as A becomes large, the magnitude of $-1/N(A)$ approaches infinity and the phase approaches -270 degrees. As A decreases, the magnitude of $-1/N(A)$ decreases and the phase approaches -180 degrees. In the limit as $A \to 0$, $-1/N(A)$ goes to $-1/\gamma T_{GFO}^2$.

Asymptotic Behavior of -1/N(A) for Very Small Values of A

Figure 5-1 shows that as A approaches zero, the magnitude of $-1/N(A)$ in db approaches $20 \log_{10}[1/\gamma T_{GFO}^2]$ and the phase is -180 degrees. The asymptotic behavior of $-1/N(A)$ for very small values of A is derived here analytically.

Table 5-I

```
L
      .100 "   LST CONTINOUS DESCRIBING FUNCTION - EXACT CMG NONLINEARITY
    1.000 COMPLEX GV,GN*16
    1.500 REAL*8 P(20),PI,RAD,TO,GAMMA,ESTART,E,AA,R,TGFI,TGFN,TGFP,C1,C2
,A1,B1
    1.600 REAL*8 A2
    2.000 PI=3.14159
    3.000 RAD=180./PI
    4.000 TO=.1
    4.500 S=10.
    5.000 GAMMA=S*1.38E5
    6.000 ESTART=1.E-13
    7.000 NP=2
    8.000 ND=15
    9.000 P(1)=1.
   10.000 P(2)=5.
   10.200 WRITE(6,100)
   10.400 WRITE(6,101)
   11.000 DO 1 J=1,ND
   12.000 DO 1 I=1,NP
   13.000 E=ESTART*P(I)*(10.**(J-1))
   14.000 AA=2.*GAMMA*E*TO
   15.000 R=(-1./AA)+DSQRT((AA*AA+1.)/(AA*AA))
   16.000 TGFI=R*TO
   17.000 TGFN=TGFI
   18.000 TGFP=-TGFI
   19.000 C1=E-1./(GAMMA*(TGFP-TO))
   20.000 C2=-E-1./(GAMMA*(TGFN+TO))
   21.000 A1=(-4.*TO/PI)+(1./(PI*GAMMA*E))*DLOG(((C1+E)*(C2-E))/((C1-E)*%
   21.100 (C2+E)))
   21.500 A2=DLOG(((C1+E)*(C2-E))/((C1-E)*(C2+E)))
   21.600 A1=(-4.*TO/PI)+(A2/(PI*GAMMA*E))
   22.000 B1=(-1./(GAMMA*E))*(2.+C2/DSQRT(C2*C2-E*E)-C1/DSQRT(C1*C1-E*E))
   22.100 A1=A1/E
   22.200 B1=B1/E
   23.000 GN=DCMPLX(B1,-A1)
   24.000 GV=-1./GN
   25.000 G1=REAL(GV)
   26.000 G2=AIMAG(GV)
   27.000 GMAG=CABS(GV)
   28.000 GDB=20.*ALOG10(GMAG)
   29.000 GPHASE=RAD*ATAN2(G2,G1)
   30.000 IF(GPHASE.GE.0.)GPHASE=GPHASE-360.
   33.000 WRITE(6,102)E,TGFI,GPHASE,GDB,GMAG
   34.000 1 CONTINUE
   35.000 100 FORMAT('   CONTINOUS DESCRIBING FUNCTION FOR CMG NONLINEARI
TY')
   36.000 101 FORMAT(/,8X,'E',11X,'TGFI',10X,'PHASE',10X,'DB',9X,'MAGNITU
DE'/)
   37.000 102 FORMAT(1P5E14.5)
   39.000 STOP
   40.000 END
C
```

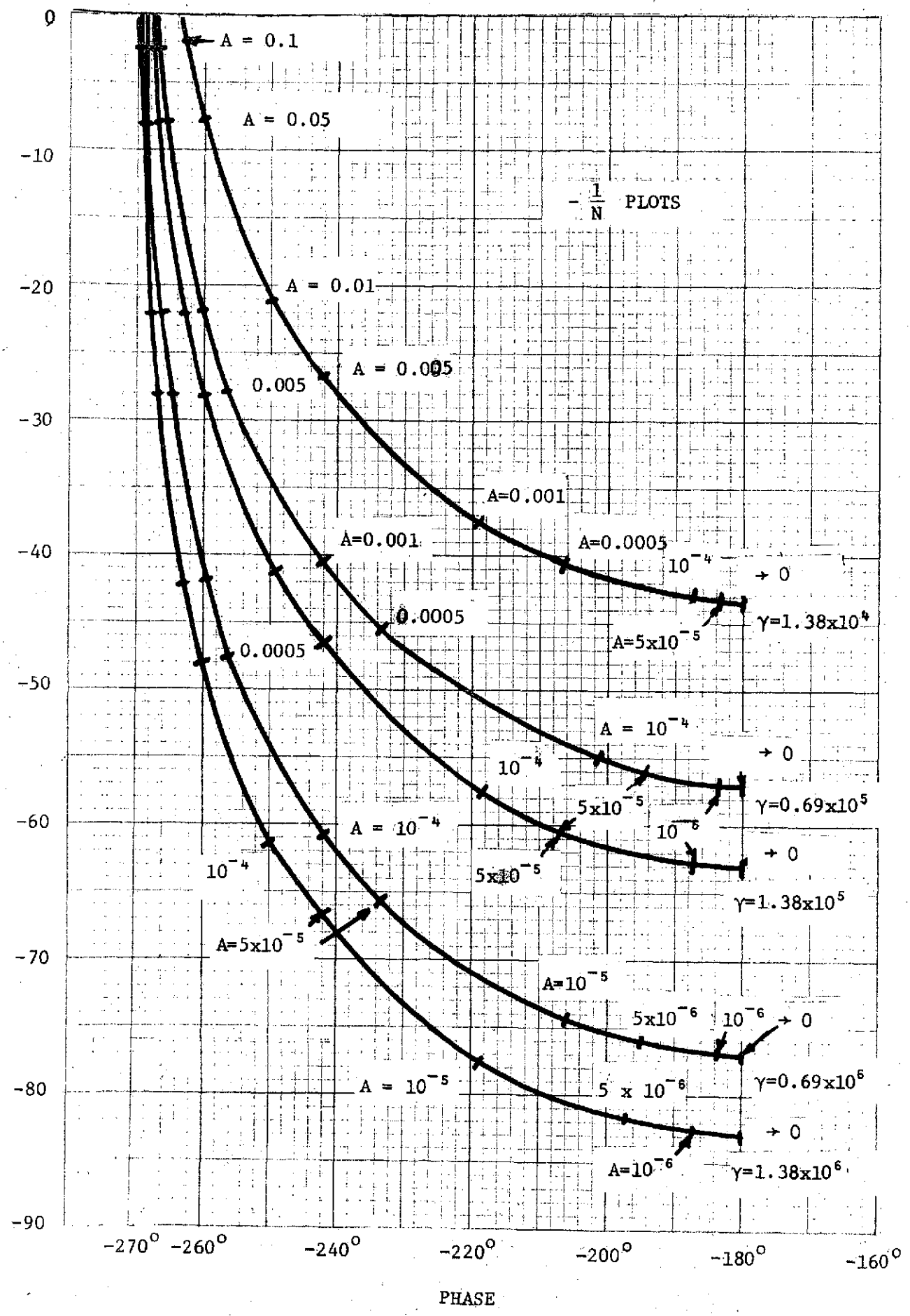
0
-10
-20
-30
-40
-50
-60
-70
-80
-90
DECIBELS
-270° -260° -240° -220° -200° -180° -160°
PHASE
$-\frac{1}{N}$ PLOTS
A = 0.1
A = 0.05
A = 0.01
A = 0.005
0.005
A=0.001
A=0.001
A=0.0005
10^{-4} → 0
$\gamma=1.38\times10^{4}$
$A=5\times10^{-5}$
0.0005
0.0005
$A = 10^{-4}$
→ 0
10^{-4}
5×10^{-5}
10^{-6}
$\gamma=0.69\times10^{5}$
$A = 10^{-4}$
→ 0
10^{-4}
5×10^{-5}
$\gamma=1.38\times10^{5}$
$A=5\times10^{-5}$
$A=10^{-5}$
5×10^{-6}
10^{-6} → 0
$\gamma=0.69\times10^{6}$
$A = 10^{-5}$
5×10^{-6}
→ 0
$A=10^{-6}$
$\gamma=1.38\times10^{6}$

Figure 5-1

Dividing both sides of Eq. (5-24) by A and expanding the logarithmic term into a power series, we have

$$\frac{A_1}{A} = -\frac{4}{\pi A}T_{GFO} + \frac{4}{\pi A^2\gamma}\left(\frac{A}{C_1} + \frac{A^3}{C_1^3} + \frac{A^5}{C_1^5} + \cdots\right)$$

$$= -\frac{4}{\pi A}T_{GFO} + \frac{4}{\gamma\pi}\left(\frac{1}{C_1 A} + \frac{A}{C_1^3} + \frac{A^3}{C_1^5} + \cdots\right) \qquad (5\text{-}32)$$

Taking the limit on both sides of Eq. (5-32) as A→0, and using the fact that

$$\lim_{A\to 0} C_1 = \frac{1}{\gamma T_{GFO}} \qquad (5\text{-}33)$$

we have

$$\lim_{A\to 0}\left(\frac{A_1}{A}\right) = \lim_{A\to 0}\left[-\frac{4}{\pi A}T_{GFO} + \frac{4}{\pi\gamma}\left(\frac{1}{C_1 A} + \frac{A}{C_1^3} + \frac{A^3}{C_1^5} + \cdots\right)\right]$$

$$= \lim_{A\to 0}\left[-\frac{4}{\pi A}T_{GFO} + \frac{4}{\pi\gamma}\,\frac{\gamma T_{GFO}}{A} + \frac{4A\gamma^2 T_{GFO}^3}{\pi} + \cdots\right]$$

Substituting Eq. (5-33) into the last equation we have

$$\lim_{A\to 1}\left(\frac{A_1}{A}\right)=\lim_{A\to 0}\left[\frac{4A}{\pi}[\gamma^2 T_{GFO}{}^3+A^2\gamma^4 T_{GFO}{}^5+\ldots]\right]=0 \qquad (5\text{-}34)$$

Dividing both sides of Eq. (5-30) by A and taking the limit as A approaches zero, we have

$$\lim_{A\to 0}\left(\frac{B_1}{A}\right)=\lim_{A\to 0}\frac{2}{\gamma A^2}\left(\frac{C_1}{\sqrt{C_1^2-A^2}}-1\right)$$

$$=\lim_{A\to 0}\frac{2}{\gamma A^2}\left(\frac{1}{\sqrt{1-(A/C_1)^2}}-1\right) \qquad (5\text{-}35)$$

Expanding $[1-(A/C_1)^2]^{-1/2}$ into a power series, and using only the first two terms, Eq. (5-35) becomes

$$\lim_{A\to 0}\left(\frac{B_1}{A}\right)=\lim_{A\to 0}\frac{2}{\gamma A^2}\left[\frac{1}{2}\left(\frac{A}{C_1}\right)^2\right]$$

$$=\lim_{A\to 0}\frac{1}{\gamma C_1^2}=\gamma T_{GFO}^2 \qquad (5\text{-}36)$$

Thus,

$$\lim_{A\to 0} 1/N(A)=\lim_{A\to 0}\frac{1}{\frac{B_1}{A}-j\frac{A_1}{A}}=\frac{1}{\gamma T_{GFO}{}^2} \qquad (5\text{-}37)$$

As shown in Fig. 5-1, the gain-phase plot of $-1/N(A)$ as A approaches zero is a point which lies on the -180 deg line with a magnitude of $20\log_{10}[1/\gamma T_{GFO}{}^2]$.

Asymptotic Behavior of -1/N(A) For Very Large Values of A

For very large values of A, the value of C_1 becomes

$$\lim_{A\to\infty} C_1 = \lim_{A\to\infty}\left[A + \frac{2}{\gamma T_{GFO}}\right] \tag{5-38}$$

Then

$$\lim_{A\to\infty} \frac{A_1}{A} = \lim_{A\to\infty}\left(-\frac{4}{\pi A} T_{GFO} + \frac{2}{\pi\gamma}\left(\frac{1}{C_1 A} + \frac{A}{C_1^3} + \frac{A^3}{C_1^5} + \cdots\right)\right)$$

$$= \lim_{A\to\infty}\left(-\frac{4}{\pi A} T_{GFO}\right) = -0 \tag{5-39}$$

Similarly we can show that

$$\lim_{A\to\infty} \frac{B_1}{A} = +0 \tag{5-40}$$

Thus,

$$\lim_{A\to\infty}\left[-1/N(A)\right] = -j/0 = \infty\angle\underline{-270} \tag{5-41}$$

As shown in Figure 5-1, the gain-phase plots of -1/N(A) approach $\infty\angle\underline{-270}°$ as $A \to \infty$ for all values of γ and T_{GFO}.

6. Computer Simulation of the Simplified LST System with the Analytical Torque Expressions

A computer simulation of the LST system is presented here to corroborate the results of the describing function analysis of the last chapter. Since the describing function analysis has been carried out with the analytical torque expressions for the CMG frictional nonlinearity, the simulation model of the nonlinearity also has the same characteristics. This model of the nonlinearity is implemented by using the expressions for T_{GF} in Eqs. (2-38) and (2-39) with initial conditions for θ_G and T_{GF} being redefined each time a sign change in $\dot{\theta}_G$ occurs.

The simplified LST system is represented by the block diagram of Figure 1-7. The linear transfer function which the nonlinear element NL sees is given by

$$G(s) = \frac{J_V s^2}{J_G J_V s^4 + J_V K_p s^3 + J_V K_I s^2 + K_I H K_1 s + K_I H K_0}$$

Two sets of numerical values are considered as follows:

	System 1	System 2
J_V	10^5	10^5
J_G	2.1	3.7
K_p	216.	280.
K_I	9700.	10000
H	600	200
K_1	1371.02	3000
K_0	5758.35	20000

The frequency-domain plots of G(s) for both systems are given in Figure 6-1 in db versus phase coordinates. Figure 6-1 also contains the -1/N curves of Figure 5-1 for $\gamma = 1.38 \times 10^5$, 1.38×10^6 and 1.38×10^7.

With $\gamma = 1.38 \times 10^7$, the -1/N curve intersects the G(s) curves of the two systems at two points each. Among these the stable points for sustained oscillations are the ones on the left at the higher frequencies. The approximate magnitudes and frequencies of the oscillations are 6×10^{-6} rad and 4.4 rad/sec, respectively, for system 1, and 2×10^{-5} rad and 5.6 rad/sec, respectively, for system 2. The curves in Figure 6.1 also show that for γ considerably smaller than 1.38×10^7, both systems will exhibit a stable response, although for certain values of γ system 2 will show sustained oscillations while system 1 is stable.

For the computer simulation, the input to the LST system, χ, is set to zero, along with all the initial states, except for the vehicle position θ_V. The initial value of θ_V is set at 5×10^{-5} rad, which is chosen so that the input signal to the nonlinearity, θ_G, would be large enough to cause the torque to saturate, while at the same time the limiting value of the input signal is not exceeded.

The following quantities are plotted from the simulation runs:

θ_V = vehicle position (rad)

ω_V = vehicle velocity (rad/sec)

θ_G = Gimbal position (rad)

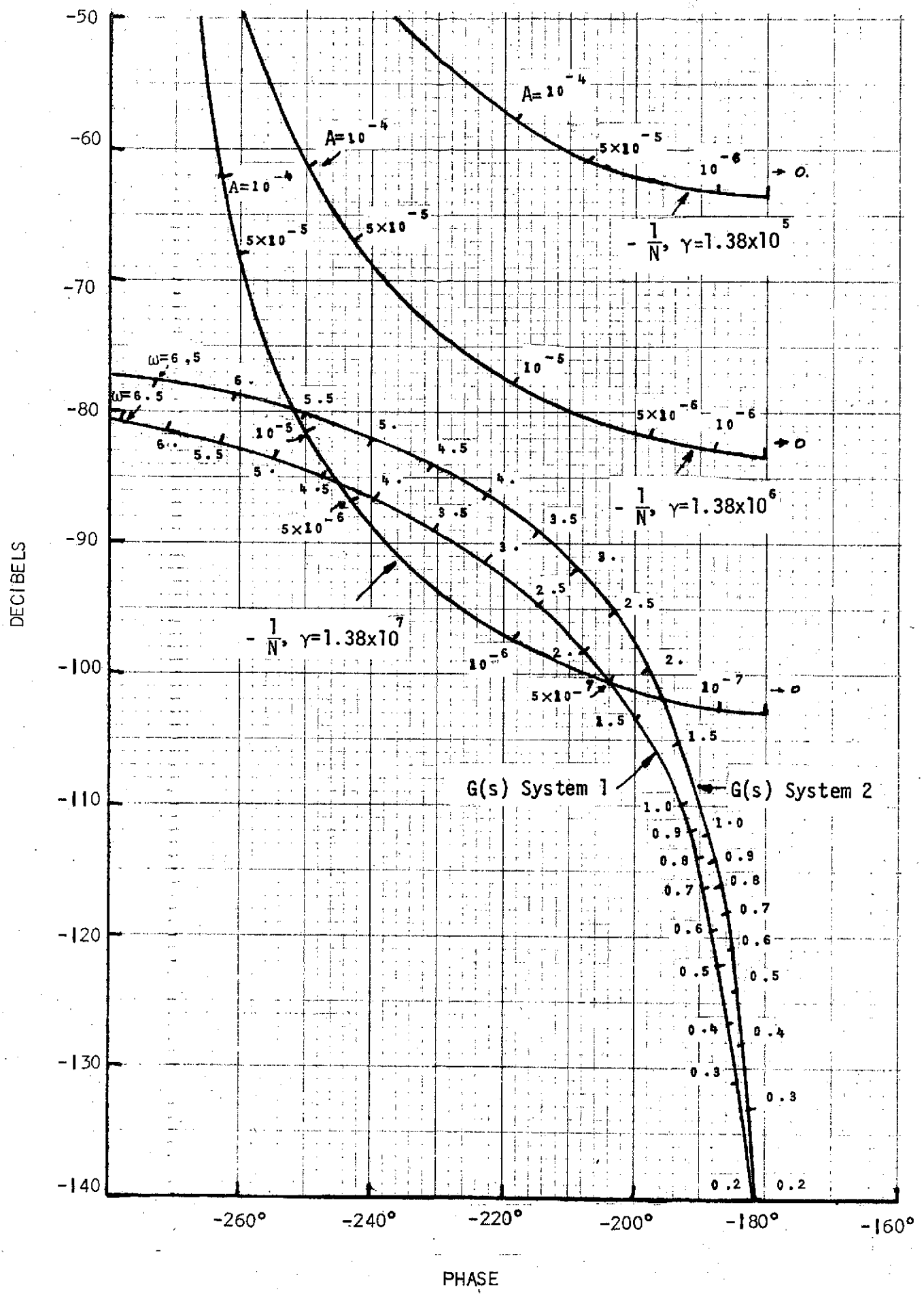
-50
-60
-70
-80
-90
-100
-110
-120
-130
-140
DECIBELS
-260°
-240°
-220°
-200°
-180°
-160°
PHASE
A=10^-4
5×10^-5
10^-5
5×10^-6
10^-6
10^-7
5×10^-7
→0
- 1/N, γ=1.38x10^5
- 1/N, γ=1.38x10^6
- 1/N, γ=1.38x10^7
ω=6.5
ω=6.5
G(s) System 1
G(s) System 2

Figure 6-1

ω_G = Gimbal velocity (rad/sec)

T_{GF} = Torque output of the nonlinearity (ft-lb)

Error = Error input command (rad/sec) to the CMG

$= \chi - K_0\theta_V - K_1\omega_V$

Figures 6-2 and 6-3 show the plots of the above listed quantities for system 1 with $\gamma = 1.38 \times 10^7$. It may be noted from the plot of T_{GF} in Figure 6-3 that the system has a sustained oscillation. This oscillation is not seen on the other plots because of the large initial transients. Figure 6-4 through 6-5 show the continuation of Figures 6-2 and 6-3 with proper scales. Figures 6-6 and 6-7 show the response plots for system 2 with $\gamma = 1.38 \times 10^7$, and Figures 6-8 and 6-9 show the continuation of these plots with proper scales. The frequencies and magnitudes of oscillations obtained with the two systems are quite close to the predicted values. The small discrepancy is attributed to the discretization of the nonlinearity implementation on the digital computer.

Figures 6-10 and 6-11 show the response plots for system 1 with $\gamma = 0.69 \times 10^7$ and their continuations are shown in Figures 6-12 and 6-13, respectively. Figures 6-14 and 6-15 show the response plots for system 1 with $\gamma = 1.38 \times 10^5$. As predicted, the system is stable for both of the lower γ values.

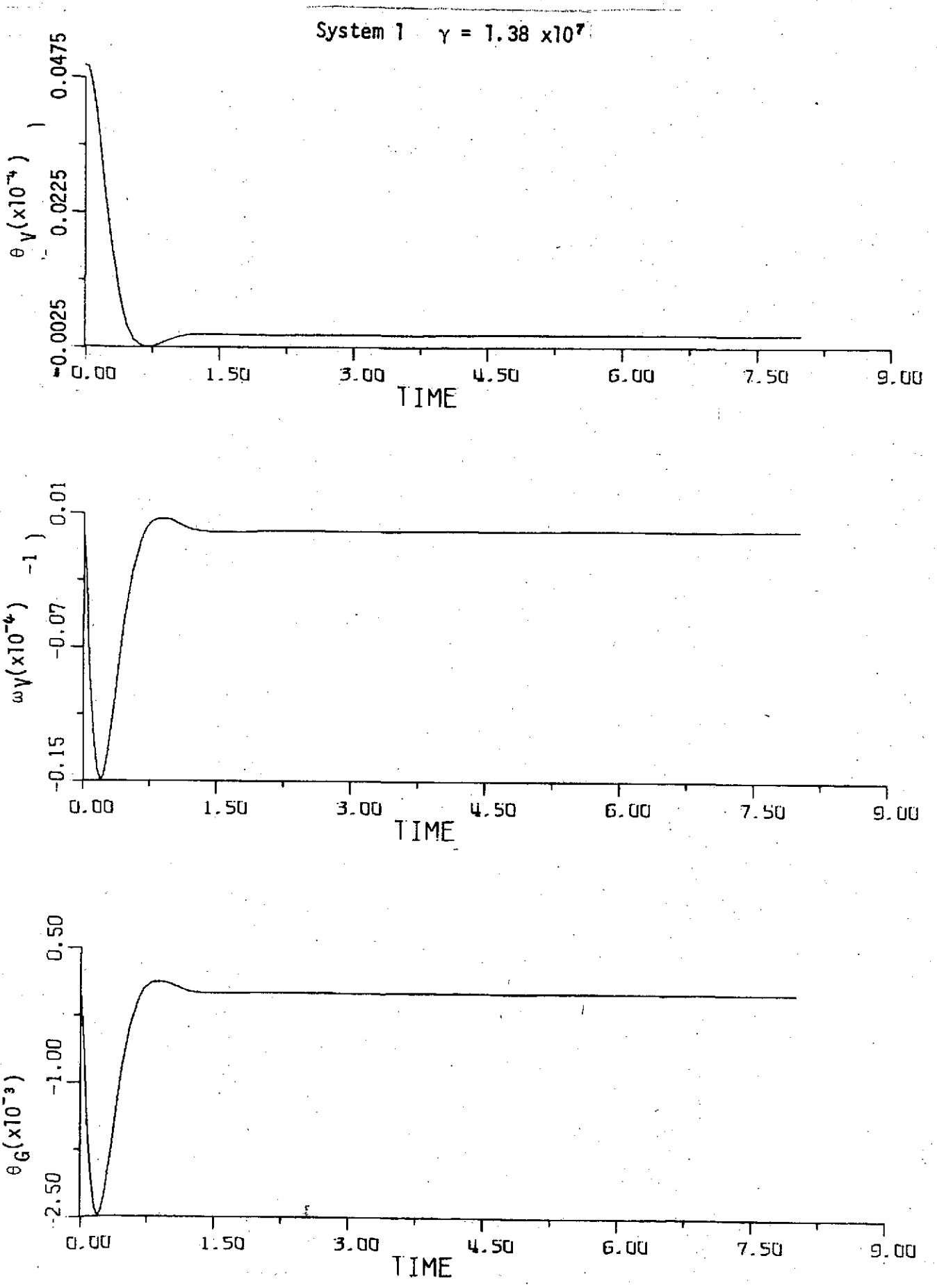
System 1 γ = 1.38 x10⁷
θγ(x10⁻⁴)
0.0475
0.0225
-0.0025
0.00
1.50
3.00
4.50
6.00
7.50
9.00
TIME
ωγ(x10⁻⁴)
-1
0.01
-0.07
-0.15
0.00
1.50
3.00
4.50
6.00
7.50
9.00
TIME
θG(x10⁻³)
0.50
-1.00
-2.50
0.00
1.50
3.00
4.50
6.00
7.50
9.00
TIME

Figure 6-2

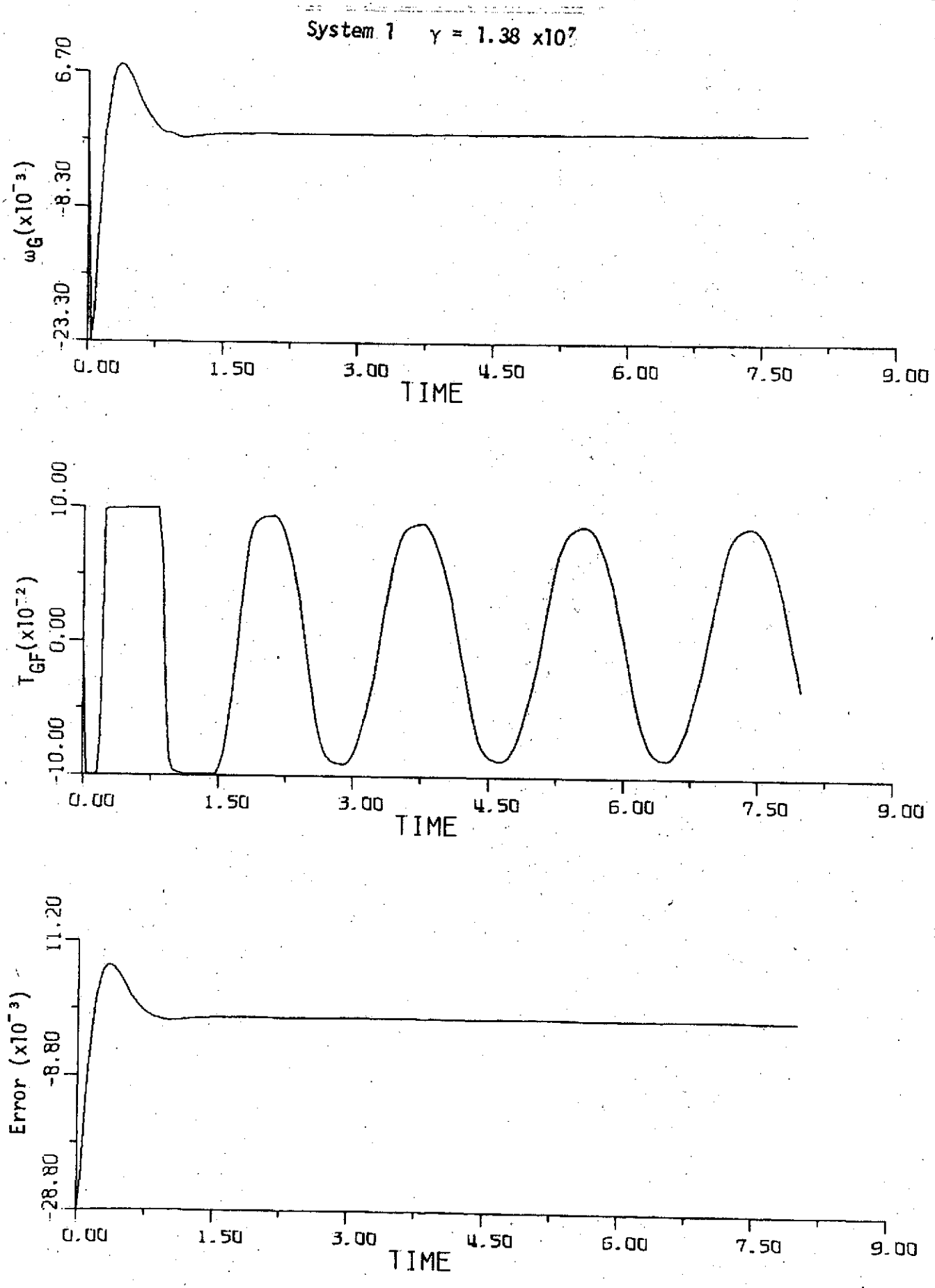
System 1 γ = 1.38 x10⁷
6.70
-8.30
-23.30
ωG(x10⁻³)
0.00
1.50
3.00
4.50
6.00
7.50
9.00
TIME
10.00
0.00
-10.00
TGF(x10⁻²)
0.00
1.50
3.00
4.50
6.00
7.50
9.00
TIME
11.20
-8.80
-28.80
Error (x10⁻³)
0.00
1.50
3.00
4.50
6.00
7.50
9.00
TIME

Figure 6-3

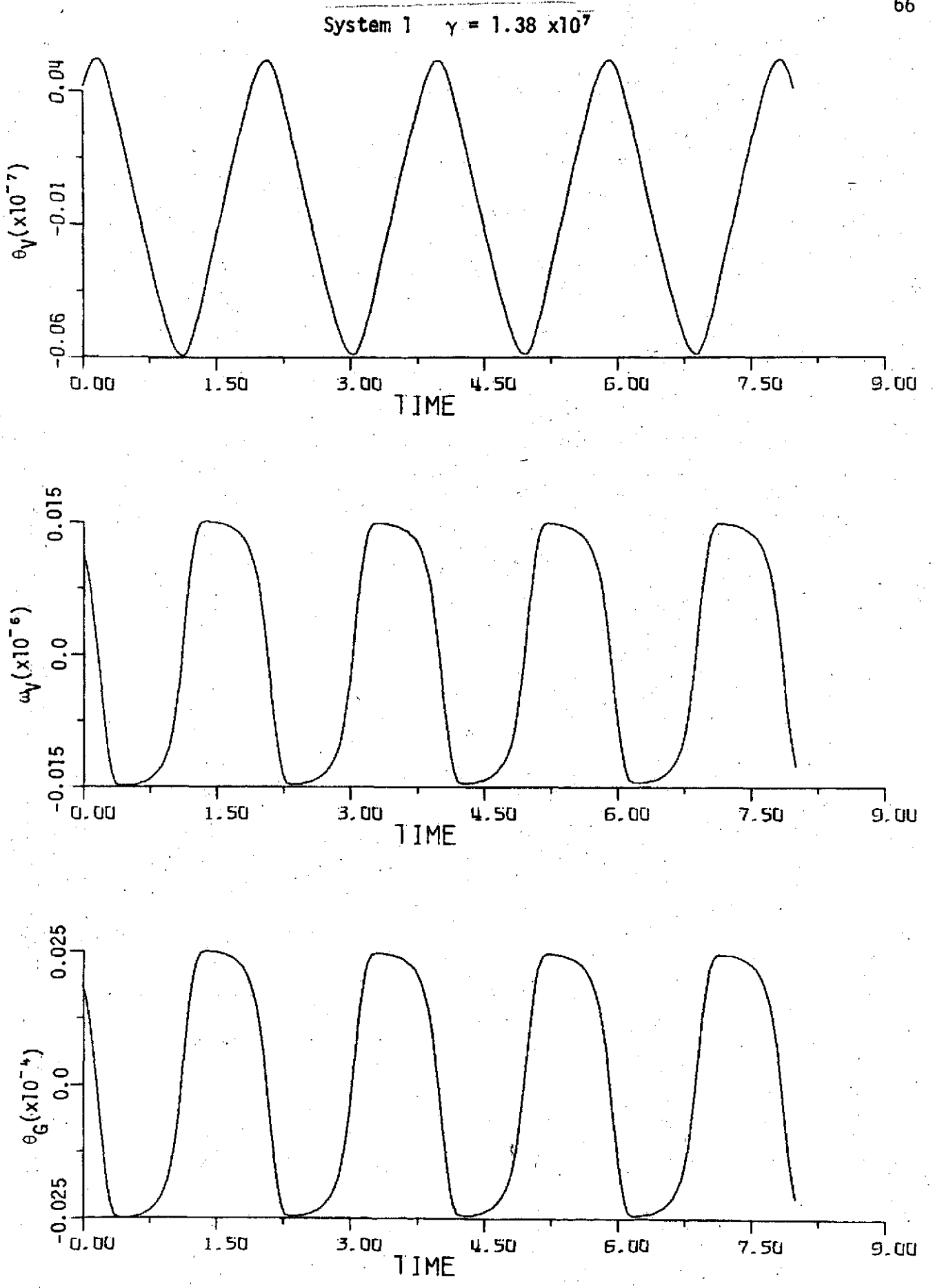
System 1 γ = 1.38 x10⁷
θV(x10⁻⁷)
0.04
-0.01
-0.06
0.00
1.50
3.00
4.50
6.00
7.50
9.00
TIME
ωV(x10⁻⁶)
0.015
0.0
-0.015
0.00
1.50
3.00
4.50
6.00
7.50
9.00
TIME
θG(x10⁻⁴)
0.025
0.0
-0.025
0.00
1.50
3.00
4.50
6.00
7.50
9.00
TIME

Figure 6-4

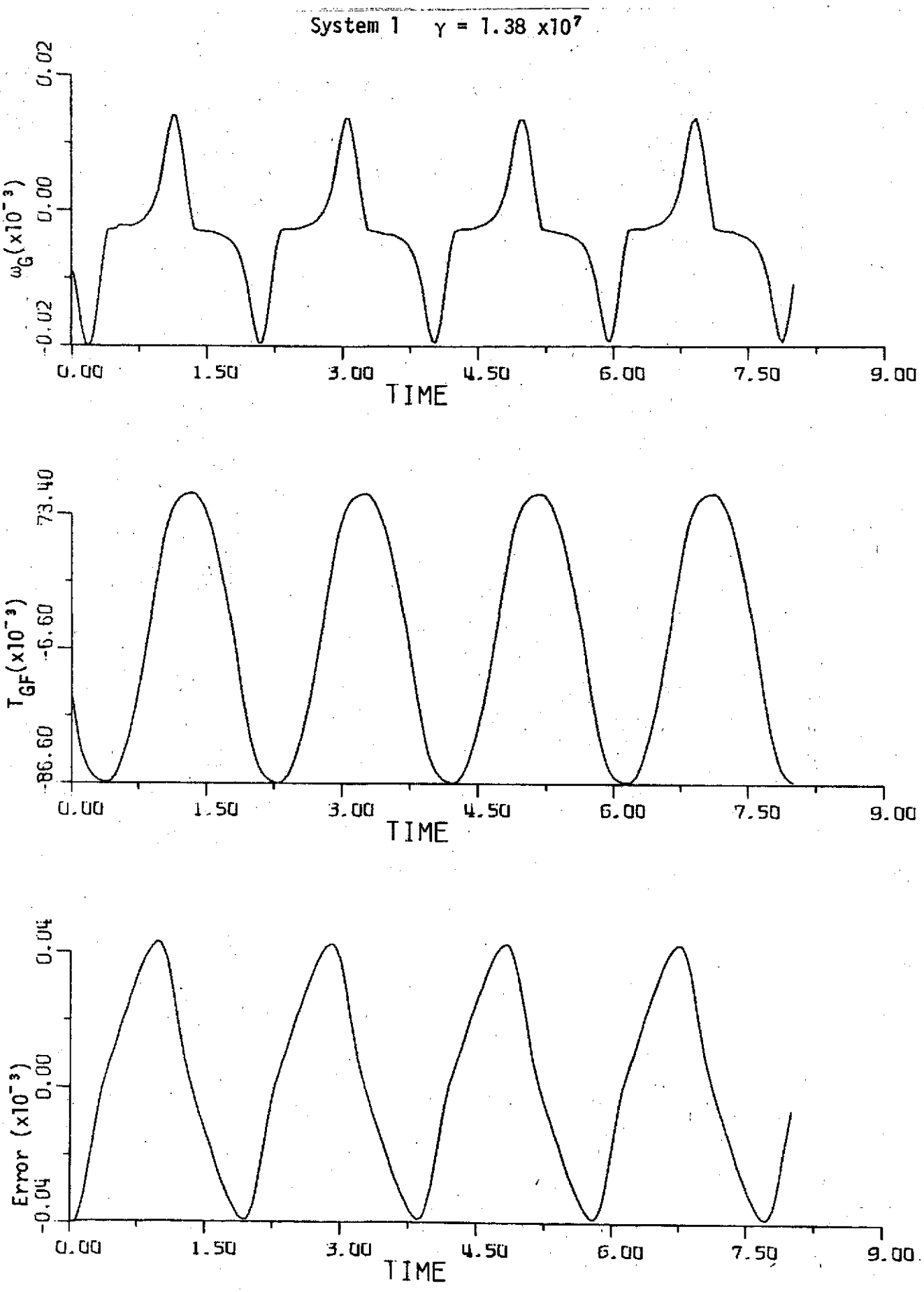
System 1 γ = 1.38 x10⁷
ωG(x10⁻³)
0.02
0.00
-0.02
0.00
1.50
3.00
4.50
6.00
7.50
9.00
TIME
TGF(x10⁻³)
73.40
-6.60
-86.60
0.00
1.50
3.00
4.50
6.00
7.50
9.00
TIME
Error (x10⁻³)
0.04
0.00
-0.04
0.00
1.50
3.00
4.50
6.00
7.50
9.00
TIME

Figure 6-5

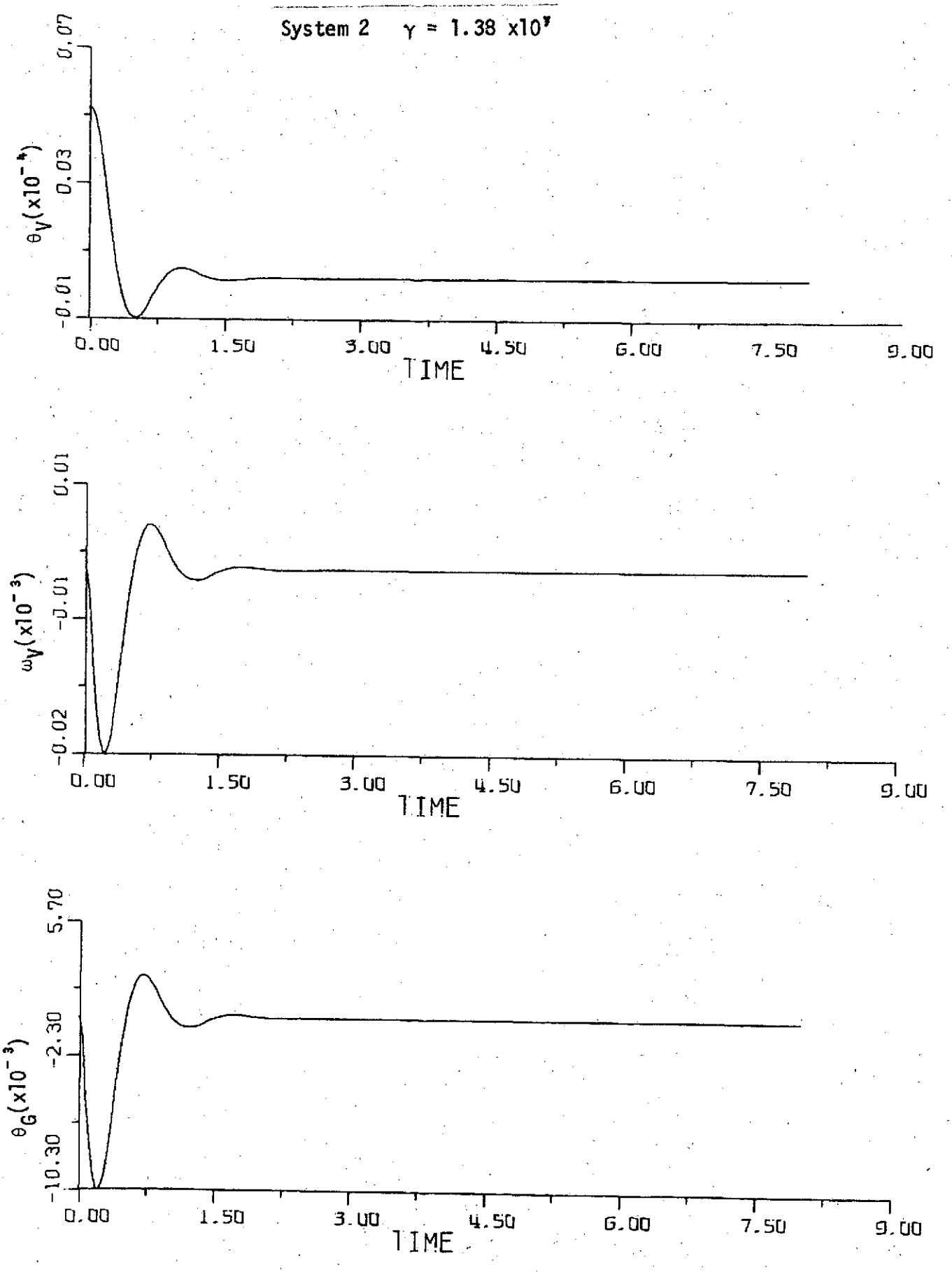
System 2 γ = 1.38 x10⁷
θV(x10⁻⁴)
0.07
0.03
-0.01
0.00
1.50
3.00
4.50
6.00
7.50
9.00
TIME
ωV(x10⁻³)
0.01
-0.01
-0.02
0.00
1.50
3.00
4.50
6.00
7.50
9.00
TIME
θG(x10⁻³)
5.70
-2.30
-10.30
0.00
1.50
3.00
4.50
6.00
7.50
9.00
TIME

Figure 6-6

System 2 $\gamma = 1.38 \times 10^7$

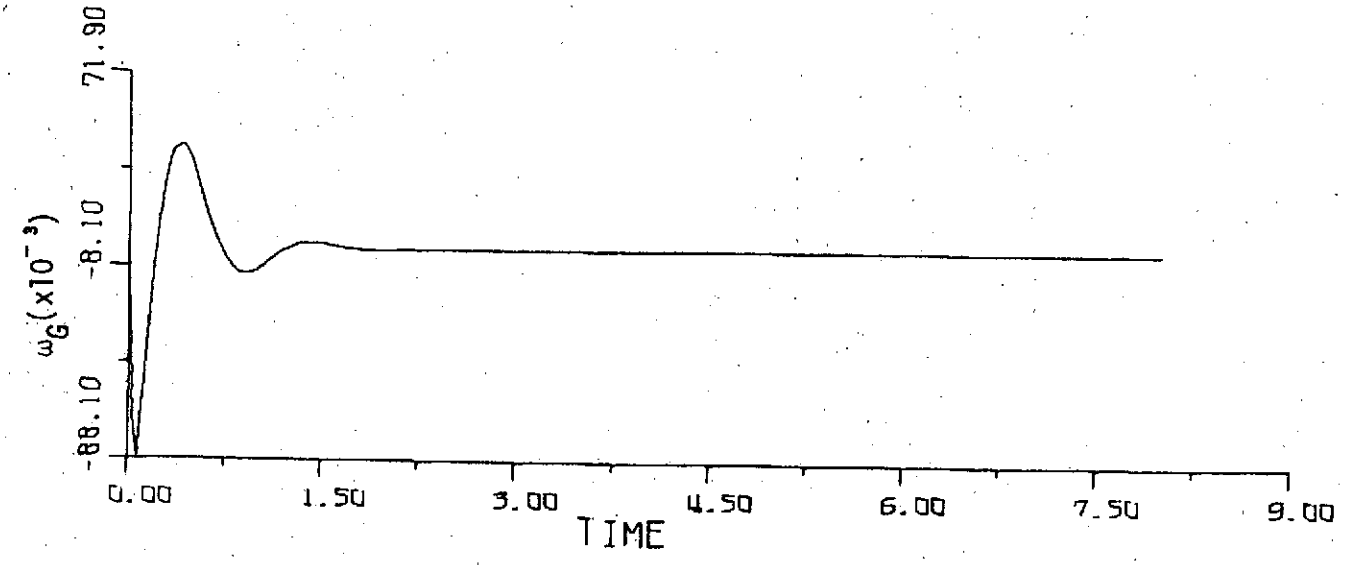

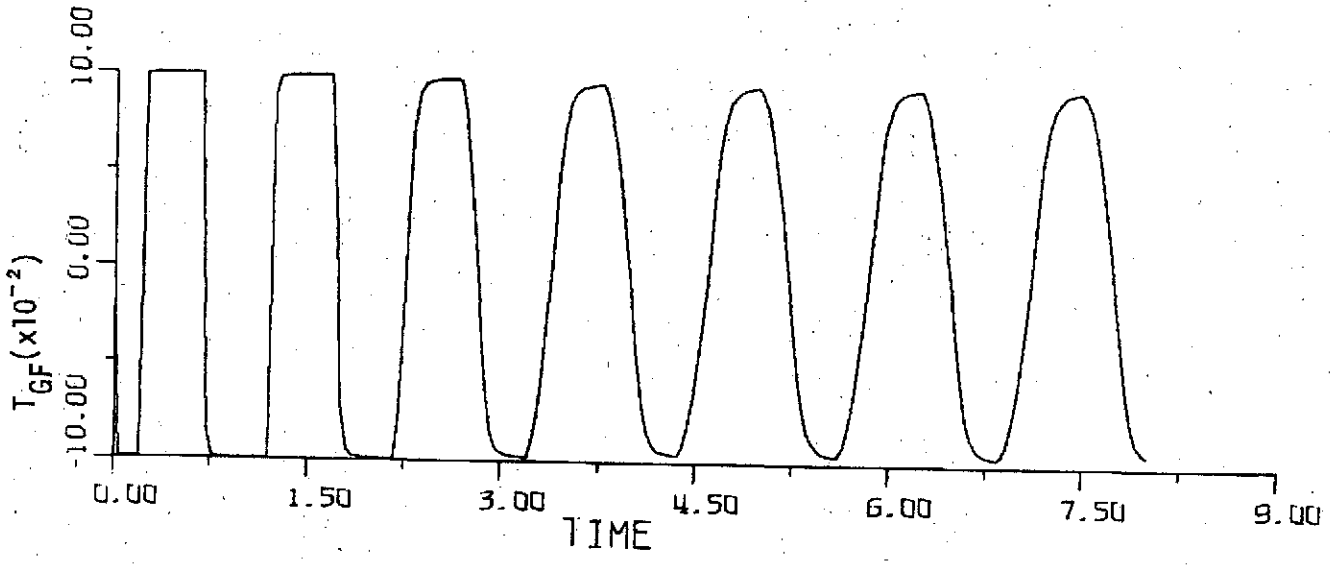

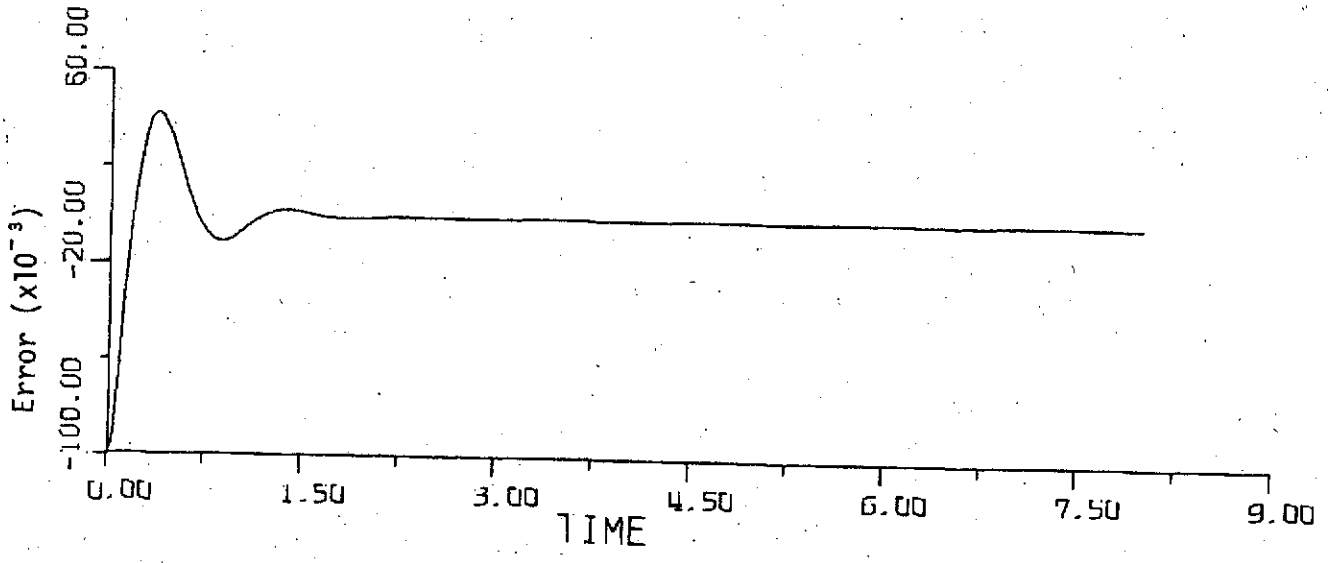

Figure 6-7

System 2 $\gamma = 1.38 \times 10^7$

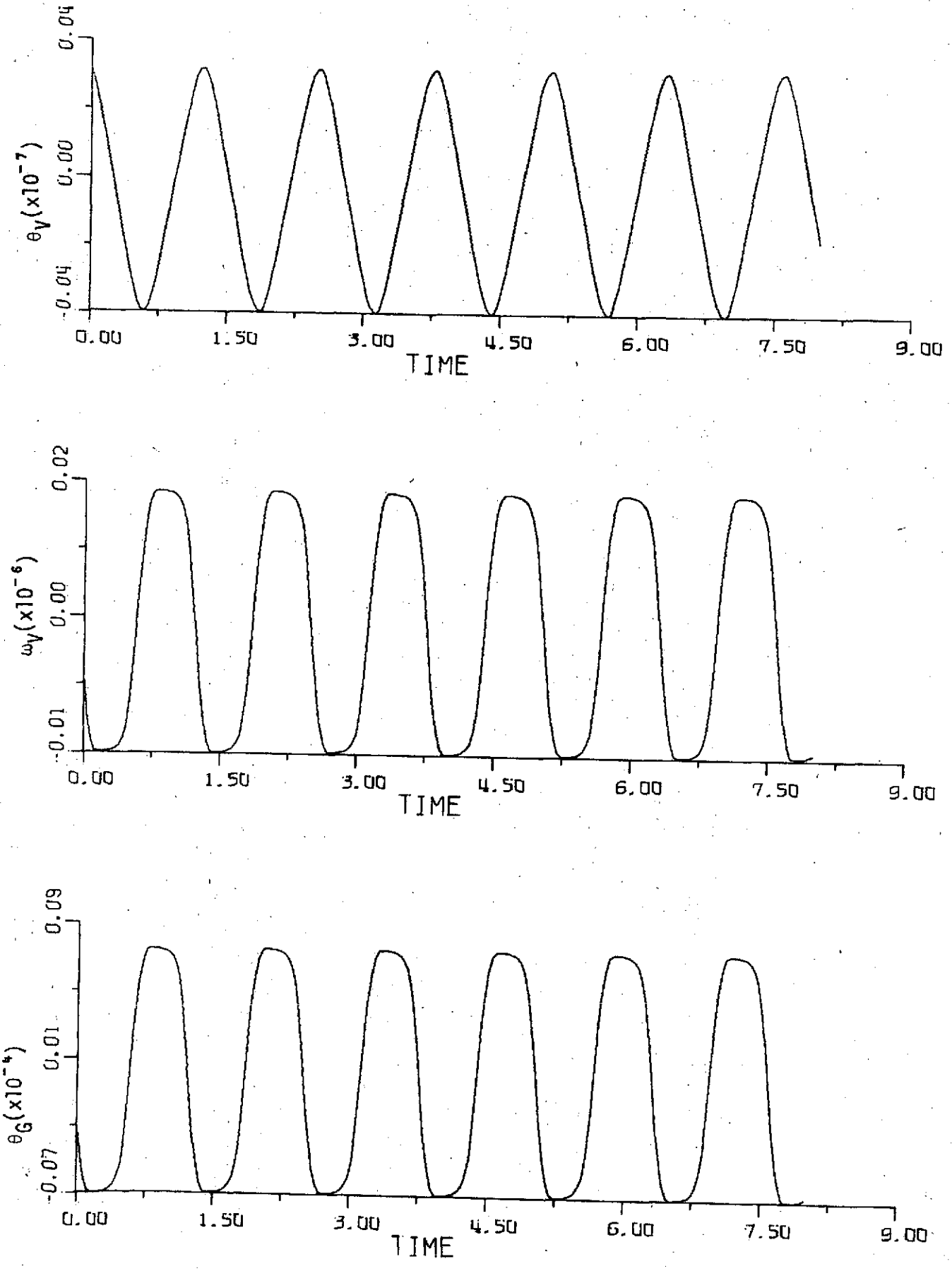

Figure 6-8

System 2 $\gamma = 1.38 \times 10^7$

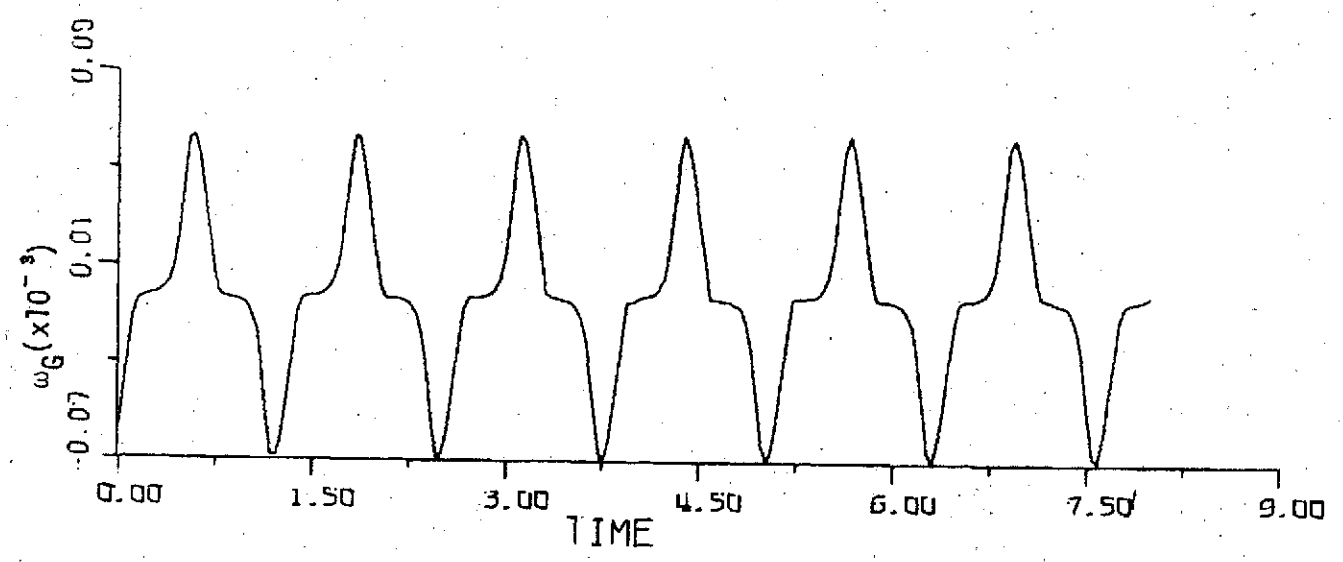

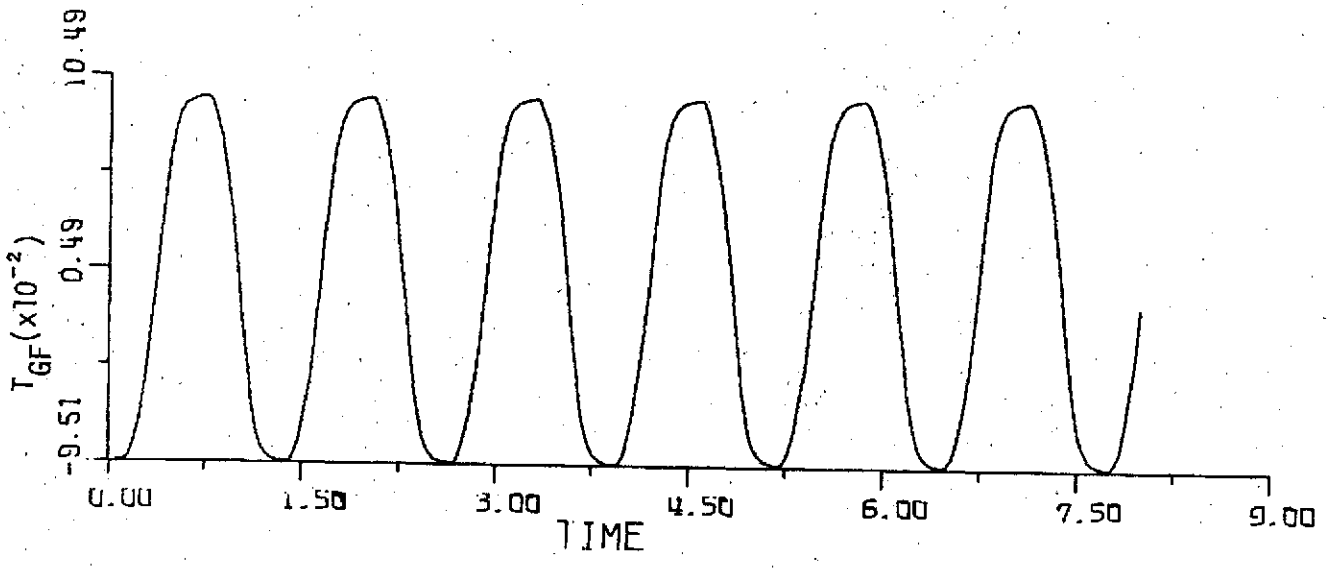

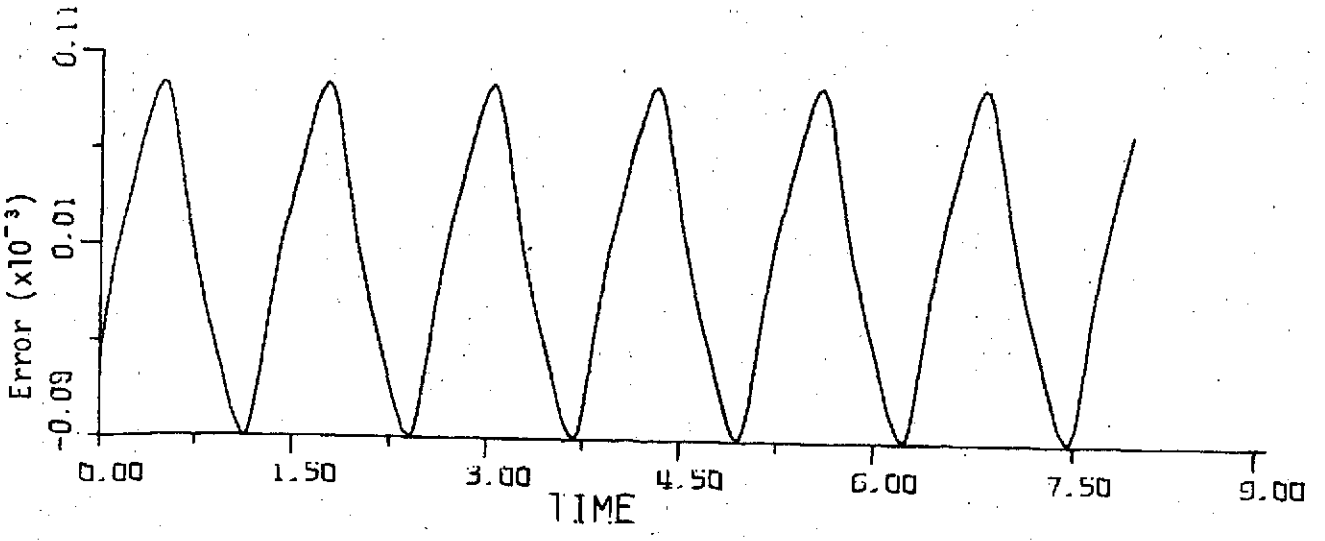

Figure 6-9

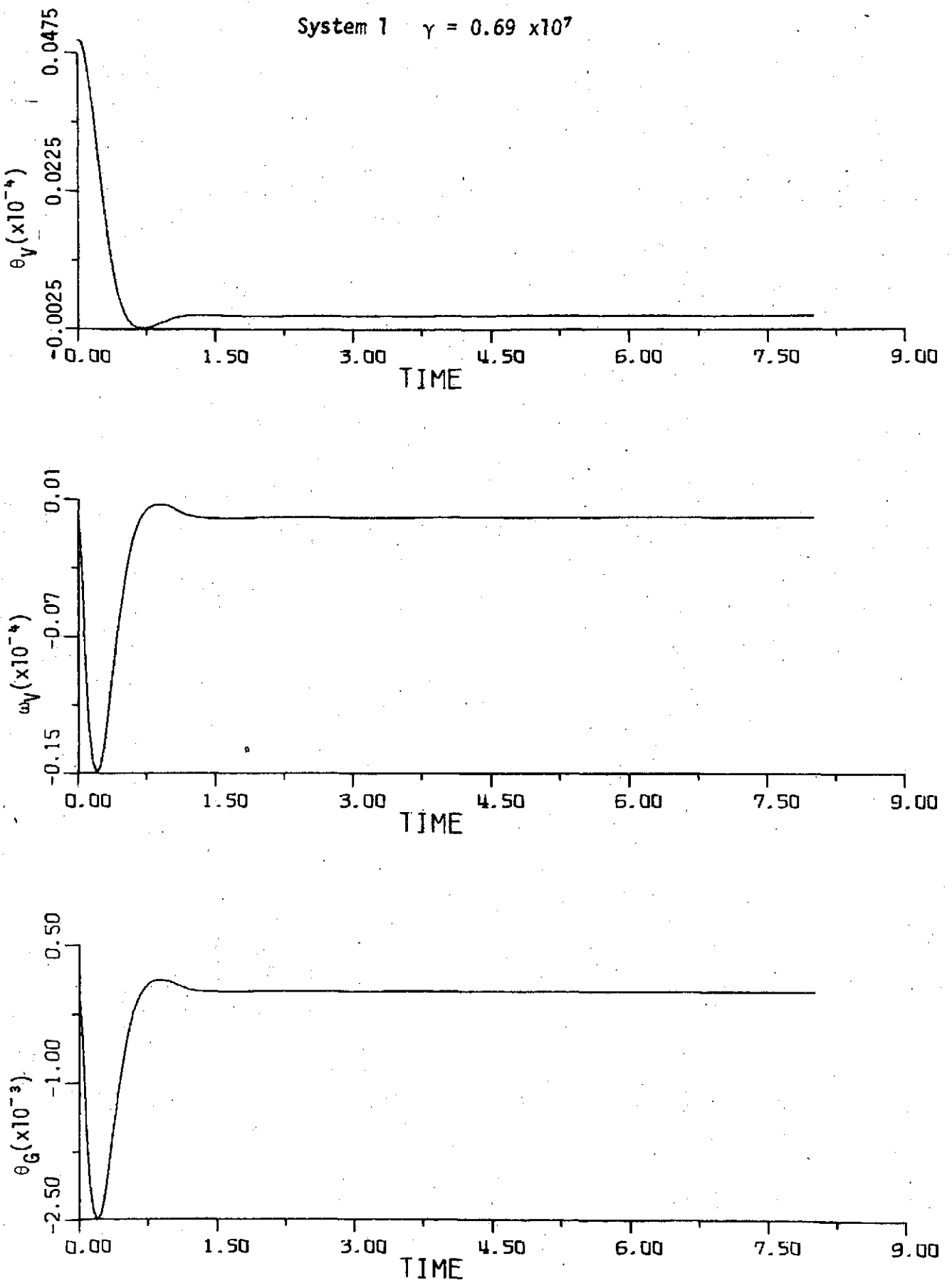
System 1 γ = 0.69 x10⁷
θV(x10⁻⁴)
0.0475
0.0225
-0.0025
0.00
1.50
3.00
4.50
6.00
7.50
9.00
TIME
ωV(x10⁻⁴)
0.01
-0.07
-0.15
0.00
1.50
3.00
4.50
6.00
7.50
9.00
TIME
θG(x10⁻³)
0.50
-1.00
-2.50
0.00
1.50
3.00
4.50
6.00
7.50
9.00
TIME

Figure 6-10

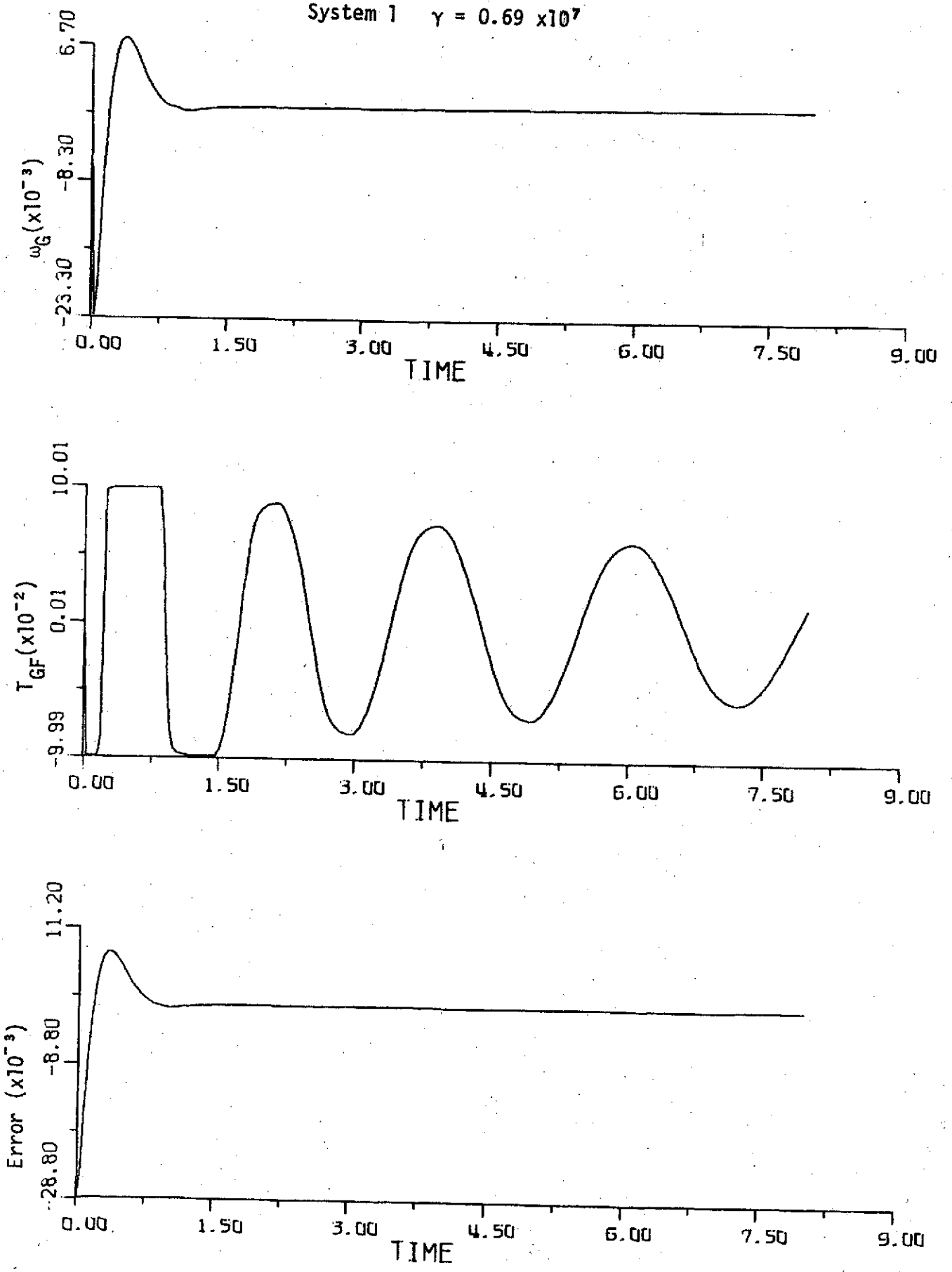
System 1 γ = 0.69 x10⁷
6.70
-8.30
-23.30
ω_G(x10⁻³)
0.00
1.50
3.00
4.50
6.00
7.50
9.00
TIME
10.01
0.01
-9.99
T_GF(x10⁻²)
0.00
1.50
3.00
4.50
6.00
7.50
9.00
TIME
11.20
-8.80
-28.80
Error (x10⁻³)
0.00
1.50
3.00
4.50
6.00
7.50
9.00
TIME

Figure 6-11

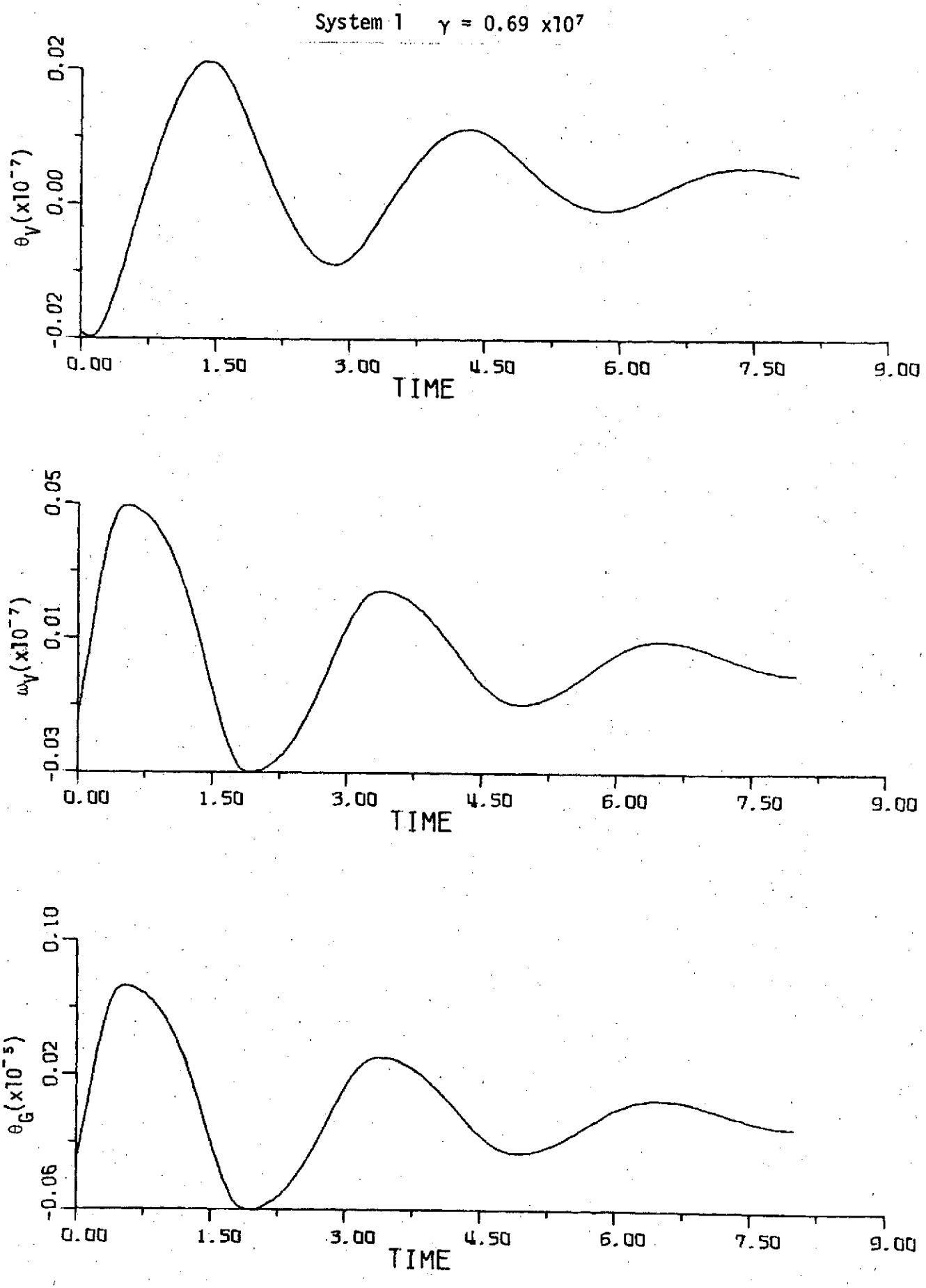
System 1 γ = 0.69 x10⁷
θV(x10⁻⁷)
0.02
0.00
-0.02
0.00
1.50
3.00
4.50
6.00
7.50
9.00
TIME
ωV(x10⁻⁷)
0.05
0.01
-0.03
0.00
1.50
3.00
4.50
6.00
7.50
9.00
TIME
θG(x10⁻⁵)
0.10
0.02
-0.06
0.00
1.50
3.00
4.50
6.00
7.50
9.00
TIME

Figure 6-12

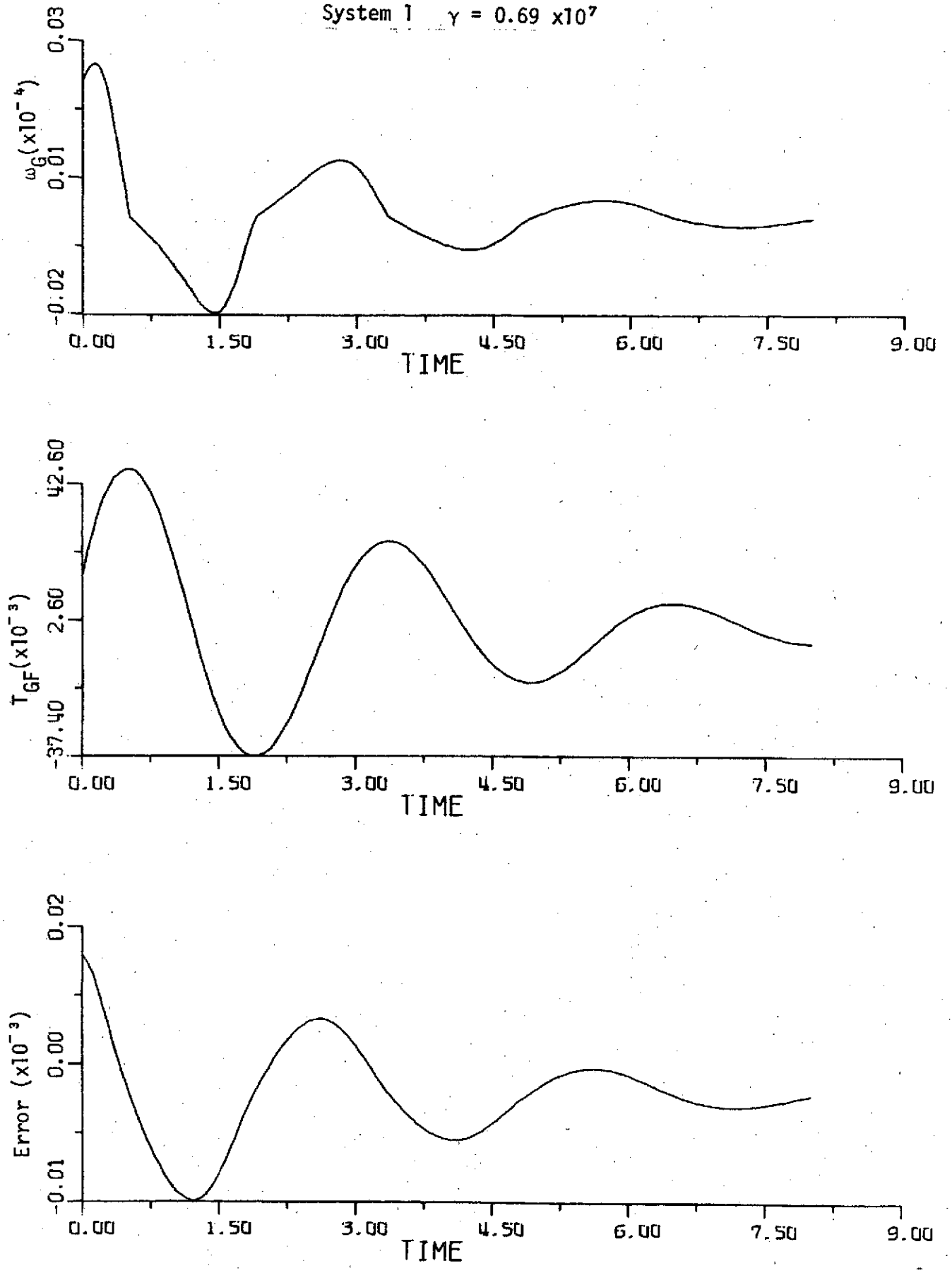
System 1 γ = 0.69 x10⁷
ω_G(x10⁻⁴)
0.03
0.01
-0.02
0.00
1.50
3.00
4.50
6.00
7.50
9.00
TIME
T_GF(x10⁻³)
42.60
2.60
-37.40
0.00
1.50
3.00
4.50
6.00
7.50
9.00
TIME
Error (x10⁻³)
0.02
0.00
-0.01
0.00
1.50
3.00
4.50
6.00
7.50
9.00
TIME

Figure 6-13

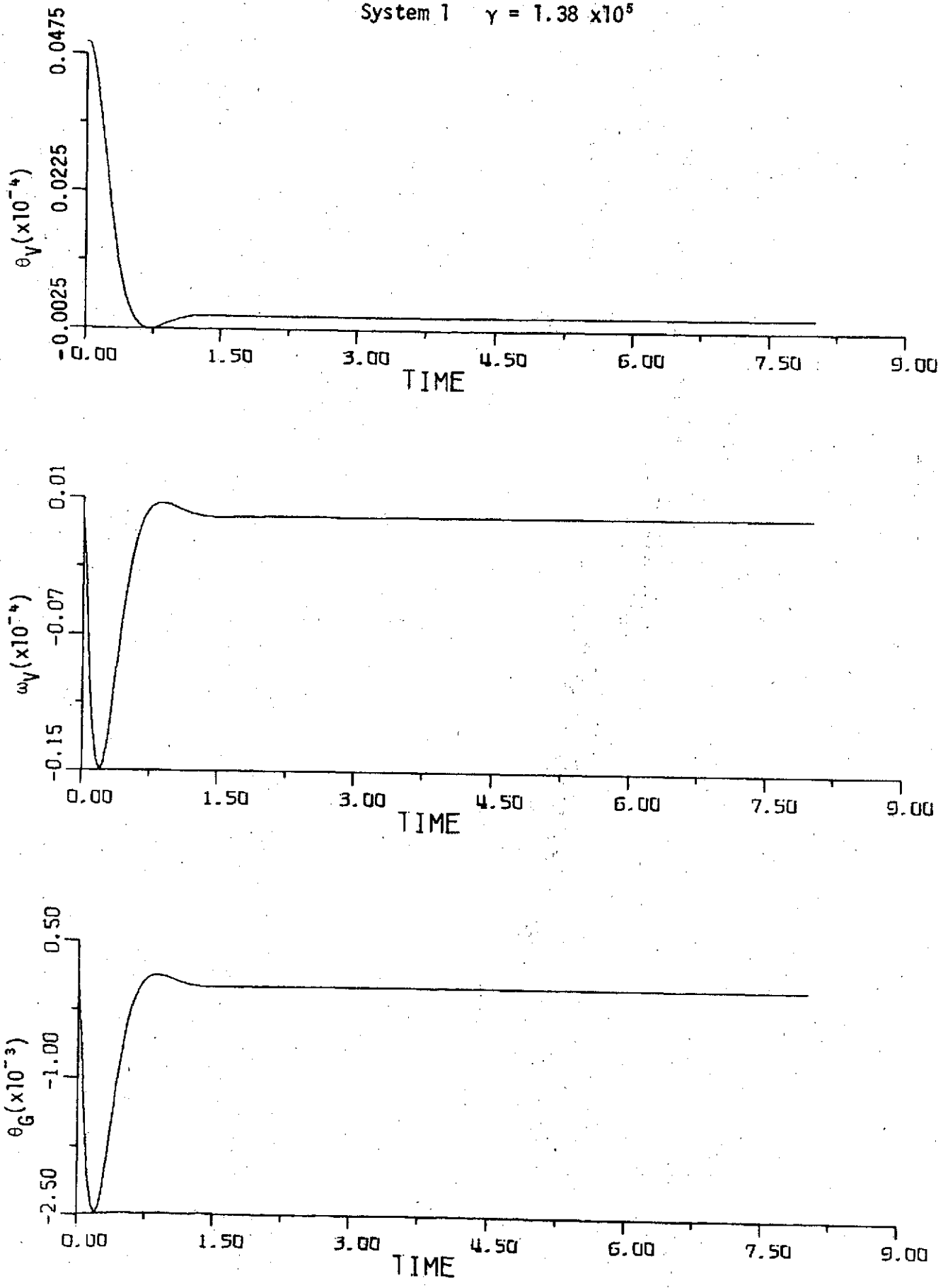
System 1 γ = 1.38 x10⁵
θV(x10⁻⁴)
0.0475
0.0225
-0.0025
0.00
1.50
3.00
4.50
6.00
7.50
9.00
TIME
ωV(x10⁻⁴)
0.01
-0.07
-0.15
0.00
1.50
3.00
4.50
6.00
7.50
9.00
TIME
θG(x10⁻³)
0.50
-1.00
-2.50
0.00
1.50
3.00
4.50
6.00
7.50
9.00
TIME

Figure 6-14

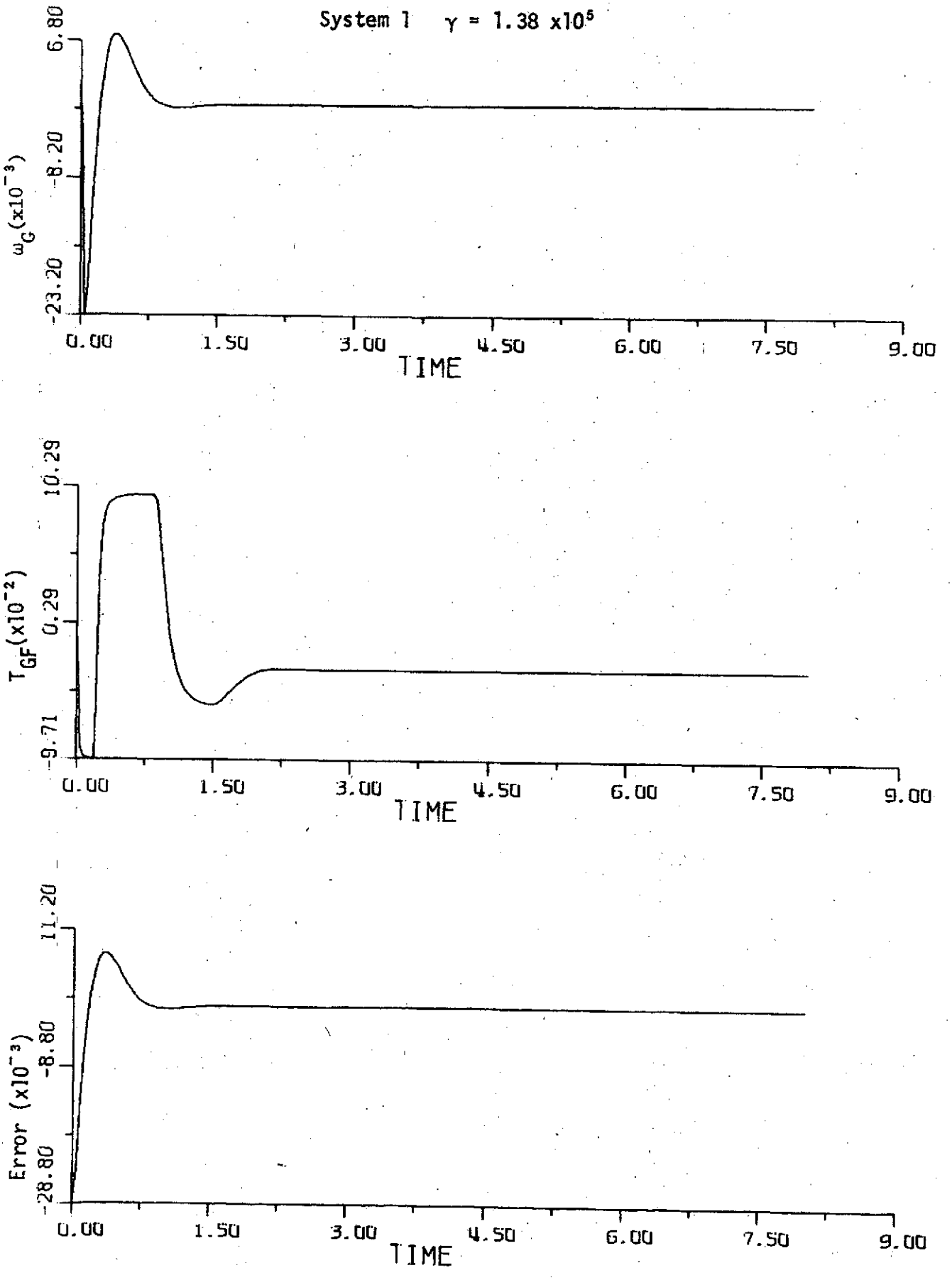
System 1 γ = 1.38 x10⁵
6.80
-8.20
-23.20
ω_G(x10⁻³)
0.00
1.50
3.00
4.50
6.00
7.50
9.00
TIME
10.29
0.29
-9.71
T_GF(x10⁻²)
0.00
1.50
3.00
4.50
6.00
7.50
9.00
TIME
11.20
-8.80
-28.80
Error (x10⁻³)
0.00
1.50
3.00
4.50
6.00
7.50
9.00
TIME

Figure 6-15

7. Transfer Functions of the Sampled-Data LST System

Since the actual LST system has sample-and-hold between the vehicle controller and the CMG controller, the system should be modelled as a sampled-data control system. Figure 7-1 shows the block diagram of the simplified LST system with sampled data. Since it is necessary to isolate the CMG nonlinearity from the linear dynamics for analytical purposes, a sample-and-hold is inserted in front of the nonlinearity as an approximation.

Referring to Figure 7-1, the following equations are written using e^*, θ_G^* and θ_V^* as outputs.

$$e^* = (G_1\chi)^* + N^*\left[\frac{G_{ho}G_1G_6G_7}{\Delta_0}\right]^* \theta_G^* - \left[\frac{G_{ho}G_1G_2G_3G_6G_7}{\Delta_0}\right]^* e^* \qquad (7\text{-}1)$$

$$\theta_G^* = -N^*\left[\frac{G_{ho}G_6}{s\Delta_0}\right]^* \theta_G^* + \left[\frac{G_{ho}G_2G_3G_6}{s\Delta_0}\right]^* e^* \qquad (7\text{-}2)$$

$$\theta_V^* = \left[\frac{G_{ho}G_2G_3G_6G_7}{\Delta_0}\right]^* e^* - N^*\left[\frac{G_{ho}G_6G_7}{\Delta_0}\right]^* \theta_G^* \qquad (7\text{-}3)$$

where the symbol * denotes the z-transform operation, and N^* represents the discrete describing function of the CMG frictional nonlinearity;

$$\Delta_0 = 1 + G_3G_6 \qquad (7\text{-}4)$$

Equations (7-1) through (7-3) are portrayed by the sampled signal flow graph of Figure 7-2. Applying Mason's gain formula to this flow graph yields the determinant of the graph as

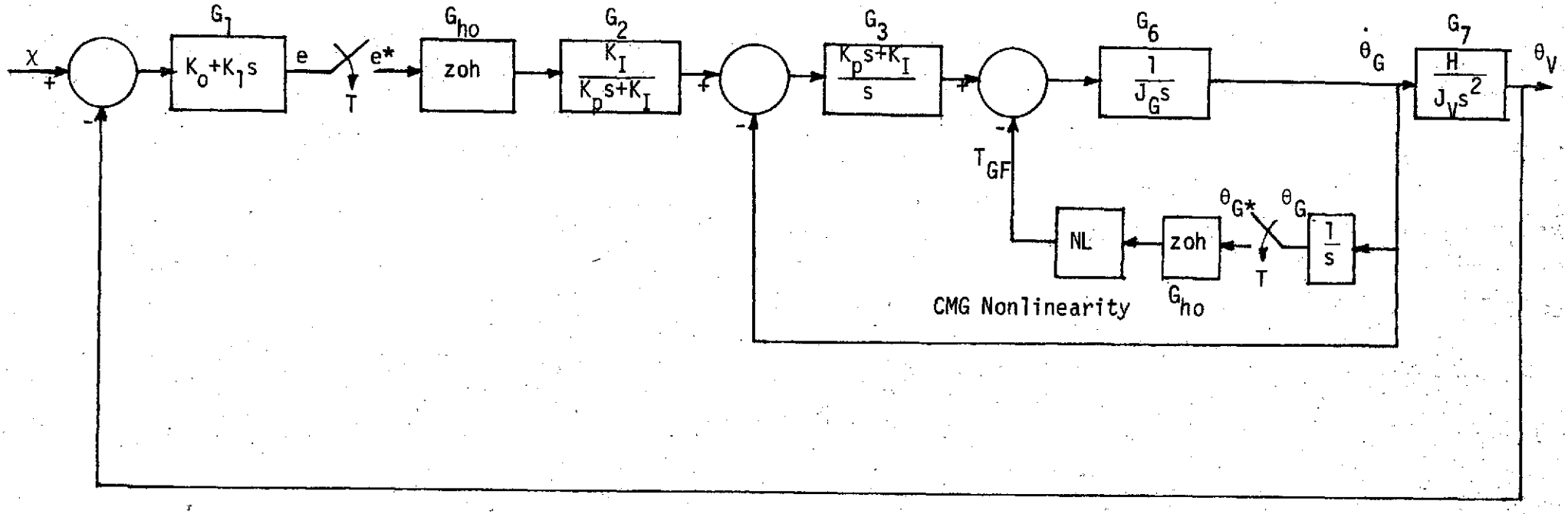

Figure 7-1. A block diagram of the simplified LST control system with sampled data

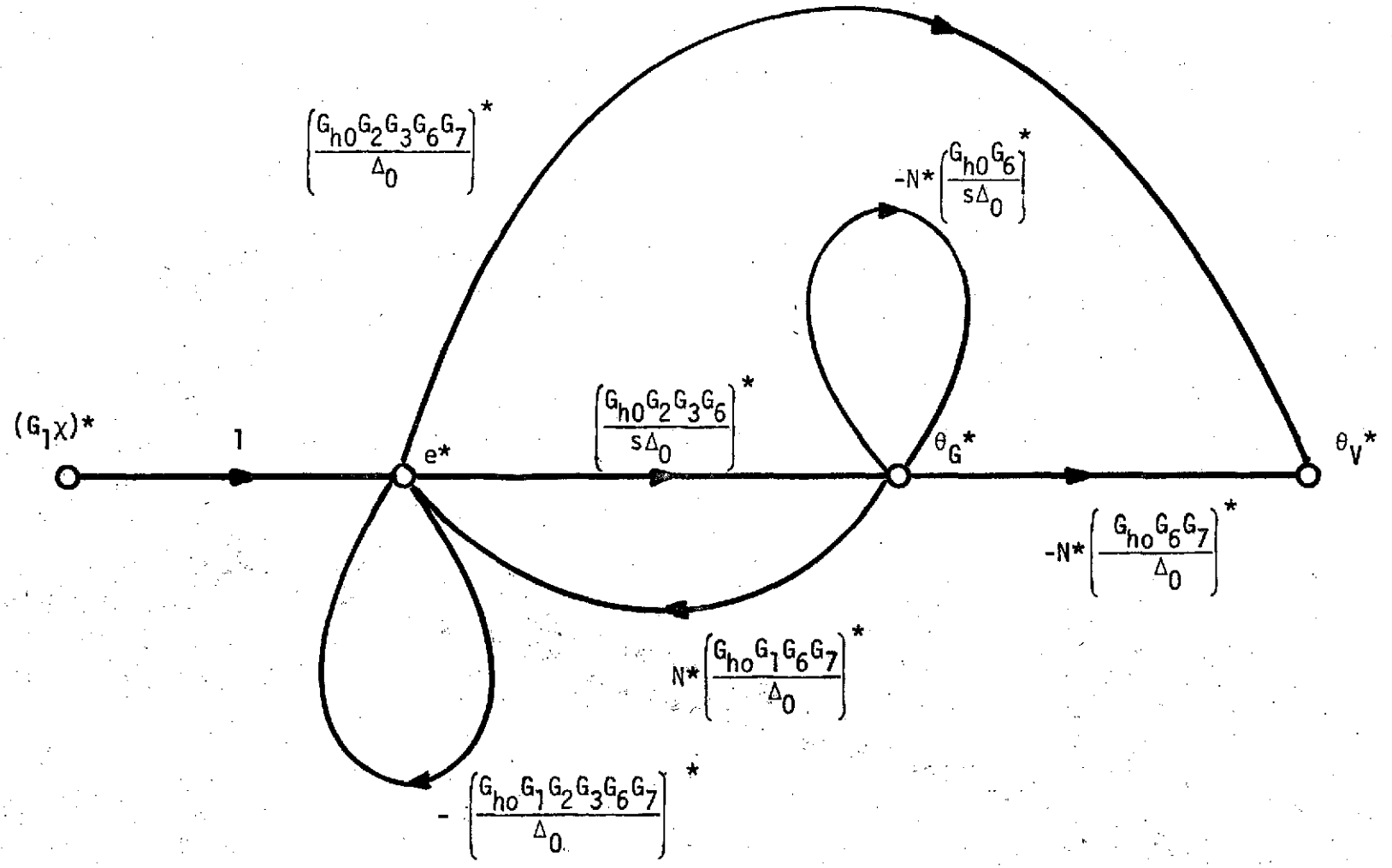

Figure 7-2. The Sampled Signal Flow Graph for the Equivalent System.

$$\Delta = 1 + N^*\left(\left[\frac{G_{ho}G_6}{s\Delta_0}\right]^* - \left[\frac{G_{ho}G_6G_7G_1}{\Delta_0}\right]^* \left[\frac{G_{ho}G_2G_3G_6}{s\Delta_0}\right]^* \right)$$

$$+ N^* \left[\frac{G_{ho}G_1G_2G_3G_6G_7}{\Delta_0}\right]^* \left[\frac{G_{ho}G_6}{s\Delta_0}\right]^* + \left[\frac{G_{ho}G_1G_2G_3G_6G_7}{\Delta_0}\right]^* \quad (7\text{-}5)$$

The last equation is put into the form of (with $N(z) = N^*$)

$$1 + N(z)G(z) = 0 \quad (7\text{-}6)$$

where

$$G(z) = \frac{A_1(z) - A_2(z)A_3(z) + A_4(z)A_1(z)}{1 + A_4(z)} \quad (7\text{-}7)$$

$$A_1(z) = (1-z^{-1})\mathcal{Z}\left[\frac{G_6}{s^2\Delta_0}\right] \quad (7\text{-}8)$$

$$A_2(z) = (1-z^{-1})\mathcal{Z}\left[\frac{G_6G_7G_1}{s\Delta_0}\right] \quad (7\text{-}9)$$

$$A_3(z) = (1-z^{-1})\mathcal{Z}\left[\frac{G_2G_3G_6}{s^2\Delta_0}\right] \quad (7\text{-}10)$$

$$A_4(z) = (1-z^{-1})\mathcal{Z}\left[\frac{G_1G_2G_3G_6G_7}{s\Delta_0}\right] \quad (7\text{-}11)$$

Substitution of the system transfer functions into the above expressions yields

$$\Delta_0 = \frac{J_G s^2 + K_p s + K_I}{J_G s^2} \quad (7\text{-}12)$$

$$A_1(z) = (1-z^{-1})\mathcal{Z}\left[\frac{1}{J_G s^3 + K_p s^2 + K_I s}\right] \quad (7\text{-}13)$$

$$A_2(z) = (1-z^{-1})\mathcal{Z}\left[\frac{H(K_0 + K_1 s)}{J_V s^2 (J_G s^2 + K_p s + K_I)}\right] \quad (7\text{-}14)$$

$$A_3(z) = (1-z^{-1})\mathcal{Z}\left[\frac{K_I}{s^2(J_G s^2+K_p s+K_I)}\right] \tag{7-15}$$

$$A_4(z) = (1-z^{-1})\mathcal{Z}\left[\frac{K_I H(K_0+K_1 s)}{J_V s^3(J_G s^2+K_p s+K_I)}\right] \tag{7-16}$$

The following system parameters are used for System 1:

$H = 600$ ft-lb-sec

$J_G = 2.1$ ft-lb-sec^2

$K_0 = 5.75835 \times 10^3$

$K_1 = 1.37102 \times 10^3$

$K_p = 216$ ft-lb/rad/sec

$K_I = 9700$ ft-lb/rad

$J_V = 10^5$ ft-lb-sec^2

Taking the z-transforms of the functions inside the brackets in Eqs. (7-13) through (7-16), we have the following results:

$$A_1(z) = A_{13} + A_{14}\frac{z-1}{z-e^{aT}} + A_{15}\frac{z-1}{z-e^{\bar{a}T}} \tag{7-17}$$

$a = -51.429993 - j44.42923$

$\bar{a} = -51.429993 + j44.42923$

$A_{13} = 1.0309376 \times 10^{-4}$

$A_{14} = -5.15469 \times 10^{-5} - j5.9669183 \times 10^{-5}$

$A_{15} = -5.15469 \times 10^{-5} + j5.9669183 \times 10^{-5}$

$$A_2(z) = A_{22}\frac{T}{z-1} + A_{23} + A_{24}\frac{z-1}{z-e^{aT}} + A_{25}\frac{z-1}{z-e^{\bar{a}T}} \tag{7-18}$$

$$A_{22} = 3.5616776 \times 10^{-3}$$

$$A_{23} = 7.6870434 \times 10^{-4}$$

$$A_{24} = -3.8435217 \times 10^{-4} - j4.8499764 \times 10^{-4}$$

$$A_{25} = 3.8435217 \times 10^{-4} + j4.8499764 \times 10^{-4}$$

$$A_3(z) = A_{32} \frac{T}{z-1} + A_{33} + A_{34} \frac{z-1}{z-e^{aT}} + A_{35} \frac{z-1}{z-e^{\overline{aT}}} \qquad (7\text{-}19)$$

$$A_{32} = 1.0$$

$$A_{33} = -2.2268891 \times 10^{-2}$$

$$A_{34} = 1.1134446 \times 10^{-2} + j1.6350537 \times 10^{-3}$$

$$A_{35} = 1.1134446 \times 10^{-2} - j1.6350537 \times 10^{-3}$$

$$A_4(z) = A_{41} \frac{T^2(z+1)}{2(z-1)^2} + A_{42} \frac{T}{z-1} + A_{43} + A_{44} \frac{z-1}{z-e^{aT}} + A_{45} \frac{z-1}{z-e^{\overline{aT}}} \qquad (7\text{-}20)$$

$$A_{41} = 34.54837$$

$$A_{42} = 7.4564409$$

$$A_{43} = -0.17352653$$

$$A_{44} = 8.6763263 \times 10^{-2} + j1.6520832 \times 10^{-2}$$

$$A_{45} = 8.6763263 \times 10^{-2} - j1.6520832 \times 10^{-2}$$

The following system parameters are used for System 2. The same expressions for $A_1(z)$, $A_2(z)$, $A_3(z)$ and $A_4(z)$ are preserved.

$$H = 200 \text{ ft-lb-sec}$$

$$J_G = 3.7 \text{ ft-lb-sec}^2$$

$$K_0 = 2 \times 10^4$$

$$K_1 = 3 \times 10^3$$

$K_p = 280$ ft-lb/rad/sec

$K_I = 10^4$ ft-lb/rad

$J_V = 10^5$ ft-lb-sec^2

The corresponding coefficients in Eqs. (7-17) through (7-20) are

$$a = -37.83783 - j35.651077$$

$$\bar{a} = -37.83783 + j35.651077$$

$$A_{13} = 9.9999976 \times 10^{-5}$$

$$A_{14} = -4.9999973 \times 10^{-5} - j5.3066848 \times 10^{-5}$$

$$A_{15} = -4.9999973 \times 10^{-5} + j5.3066848 \times 10^{-5}$$

$$A_{22} = 3.9999932 \times 10^{-3}$$

$$A_{23} = 4.8799929 \times 10^{-4}$$

$$A_{24} = -2.43997 \times 10^{-4} - j3.150655 \times 10^{-4}$$

$$A_{25} = -2.43997 \times 10^{-4} + j3.150655 \times 10^{-4}$$

$$A_{32} = 9.9999982 \times 10^{-1}$$

$$A_{33} = -2.8 \times 10^{-2}$$

$$A_{34} = 1.4000002 \times 10^{-2} + j8.3391555 \times 10^{-4}$$

$$A_{35} = 1.4000002 \times 10^{-2} - j8.3391555 \times 10^{-4}$$

$$A_{41} = 39.999985$$

$$A_{42} = 4.8800011$$

$$A_{43} = -1.5144014 \times 10^{-1}$$

$$A_{44} = 7.5720072 \times 10^{-2} + j1.1923421 \times 10^{-2}$$

$$A_{45} = 7.5720072 \times 10^{-2} - j1.1923421 \times 10^{-2}$$

It can be shown that if T approaches zero, the z-transfer function G(z) in Eq. (7-7) reverts to that of the continuous transfer function G(s) of Eq. (1-16).

The G(z) plots for system 1 and 2 are shown in Figures 7-3 through 7-6. Since these plots are to be used for predicting the existence of self-sustained oscillations in the sampled-data system, the frequency of oscillations is expressed as an integral multiple of the sampling period T. Thus, the frequency of oscillation is represented as

$$\omega_c = \frac{2\pi}{NT} \tag{7-21}$$

for N = 2, 3, ...

The various plots of each system correspond to different values of N, with T as a parameter. Figures 7-3 and 7-5 are for lower values of T where as Figures 7-4 and 7-6 are for higher values of T.

Notice that for large N and small T, the G(z) curves approach that of the continuous system transfer function G(s).

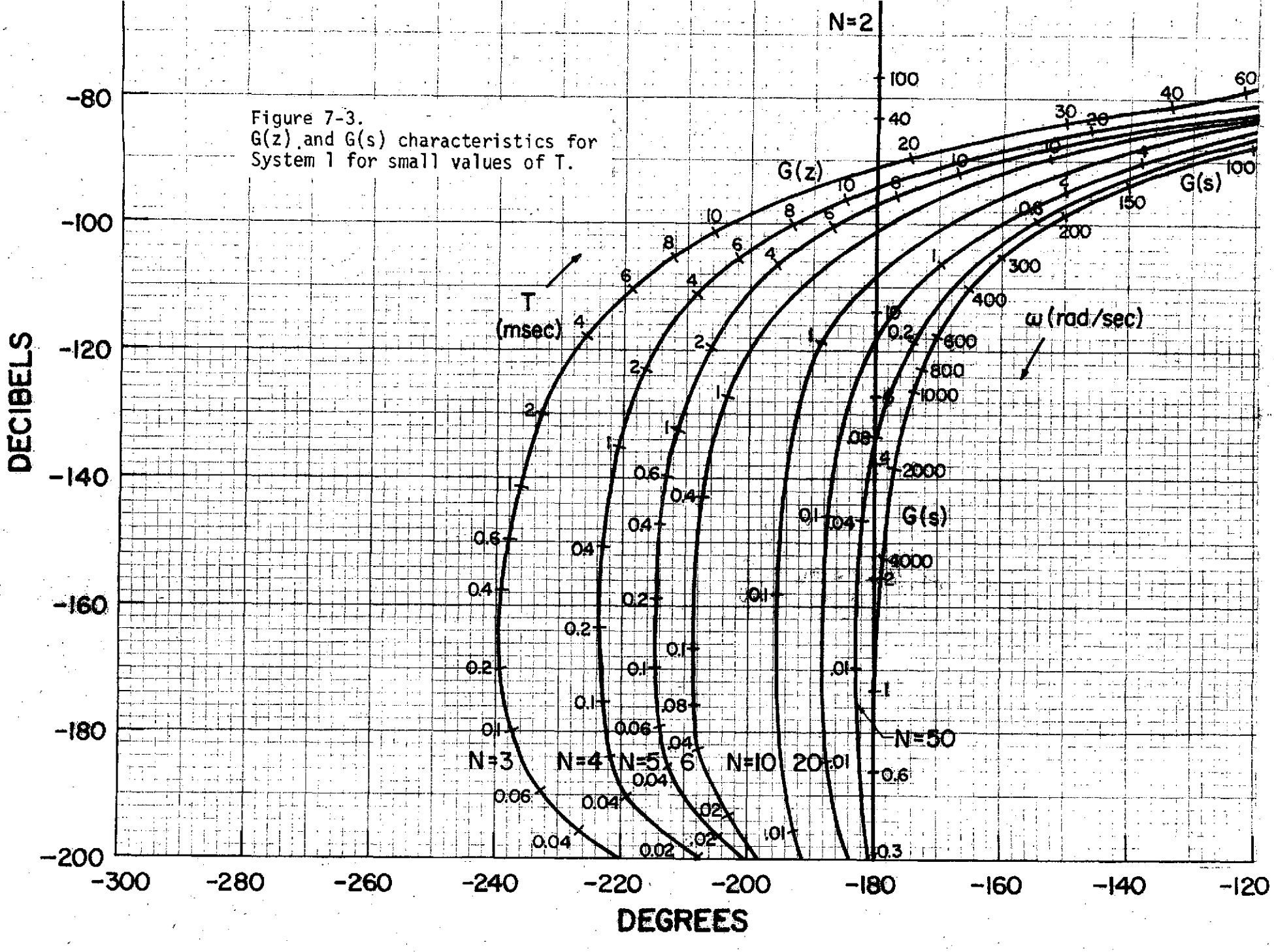

Figure 7-3.
G(z) and G(s) characteristics for System 1 for small values of T.

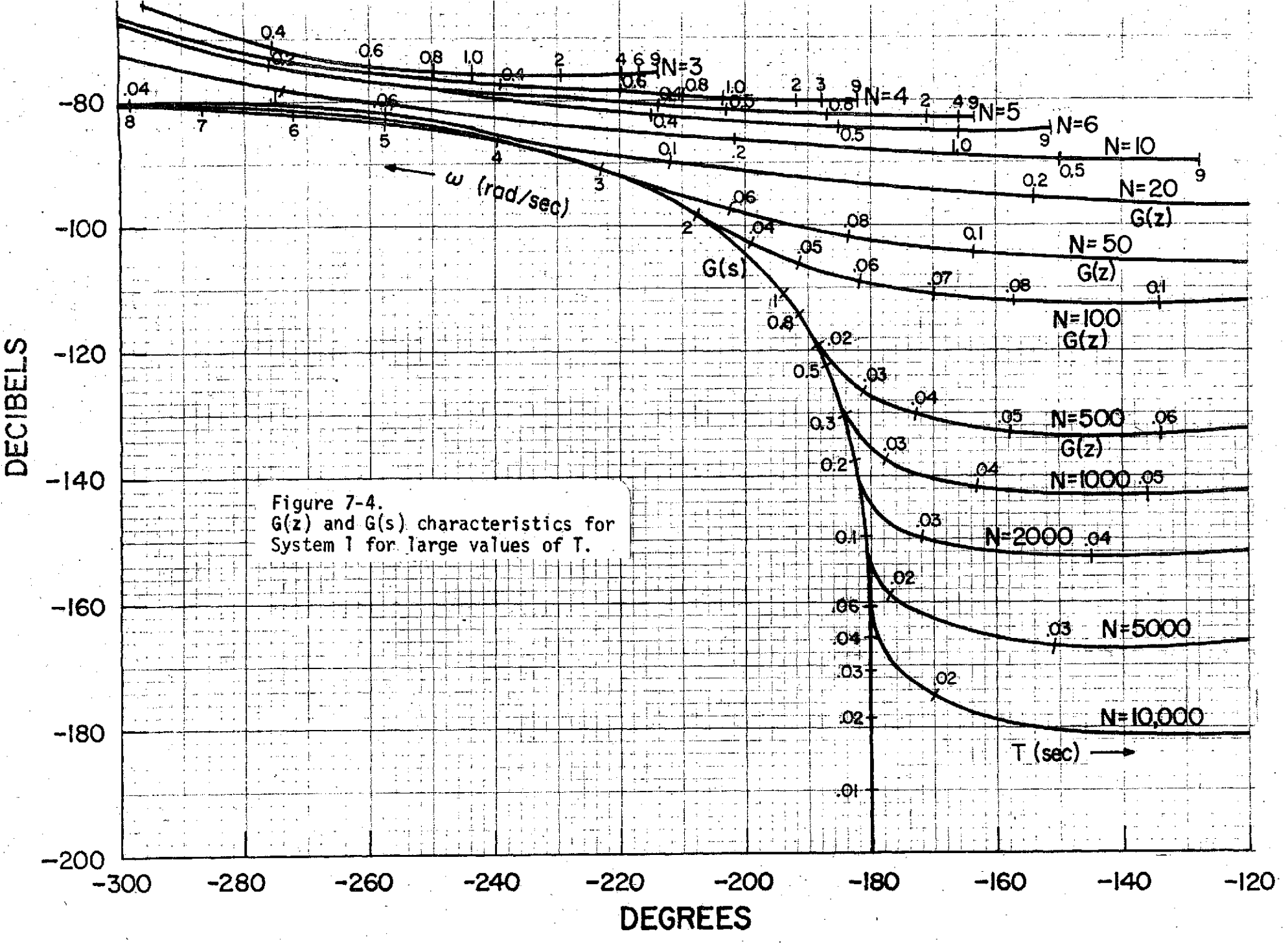

Figure 7-4.
G(z) and G(s) characteristics for System 1 for large values of T.

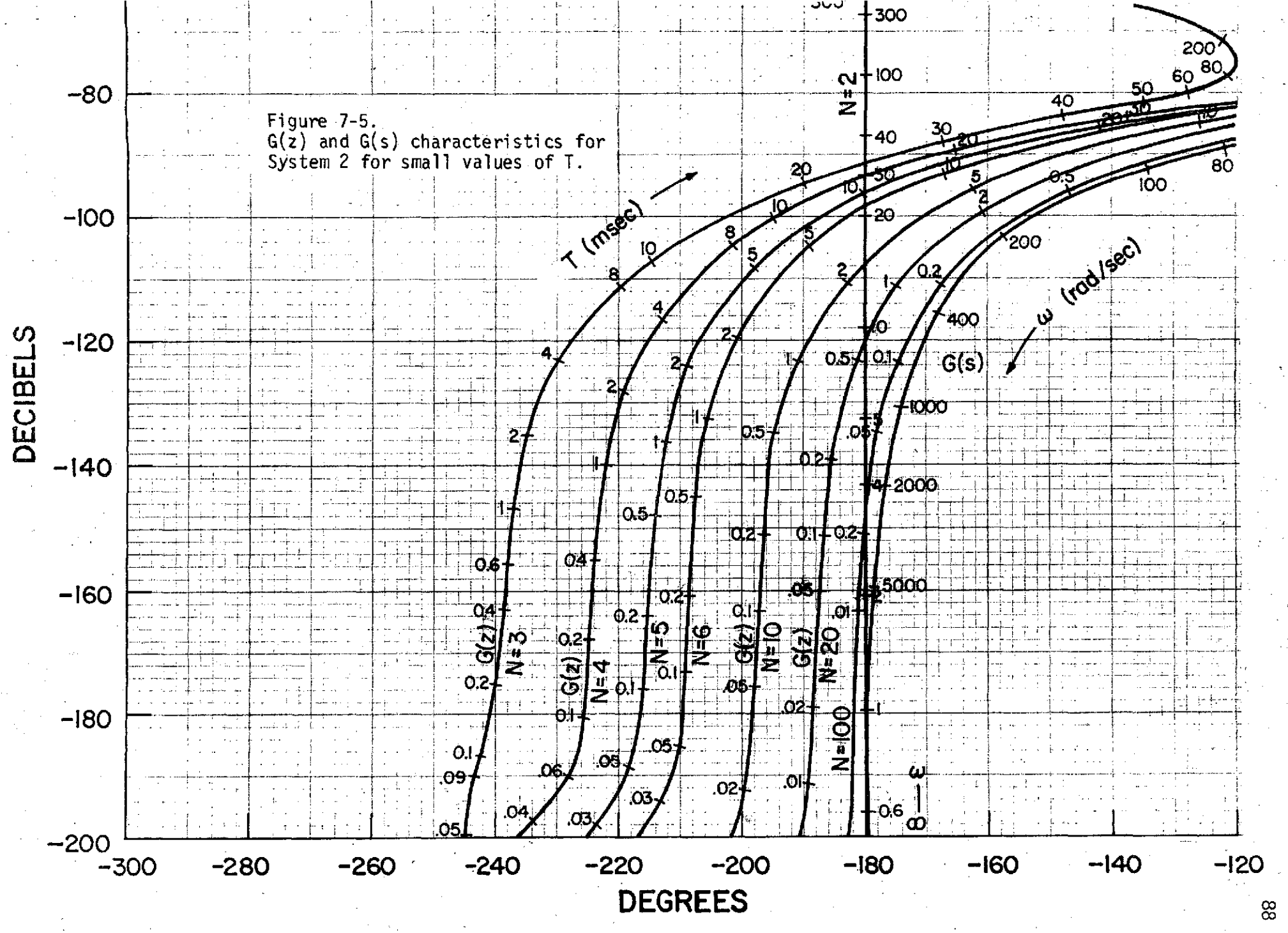

Figure 7-5.
G(z) and G(s) characteristics for System 2 for small values of T.

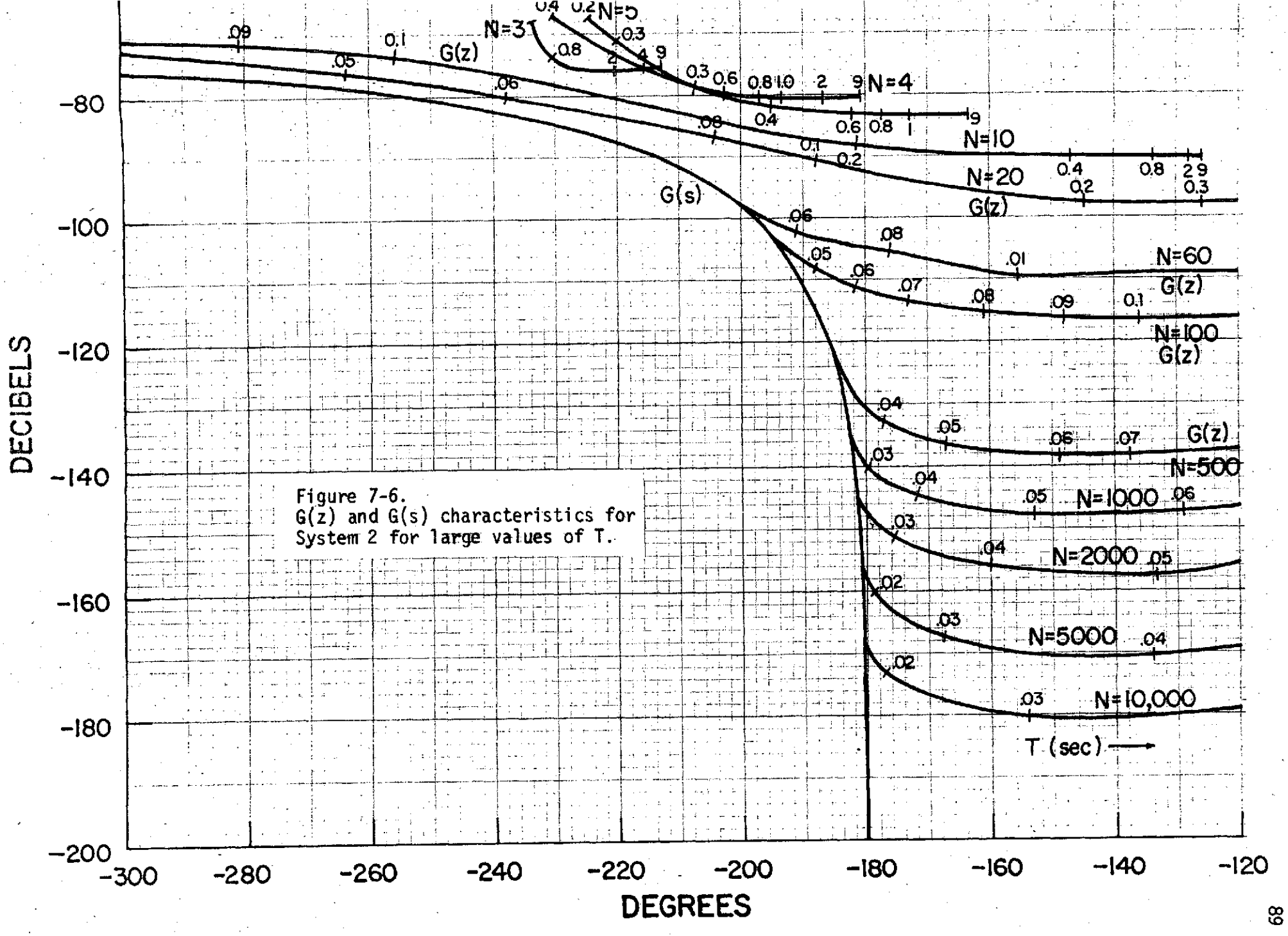

Figure 7-6.
G(z) and G(s) characteristics for System 2 for large values of T.

8. The Discrete Describing Function of the CMG Frictional Nonlinearity

In order to study the condition of self-sustained oscillations of the LST system with sampled data, it is necessary to evaluate the discrete describing function of the CMG frictional nonlinearity, $N(z)$.

The first step in the derivation of $N(z)$ involves the interchanging of the positions of the nonlinearity and the zero-order hold in Figure 8-1a. This step is justified since the nonlinearity is amplitude dependent only, so that the signal of T_{GF} is not affected by this interchange. Figure 8-1b illustrates the transposition between NL and zoh.

The second step involves the assumption that θ_G is sinusoidal; that is,

$$\theta_G(t) = A\cos(\omega t + \phi) \tag{8-1}$$

where A, ω, and ϕ denote the amplitude, the frequency in radians, and the phase in degrees of the sinusoid, respectively.

The z-transform of $\theta_G(t)$ is

$$\theta_G(z) = \sum_{k=0}^{\infty} A\cos\left(\frac{2\pi k}{N} + \phi\right)z^{-k} \tag{8-2}$$

or in closed form,

$$\theta_G(z) = \frac{Az\left[\left(z - \cos\frac{2\pi}{N}\right)\cos\phi - \sin\frac{2\pi}{N}\sin\phi\right]}{z^2 - 2z\cos\frac{2\pi}{N} + 1} \tag{8-3}$$

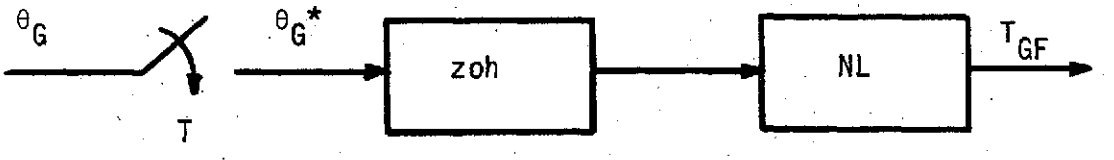

(a)

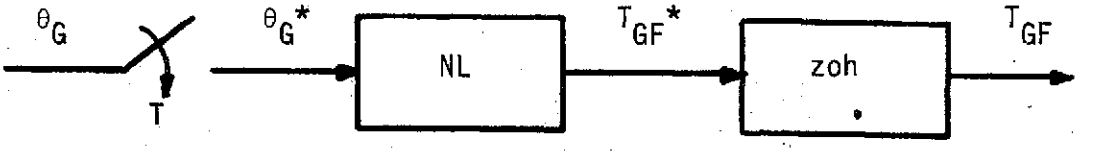

(b)

Figure 8-1

An important consideration is that because of the periodic nature of the sampler, $\theta_G(t)$, $\theta_G^*(t)$, and $T_{GF}^*(t)$ are all periodic functions of period NT, where N is a positive integer ≥ 2. Therefore, $\omega = 2\pi/NT$, and $\omega T = 2\pi/N$.

The output of the nonlinearity in Figure 8-1b is denoted by $T_{GF}^*(t)$, and its z-transform is $T_{GF}(z)$. The discrete describing function (DDF) of the nonlinearity is defined as

$$N(z) = \frac{T_{GF}(z)}{\theta_G(z)} \tag{8-4}$$

It turns out that the discrete describing function (DDF) for N = 2 must be derived separately, and a general expression for N(z) can be obtained for all $N \geq 3$.

The DDF for N = 2

Let $T_{GF}(kT)$ denote the value of $T_{GF}^*(t)$ at t = kT. For N = 2, the signal $T_{GF}^*(t)$ is a periodic function with a period of 2T. The z-transform of $T_{GF}^*(t)$ is written

$$T_{GF}(z) = T_{GF}(0)(1 + z^{-2} + z^{-4} + \ldots) + T_{GF}(T)(z^{-1} + z^{-3} + \ldots)$$

$$= \frac{T_{GF}(0)z^2 + T_{GF}(T)z}{z^2 - 1} \tag{8-5}$$

For the CMG frictional nonlinearity, it has been established in chapter 2 that

$$T_{GF}(t) = T_{GF0}\frac{\frac{R}{R+1} - \frac{a}{2}[1 - \cos(\omega t + \phi)]}{\frac{1}{R+1} + \frac{a}{2}[1 - \cos(\omega t + \phi)]} \qquad \dot{\theta}_G \leq 0 \tag{8-6}$$

$$T_{GF}(t) = T_{GFO}\frac{\frac{R}{R-1} + \frac{a}{2}[1 - \cos(\omega t + \phi)]}{\frac{1}{R-1} + \frac{a}{2}[1 - \cos(\omega t + \phi)]} \qquad \dot{\theta} \geq 0 \quad (8\text{-}7)$$

Let us introduce the following notation:

$$T_{GF}^{-}(kT) = T_{GF}(t)\Big|_{t=kT} \qquad \dot{\theta}_G \leq 0 \quad (8\text{-}8)$$

$$T_{GF}^{+}(kT) = T_{GF}(t)\Big|_{t=kT} \qquad \dot{\theta}_G \geq 0 \quad (8\text{-}9)$$

We have,

$$T_{GF}^{-}(kT) = T_{GFO}\frac{\frac{R}{R+1} - \frac{a}{2}[1 - \cos(\frac{2\pi k}{N} + \phi)]}{\frac{1}{R+1} + \frac{a}{2}[1 - \cos(\frac{2\pi k}{N} + \phi)]} \quad \dot{\theta}_G \leq 0 \quad (8\text{-}10)$$

$$T_{GF}^{+}(kT) = T_{GFO}\frac{\frac{R}{R-1} + \frac{a}{2}[1 - \cos(\frac{2\pi k}{N} + \phi)]}{\frac{1}{R-1} + \frac{a}{2}[1 - \cos(\frac{2\pi k}{N} + \phi)]} \quad \dot{\theta}_G \geq 0 \quad (8\text{-}11)$$

For N = 2, $(\phi \neq \pm \pi/2)$

$$\begin{aligned} T_{GF}(0) &= T_{GF}^{-}(0) && 0 \leq \phi < \pi \\ &= T_{GF}^{+}(0) && \pi \leq \phi < 2\pi \\ T_{GF}(T) &= T_{GF}^{+}(T) && 0 \leq \phi < \pi \\ &= T_{GF}^{-}(T) && \pi \leq \phi < 2\pi \end{aligned} \qquad (8\text{-}12)$$

Substituting N = 2 into Eq. (8-3), we have

$$\theta_G(z) = \frac{Az\cos\phi}{z + 1} \tag{8-13}$$

Using Eqs. (8-5) and (8-13), the DDF for N = 2 is determined,

$$N(z) = \frac{T_{GF}(0)z + T_{GF}(T)}{A(z - 1)\cos\phi} \tag{8-14}$$

Also, for N = 2, z = -1, the last equation becomes

$$N(z) = \frac{T_{GF}(0) - T_{GF}(T)}{2A\cos\phi} \tag{8-15}$$

For stability analysis, we define

$$F(z) = -\frac{1}{N(z)} = \frac{2A\cos\phi}{T_{GF}(T) - T_{GF}(0)} \tag{8-16}$$

The DDF for $N \geq 3$

In general, the z-transform of the output of the nonlinearity may be written as

$$T_{GF}(z) = \sum_{m=0}^{\infty} \sum_{k=0}^{N-1} T_{GF}(kT)z^{-k-mN}$$

$$= \frac{\sum_{k=0}^{N-1} T_{GF}(kT)z^{N-k}}{z^N - 1} \tag{8-17}$$

Using Eq. (8-2) for $\theta_G(z)$, the discrete describing function N(z) is written

$$N(z) = \frac{T_{GF}(z)}{\theta_G(z)} = \frac{\sum_{k=0}^{N-1} T_{GF}(kT)z^{N-k}}{(z^N - 1)\sum_{k=0}^{\infty} A\cos(\frac{2\pi k}{N} + \phi)z^{-k}} \tag{8-18}$$

The denominator of N(z) may be simplified as follows:

$$(z^N - 1)\sum_{k=0}^{\infty} A\cos(\frac{2\pi k}{N} + \phi)z^{-k} = A\sum_{k=0}^{\infty} z^{N-k}\cos(\frac{2\pi k}{N} + \phi) - A\sum_{k=0}^{\infty} z^{-k}\cos(\frac{2\pi k}{N} + \phi)$$

$$= A\sum_{k=0}^{N-1} \cos(\frac{2\pi k}{N} + \phi)z^{N-k-1} \tag{8-19}$$

Thus,

$$N(z) = \frac{\sum_{k=0}^{N-1} T_{GF}(kT)z^{N-k-1}}{A\sum_{k=0}^{N-1} \cos(\frac{2\pi k}{N} + \phi)z^{N-k-1}} \qquad (N \geq 3) \tag{8-20}$$

As an alternative we may expand $z^N - 1$ as

$$z^N - 1 = \prod_{k=0}^{N-1} (z - e^{j2\pi k/N}) \tag{8-21}$$

Then, using Eq. (8-3) for $\theta_G(z)$, N(z) is written

$$N(z) = \frac{\sum_{k=0}^{N-1} T_{GF}(kT) z^{N-k} [z^2 - 2z\cos\frac{2\pi}{N} + 1]}{\prod_{k=0}^{N-1} (z - e^{j2\pi k/N}) Az[(z - \cos\frac{2\pi}{N})\cos\phi - \sin\frac{2\pi}{N}\sin\phi]} \tag{8-22}$$

For N = 3, N(z) is simplified to

$$N(z) = \frac{T_{GF}(0)z^2 + T_{GF}(T)z + T_{GF}(2T)}{A(z - 1)[(z + 0.5)\cos\phi - 0.866\sin\phi]} \tag{8-23}$$

For N > 3,

$$N(z) = \frac{\sum_{k=0}^{N-1} T_{GF}(kT) z^{N-k-1}}{A(z - 1) \prod_{k=2}^{N-2} (z - e^{j2\pi k/N})[(z - \cos\frac{2\pi}{N})\cos\phi - \sin\frac{2\pi}{N}\sin\phi]} \tag{8-24}$$

where in general,

$$\begin{aligned} T_{GF}(kT) &= T_{GF}^{-}(kT) \qquad 0 < \frac{2\pi k}{N} + \phi < \pi \\ &= T_{GF}^{+}(kT) \qquad \pi < \frac{2\pi k}{N} + \phi < 2\pi \end{aligned} \tag{8-25}$$

where $0 \leq (2\pi k/N + \phi) \leq 2\pi$ must be satisfied by appropriate conversion of the angle $2\pi k/N + \phi$.

For stability studies the critical regions of $F(z) = -1/N(z)$ should be constructed for N = 2, 3, ..., with ϕ varied from 0^o to 360^o, and A from 0 to infinity.

The following theorems on the properties of $-1/N(z)$ are useful for simplifying the task of the construction of the critical regions.

Theorem 8-1

For any integral N, the magnitude and phase of $-1/N(z)$ repeat for every $\phi = 2\pi/N$ radians.

Proof: The negative inverse of the discrete describing function is written

$$F(z) = -\frac{1}{N(z)} = \frac{-A[(z - \cos\frac{2\pi}{N})\cos\phi - \sin\frac{2\pi}{N}\sin\phi](z^N - 1)}{\left[\sum_{k=0}^{N-1} T_{GF}(kT)z^{N-k-1}\right](z^2 - 2z\cos\frac{2\pi}{N} + 1)} \tag{8-26}$$

Let

$$F(z) = \frac{F_1(z)F_2(z)}{F_3(z)F_4(z)} \tag{8-27}$$

where

$$F_1(z) = -A[(z - \cos\frac{2\pi}{N})\cos\phi - \sin\frac{2\pi}{N}\sin\phi] \tag{8-28}$$

$$F_2(z) = z^N - 1 \tag{8-29}$$

$$F_3(z) = \sum_{k=0}^{N-1} T_{GF}(kT)z^{N-k-1} \tag{8-30}$$

$$F_4(z) = (z^2 - 2z\cos\frac{2\pi}{N} + 1) \tag{8-31}$$

Let

$$F(z)_N = [F(z)]_\phi = \phi + 2\pi/N \tag{8-32}$$

$$F_1(z)_N = [F_1(z)]_\phi = \phi + 2\pi/N \tag{8-33}$$

$$F_3(z)_N = [F_3(z)]_\phi = \phi + 2\pi/N \tag{8-34}$$

Then,

$$\frac{|F(z)|}{|F(z)_N|} = \frac{|F_1(z)|}{|F_3(z)|}\frac{|F_3(z)_N|}{|F_1(z)_N|} \tag{8-35}$$

and

$$\text{Arg}[F(z)] - \text{Arg}[F(z)_N] = \text{Arg}[F_1(z)] - \text{Arg}[F_3(z)] - \text{Arg}[F_1(z)_N] + \text{Arg}[F_3(z)_N] \tag{8-36}$$

Also,

$$|F_1(z)| = \left|A\sin\frac{2\pi}{N}\right| \tag{8-37}$$

$$|F_1(z)_N| = \left|A\sin\frac{2\pi}{N}\right| = |F_1(z)| \tag{8-38}$$

Let us express $F_3(z)_N$ as

$$F_3(z)_N = \sum_{k=0}^{N-1} T_{GF}(kT)_N z^{N-k-1} \tag{8-39}$$

where

$$T_{GF}(kT)_N = [T_{GF}(kT)]_{\phi} = \phi + 2\pi/N \tag{8-40}$$

It can be shown that for any integral N,

$$F_3(z)_N = zF_3(z) = \sum_{k=0}^{N-1} T_{GF}(kT) z^{N-k} \tag{8-41}$$

Then, Eq. (8-35) becomes

$$\frac{|F(z)|}{|F(z)_N|} = \frac{|F_3(z)_N|}{|F_3(z)|} = \frac{|zF_3(z)|}{|F_3(z)|} = 1 \tag{8-42}$$

The argument of $F_1(z)$ is

$$\text{Arg}[F_1(z)] = \phi - \pi/2 \tag{8-43}$$

Then

$$\text{Arg}[F_1(z)_N] = \phi - \pi/2 + 2\pi/N \tag{8-44}$$

Thus, Eq. (8-36) becomes

$$\text{Arg}[F(z)] - \text{Arg}[F(z)_N] = -\frac{2\pi}{N} - \text{Arg}[F_3(z)] + \text{Arg}[F_3(z)_N]$$

$$= -\frac{2\pi}{N} - \text{Arg}[F_3(z)] + \text{Arg}[zF_3(z)]$$

$$= -\frac{2\pi}{N} - \text{Arg}[F_3(z)] + \frac{2\pi}{N} + \text{Arg}[F_3(z)]$$

$$= 0 \qquad (8\text{-}45)$$

Q.E.D.

As an illustrative example of Theorem 8-1, let us consider the case of N = 4.

Let $\frac{a}{2} = \gamma T_{GF0} A = K$

Then

$$T_{GF}^{-}(kT) = \frac{R + K(R+1)[\cos(\phi + 2\pi k/N) - 1]}{1 - K(R+1)[\cos(\phi + 2\pi k/N) - 1]} T_{GF0} \qquad (8\text{-}46)$$

$$T_{GF}^{+}(kT) = \frac{R - K(R-1)[\cos(\phi + 2\pi k/N) - 1]}{1 - K(R-1)[\cos\ \phi + 2\pi k/N) - 1]} T_{GF0} \qquad (8\text{-}47)$$

For $0 < \phi < \pi$,

$$F_3(z) = T_{GF}^{-}(0)z^3 + T_{GF}^{-}(T)z^2 + T_{GF}^{+}(2T)z + T_{GF}^{+}(3T) \qquad (8\text{-}48)$$

$$F_3(z)_N = T_{GF}^{-}(0)_N z^3 + T_{GF}^{+}(T)_N z^2 + T_{GF}^{+}(2T)_N z + T_{GF}^{-}(3T)_N \qquad (8\text{-}49)$$

It is easy to see that

$$T_{GF}^{-}(0)_N = T_{GF}^{-}(T)$$

$$T_{GF}^{+}(T)_N = T_{GF}^{+}(2T)$$

$$T_{GF}^{+}(2T)_N = T_{GF}^{+}(3T) \qquad (8\text{-}50)$$

$$T_{GF}^{-}(3T)_N = T_{GF}^{-}(0)$$

which proves that $F_3(z)_N = zF_3(z)$.

Similar results are obtained for $\pi < \phi < 2\pi$.

Theorem 8-2

For odd N ($N \geq 3$), the magnitude and phase of $-1/N(z)$ repeat for every $\phi = \pi/N$.

Proof: Let $F(z)_N$, $F_1(z)_N$, $F_3(z)_N$ now be defined as $F(z)$, $F_1(z)$, and $F_3(z)$ with ϕ replaced by $\phi + \pi/N$, respectively. Then,

$$\text{Arg}[F_1(z)_N] = \phi - \frac{\pi}{2} + \frac{\pi}{N} \qquad (8\text{-}51)$$

$$\text{Arg}[F(z)] - \text{Arg}[F(z)_N] = -\frac{\pi}{N} + \text{Arg}[F_3(z)_N] - \text{Arg}[F_3(z)] \qquad (8\text{-}52)$$

Using the same notation as in Theorem 8-1, it can be shown that for odd $N \geq 3$,

$$F_3(z)_N = -z^{-(N-1)/2} F_3(z) \tag{8-53}$$

Thus,

$$\begin{aligned} \text{Arg}[F_3(z)_N] &= \pi - \frac{(N-1)}{2}\frac{2\pi}{N} + \text{Arg}[F_3(z)] \\ &= \frac{\pi}{N} + \text{Arg}[F_3(z)] \end{aligned} \tag{8-54}$$

Again,

$$\frac{|F(z)|}{|F(z)_N|} = \frac{|F_3(z)_N|}{|F_3(z)|} = 1 \tag{8-55}$$

and

$$\begin{aligned} \text{Arg}[F(z)] - \text{Arg}[F(z)_N] &= -\frac{\pi}{N} + \text{Arg}[F_3(z)_N] - \text{Arg}[F_3(z)] \\ &= 0 \end{aligned} \tag{8-56}$$

Q.E.D.

As an illustrative example of Theorem 8-2, consider the case N = 3.

For $0 < \phi < \pi$,

$$F_3(z) = T_{GF}^{-}(0)z^2 + T_{GF}^{-}(T)z + T_{GF}^{+}(2T) \tag{8-57}$$

$$F_3(z)_N = T_{GF}^{-}(0)_N z^2 + T_{GF}^{+}(T)_N z + T_{GF}^{+}(2T)_N \tag{8-58}$$

It can readily be shown that

$$T_{GF}^{-}(0)_N = -T_{GF}^{+}(2T)$$

$$T_{GF}^{+}(T)_N = -T_{GF}^{-}(0) \qquad (8\text{-}59)$$

$$T_{GF}^{+}(2T)_N = -T_{GF}^{-}(T)$$

To carry out one of the identities above,

$$T_{GF}^{-}(T)_N = T_{GFO}\frac{R - K(R-1)[\cos(\phi+\pi) - 1]}{1 - K(R-1)[\cos(\phi+\pi) - 1]} = \frac{R + K(R-1)(\cos\phi + 1)}{1 + K(R-1)(\cos\phi + 1)}T_{GFO} \qquad (8\text{-}60)$$

$$T_{GF}^{-}(0) = T_{GFO}\frac{R + K(R+1)(\cos\phi - 1)}{1 - K(R+1)(\cos\phi - 1)} \qquad (8\text{-}61)$$

Using the relation, $R^2 + R/K - 1 = 0$, we have

$$T_{GF}^{-}(T)_N = -T_{GF}^{-}(0) \qquad (8\text{-}62)$$

Thus,

$$F_3(z)_N = -z^{-1}F_3(z) \qquad (8\text{-}63)$$

The significance of the last two theorems is that the critical regions of $-1/N(z)$ need be computed only for $0^o < \phi \leq \pi/N$ for odd N, and $0^o < \phi \leq 2\pi/N$ for even N.

Theorem 8-3.

Asympotic Behavior of -1/N(z) as A approaches infinity.

(a) $\lim_{A\to\infty} |-1/N(z)| = \infty$ (8-64)

(b) For even $N \geq 4$, $0 < \phi \leq 2\pi/N$.

$$\lim_{A\to\infty} \text{Arg}[-1/N(z)] = (\frac{1}{2} - \frac{1}{N})\pi + \phi \quad (8\text{-}65)$$

For odd $N > 3$, $0 < \phi \leq \pi/N$.

$$\lim_{A\to\infty} \text{Arg}[-1/N(z)] = (1 - \frac{1}{N})\frac{\pi}{2} + \phi \quad (8\text{-}66)$$

(c) For $N = 2$ $\quad 0 < \phi \leq \pi$

$$\lim_{A\to\infty} \text{Arg}[-1/N(z)] = 0^{o} \qquad 0 < \phi \leq \pi/2$$

$$= \pi \qquad \pi/2 < \phi \leq \pi \quad (8\text{-}67)$$

(d) For $N = 3$ $\quad 0 < \phi \leq \pi/3$

$$\lim_{A\to\infty} \text{Arg}[-1/N(z)] = -\frac{5\pi}{3} + \phi \quad (8\text{-}68)$$

Proof:

We can easily show that

$$\lim_{A\to\infty} T_{GF}^{-}(kT) = -T_{GFO} \qquad \dot{\theta}_G \leq 0 \quad (8\text{-}69)$$

$$\lim_{A\to\infty} T_{GF}^{+}(kT) = T_{GFO} \qquad \dot{\theta}_G \geq 0 \quad (8\text{-}70)$$

The magnitude of -1/N(z) is directly proportional to A as A approaches infinity; thus (a) is proved.

For N = 2 $0 < \phi \leq \pi/2$

$$F(z) = -1/N(z) = \frac{2A\cos\phi}{T_{GF}(T) - T_{GF}(0)} \tag{8-71}$$

Thus,

$$\lim_{A\to\infty} \text{Arg}[F(z)] = \lim_{A\to\infty} \text{Arg}\left[\frac{2A\cos\phi}{T_{GF}(T) - T_{GF}(0)}\right]$$

$$= \text{Arg}\,\frac{2A\cos\phi}{2T_{GF0}} = 0^{o} \qquad 0 < \phi \leq \pi/2$$

$$= \pi \qquad \pi/2 < \phi \leq \pi \tag{8-72}$$

This proves item (c).

For N = 3 $0 < \phi \leq \pi/3$

$$F(z) = \frac{-A[(z + 0.5)\cos\phi - 0.866\sin\phi](z - 1)}{T_{GF}(0)z^2 + T_{GF}(T)z + T_{GF}(2T)} \tag{8-73}$$

$$\lim_{A\to\infty} \text{Arg}[F(z)] = -\frac{5\pi}{3} - \lim_{A\to\infty} \text{Arg}[T_{GF}(0)z^2 + T_{GF}(T)z + T_{GF}(2T)] + \phi$$

$$= -\frac{5\pi}{3} - \text{Arg}[-z^2 - z + 1] + \phi$$

$$= -\frac{5\pi}{3} + \phi \tag{8-74}$$

This proves item (d).

For $N \geq 4$ and even $\quad 0 < \phi \leq 2\pi/N$

Using Eqs. (8-27) through (8-31), we have

$$\lim_{A\to\infty} \text{Arg}[F(z)] = \lim_{A\to\infty} \left\{\text{Arg}[F_1(z)] + \text{Arg}[F_2(z)] - \text{Arg}[F_3(z)] - \text{Arg}[F_4(z)]\right\}$$

$$= \phi - \frac{\pi}{2} - \lim_{A\to\infty} \left\{\text{Arg}[F_3(z)]\right\} + \text{Arg}[F_2(z)] - \text{Arg}[F_4(z)] \tag{8-75}$$

$$\text{Arg}[F_2(z)] - \text{Arg}[F_4(z)] = \text{Arg}[(z-1)\prod_{k=2}^{N-2}(z - e^{j2\pi k/N})]$$

$$= \text{Arg}[e^{j\pi/N}(e^{j\pi/N} - e^{-j\pi/N})\prod_{k=2}^{N-2} e^{j2\pi/N}(1 - e^{j2\pi/N(k-1)})] \tag{8-76}$$

$$\text{Arg}[F_2(z)] - \text{Arg}[F_4(z)] = \text{Arg}[e^{j\pi/N}(e^{j\pi/N} - e^{-j\pi/N})(e^{j2\pi/N})^{N-3}\prod_{k=1}^{N-3}(1 - e^{j2\pi k/N})]$$

$$= \frac{\pi}{N} + \frac{\pi}{2} + (N-3)\left(\frac{2\pi}{N}\right) + \text{Arg}\prod_{k=1}^{N-3} e^{j\pi k/N}(e^{-j\pi k/N} - e^{+j\pi k/N})$$

$$= \frac{\pi}{N} + (N-3)\left(\frac{2\pi}{N}\right) + (N-4)\left(-\frac{\pi}{2}\right) + \sum_{k=1}^{N-3}\frac{k\pi}{N} \tag{8-77}$$

$$\lim_{A\to\infty} \text{Arg}[F_3(z)] = \lim_{A\to\infty} \text{Arg}\sum_{k=0}^{N-1} T_{GF}(kT)z^{N-k-1}$$

$$= \text{Arg} \sum_{k=0}^{N/2-1} - T_{GFO} z^{N-k-1} + \text{Arg} \sum_{k=N/2}^{N-1} T_{GFO} z^{N-k-1}$$

$$= \text{Arg} \sum_{k=0}^{N/2-1} - T_{GFO} z^{N-k-1} = \frac{(\frac{N}{2} - 1)\pi}{N} = \frac{\pi}{2} - \frac{\pi}{N} \qquad (8\text{-}78)$$

Thus,

$$\lim_{A \to \infty} \text{Arg}[F(z)] = \phi - \frac{\pi}{2} + \frac{\pi}{N} + (N - 4)(-\frac{\pi}{2}) + (N - 3)(\frac{2\pi}{N}) + \sum_{k=1}^{N-3} \frac{k\pi}{N} - \frac{\pi}{2} + \frac{\pi}{N}$$

$$= (3 - \frac{N}{2} - \frac{4}{N} + \sum_{k=1}^{N-3} \frac{k}{N})\pi + \phi$$

$$= (\frac{1}{2} - \frac{1}{N})\pi + \phi \qquad (8\text{-}79)$$

<u>For N > 3 and odd</u> $0 < \phi \leq \pi/N$

For this case,

$$\lim_{A \to \infty} \text{Arg}[F_3(z)] = \text{Arg} \sum_{k=0}^{(N-1)/2} - T_{GFO} z^{N-k-1} + \text{Arg} \sum_{k=(N+1)/2}^{N-1} T_{GFO} z^{N-k-1}$$

$$= \frac{(N - 3)\pi}{2N} \qquad (8\text{-}80)$$

Thus,

$$\lim_{A\to\infty} \text{Arg}[F(z)] = \phi - \frac{\pi}{2} + \frac{\pi}{N} + (N-4)(-\frac{\pi}{2}) + (N-3)(\frac{2\pi}{N}) + \sum_{k=1}^{N-3} \frac{k\pi}{N} - \frac{(N-3)\pi}{2N}$$

$$= (3 - \frac{N}{2} - \frac{7}{2N} + \sum_{k=1}^{N-3} \frac{k}{N})\pi + \phi$$

$$= (1 - \frac{1}{N})\frac{\pi}{2} + \phi \qquad (8\text{-}81)$$

and (b) is proved. Q.E.D.

Theorem 8-4.

Asymptotic Behavior of -1/N(z) as A approaches zero.

$$\lim_{A\to 0} F(z) = -\frac{1}{\gamma T_{GFO}^2} \qquad (8\text{-}82)$$

for all ϕ and all N.

Proof: From Eq. (8-20), for $N \geq 3$,

$$F(z) = -\frac{1}{N(z)} = \frac{-A\sum_{k=0}^{N-1} \cos(\frac{2k\pi}{N} + \phi)z^{N-k-1}}{\sum_{k=0}^{N-1} T_{GF}(kT)z^{N-k-1}} \qquad (8\text{-}83)$$

$$\lim_{A\to 0} F(z) = \frac{-\sum_{k=0}^{N-1} \cos(\frac{2k\pi}{N} + \phi)z^{N-k-1}}{\lim_{A\to 0} \sum_{k=0}^{N-1} \frac{T_{GF}(kT)}{A} z^{N-k-1}}$$

$$= \frac{-\sum_{k=0}^{N-1} \cos\left(\frac{2k\pi}{N} + \phi\right) z^{N-k-1}}{\sum_{k=0}^{N-1} \lim_{A\to 0} \frac{T_{GF}(kT)}{A} z^{N-k-1}} \qquad (8\text{-}84)$$

Therefore, the problem is that of finding $\lim_{A\to 0} \frac{T_{GF}(kT)}{A}$.

First, let $T_{GF}(kT) = T_{GF}^{-}(kT)$. Then

$$\lim_{A\to 0} \frac{T_{GF}^{-}(kT)}{A} = \lim_{A\to 0} T_{GFO} \frac{\frac{R}{A(R+1)} - \gamma T_{GFO} + \gamma T_{GFO} \cos\left(\frac{2\pi k}{N} + \phi\right)}{\gamma T_{GFO} A - \gamma T_{GFO} A \cos\left(\frac{2\pi k}{N} + \phi\right) + \frac{1}{R+1}}$$

$$\cong T_{GFO} \lim_{A\to 0} \frac{R}{A(R+1)} + \gamma T_{GFO}^{2} \left[\cos\left(\frac{2\pi k}{N} + \phi\right) - 1\right] \qquad (8\text{-}85)$$

where the fact that $\lim_{A\to 0} [1/(R+1)] = 1$ has been used.

$$\lim_{A\to 0} \frac{R}{A(R+1)} \cong \lim_{A\to 0} \frac{R}{A} = \lim_{A\to 0} \frac{1}{A} \left\{ -\frac{1}{2\gamma T_{GFO} A} + \sqrt{\frac{4\gamma^2 T_{GFO}^2 A^2 + 1}{4\gamma^2 T_{GFO}^2 A^2}} \right\} \qquad (8\text{-}86)$$

Or,

$$\lim_{A\to 0} \frac{R}{A(R+1)} = \lim_{A\to 0} \frac{1}{A} \left\{ -\frac{1}{2\gamma T_{GFO} A} + \frac{1}{2\gamma T_{GFO} A} \sqrt{1 + 4\gamma^2 T_{GFO}^2 A^2} \right\} \qquad (8\text{-}87)$$

Expanding $\sqrt{1 + 4\gamma^2 T_{GFO}{}^2 A^2}$ into a power series, and using only the first two terms, we have,

$$\lim_{A\to 0} \frac{R}{A(R+1)} = \lim_{A\to 0} \frac{1}{A}\left[\frac{4\gamma^2 T_{GFO}{}^2 A^2}{4\gamma T_{GFO} A}\right] = \gamma T_{GFO} \tag{8-88}$$

Thus,

$$\lim_{A\to 0} \frac{T_{GF}{}^-(kT)}{A} = \gamma T_{GFO}{}^2 + \gamma T_{GFO}{}^2[\cos(\frac{2\pi k}{N} + \phi) - 1]$$

$$= \gamma T_{GFO}{}^2 \cos(\frac{2\pi k}{N} + \phi) \tag{8-89}$$

Similarly, it can be shown that

$$\lim_{A\to 0} \frac{T_{GF}{}^+(kT)}{A} = \lim_{A\to 0} \frac{T_{GF}{}^-(kT)}{A} = \gamma T_{GFO}{}^2 \cos(\frac{2\pi k}{N} + \phi) \tag{8-90}$$

Now,

$$\lim_{A\to 0} F(z) = \frac{-\sum_{k=0}^{N-1} \cos(\frac{2\pi k}{N} + \phi) z^{N-k-1}}{\gamma T_{GFO}{}^2 \sum_{k=0}^{N-1} \cos(\frac{2\pi k}{N} + \phi) z^{N-k-1}} = -\frac{1}{\gamma T_{GFO}{}^2} \tag{8-91}$$

for all ϕ and all $N \geq 3$.

For N = 2,

$$\lim_{A\to 0} F(z) = \lim_{A\to 0} \frac{2A\cos\phi}{T_{GF}(T)-T_{GF}(0)}$$

$$= \lim_{A\to 0} \frac{2A\cos\phi}{T_{GFO}\dfrac{\dfrac{R}{R-1}+\gamma T_{GFO}A(1+\cos\phi)}{\dfrac{1}{R-1}+\gamma T_{GFO}A(1+\cos\phi)} - T_{GFO}\dfrac{\dfrac{R}{R+1}-\gamma T_{GFO}A(1-\cos\phi)}{\dfrac{1}{R+1}+\gamma T_{GFO}A(1-\cos\phi)}}$$

$$= -\frac{1}{\gamma T_{GFO}^{2}} \qquad (8\text{-}92)$$

Q.E.D.

9. Discrete Describing Function Plots of the CMG Frictional Nonlinearity

The discrete describing function, N(z), for the CMG frictional nonlinearity is derived in Chapter 8 for integral values of $N \geq 2$. The plots of -1/N(z) together with that of G(z) in the frequency-domain allow the study of the condition of self-sustained oscillations of the LST system with sampled data.

For N = 2, the expression for F(z) = -1/N(z) is given by Eq. (8-16). Figure 9-1 shows the F(z) plot for N = 2 in the gain-phase coordinates with $0 \leq A < \infty$ and various values of ϕ. The value of γ is 1.38×10^5. Note that the plot stays on the -180^0 and -360^0 axes.

In general, N(z) for $N \geq 3$ is given by Eq. (8-20). Figure 9-2 shows the gain-phase plot for F(z) when N = 3. The curves for several values of ϕ are plotted to illustrate the effect of varying the phase of the input signal to the nonlinearity. It should be noted that the values of F(z) repeat every 60 degrees starting from $\phi = 0^0$. As the magnitude of the input signal, A, approaches infinity, the bounds of F(z) are at -240^0 and -300^0. Figures 9-3 and 9-4 illustrate the F(z) plots for N = 4 and N = 5, respectively. For N = 4, the F(z) plot extends from -315^0 to -225^0, and for N = 5, the span is from -288^0 to -252^0.

For stability analysis, it is sufficient to consider only the bounds of the F(z) plot for a fixed N. Self-sustained oscillations characterized by N may occur if G(z) intersects with any part of the F(z) plot. The region bounded by all the F(z) curves for a given N is defined as the "critical region". In Figure 9-5 the critical region for N = 6 is shown, without showing all the curves of F(z) for various values of ϕ. Similarly, Figures 9-6 through 9-8 show the critical regions for N = 8, 20, and 50, respectively. The general shape of the critical

regions for other values of N is easily visualized. Furthermore, Theorems 8-3 and 8-4 on the asymptotic behavior of F(z) as $A \to \infty$ and $A \to 0$ are useful in generating the critical regions. It is interesting to note that as N approaches infinity, F(z) approaches -1/N of the continuous-data nonlinearity, as shown in Figure 9-8.

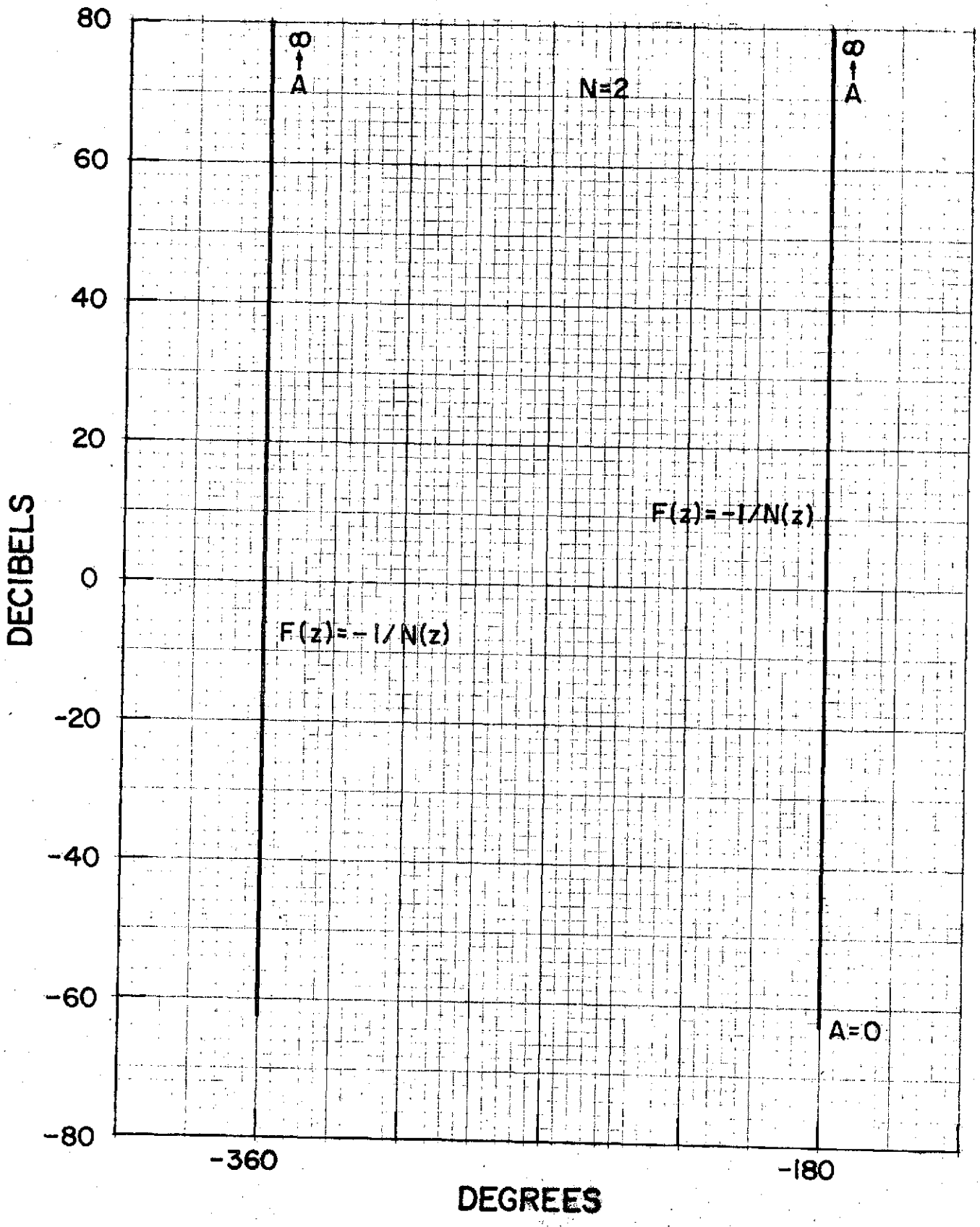

Figure 9-1. Discrete describing function plot of CMG frictional nonlinearity, $\gamma = 1.38 \times 10^5$, N = 2.

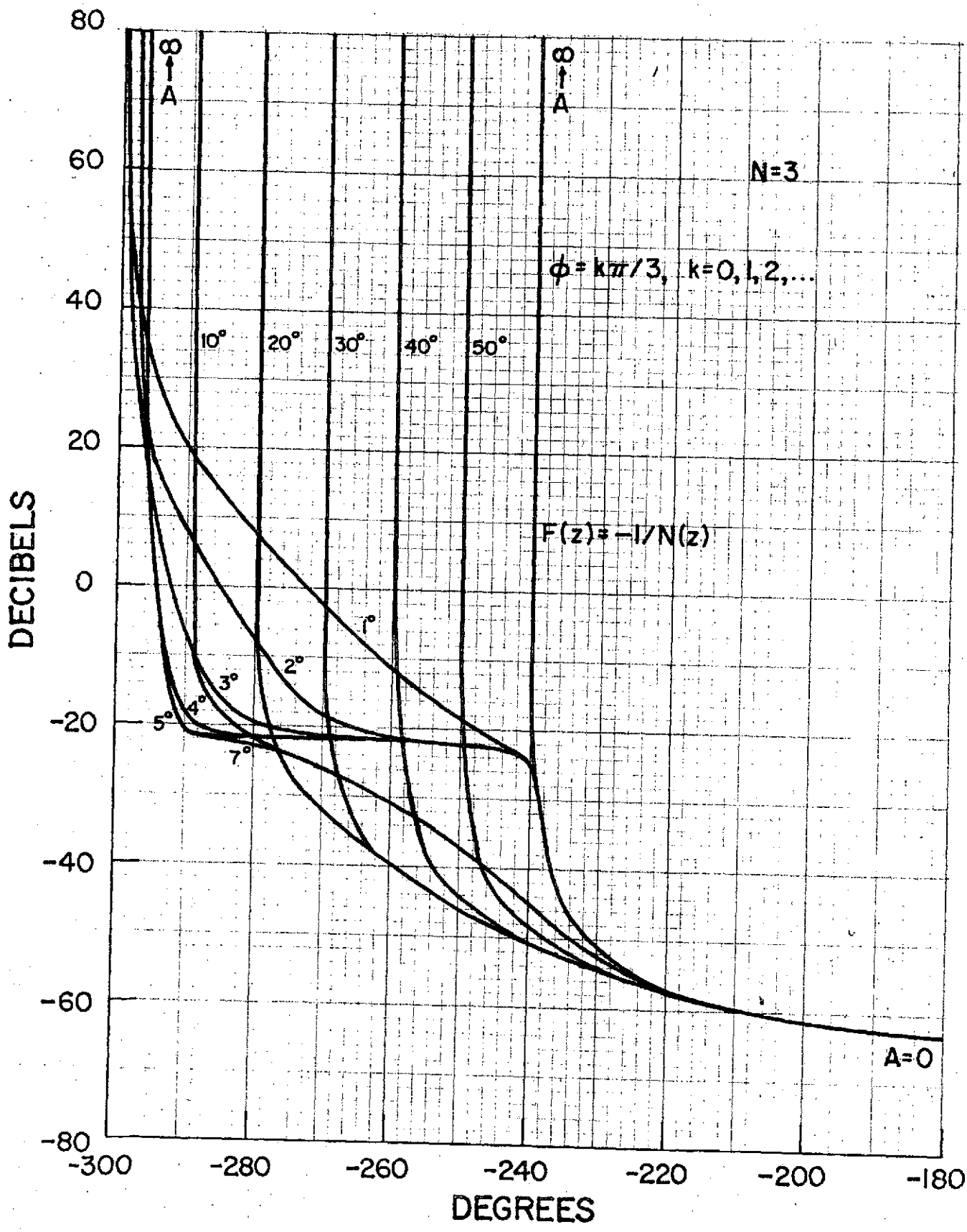

Figure 9-2. Discrete describing function plots of CMG frictional nonlinearity, $\gamma = 1.38 \times 10^5$, N = 3.

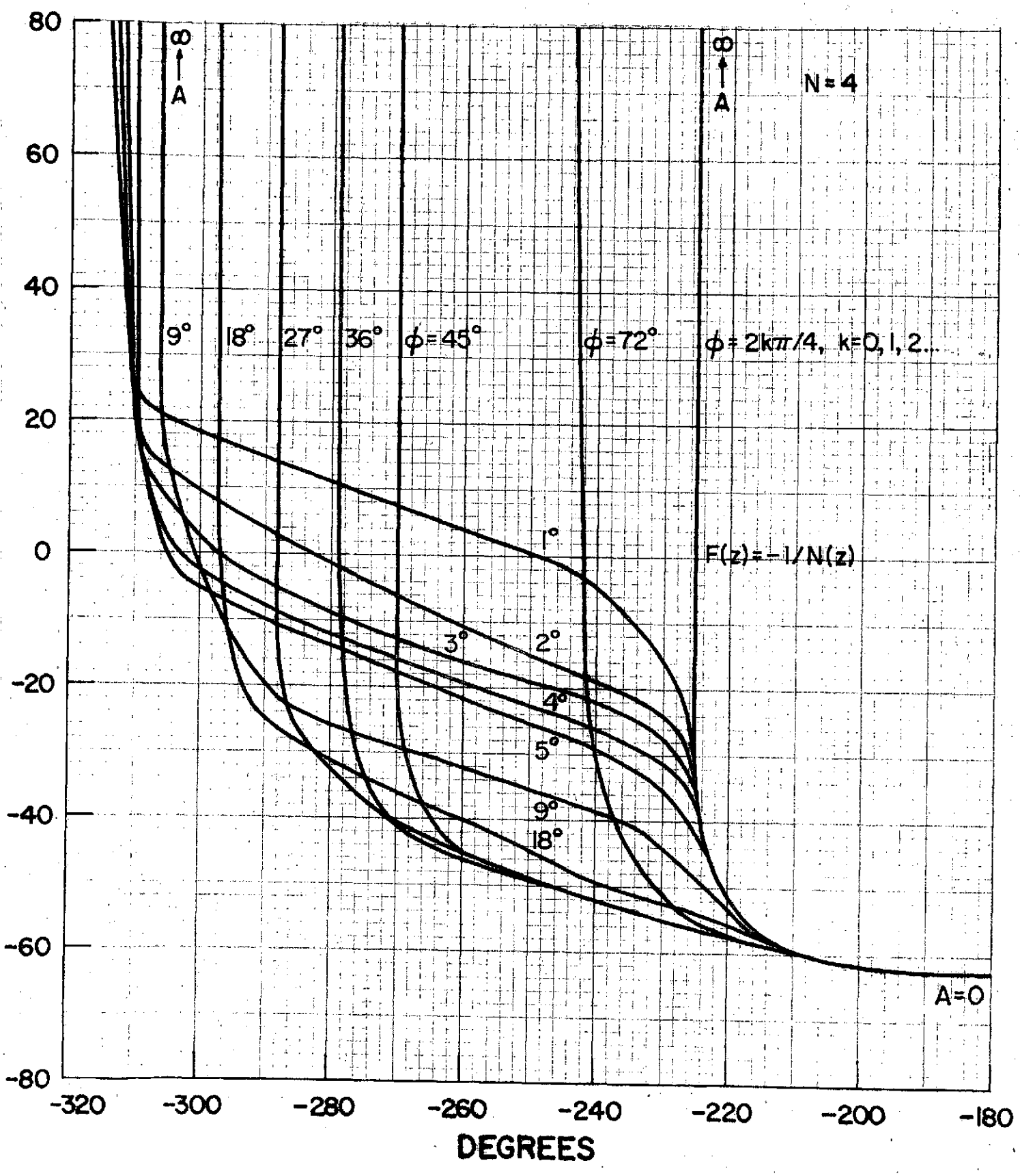

Figure 9-3. Discrete describing function plots of CMG frictional nonlinearity, $\gamma = 1.38 \times 10^5$, N = 4.

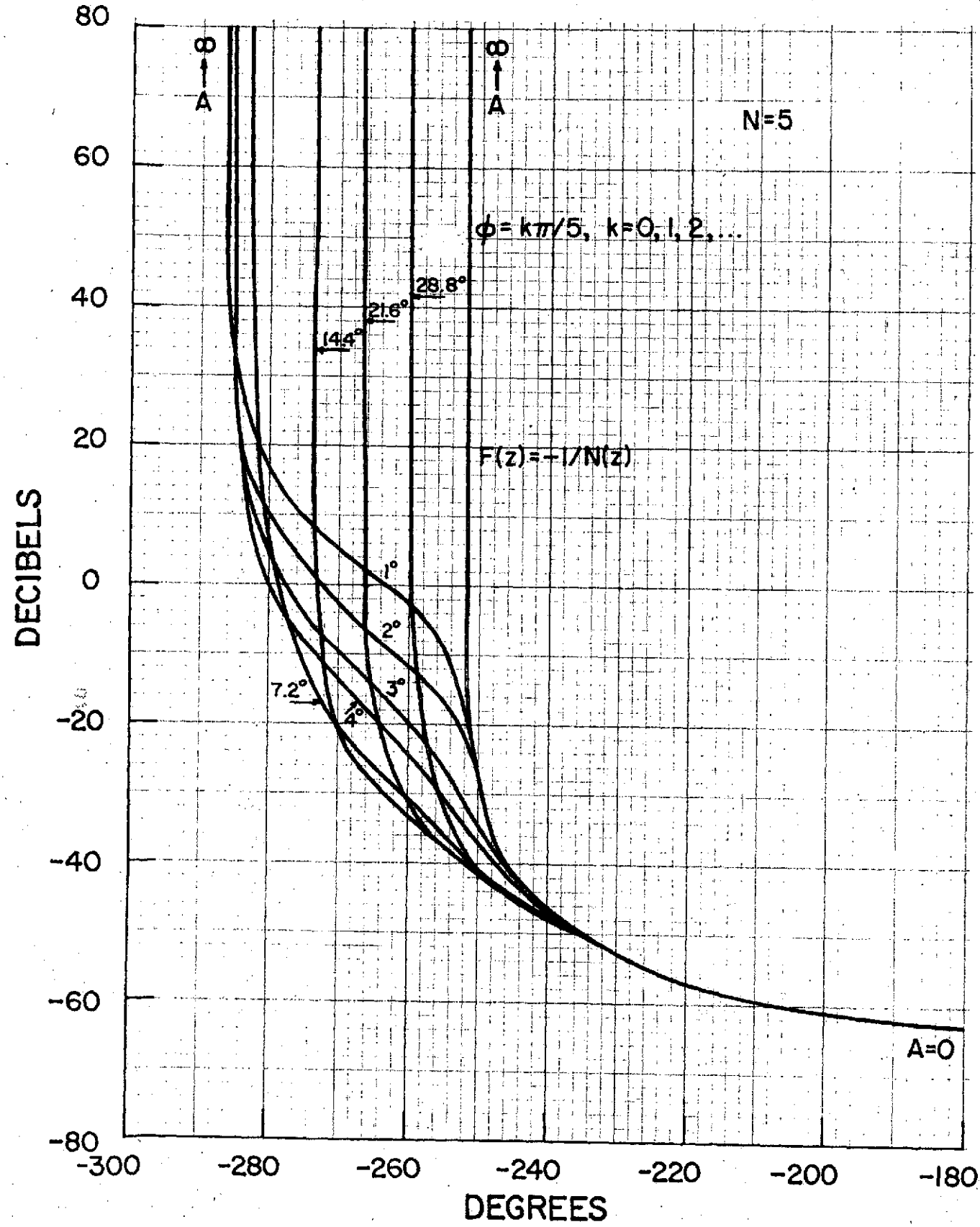

Figure 9-4. Discrete describing function plots of CMG frictional nonlinearity, $\gamma = 1.38 \times 10^5$, N = 5.

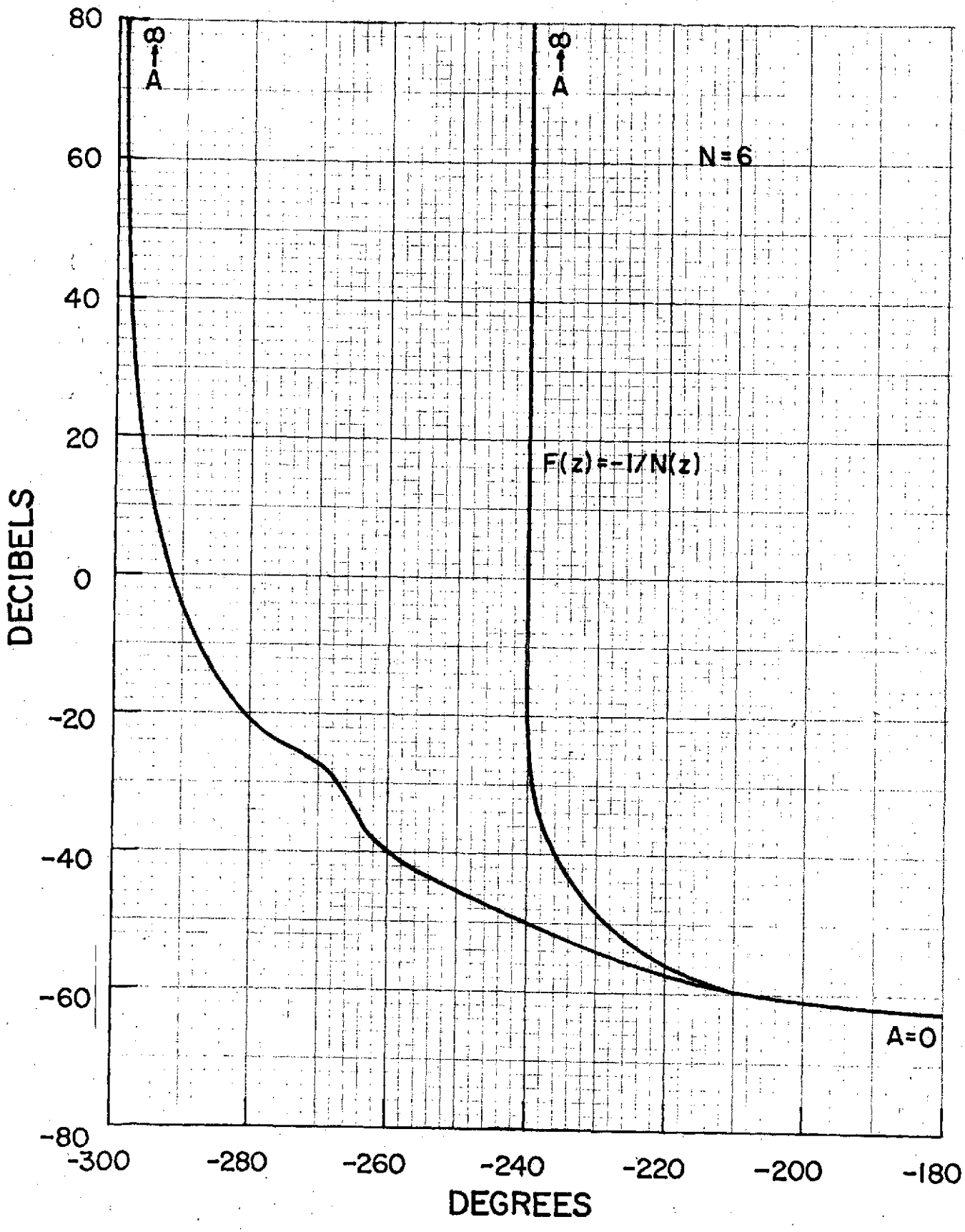

Figure 9-5. Discrete describing function plots which form the critical region of CMG frictional nonlinearity, $\gamma = 1.38 \times 10^5$, N=6.

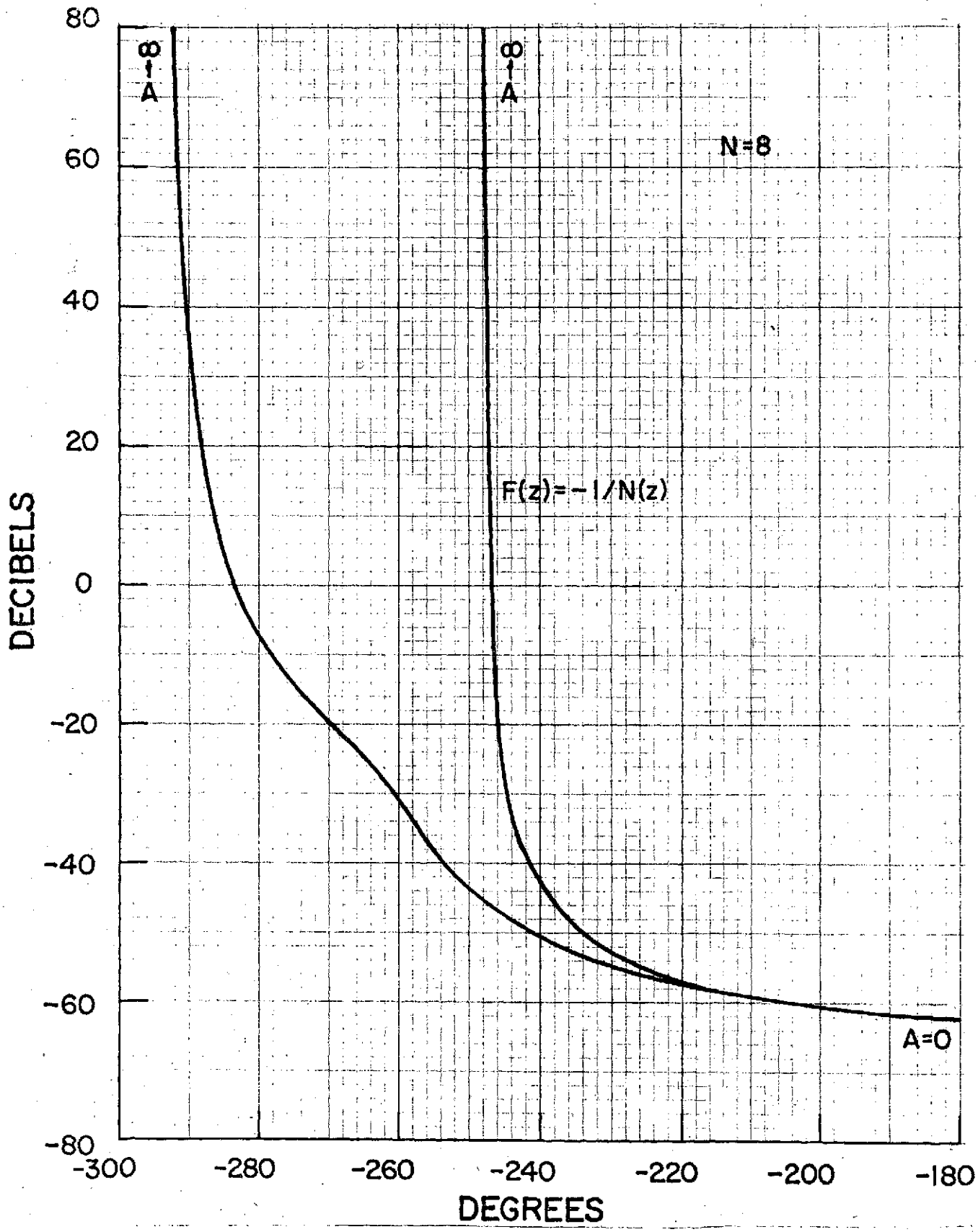

Figure 9-6. Discrete describing function plot of CMG frictional nonlinearity which form the critical region, $\gamma = 1.38 \times 10^5$, N = 8.

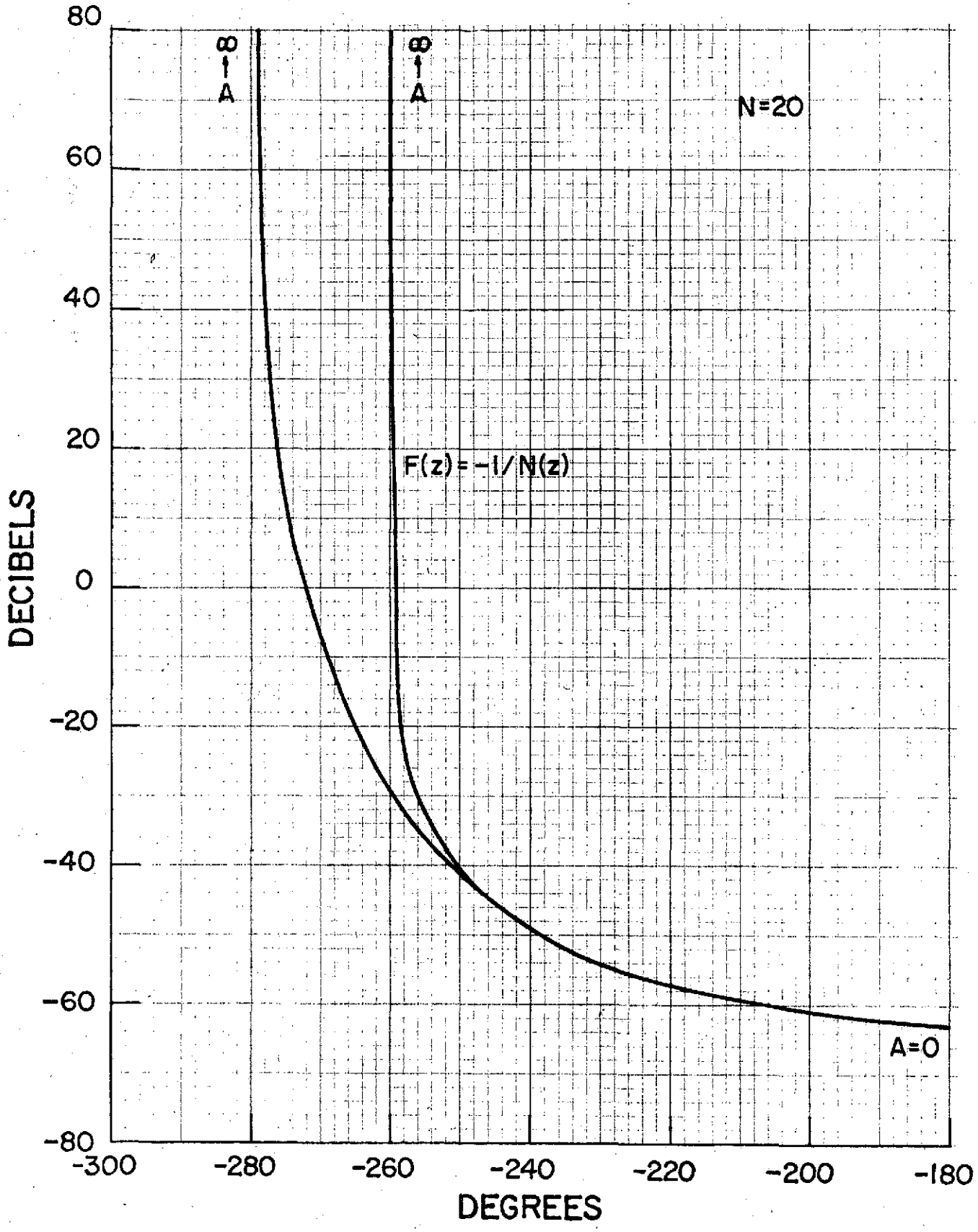

Figure 9-7. Discrete describing function plots which form the critical region of the CMG nonlinearity, $\gamma = 1.38 \times 10^5$, N = 20.

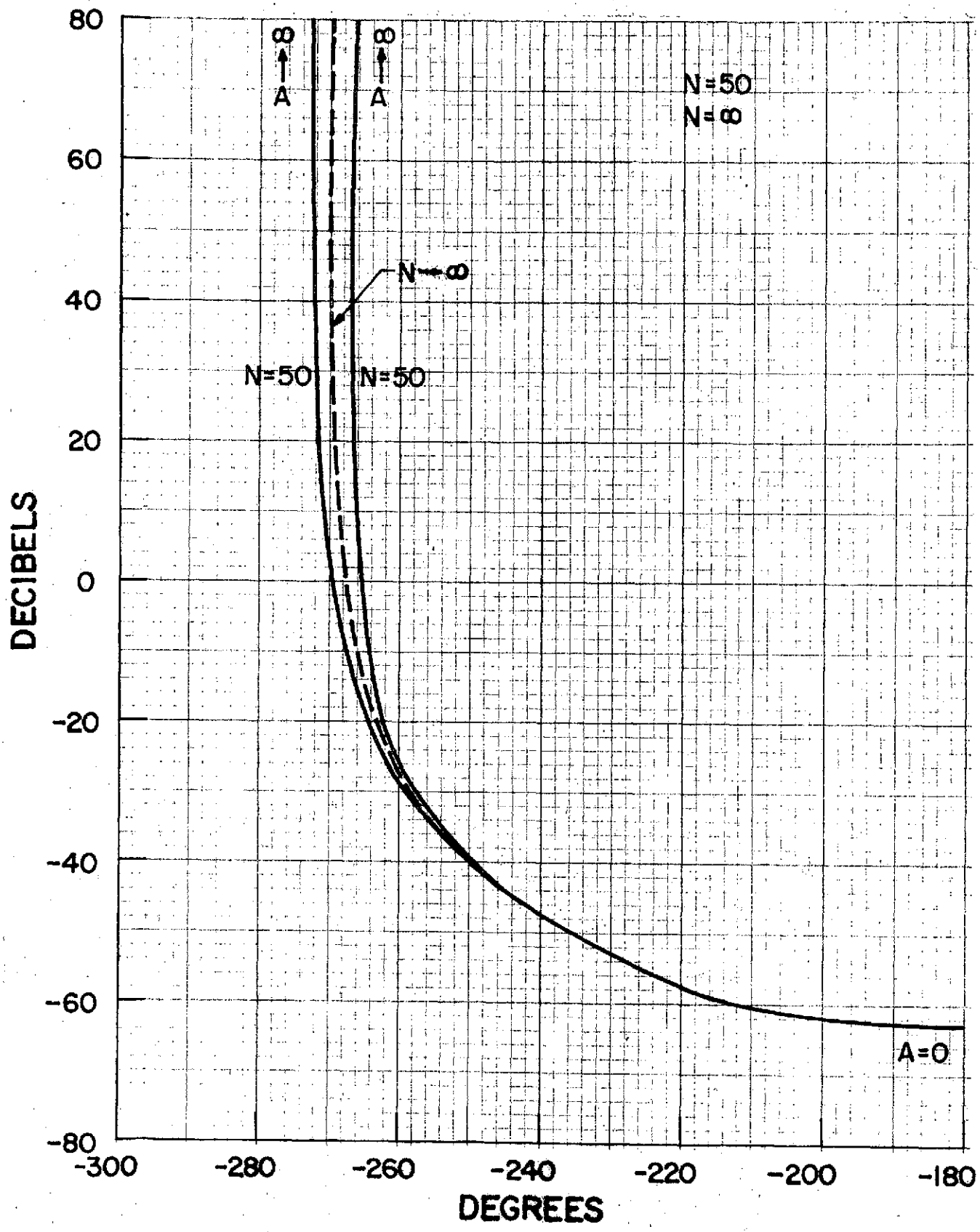

Figure 9-8. Discrete describing function plots which form the critical region of the CMG frictional nonlinearity, $\gamma = 1.38 \times 10^5$, N = 50 and N = ∞.

10. Computer Simulation of the Simplified Sampled-Data LST System with the Analytical CMG Frictional Torque Expressions

A computer simulation of the Sampled-Data LST System is presented here to corroborate the results of the discrete describing function analysis of the last two chapters. Since the analysis has been carried out with the analytical torque expressions for the CMG frictional nonlinearity, the simulation model of the nonlinearity also has the same characteristics.

The simplified sampled-data LST system is represented by the block diagram of Figure 7-1. Although for analytical convenience the discrete describing function analysis has been carried out with two samplers present in the system, the actual system has only one sampler. This is at the input to the CMG gimbal drive and there is no sampler in the nonlinearity loop. Consequently, the simulations have been performed with the two-sampler as well as the one-sampler system models. The numerical values used in the simulation model correspond to those of System 1 in Chapter 6.

The G(z) plots of Figures 7-3 and 7-4 and the -1/N(z) plots of Figures 9-1 through 9-9 show that for $\gamma = 1.38\times10^{5}$ self-sustained oscillations will not exist if T is less than 0.25 seconds approximately. For larger values of γ the plots in Figures 9-1 through 9-9 shift downward appropriately. Thus, with $\gamma = 1.38\times10^{7}$ the lowest point in the -1/N(z) curves becomes approximately -102 db, yielding a system in which self-sustained oscillations will always exist for any sampling period. The periods of these oscillations depend on the sampling period used.

For the computer simulation, the input to the LST system, χ, is set to zero, along with all the initial states, except for the vehicle position θ_V. The following quantities are plotted from the simulation runs

θ_V = vehicle position (radians)

ω_V = vehicle velocity (radians/second)

θ_G = Gimbal position (radians)

ω_G = Gimbal velocity (radians/second)

T_{GF} = Torque output of the nonlinearity (ft-lb)

Error = Error input command to the CMG (radians/second)

$$\chi - K_0\theta_V - K_1\omega_V$$

Figures 10-1 through 10-8 show the simulation results with $\gamma = 1.38\times10^5$. Two different sampling periods, T = 0.005 sec and T = 0.1 sec are considered with both the one-sampler and the two-sampler system models. Table 10-1 provides the details of each of these simulation runs. Note that, as predicted, both the system models are stable with the sampling periods considered and no self-sustained oscillations exist.

Table 10-1. Computer Simulations with $\gamma = 1.38\times10^5$.

Figure No.	No. of Samplers in System Model	Sampling Period T(sec)	Initial Value of θ_V(rad)
10-1, 10-2	2	0.005	$1.\times10^{-8}$
10-3, 10-4	1	0.005	$1.\times10^{-8}$
10-5, 10-6	2	0.1	$1.\times10^{-8}$
10-7, 10-8	1	0.1	$1.\times10^{-8}$

Figures 10-9 through 10-30 show the simulation-results with $\gamma = 1.38\times10^{7}$. Several sampling periods from T = 0.005 sec up to T = 0.25 sec are used with both the one- and 2-sampler system models. The details of the simulation parameters and the oscillation periods are shown in Table 10-2. Note that the one-sampler and two-sampler system models always oscillate with periods close to those which are predicted by the $-1/N(z)$ and $G(z)$ plots. Although the two-sampler model is in closer agreement with the theoretical predictions, these results do justify the approximation of introducing the sampler. Note also that for some sampling periods (eg. 0.02 sec) although the one-sampler model and the two-sampler model oscillate with periods which differ considerably (0.04 sec and 1.76 sec, respectively) both periods are in fact predicted by the theory.

From the standpoint of self-sustained oscillations, if γ is at its nominal value of 1.38×10^{5} any sampling period less than 0.25 seconds, approximately should yield a stable system. However, other practical considerations and stability considerations due to non-zero inputs would limit the sampling period to a much lower value.

Table 10-2. Computer Simulations with $\gamma = 1.38\times10^{7}$

Figure No.	No. of Samplers in System Model	Sampling Period T(sec)	Initial Value of θ_V(rad)	Oscillation Period (sec) (NT)
10-9, 10-10	2	0.005	$1.\times10^{-8}$	1.58 (316T)
10-11, 10-12	1	0.005	$1.\times10^{-8}$	1.88 (376T)
10-13, 10-14	2	0.02	$1.\times10^{-7}$	0.04 (2T)
10-15, 10-16	2	0.02	Continuation of 10-13, 10-14	0.04 (2T)
10-17, 10-18	1	0.02	$5.\times10^{-8}$	1.76 (88T)
10-19, 10-20	2	0.05	$1.\times10^{-8}$	0.1 (2T)
10-21, 10-22	1	0.05	$1.\times10^{-8}$	1.25 (25T)
10-23, 10-24	2	0.1	$1.\times10^{-8}$	1.0 (10T)
10-25, 10-26	1	0.1	$1.\times10^{-8}$	1.2 (12T)
10-27, 10-28	2	0.25	$1.\times10^{-7}$	0.5 (2T)
10-29, 10-30	1	0.25	$1.\times10^{-7}$	0.75 (3T)

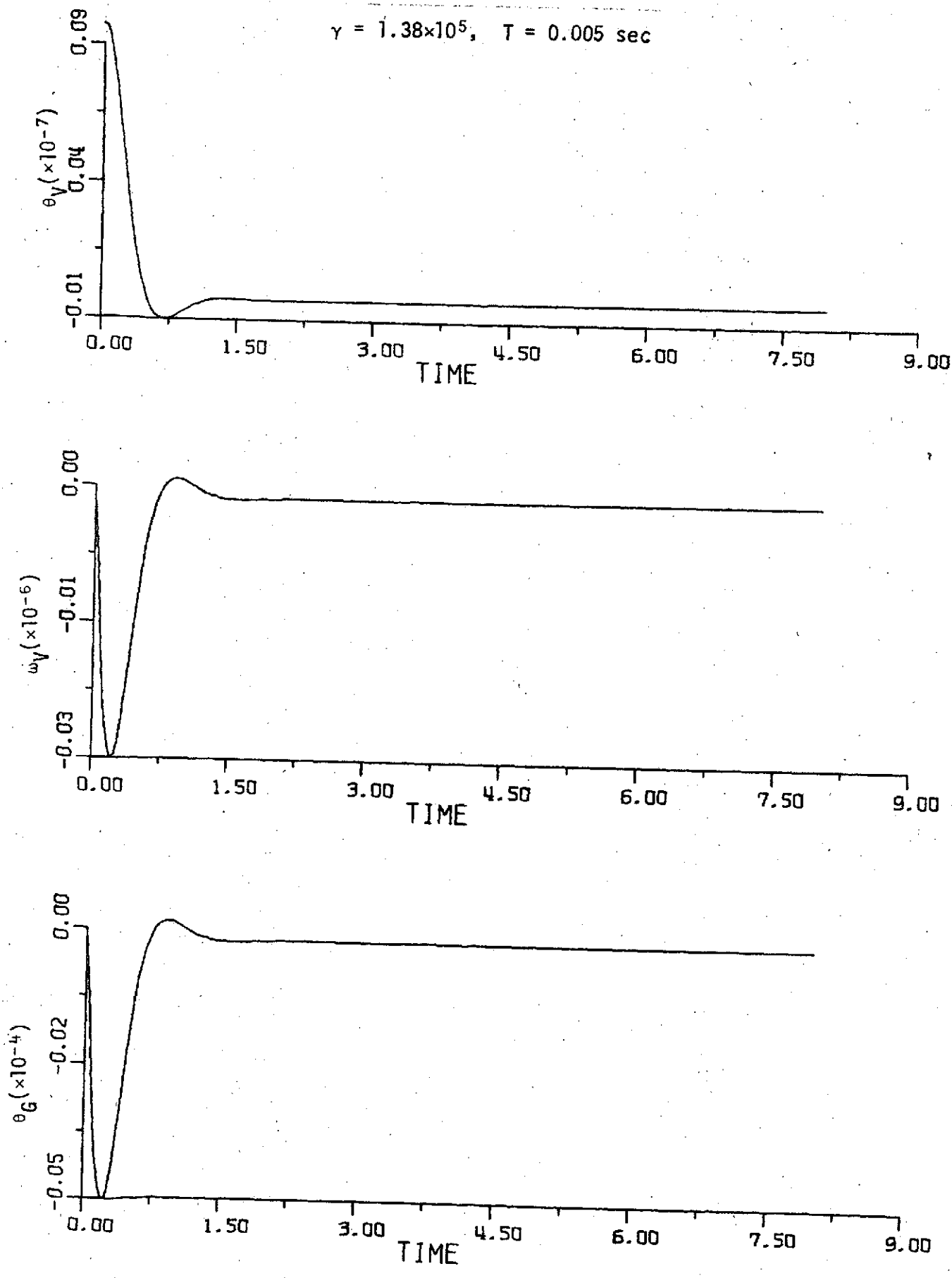
γ = 1.38×10^5, T = 0.005 sec
θV(×10-7)
0.09
0.04
-0.01
0.00
1.50
3.00
4.50
6.00
7.50
9.00
TIME
ωV(×10-6)
0.00
-0.01
-0.03
0.00
1.50
3.00
4.50
6.00
7.50
9.00
TIME
θG(×10-4)
0.00
-0.02
-0.05
0.00
1.50
3.00
4.50
6.00
7.50
9.00
TIME

Figure 10-1

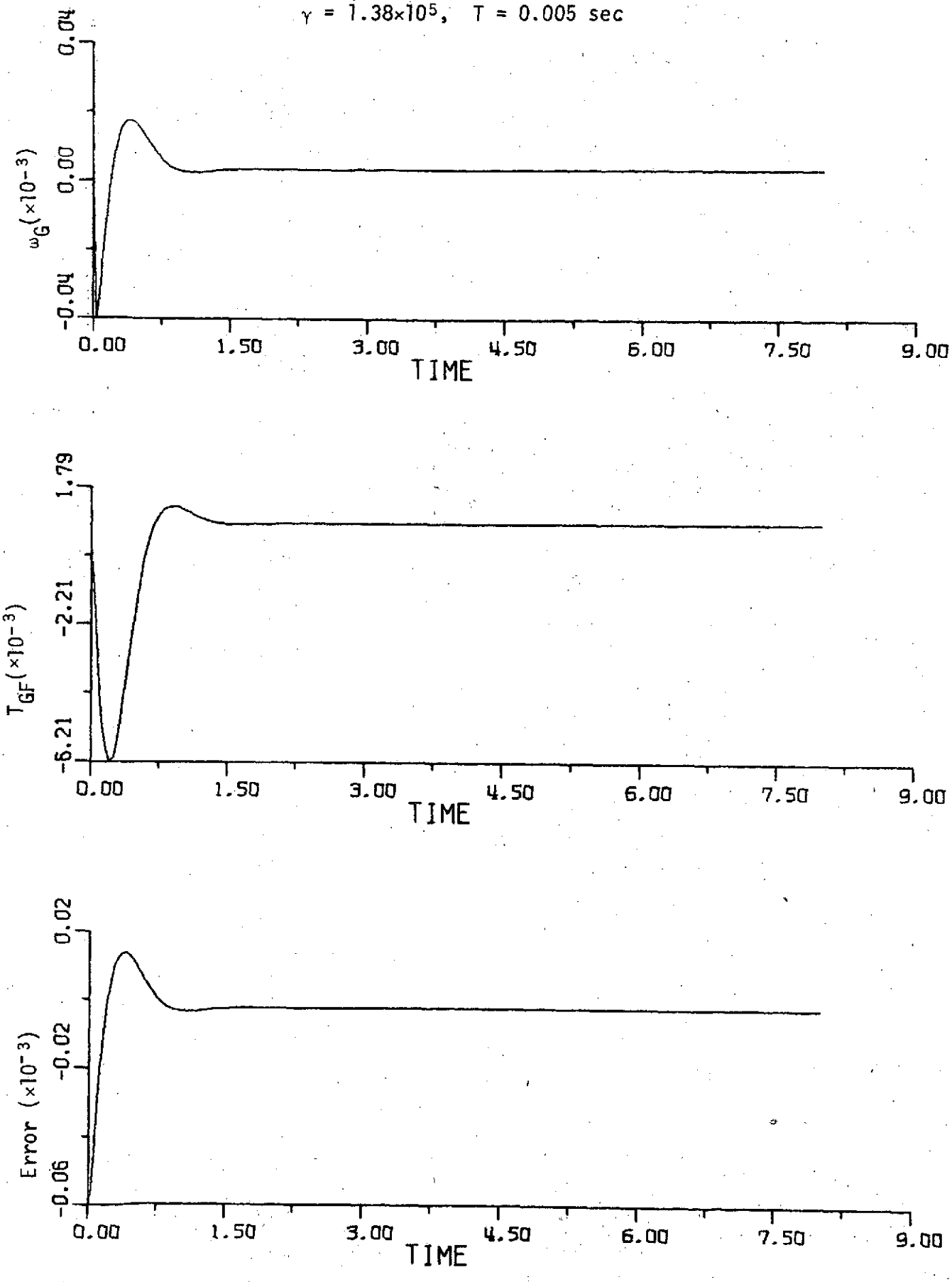
γ = 1.38×10⁵, T = 0.005 sec
0.04
0.00
-0.04
ω_G(×10⁻³)
0.00
1.50
3.00
4.50
6.00
7.50
9.00
TIME
1.79
-2.21
-6.21
T_GF(×10⁻³)
0.00
1.50
3.00
4.50
6.00
7.50
9.00
TIME
0.02
-0.02
-0.06
Error (×10⁻³)
0.00
1.50
3.00
4.50
6.00
7.50
9.00
TIME

Figure 10-2

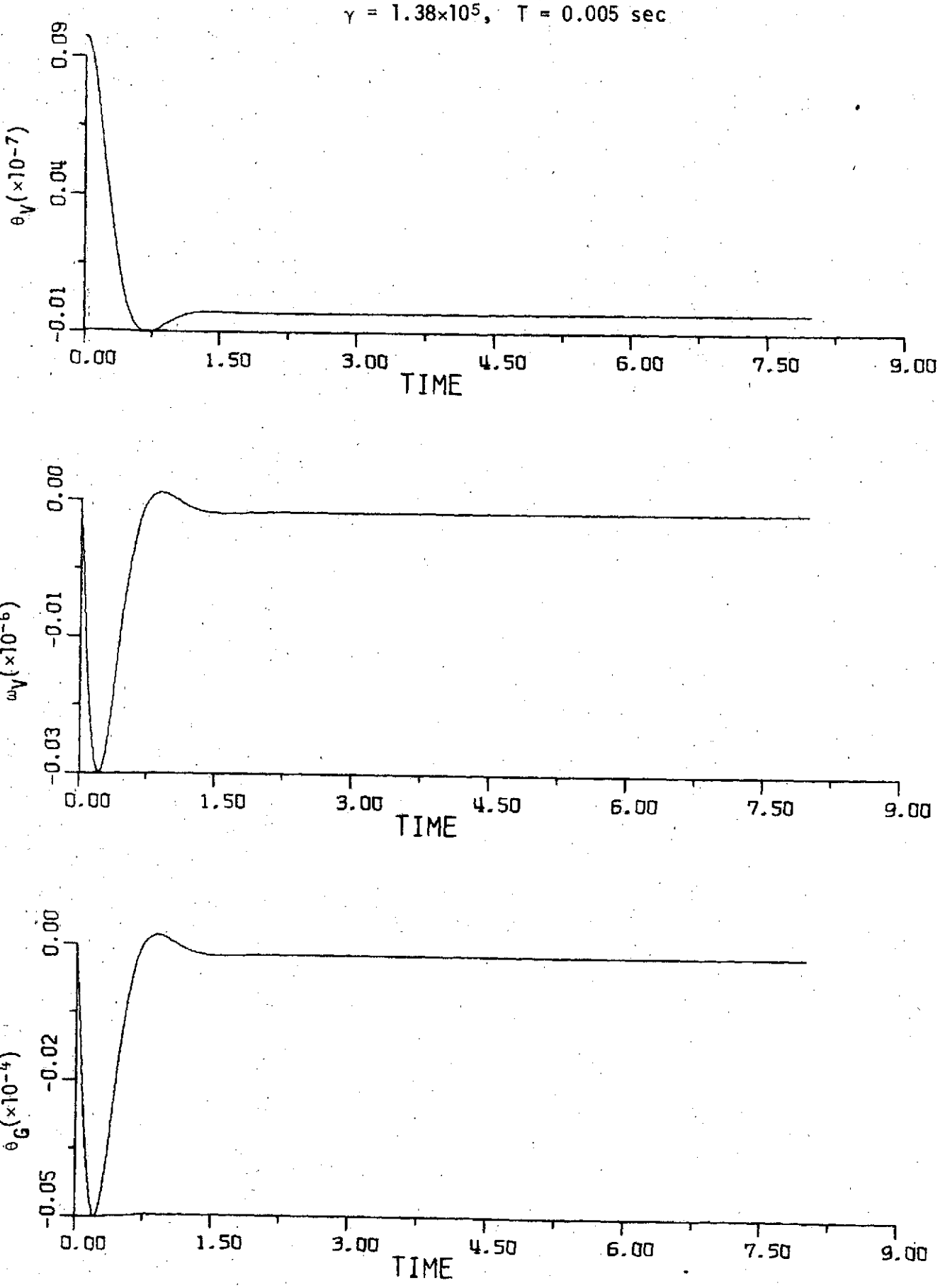
γ = 1.38×10^5, T = 0.005 sec
θV(×10-7)
0.09
0.04
-0.01
0.00
1.50
3.00
4.50
6.00
7.50
9.00
TIME
ωV(×10-6)
0.00
-0.01
-0.03
0.00
1.50
3.00
4.50
6.00
7.50
9.00
TIME
θG(×10-4)
0.00
-0.02
-0.05
0.00
1.50
3.00
4.50
6.00
7.50
9.00
TIME

Figure 10-3

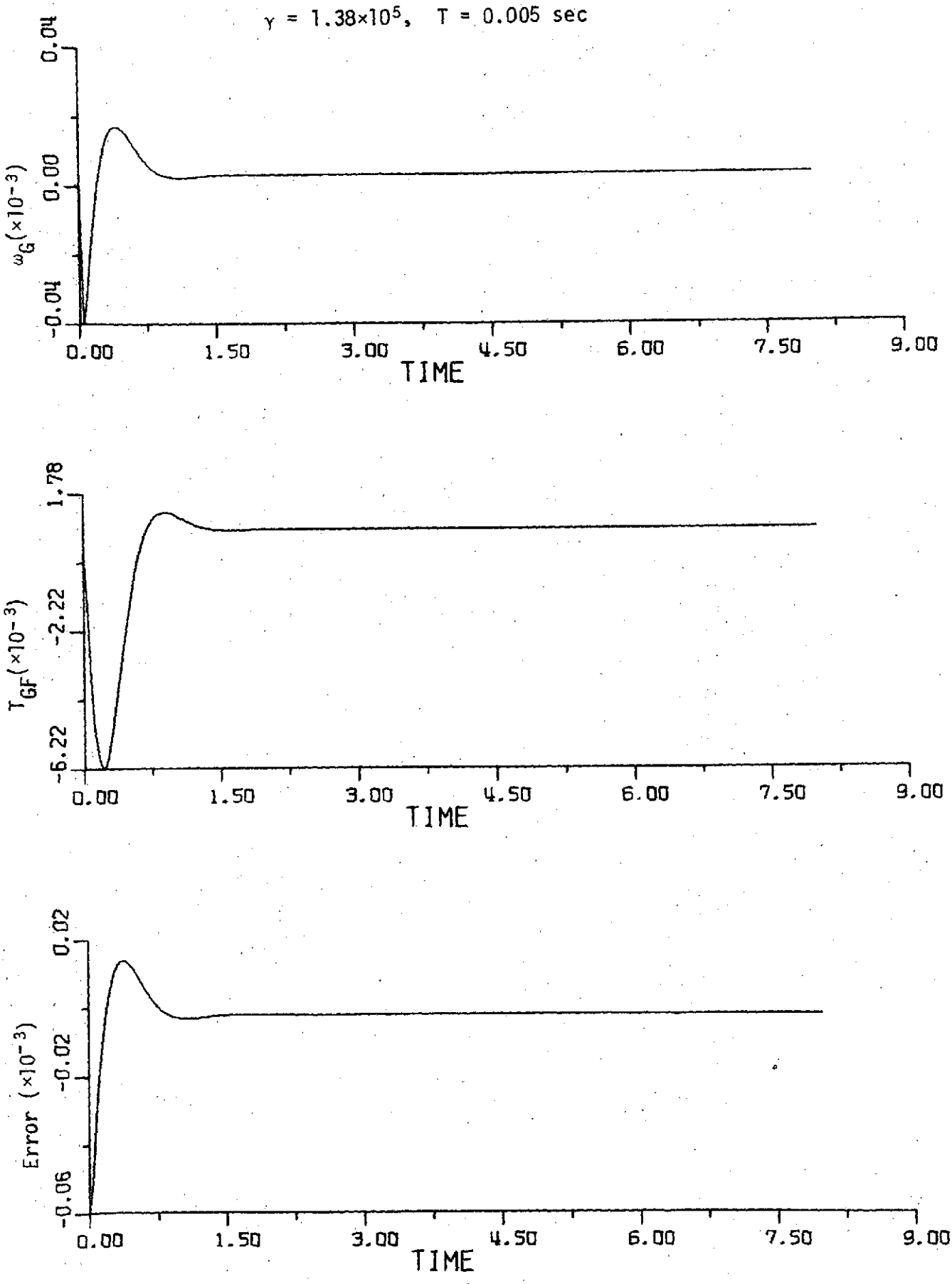
γ = 1.38×10^5, T = 0.005 sec
0.04
0.00
-0.04
ω_G(×10^-3)
0.00
1.50
3.00
4.50
6.00
7.50
9.00
TIME
1.78
-2.22
-6.22
T_GF(×10^-3)
0.00
1.50
3.00
4.50
6.00
7.50
9.00
TIME
0.02
-0.02
-0.06
Error (×10^-3)
0.00
1.50
3.00
4.50
6.00
7.50
9.00
TIME

Figure 10-4

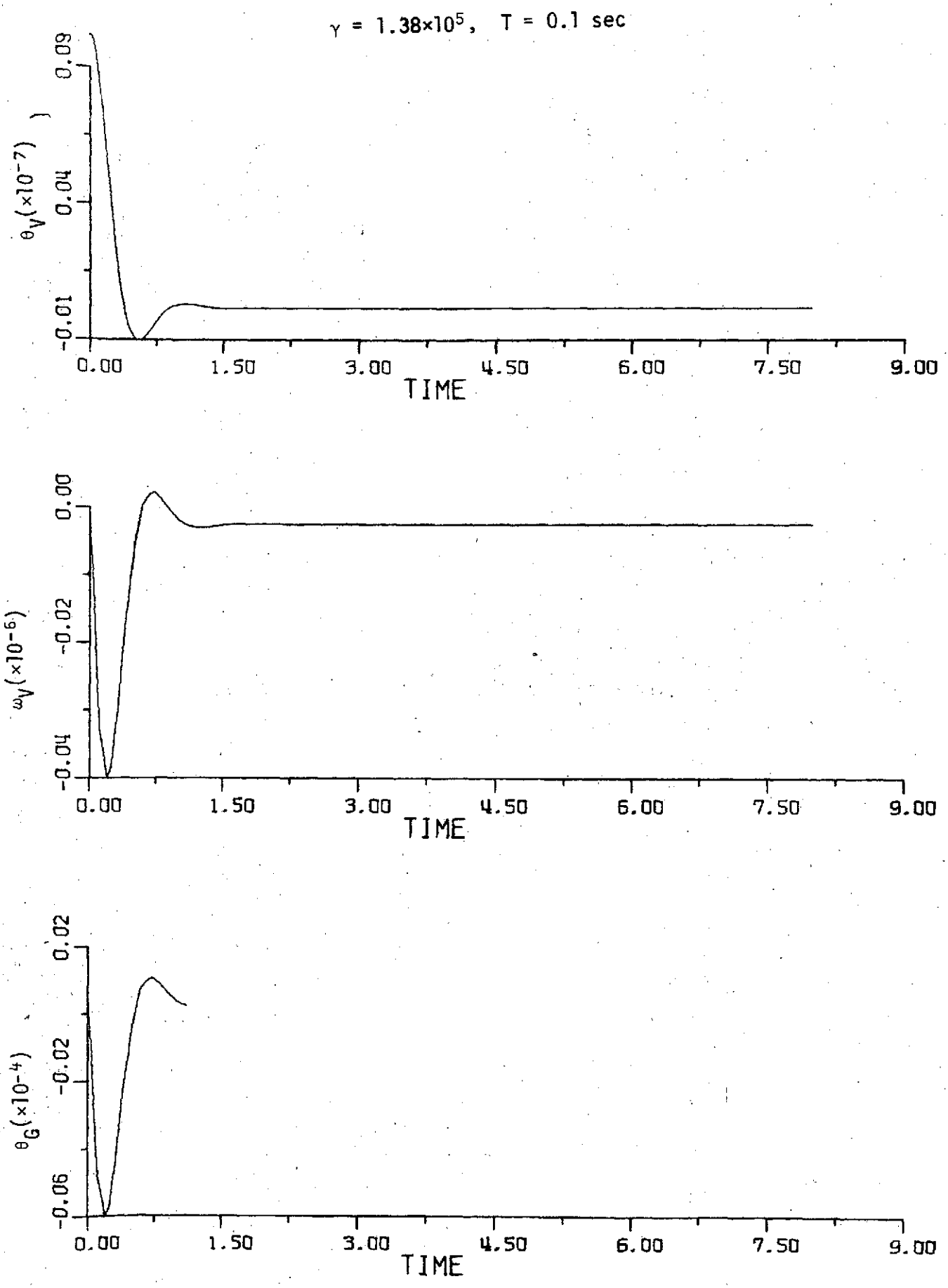
γ = 1.38×10^5, T = 0.1 sec
θV(×10^-7)
0.09
0.04
-0.01
0.00
1.50
3.00
4.50
6.00
7.50
9.00
TIME
ωV(×10^-6)
0.00
-0.02
-0.04
0.00
1.50
3.00
4.50
6.00
7.50
9.00
TIME
θG(×10^-4)
0.02
-0.02
-0.06
0.00
1.50
3.00
4.50
6.00
7.50
9.00
TIME

Figure 10-5

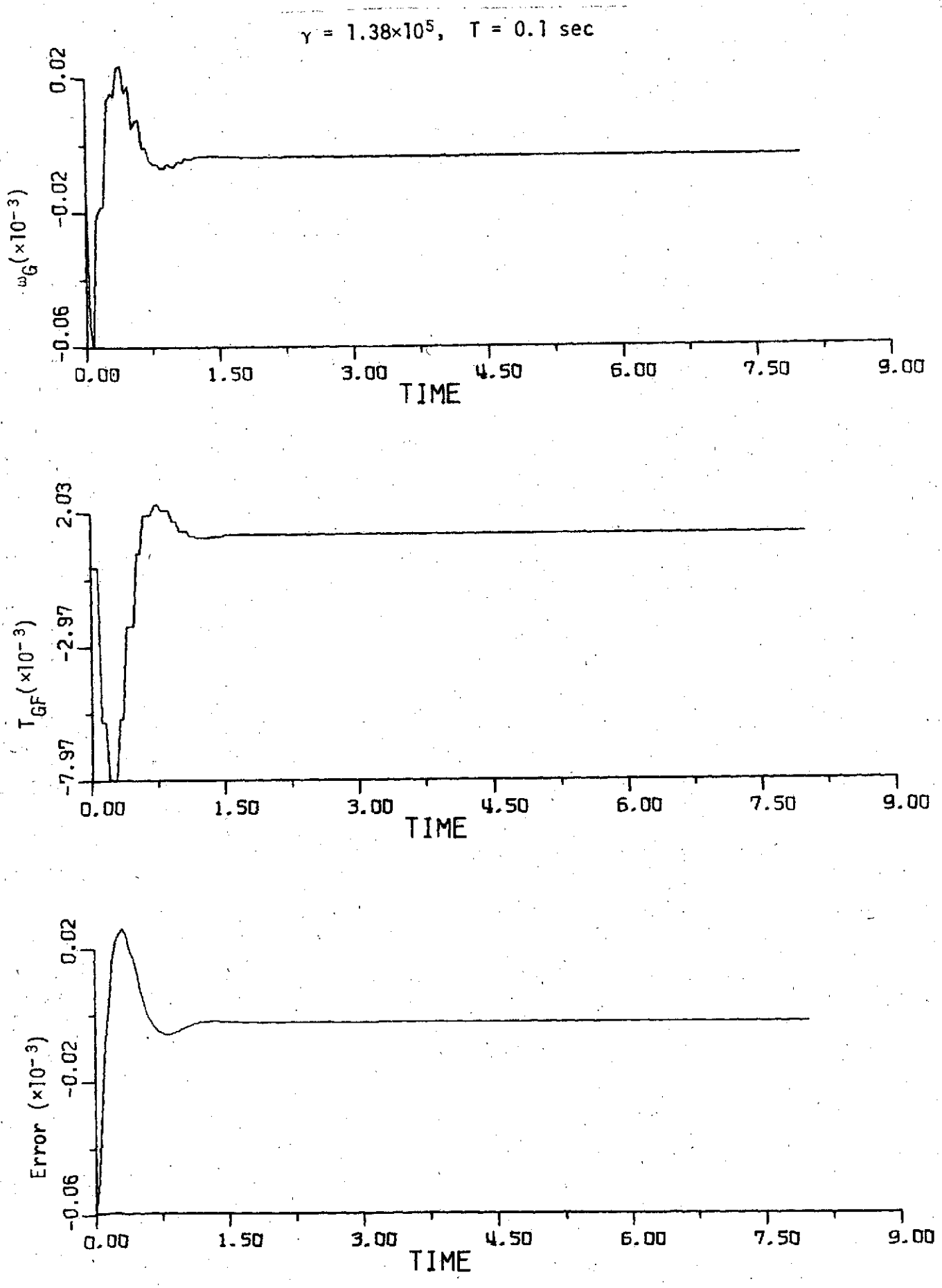
γ = 1.38×10^5, T = 0.1 sec
0.02
-0.02
-0.06
ω_G(×10^-3)
0.00
1.50
3.00
4.50
6.00
7.50
9.00
TIME
2.03
-2.97
-7.97
T_GF(×10^-3)
0.00
1.50
3.00
4.50
6.00
7.50
9.00
TIME
0.02
-0.02
-0.06
Error (×10^-3)
0.00
1.50
3.00
4.50
6.00
7.50
9.00
TIME

Figure 10-6

$\gamma = 1.38\times10^5$, T = 0.1 sec

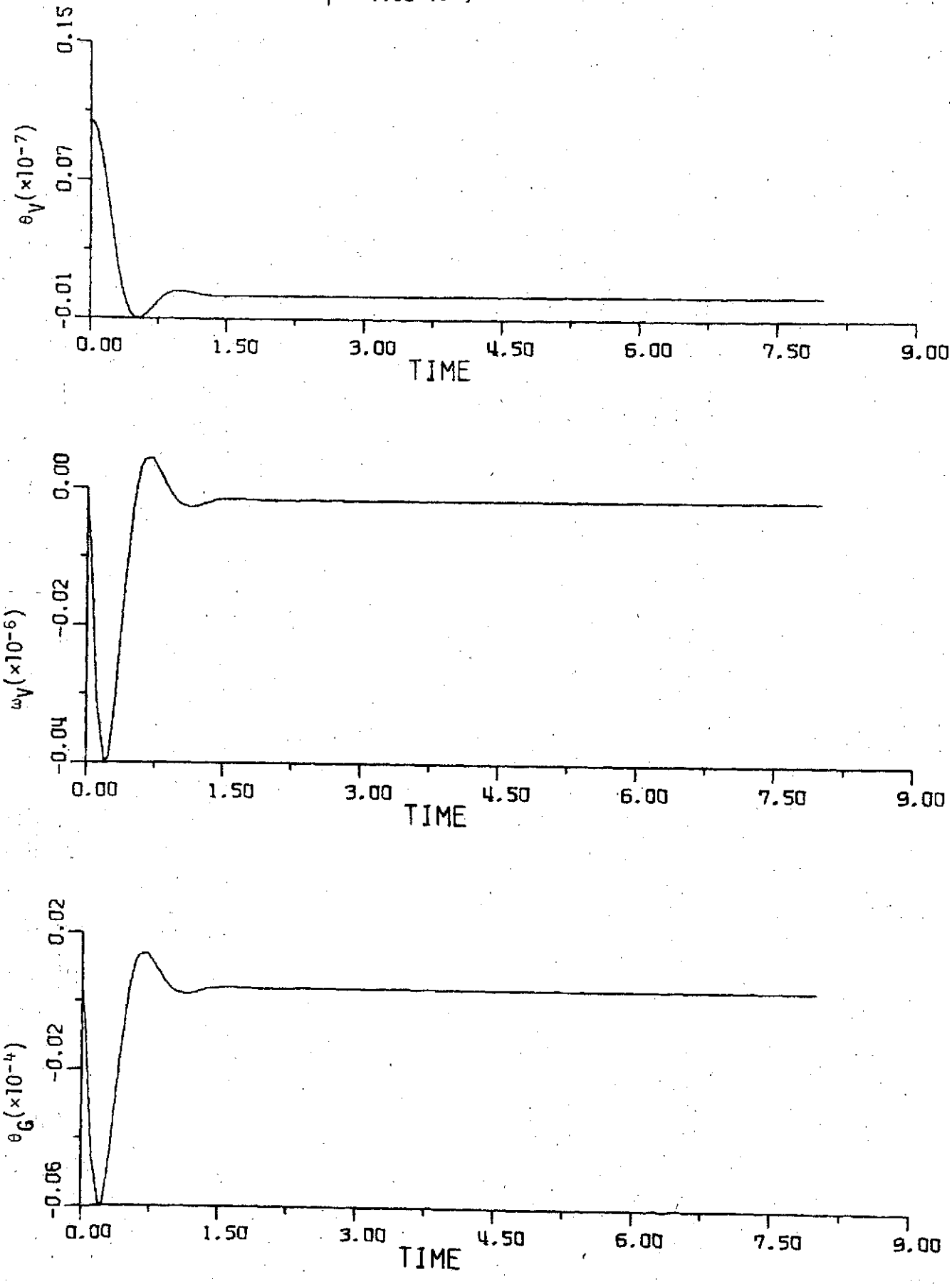

Figure 10-7

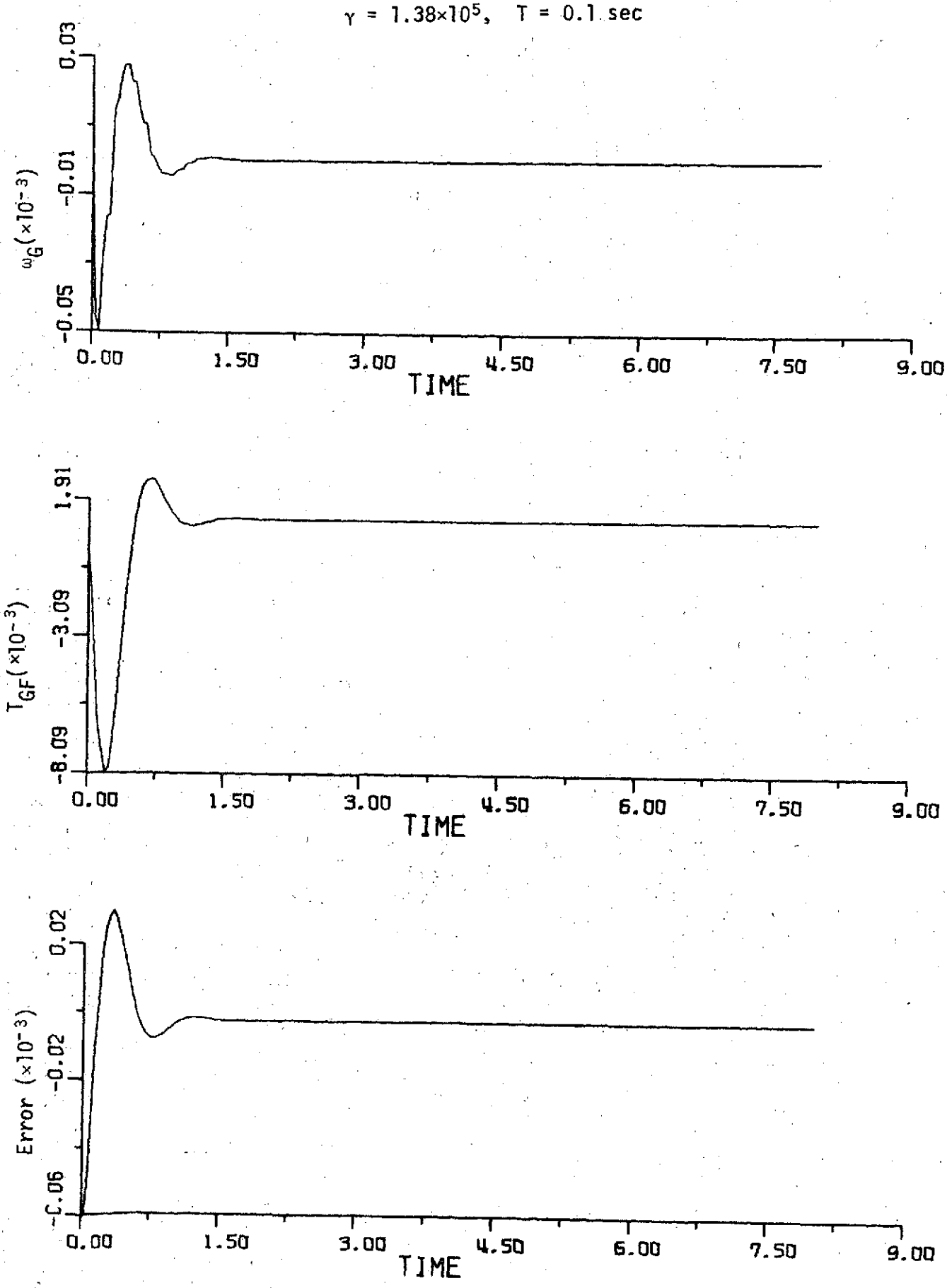
γ = 1.38×10^5, T = 0.1 sec
0.03
-0.01
-0.05
ω_G(×10^-3)
0.00
1.50
3.00
4.50
6.00
7.50
9.00
TIME
1.91
-3.09
-8.09
T_GF(×10^-3)
0.00
1.50
3.00
4.50
6.00
7.50
9.00
TIME
0.02
-0.02
-0.06
Error (×10^-3)
0.00
1.50
3.00
4.50
6.00
7.50
9.00
TIME

Figure 10-8

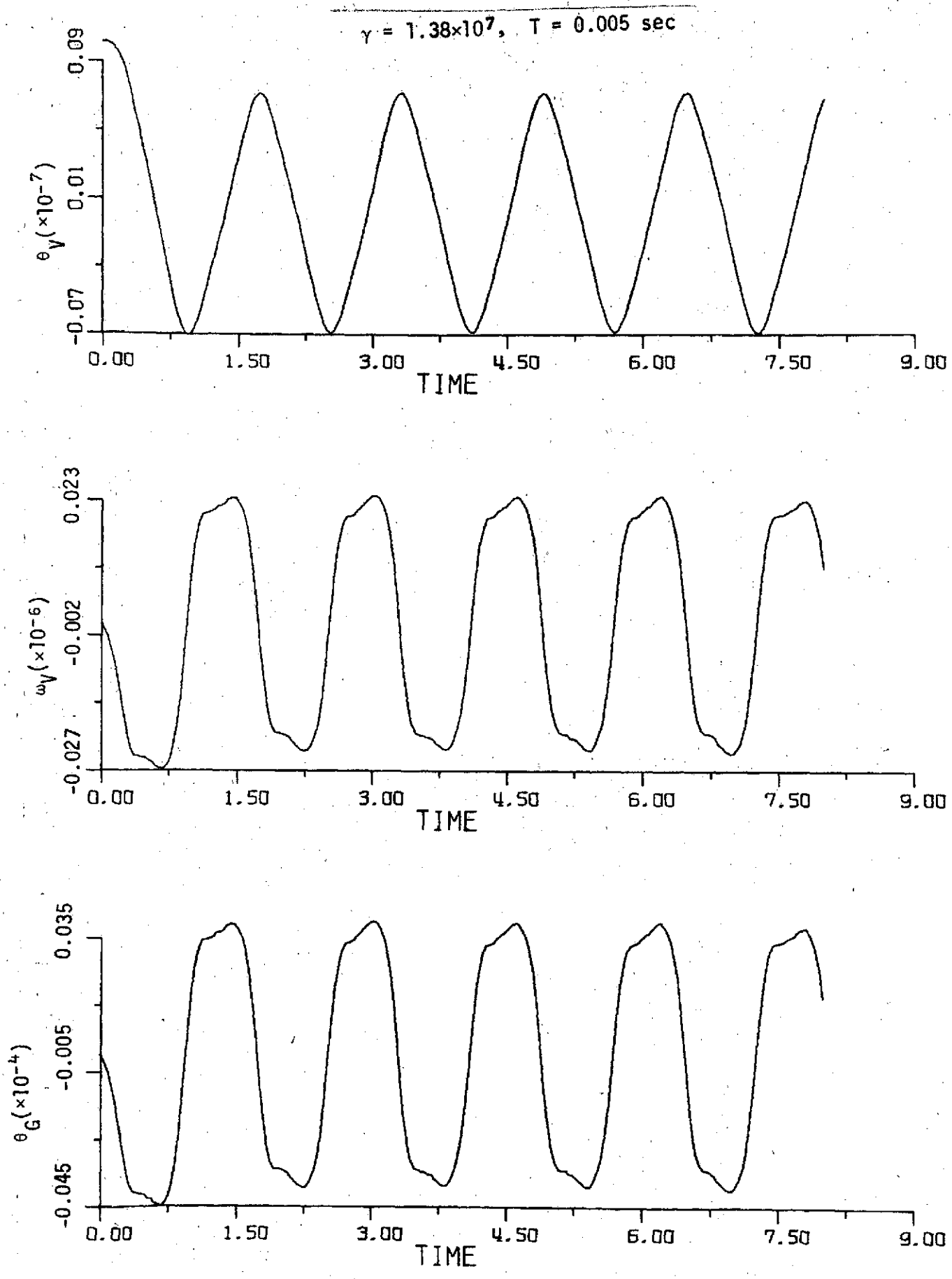
γ = 1.38×10⁷, T = 0.005 sec
θγ(×10⁻⁷)
0.09
0.01
-0.07
0.00
1.50
3.00
4.50
6.00
7.50
9.00
TIME
ωγ(×10⁻⁶)
0.023
-0.002
-0.027
0.00
1.50
3.00
4.50
6.00
7.50
9.00
TIME
θG(×10⁻⁴)
0.035
-0.005
-0.045
0.00
1.50
3.00
4.50
6.00
7.50
9.00
TIME

Figure 10-9

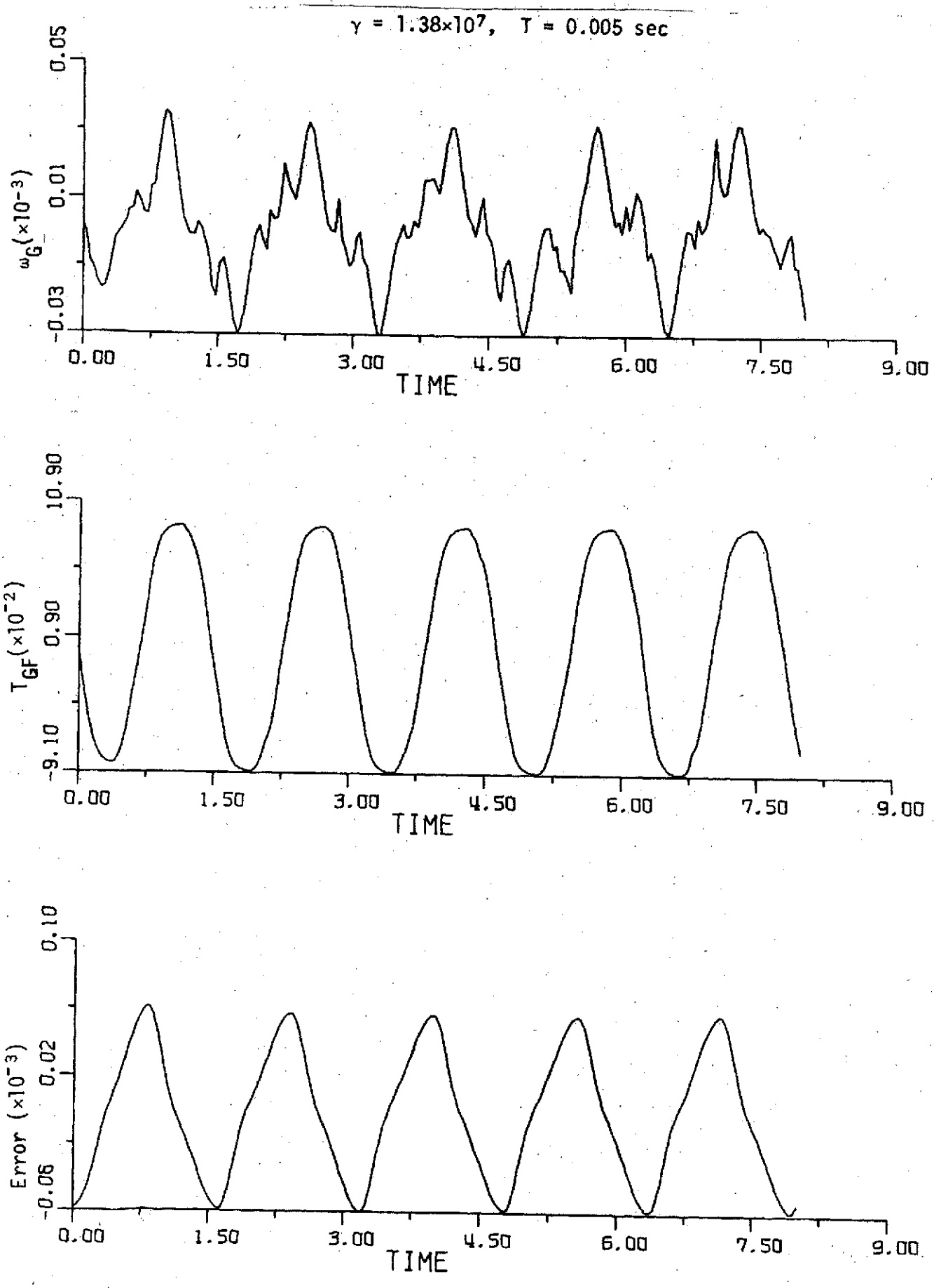
γ = 1.38×10⁷, T = 0.005 sec
0.05
0.01
-0.03
ω_G(×10⁻³)
0.00
1.50
3.00
4.50
6.00
7.50
9.00
TIME
10.90
0.90
-9.10
T_GF(×10⁻²)
0.00
1.50
3.00
4.50
6.00
7.50
9.00
TIME
0.10
0.02
-0.06
Error (×10⁻³)
0.00
1.50
3.00
4.50
6.00
7.50
9.00
TIME

Figure 10-10

$\gamma = 1.38 \times 10^7$, T = 0.005 sec

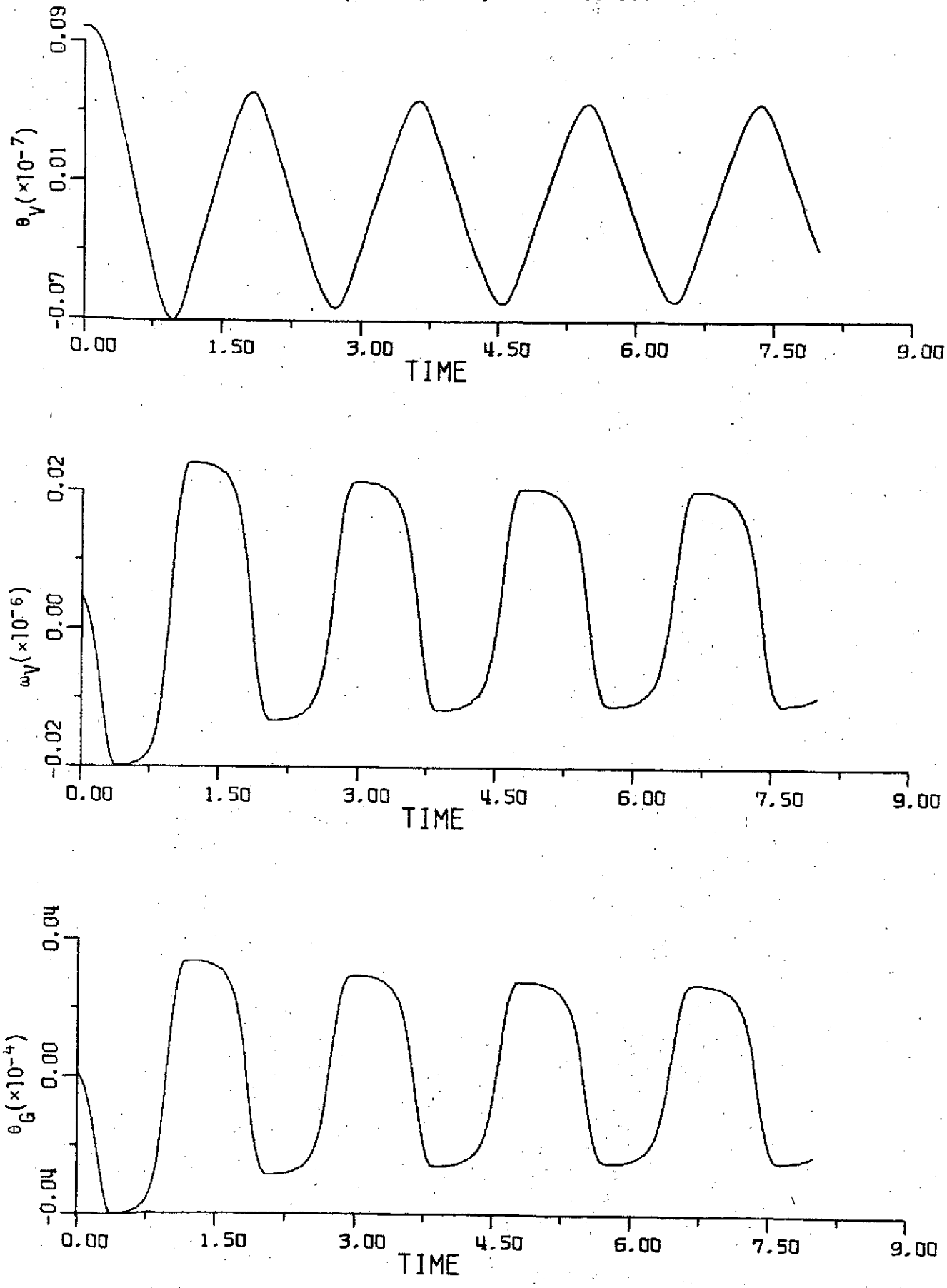

Figure 10-11

$\gamma = 1.38 \times 10^7$, $T = 0.005$ sec

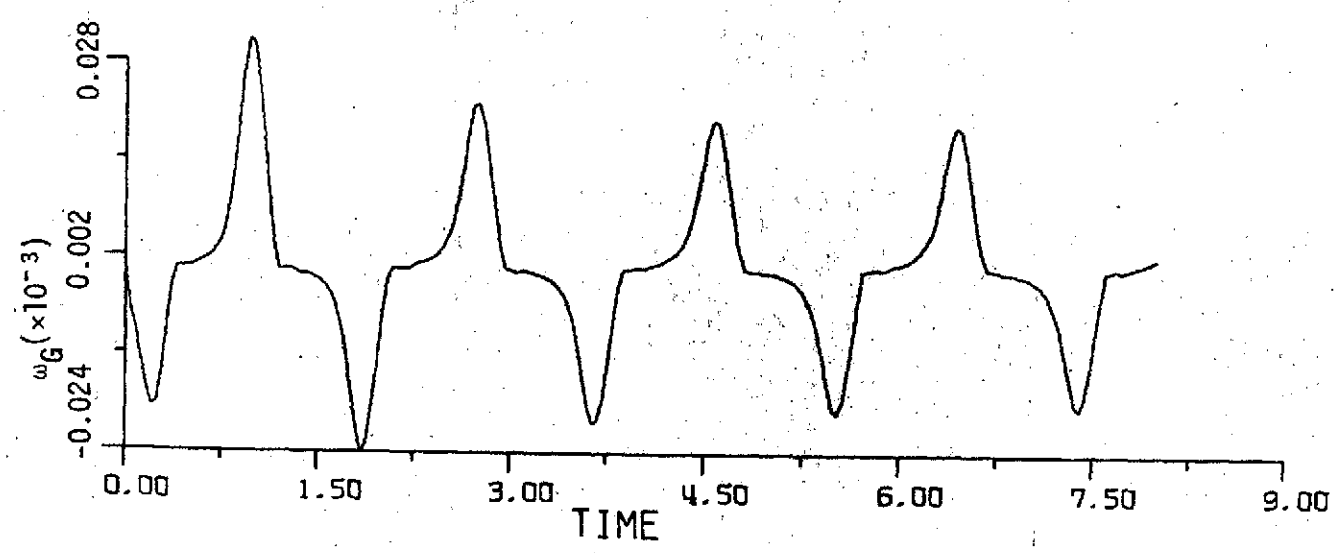

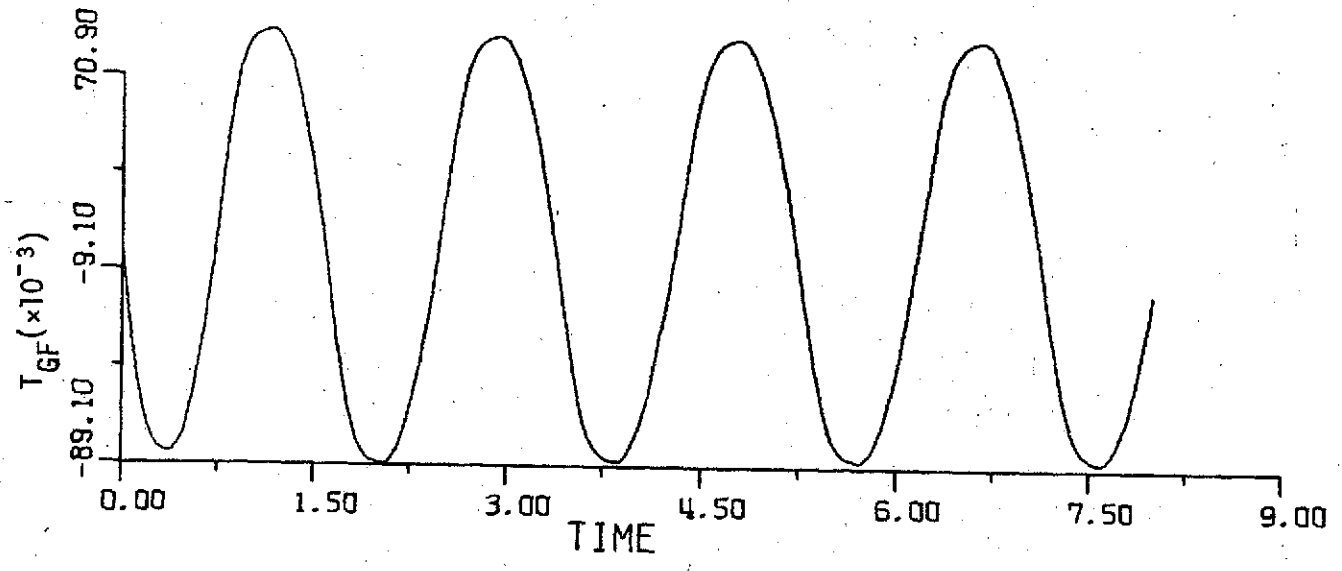

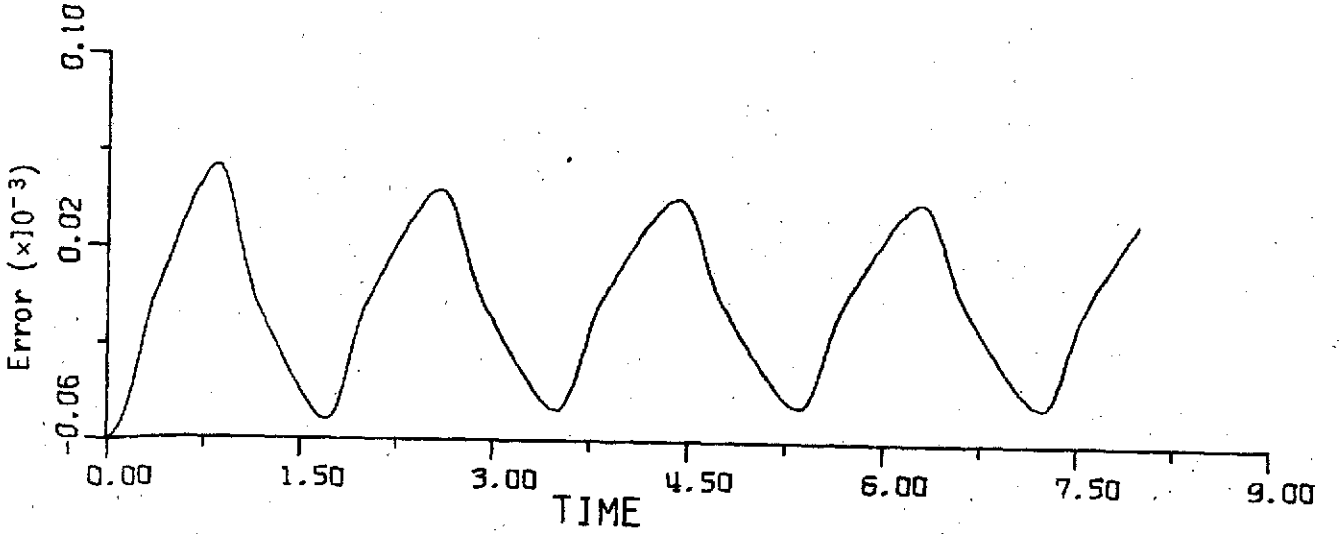

Figure 10-12

$\gamma = 1.38 \times 10^7$, $T = 0.02$ sec

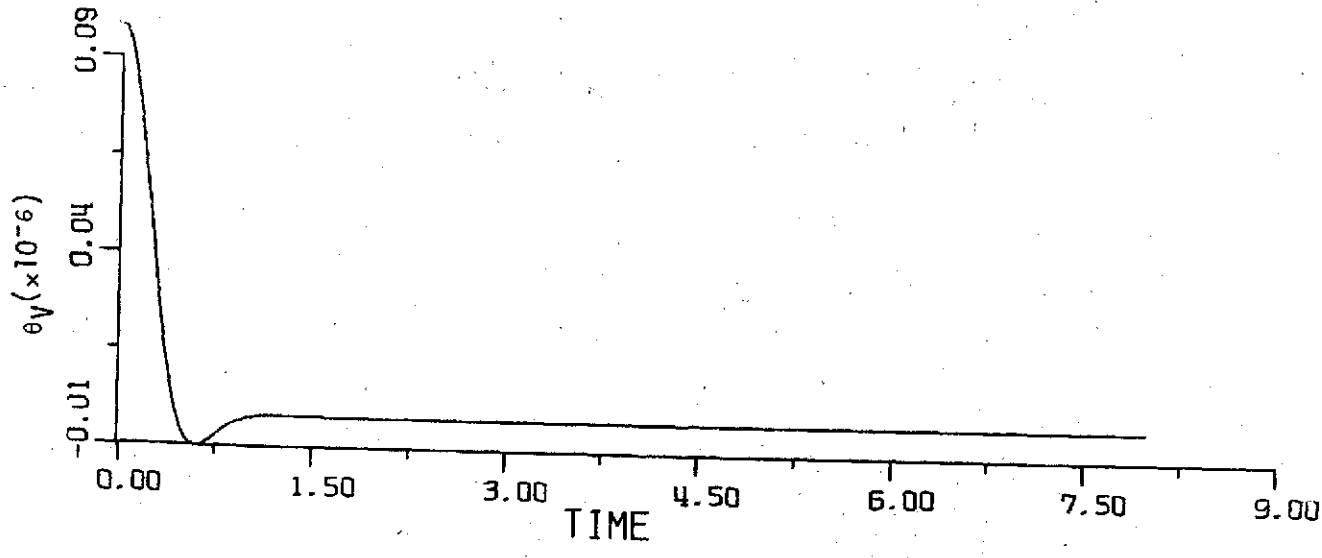

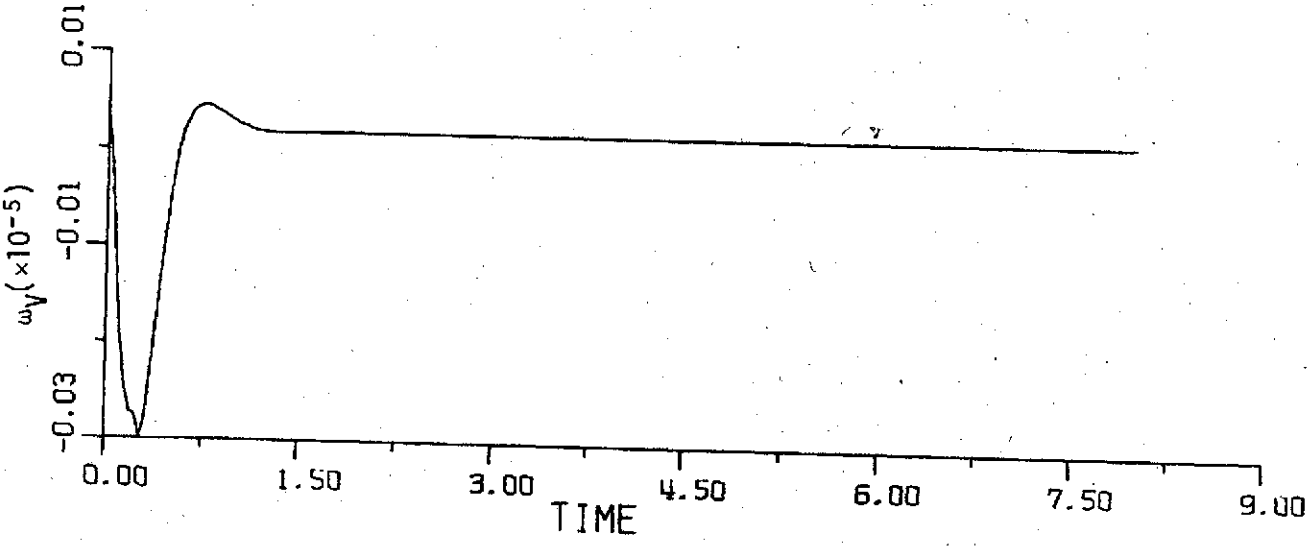

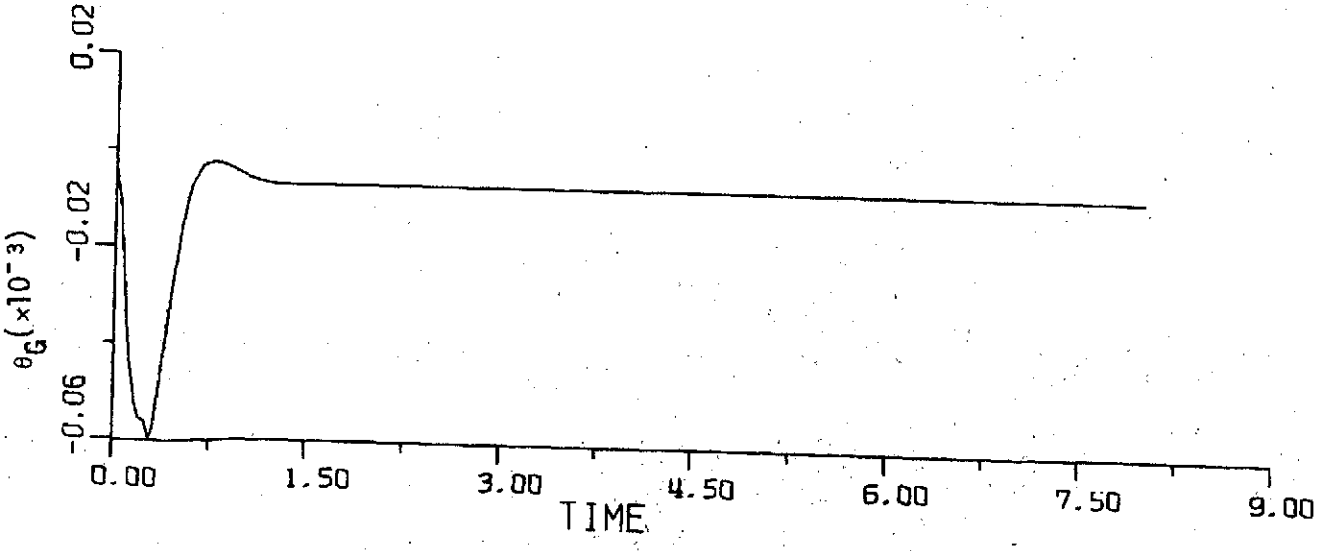

Figure 10-13

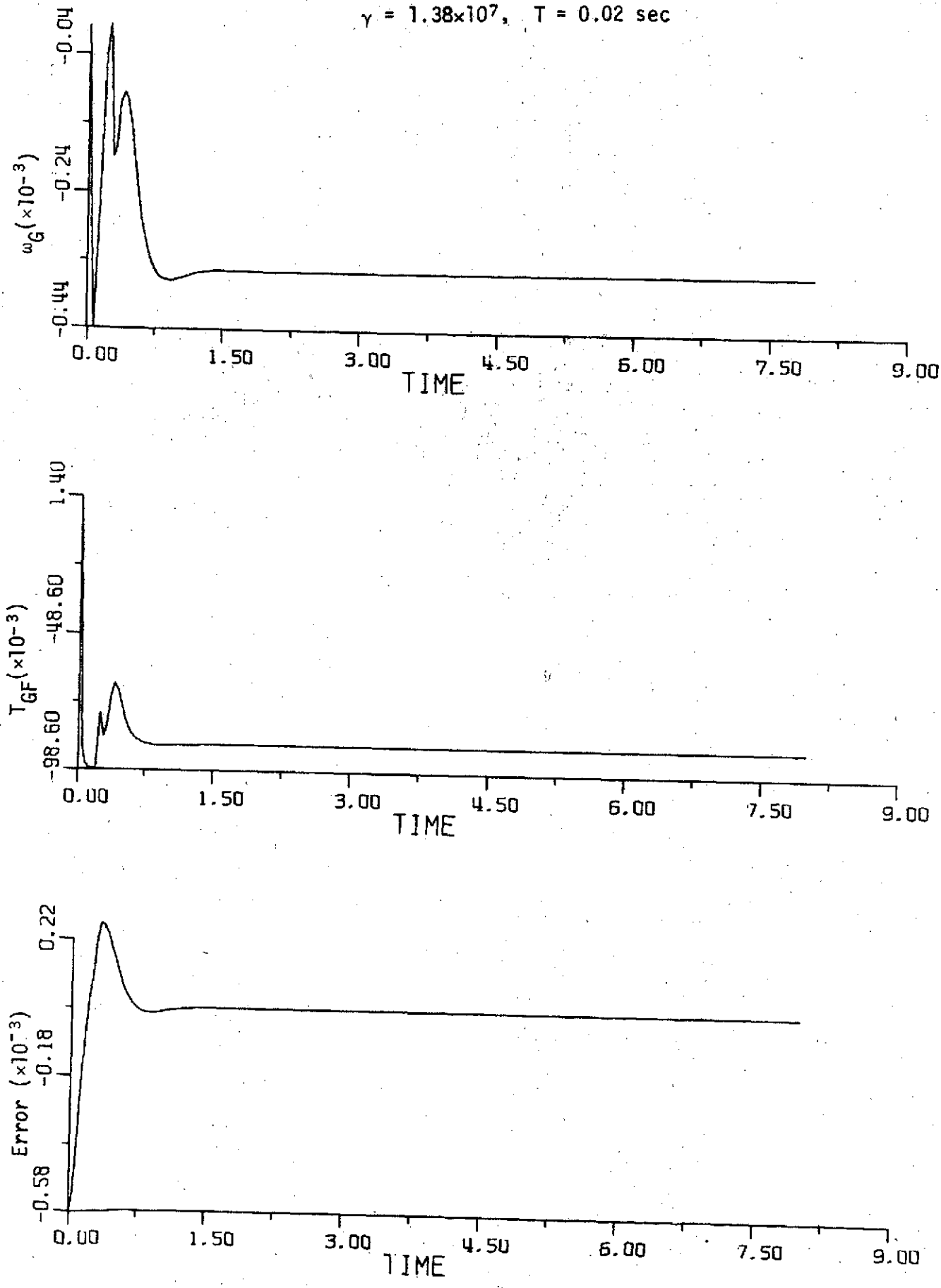
γ = 1.38×10⁷, T = 0.02 sec
ω_G(×10⁻³)
-0.04
-0.24
-0.44
0.00
1.50
3.00
4.50
6.00
7.50
9.00
TIME
T_GF(×10⁻³)
1.40
-48.60
-98.60
0.00
1.50
3.00
4.50
6.00
7.50
9.00
TIME
Error (×10⁻³)
0.22
-0.18
-0.58
0.00
1.50
3.00
4.50
6.00
7.50
9.00
TIME

Figure 10-14

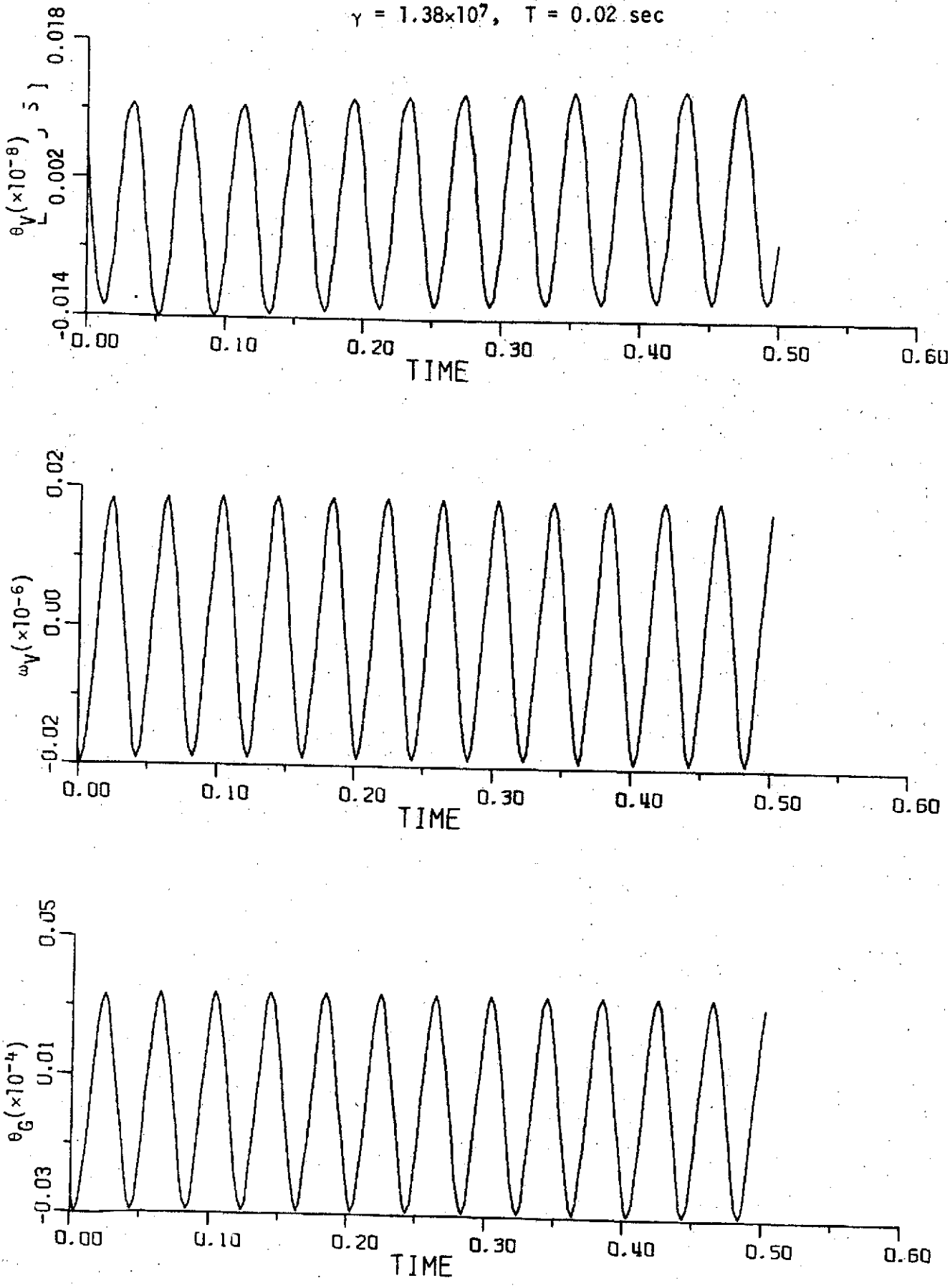
γ = 1.38×10⁷, T = 0.02 sec
θV(×10⁻⁸) [rad]
0.018
0.002
-0.014
0.00
0.10
0.20
0.30
0.40
0.50
0.60
TIME
ωV(×10⁻⁶)
0.02
0.00
-0.02
0.00
0.10
0.20
0.30
0.40
0.50
0.60
TIME
θG(×10⁻⁴)
0.05
0.01
-0.03
0.00
0.10
0.20
0.30
0.40
0.50
0.60
TIME

Figure 10-15

$\gamma = 1.38 \times 10^7$, $T = 0.02$ sec

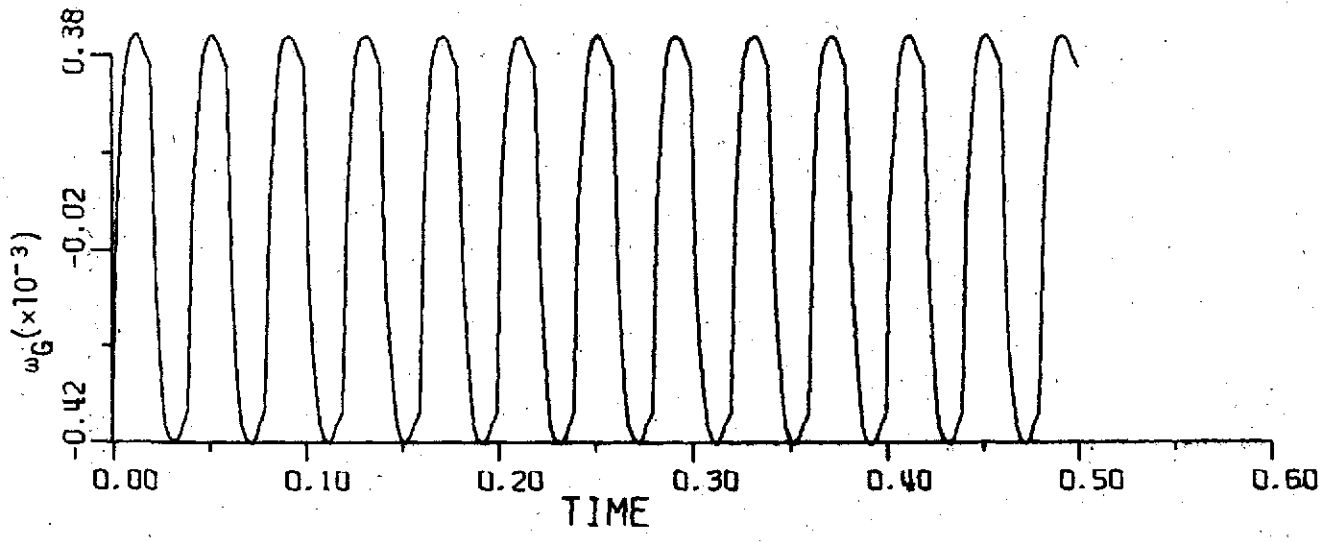

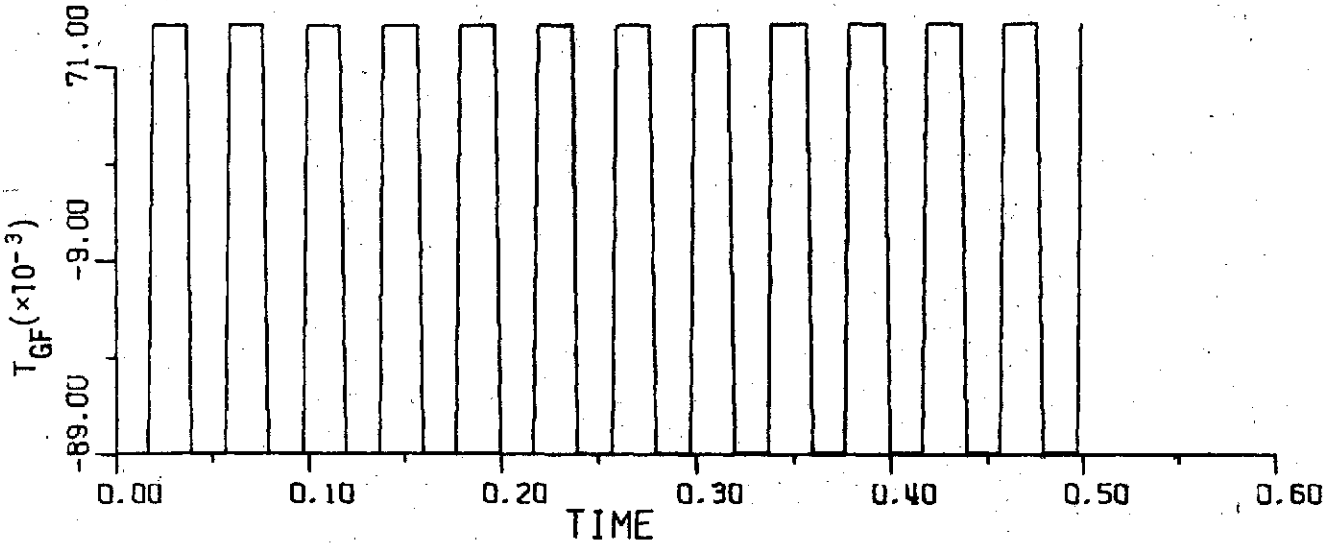

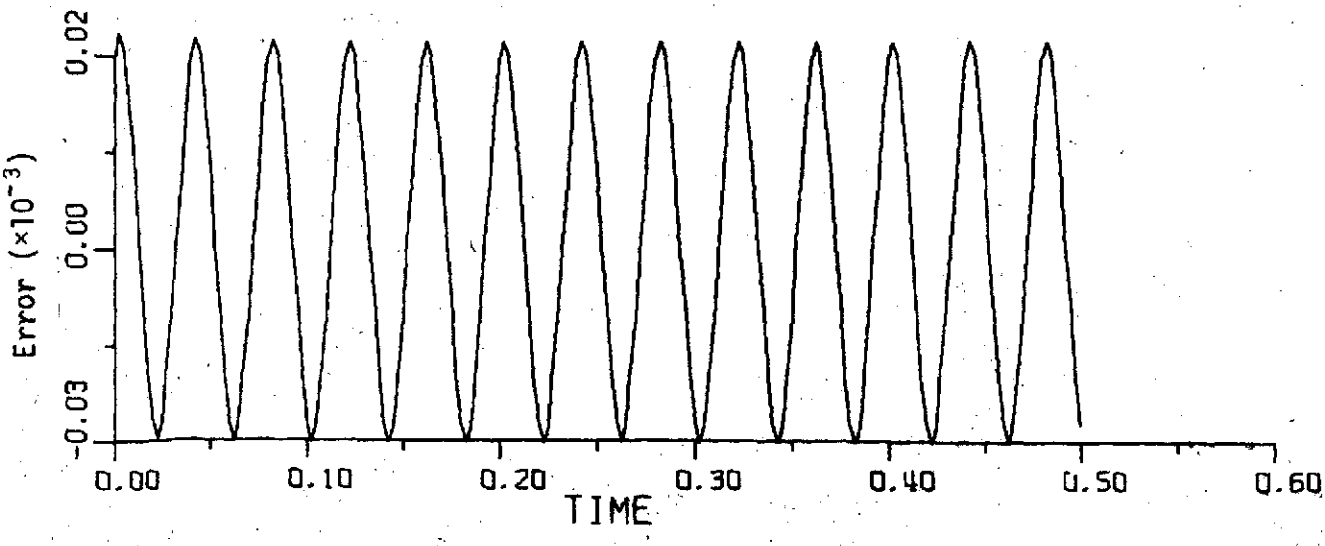

Figure 10-16

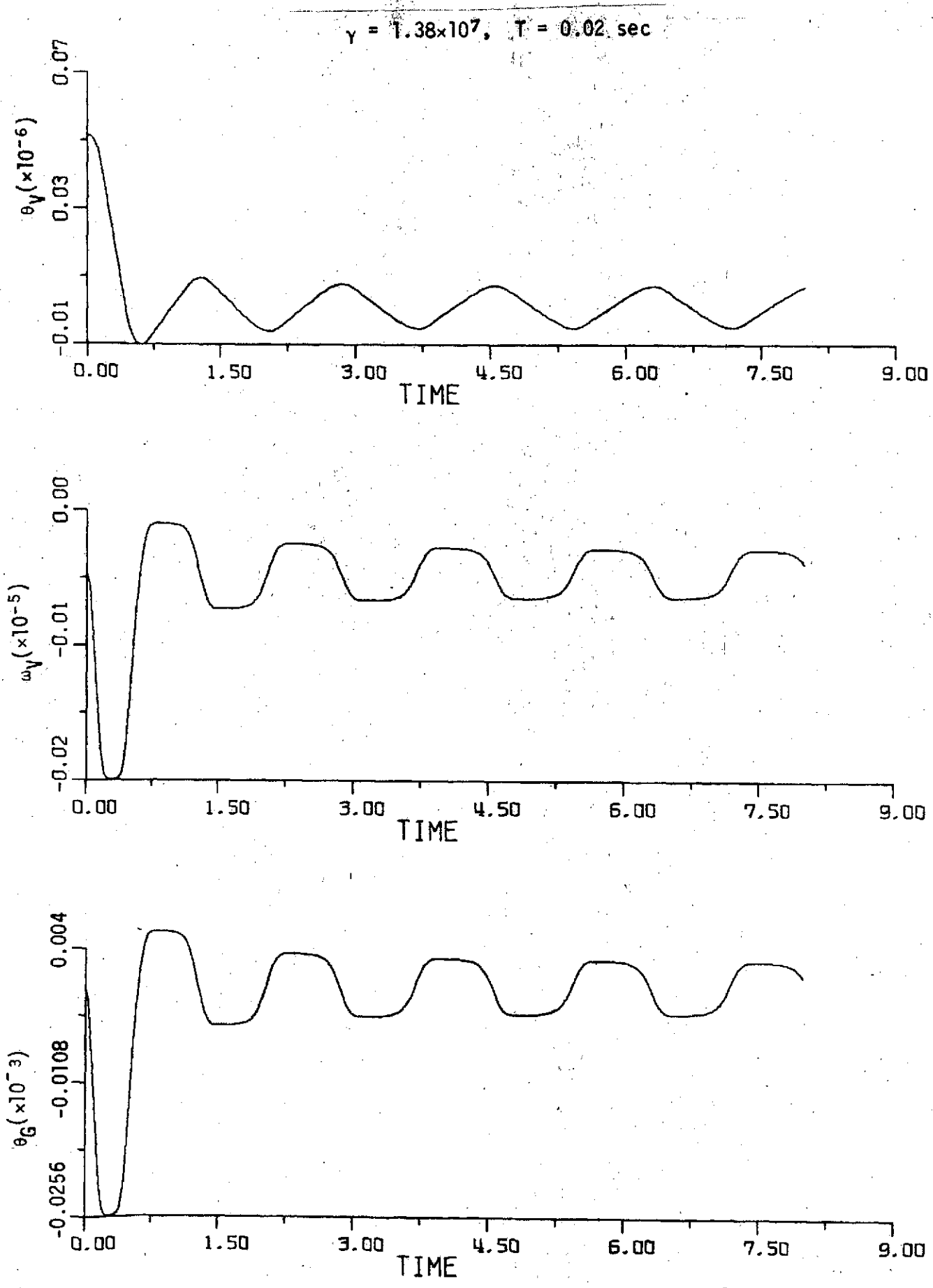
γ = 1.38×10⁷, T = 0.02 sec
θγ(×10⁻⁶)
0.07
0.03
-0.01
0.00
1.50
3.00
4.50
6.00
7.50
9.00
TIME
ωγ(×10⁻⁵)
0.00
-0.01
-0.02
0.00
1.50
3.00
4.50
6.00
7.50
9.00
TIME
θG(×10⁻³)
0.004
-0.0108
-0.0256
0.00
1.50
3.00
4.50
6.00
7.50
9.00
TIME

Figure 10-17

$\gamma = 1.38 \times 10^7$, $T = 0.02$ sec

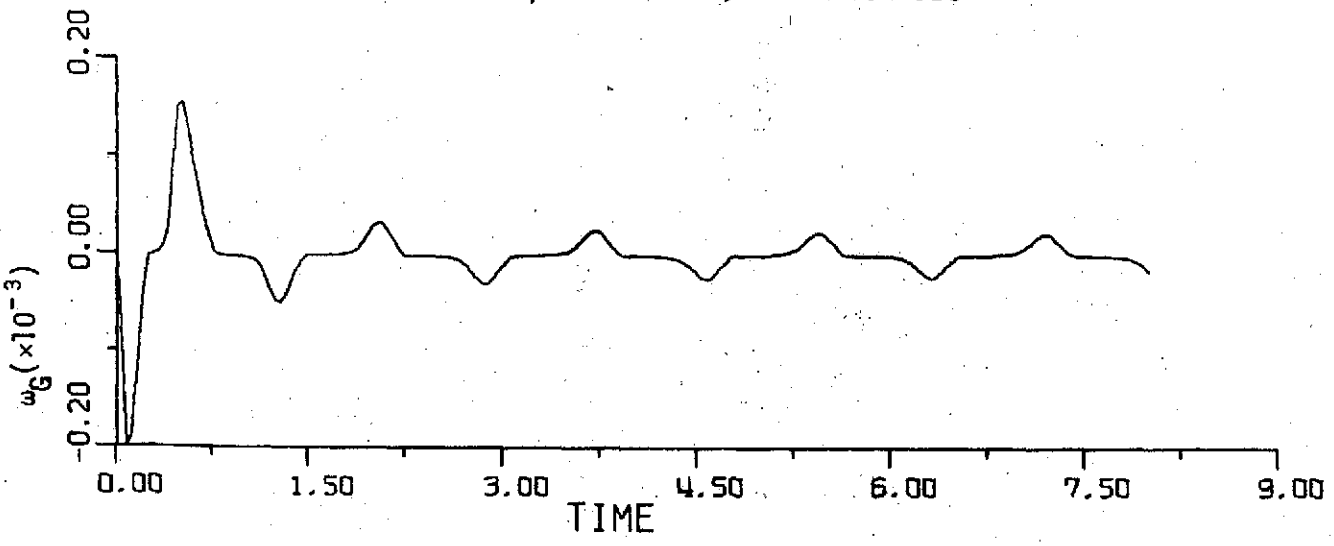

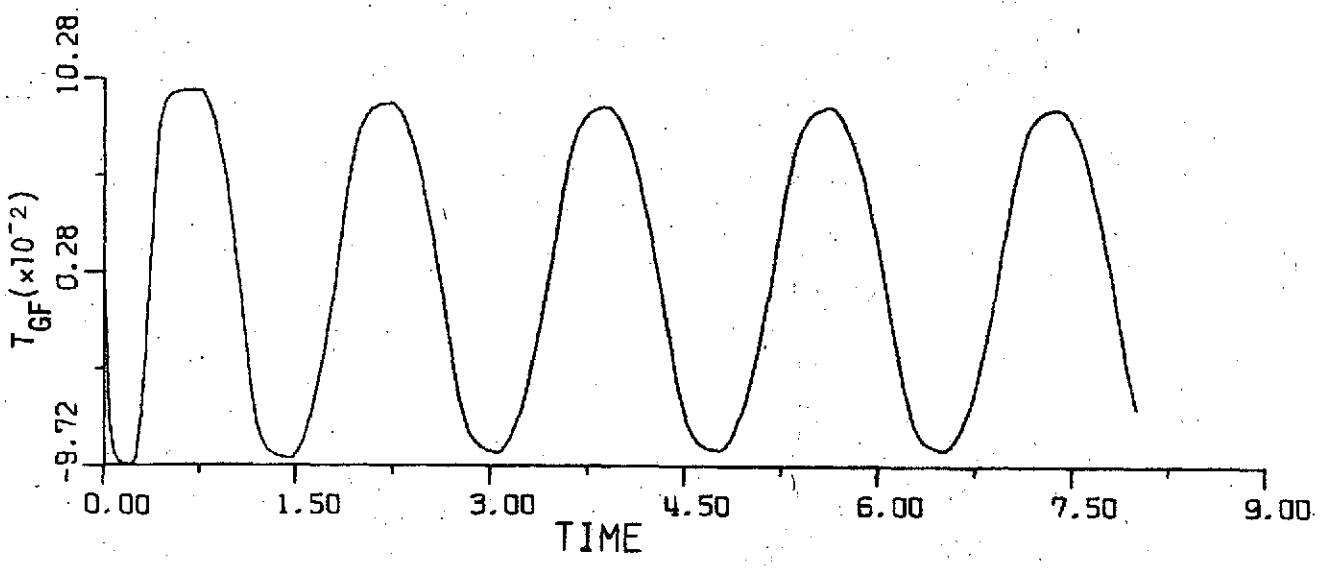

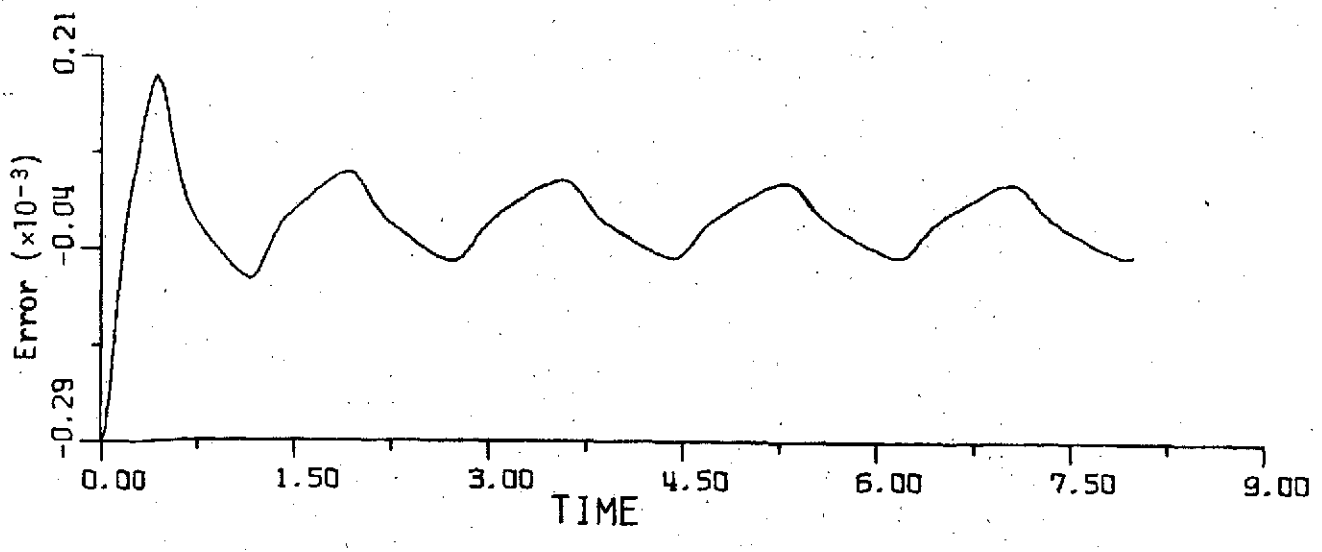

Figure 10-18

$\gamma = 1.38\times10^{7}$, T = 0.05 sec

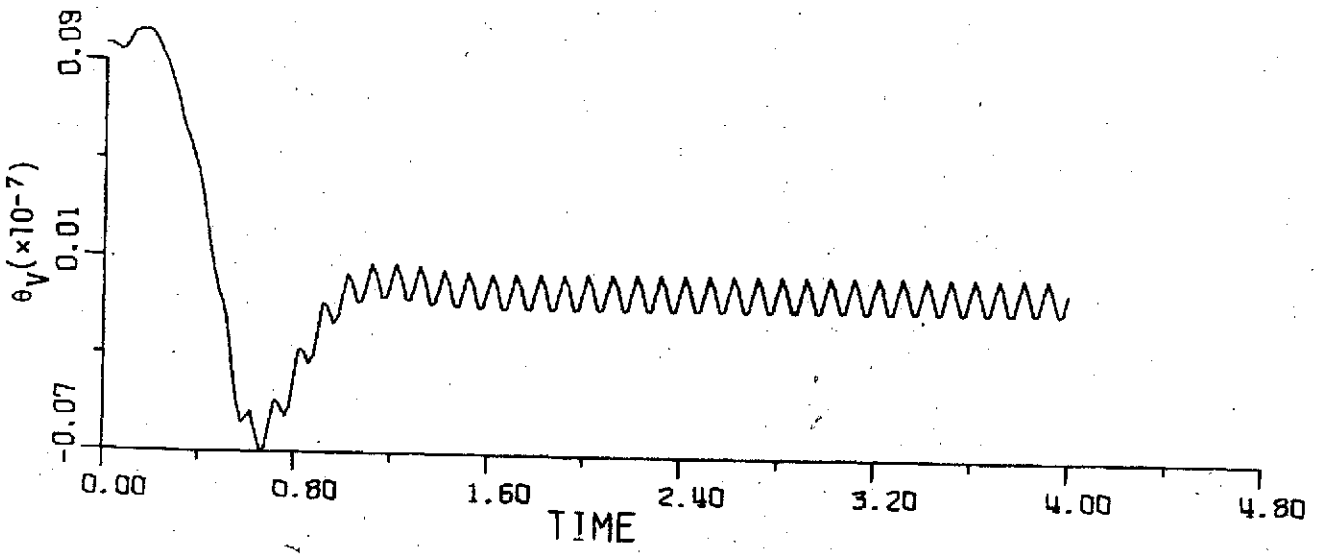

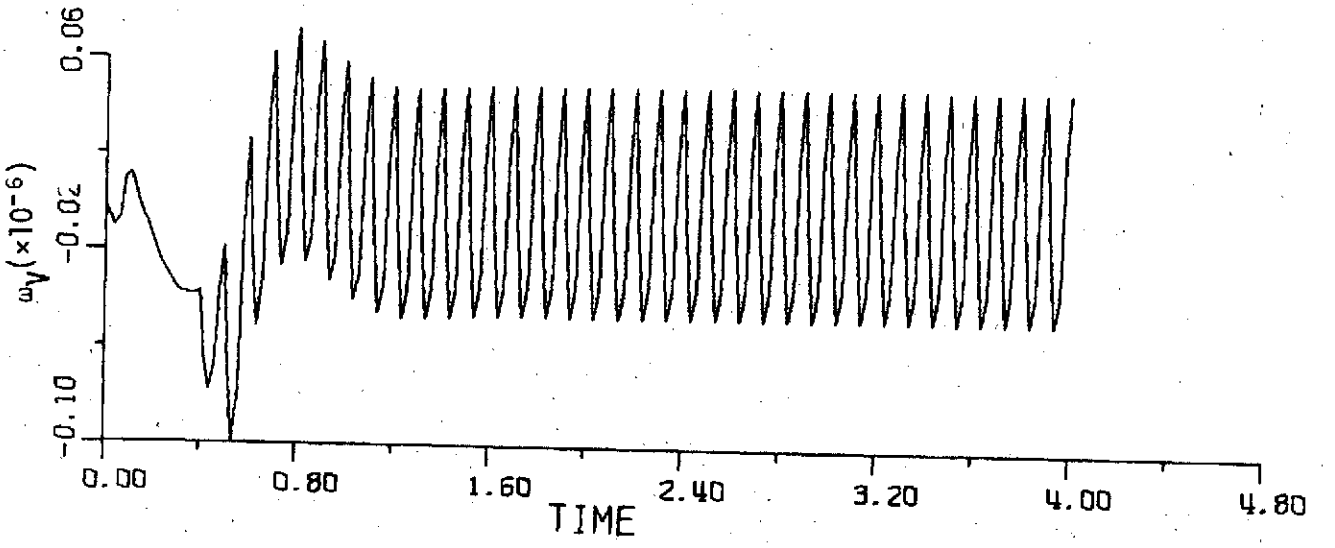

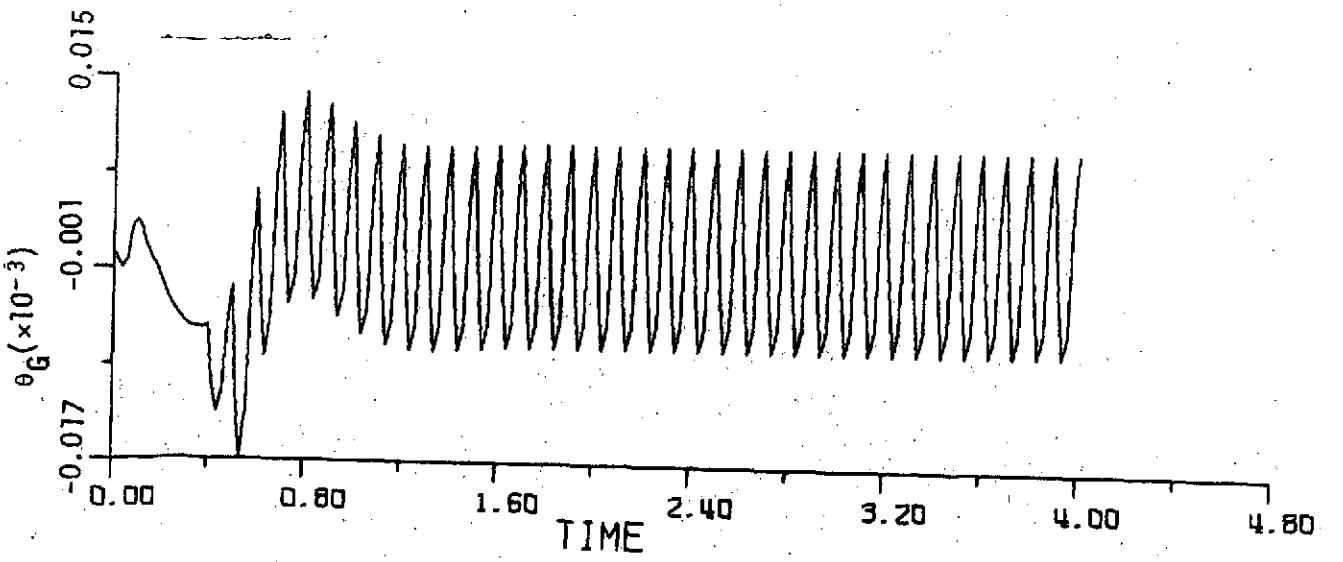

Figure 10-19

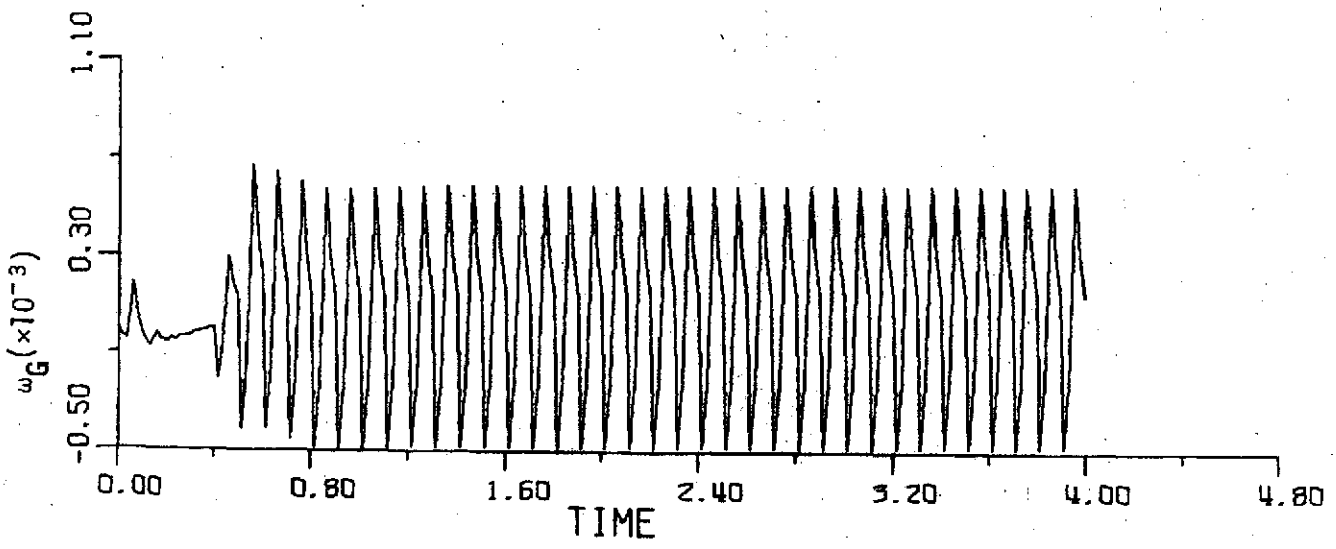
1.10
0.30
-0.50
$\omega_G(\times10^{-3})$
0.00
0.80
1.60
2.40
3.20
4.00
4.80
TIME

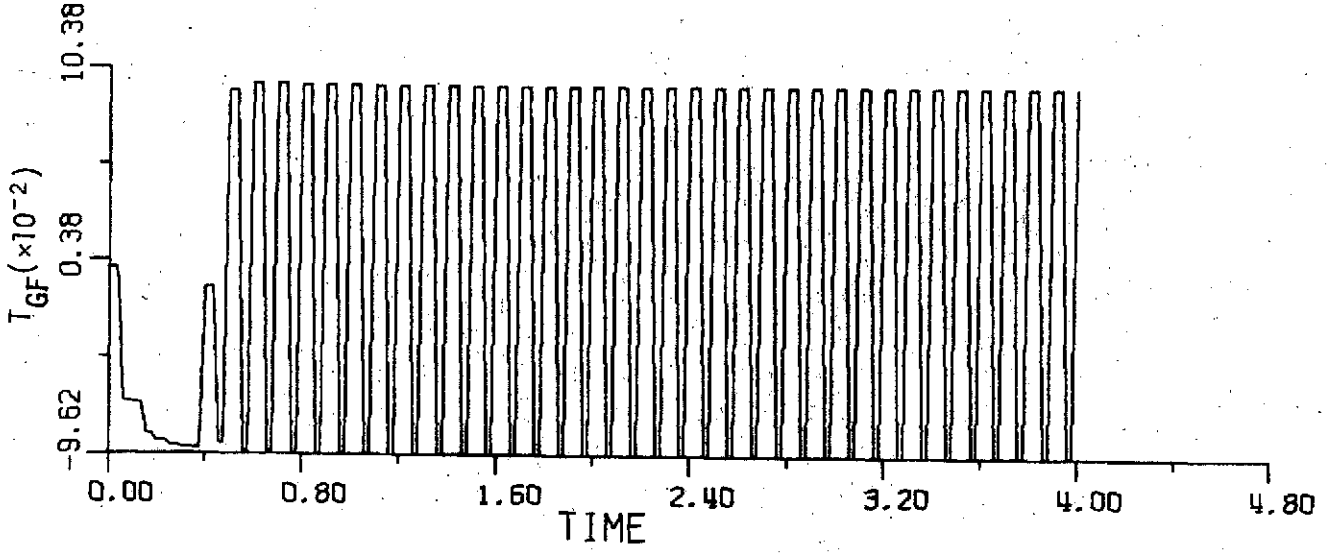
10.38
0.38
-9.62
$T_{GF}(\times10^{-2})$
0.00
0.80
1.60
2.40
3.20
4.00
4.80
TIME

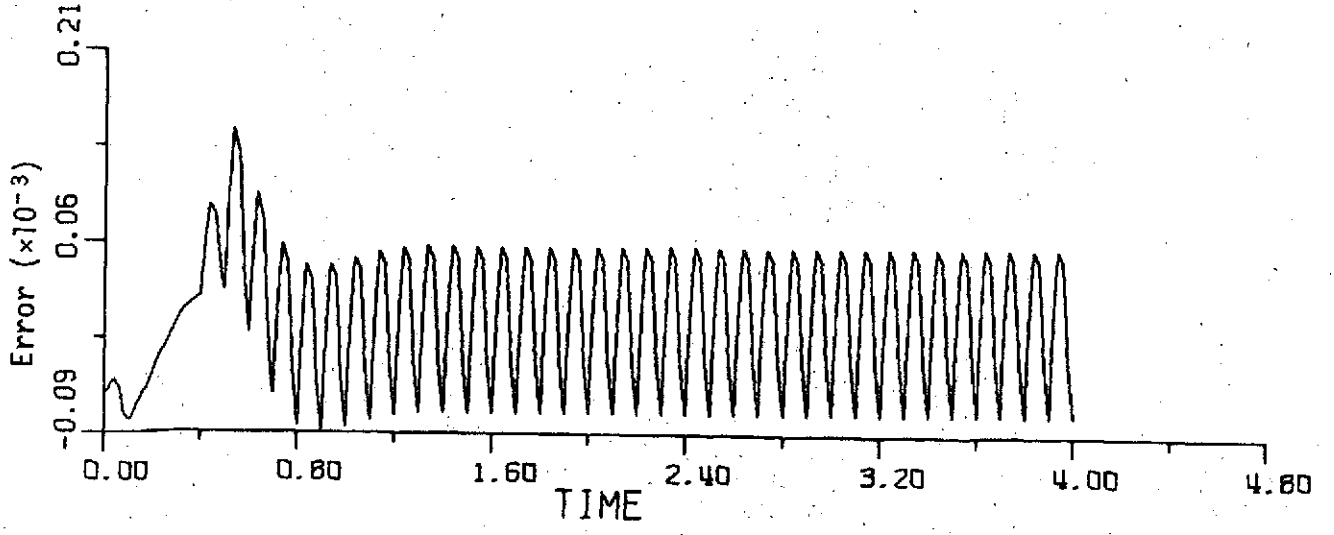
0.21
0.06
-0.09
Error $(\times10^{-3})$
0.00
0.80
1.60
2.40
3.20
4.00
4.80
TIME

Figure 10-20

$\gamma = 1.38\times10^{7}$, T = 0.05 sec

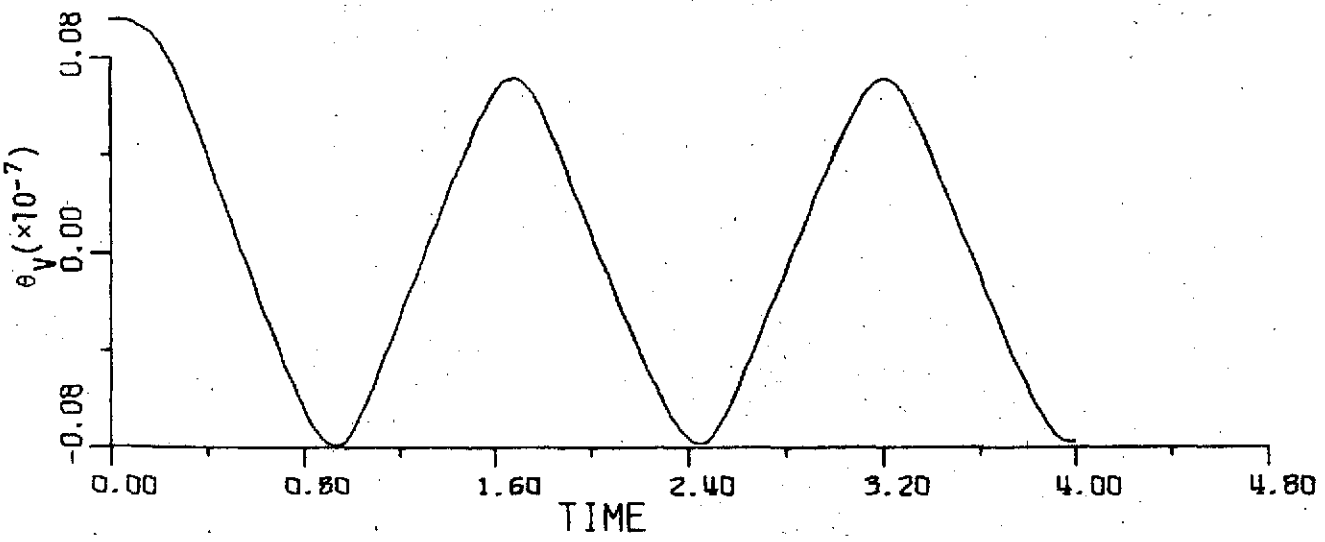

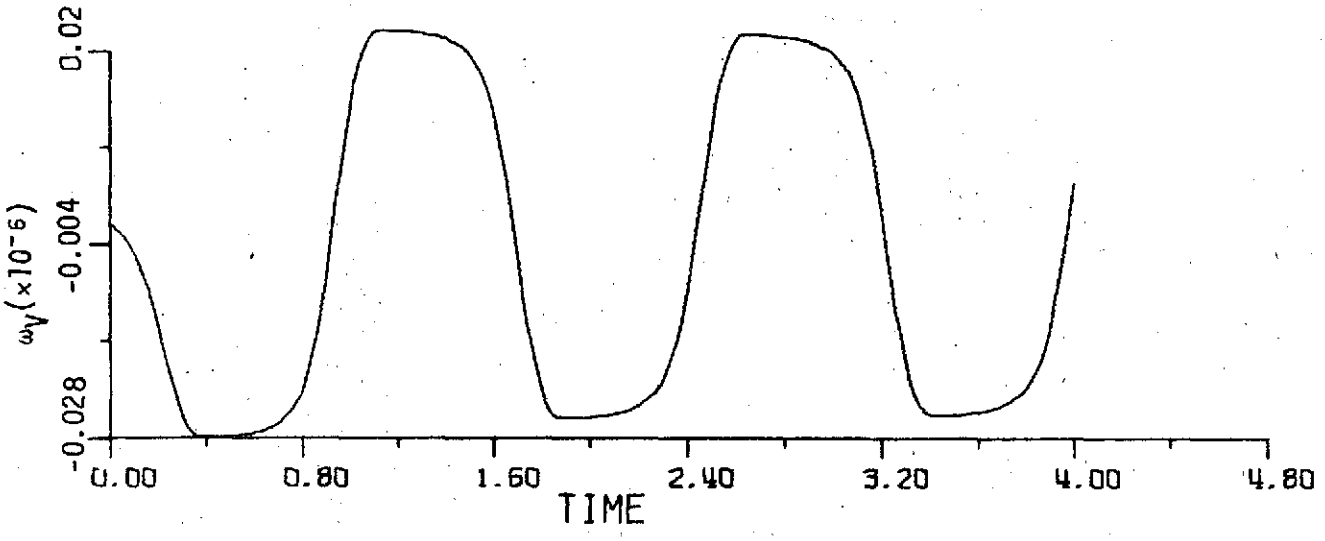

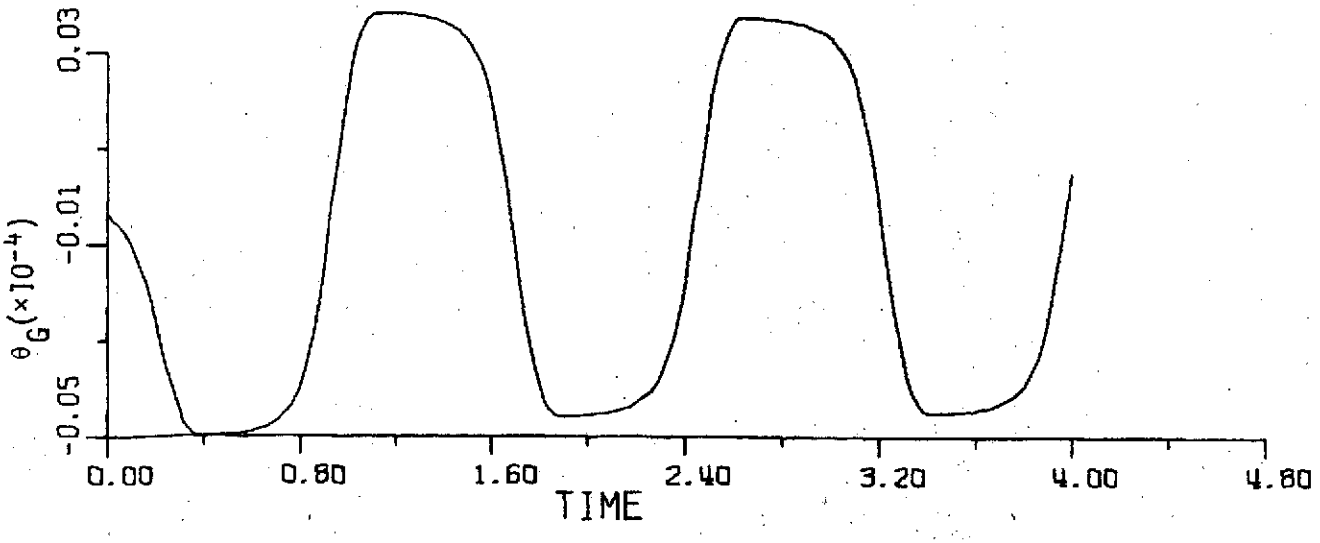

Figure 10-21

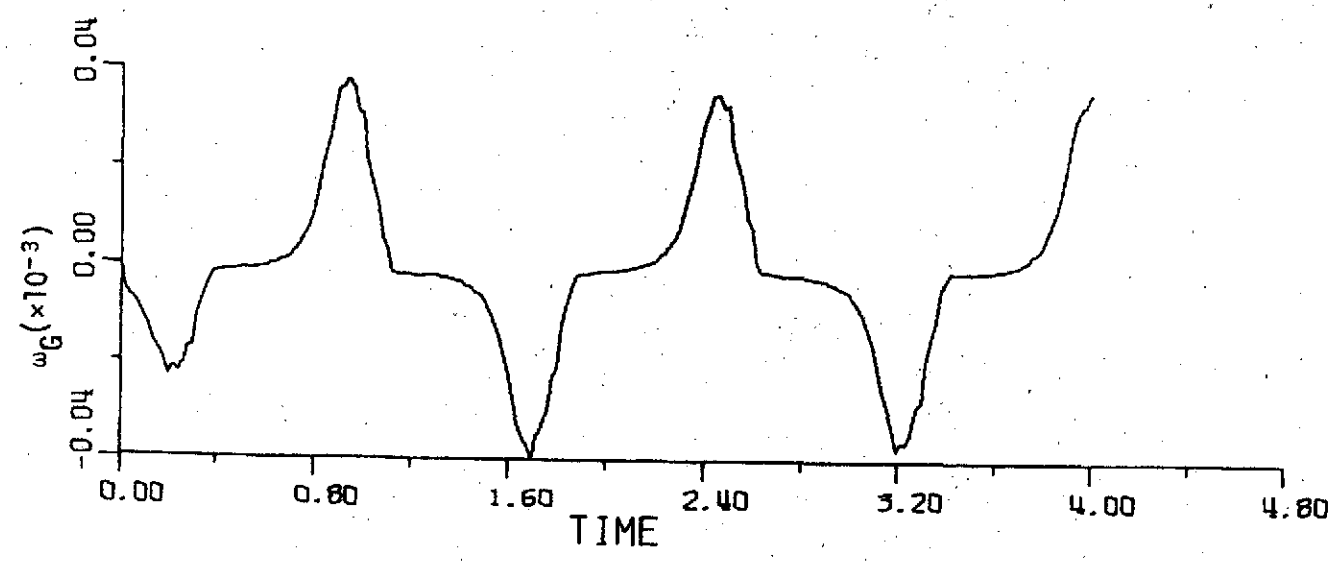
0.04
0.00
-0.04
$\omega_G(\times10^{-3})$
0.00
0.80
1.60
2.40
3.20
4.00
4.80
TIME

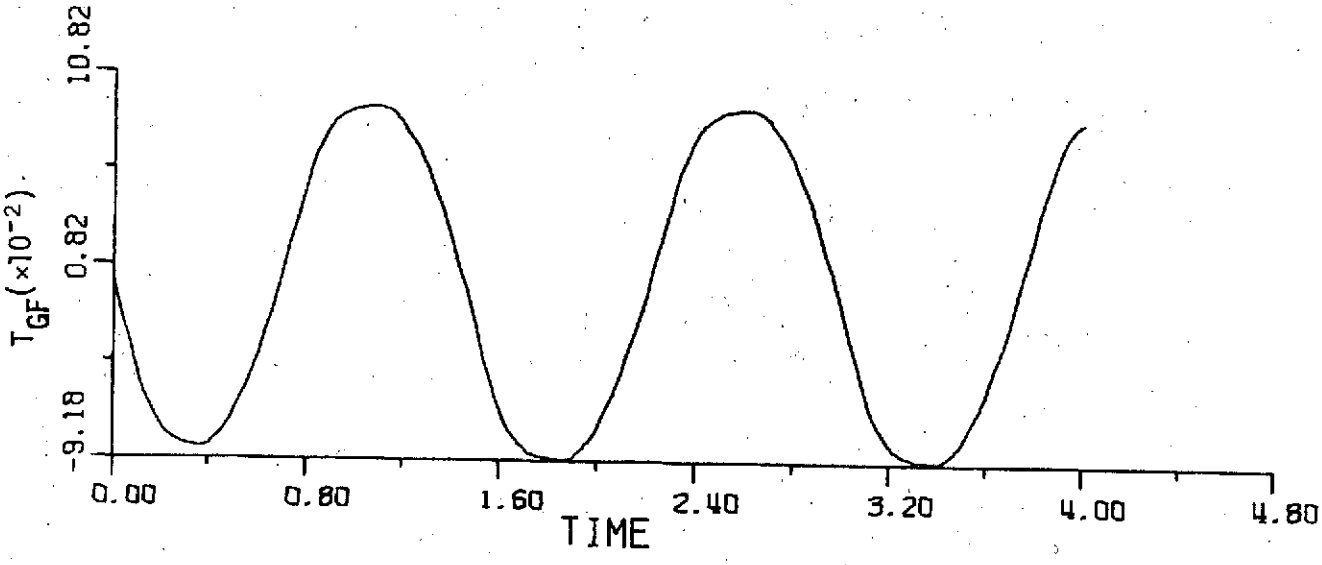
10.82
0.82
-9.18
$T_{GF}(\times10^{-2})$
0.00
0.80
1.60
2.40
3.20
4.00
4.80
TIME

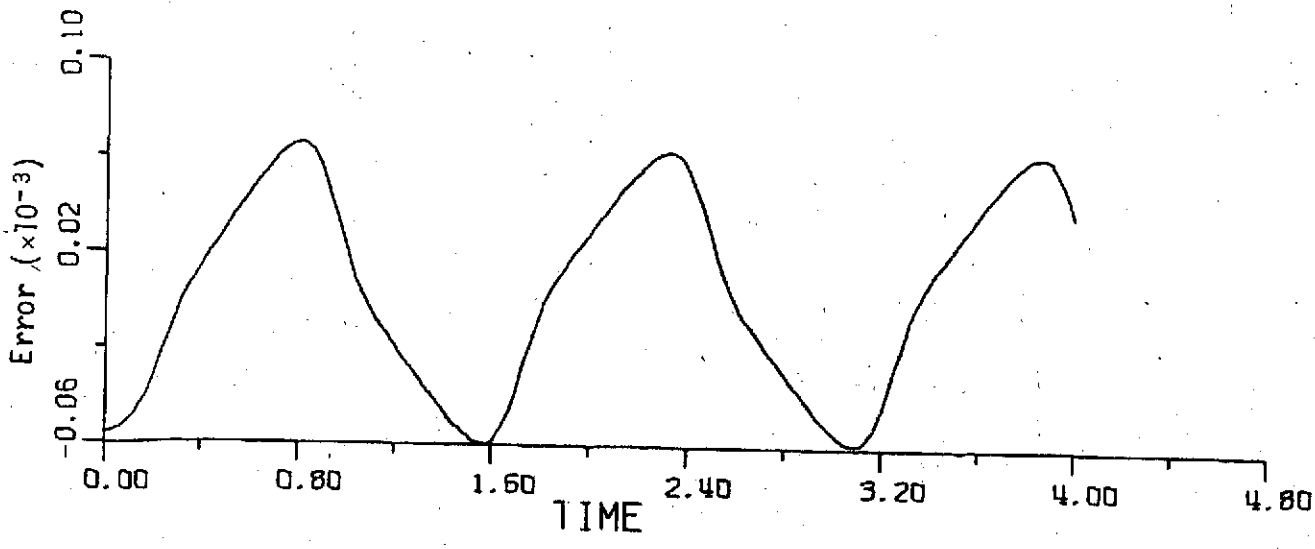
0.10
0.02
-0.06
Error $(\times10^{-3})$
0.00
0.80
1.60
2.40
3.20
4.00
4.80
TIME

Figure 10-22

$\gamma = 1.38 \times 10^7$, $T = 0.1$ sec

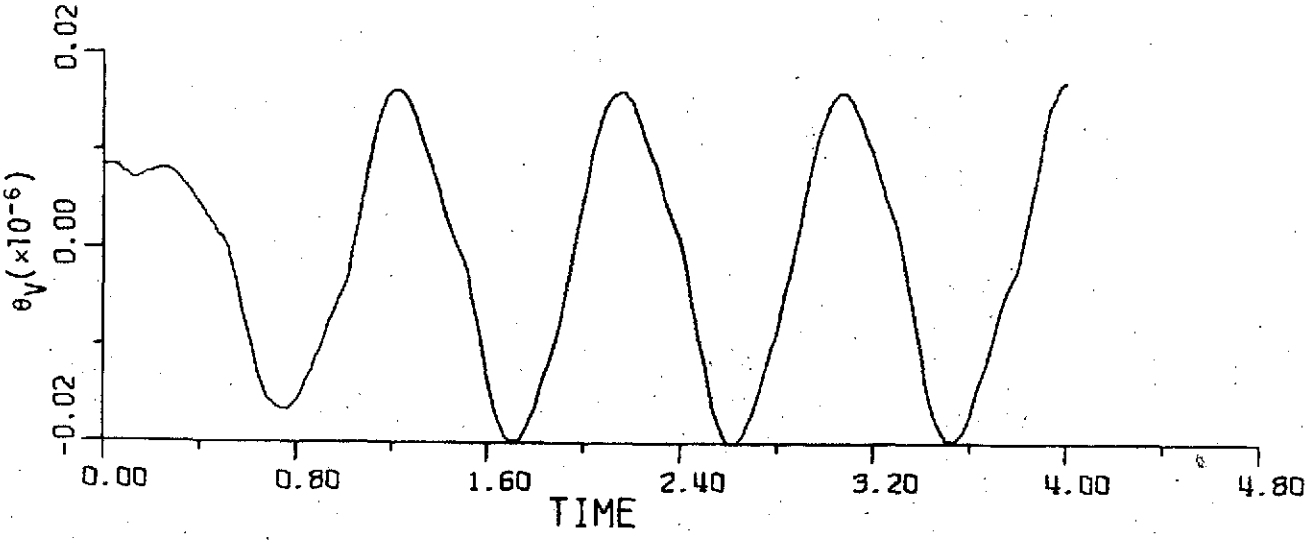

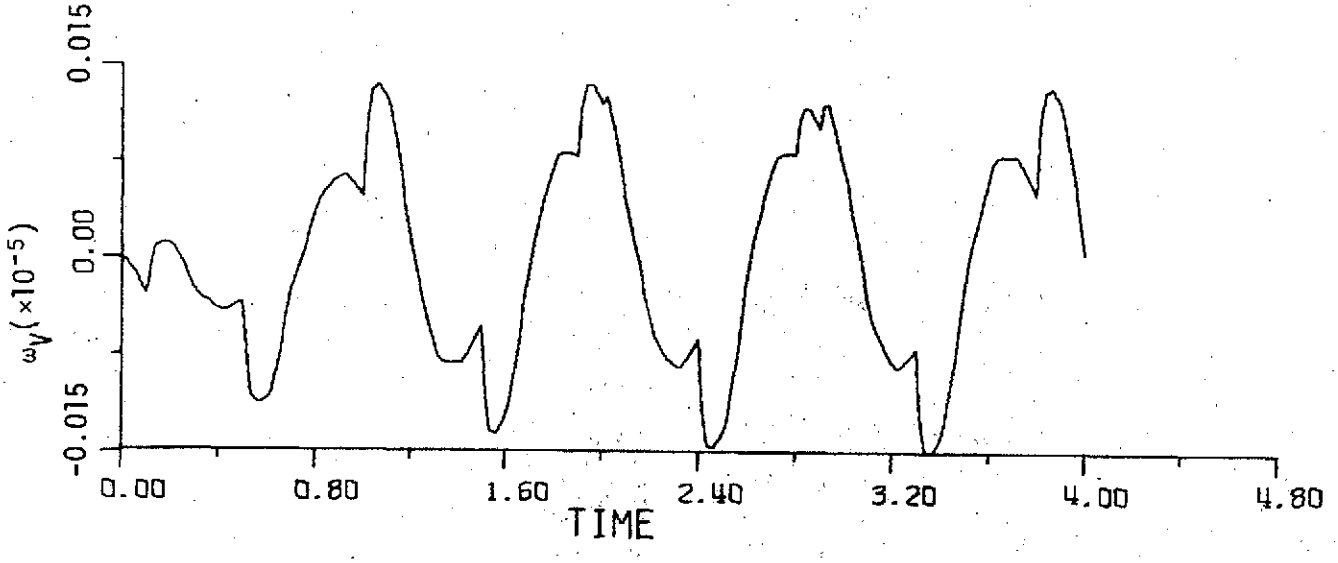

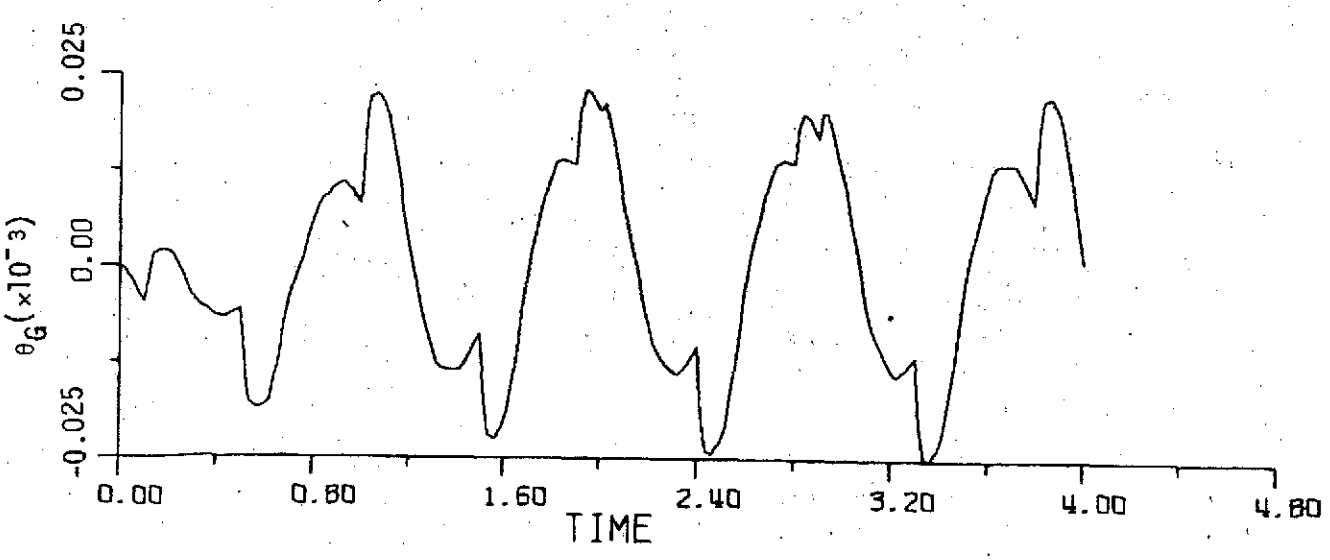

Figure 10-23

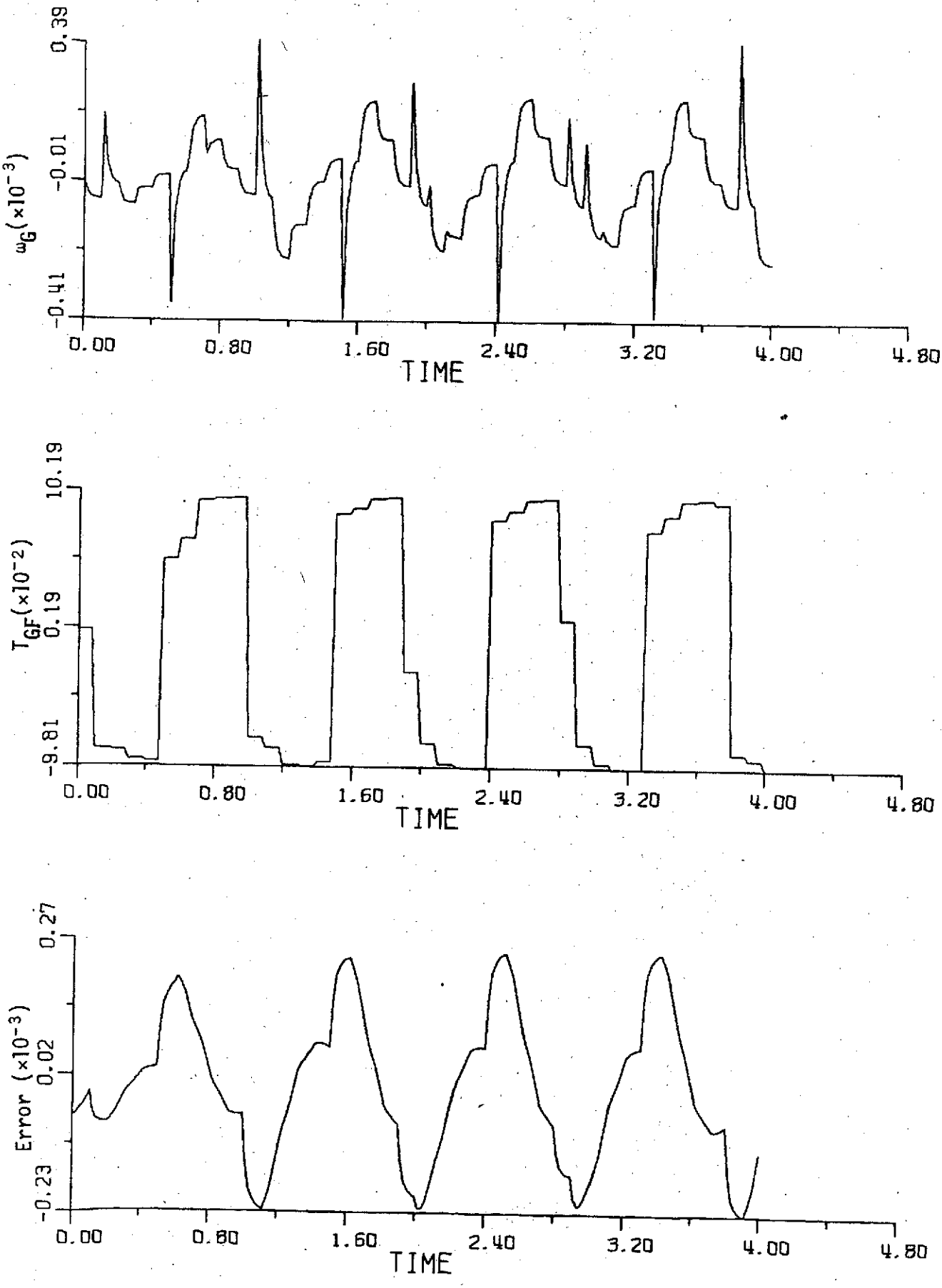
0.39
-0.01
-0.41
$\omega_G(\times10^{-3})$
0.00
0.80
1.60
2.40
3.20
4.00
4.80
TIME
10.19
0.19
-9.81
$T_{GF}(\times10^{-2})$
0.00
0.80
1.60
2.40
3.20
4.00
4.80
TIME
0.27
0.02
-0.23
Error $(\times10^{-3})$
0.00
0.80
1.60
2.40
3.20
4.00
4.80
TIME

Figure 10-24

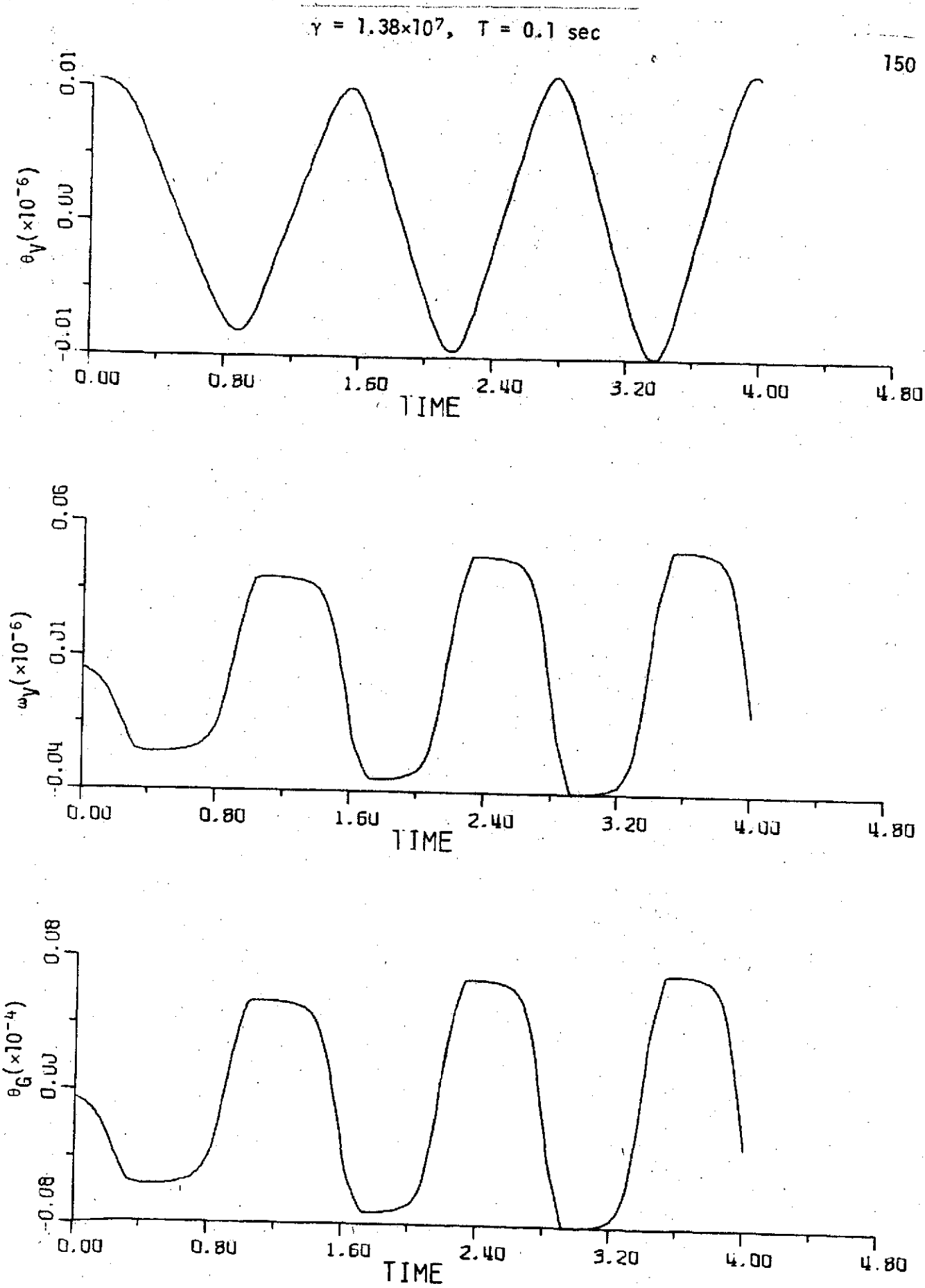
γ = 1.38×10⁷, T = 0.1 sec
θV(×10⁻⁶)
0.01
0.00
-0.01
0.00
0.80
1.60
2.40
3.20
4.00
4.80
TIME
ωy(×10⁻⁶)
0.06
0.01
-0.04
0.00
0.80
1.60
2.40
3.20
4.00
4.80
TIME
θG(×10⁻⁴)
0.08
0.00
-0.08
0.00
0.80
1.60
2.40
3.20
4.00
4.80
TIME

Figure 10-25

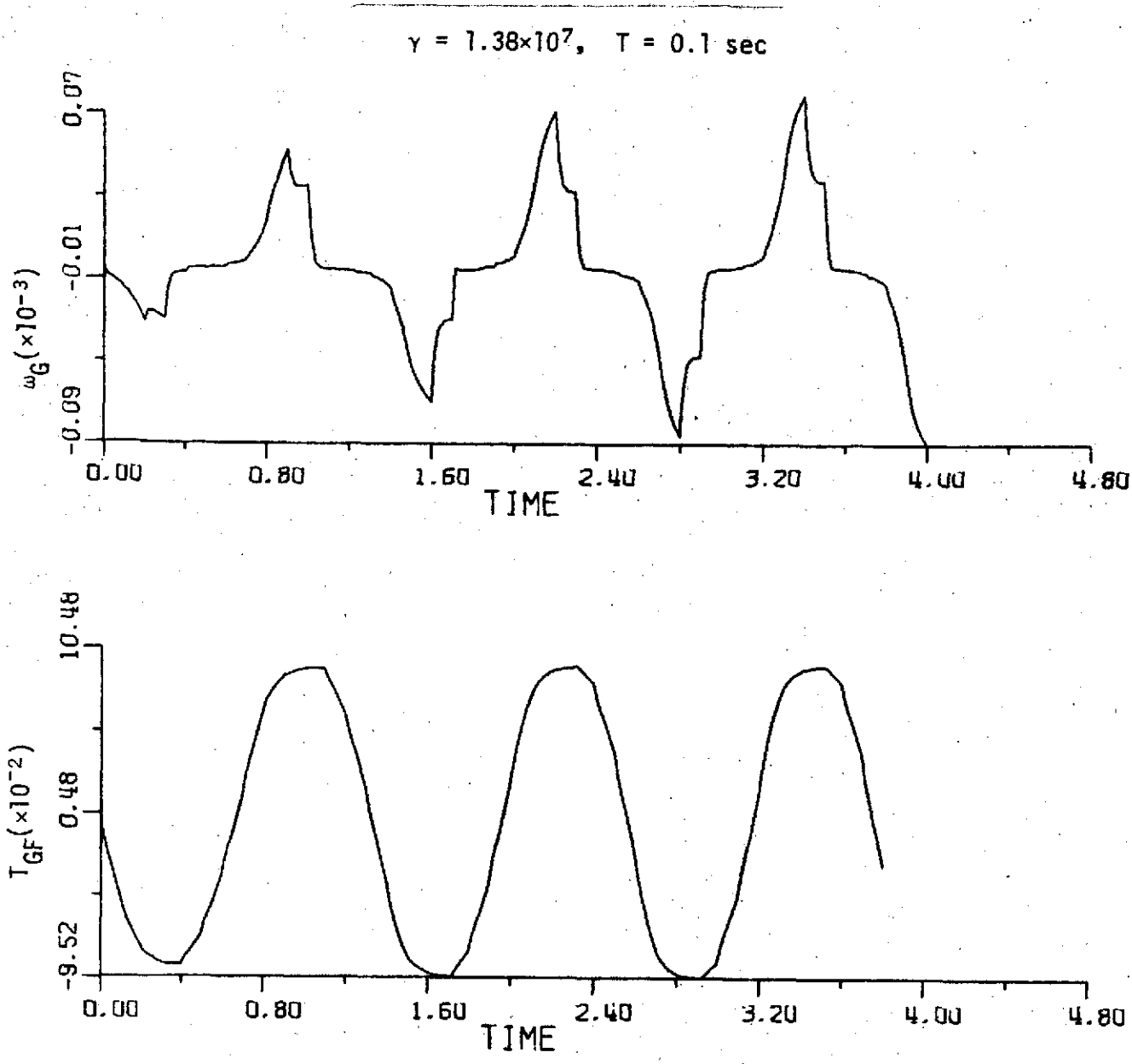
γ = 1.38×10^7, T = 0.1 sec
0.07
-0.01
-0.09
ω_G(×10^-3)
0.00
0.80
1.60
2.40
3.20
4.00
4.80
TIME
10.48
0.48
-9.52
T_GF(×10^-2)
0.00
0.80
1.60
2.40
3.20
4.00
4.80
TIME

Figure 10-26

$\gamma = 1.38\times10^{7}$, T = 0.25 sec

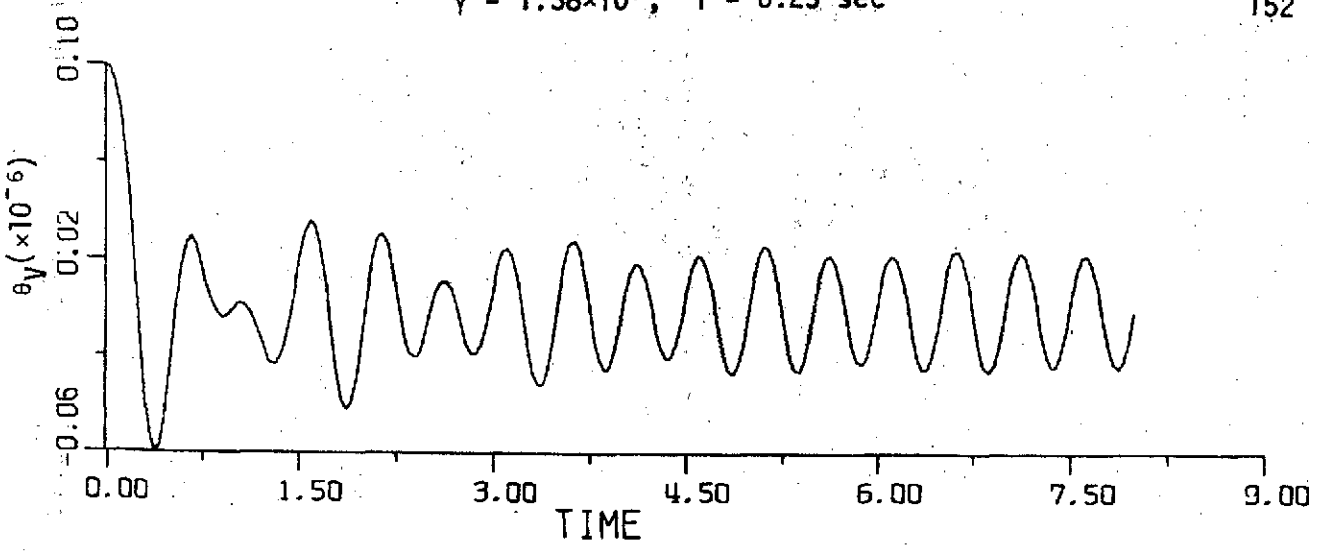

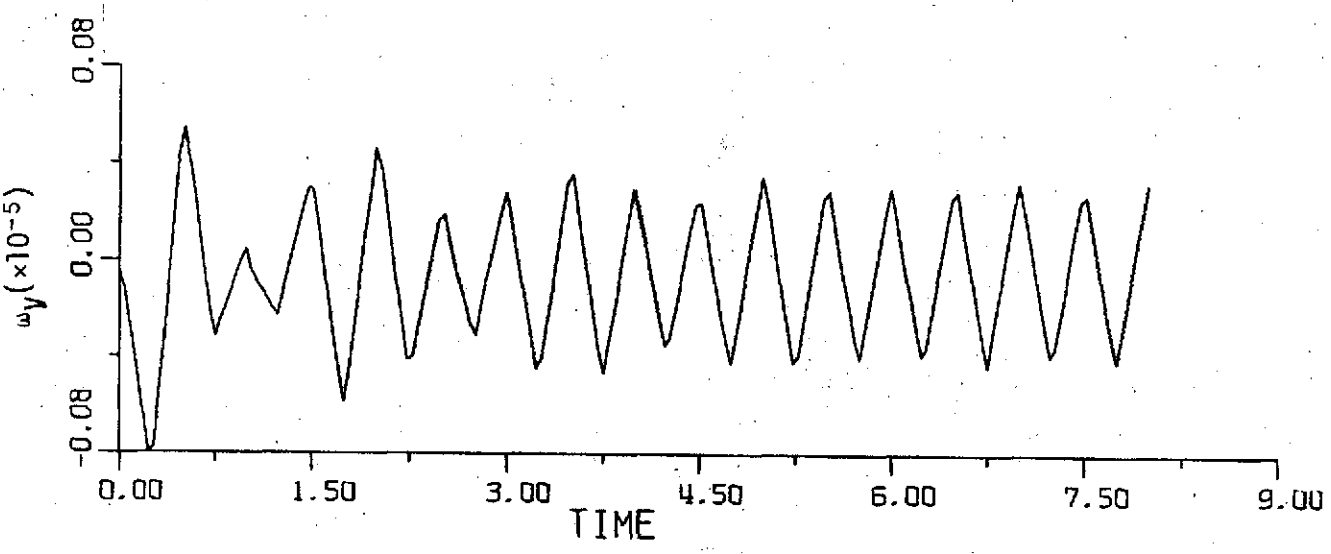

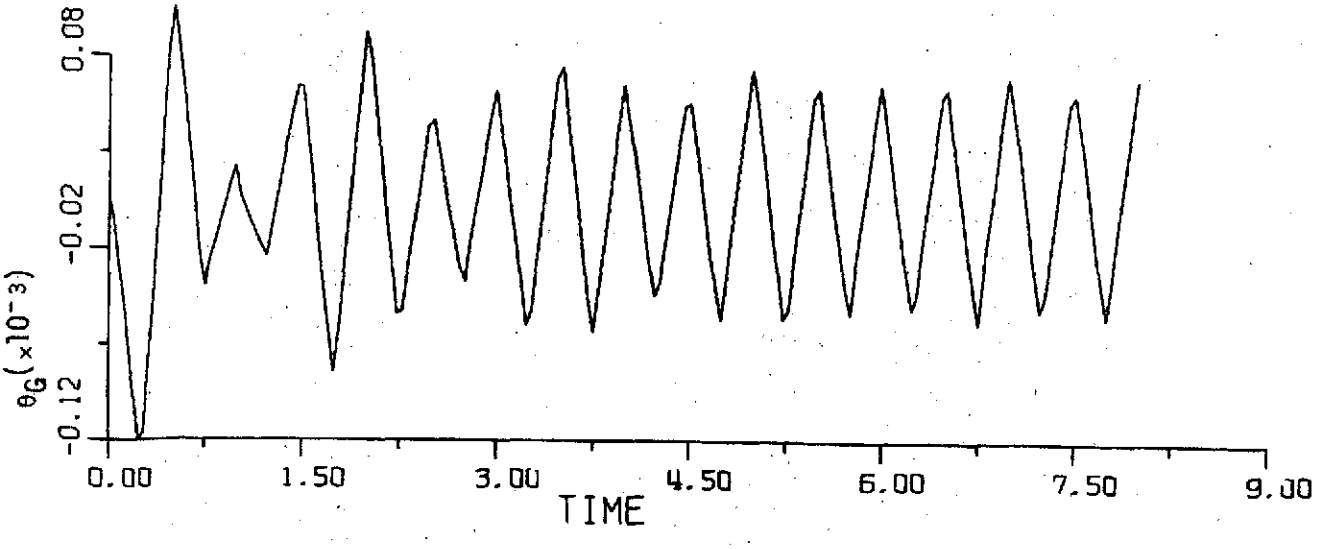

Figure 10-27

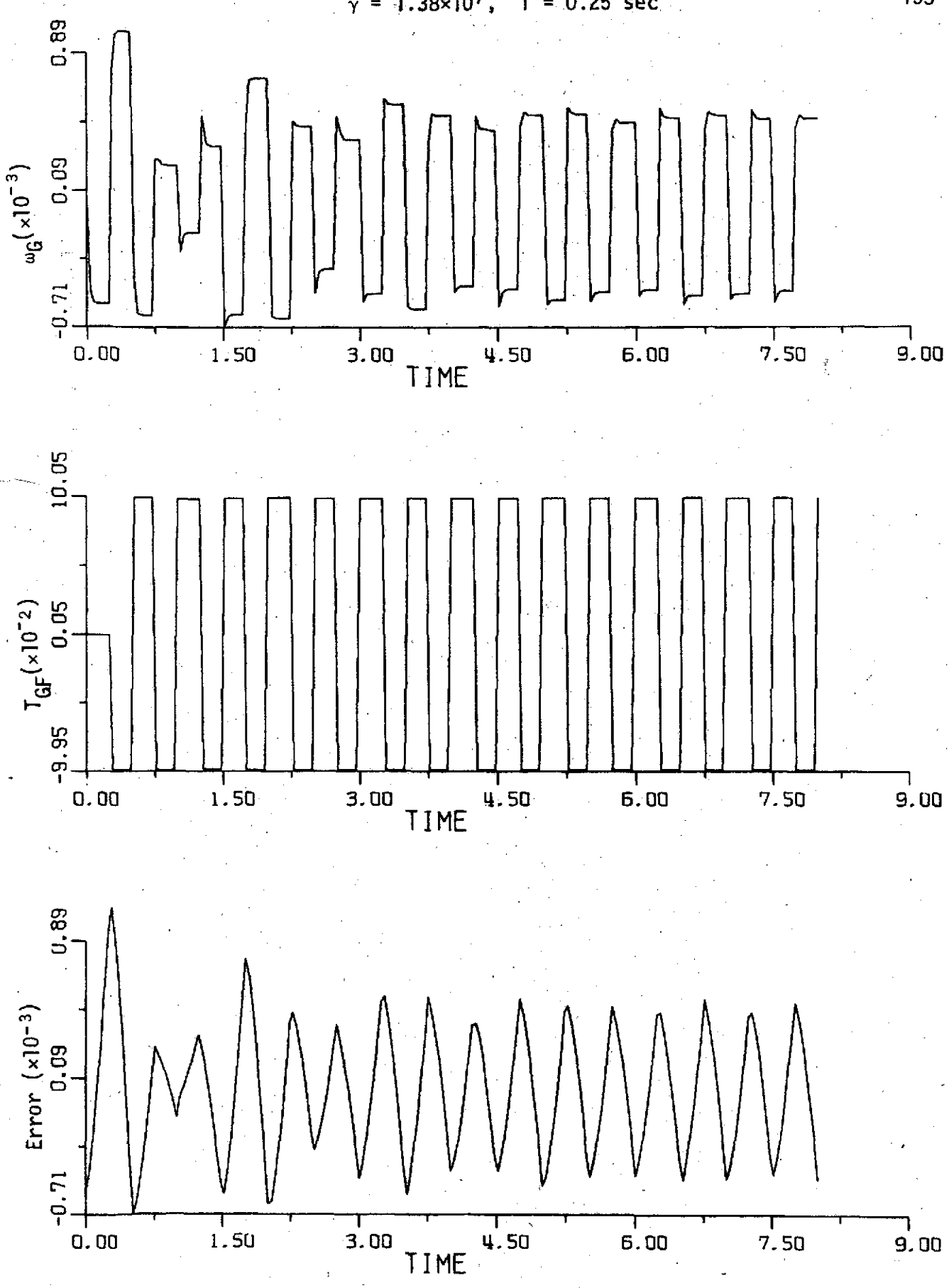
γ = 1.38×10^7, T = 0.25 sec
ω_G(×10^-3)
0.89
0.09
-0.71
0.00
1.50
3.00
4.50
6.00
7.50
9.00
TIME
T_GF(×10^-2)
10.05
0.05
-9.95
0.00
1.50
3.00
4.50
6.00
7.50
9.00
TIME
Error (×10^-3)
0.89
0.09
-0.71
0.00
1.50
3.00
4.50
6.00
7.50
9.00
TIME

Figure 10-28

$\gamma = 1.38\times10^{7}$, T = 0.25 sec

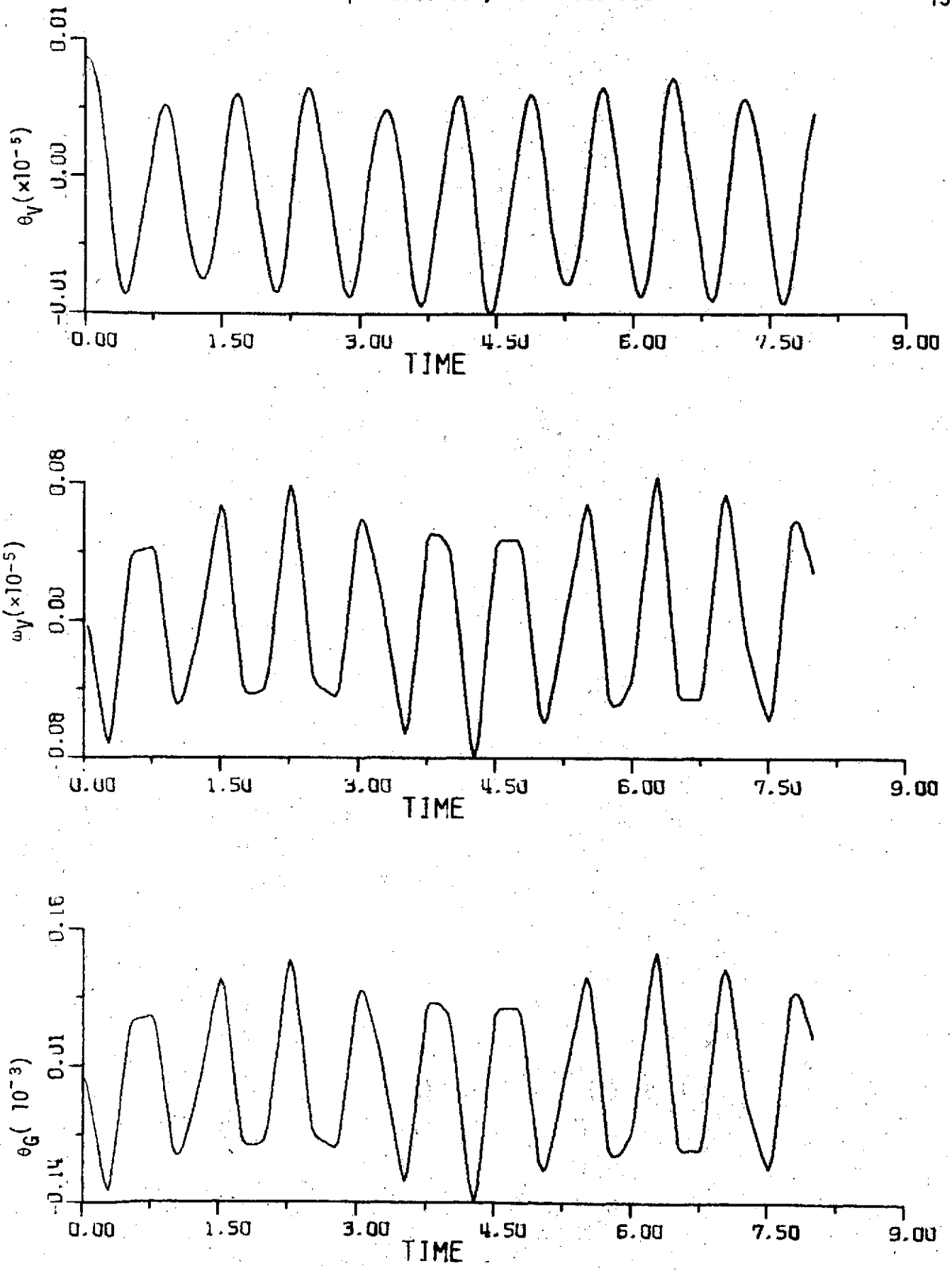

Figure 10-29

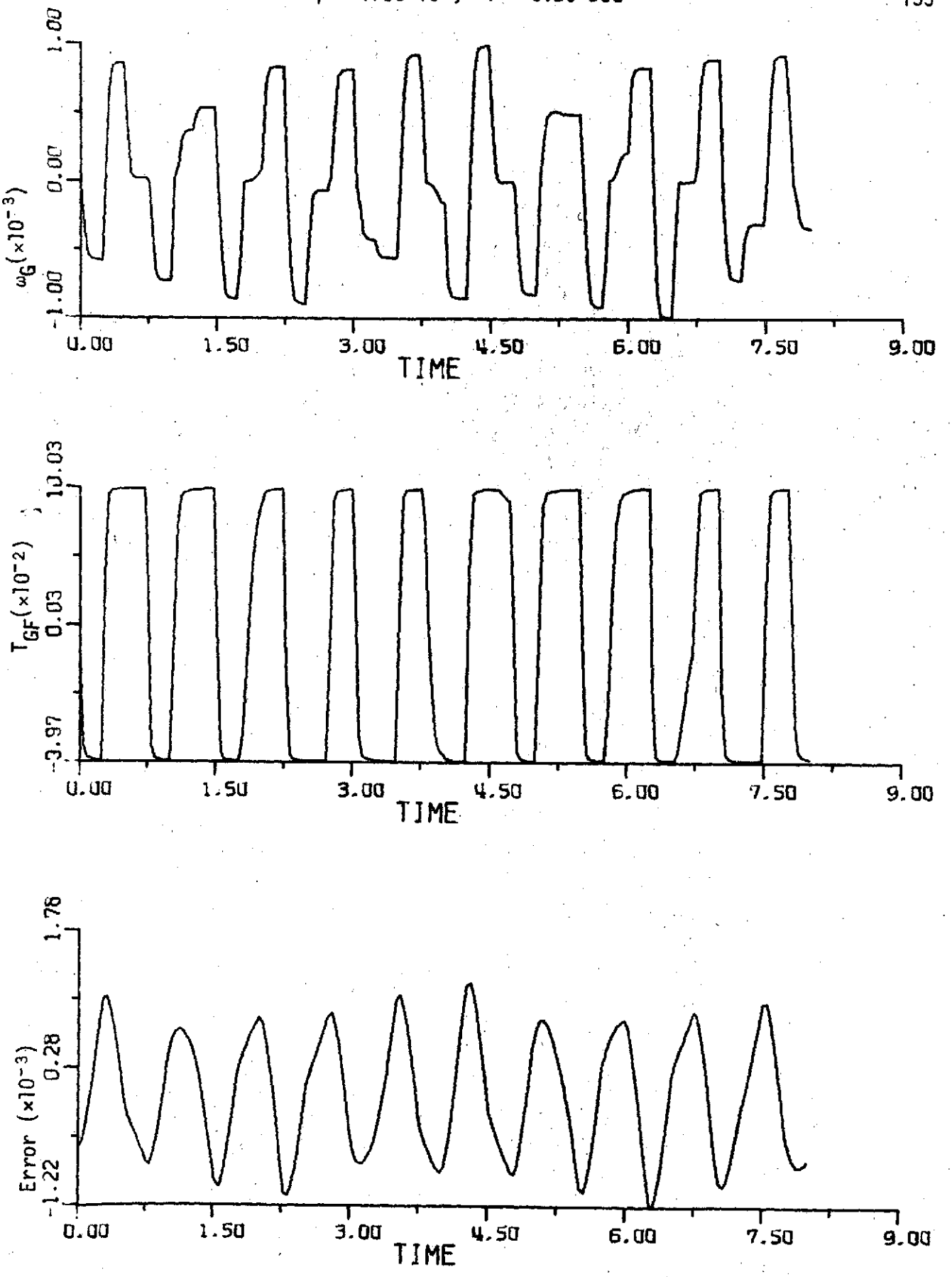
γ = 1.38×10⁷, T = 0.25 sec
ω_G(×10⁻³)
1.00
0.00
-1.00
0.00
1.50
3.00
4.50
6.00
7.50
9.00
TIME
T_GF(×10⁻²)
0.03
-3.97
TIME
Error (×10⁻³)
1.76
0.28
-1.22
TIME

Figure 10-30